CWP-284
April 1998

Seismic Data Mapping

Herman Jaramillo

— Doctoral Thesis —
Geophysics

Center for Wave Phenomena
Colorado School of Mines
Golden, Colorado 80401
303/273-3557

ABSTRACT

I introduce a seismic processing technique called Seismic Data Mapping (SDM) that transforms recorded seismic data to what would have been obtained for different recording geometries and environments. Specifically, I propose a SDM operator that can be applied to solve a variety of important geophysical processing problems such as offset continuation, Transformation to Zero Offset (TZO), Azimuthal Continuation (AMO), layer replacement and datuming etc.

The SDM operator is a cascade of prestack migration and inverse migration (demigration). Because direct implementation of the operator is computationally expensive, I present an alternative, approximate approach of attractive computational speed. I use a time–domain approach for both the demigration and migration operators as well as for the exact and approximate SDM operators.

To provide a self–contained theoretical basis, I also introduce basic concepts in diffraction theory and study the Born and Kirchhoff modeling equations. I derive the demigration and migration formulas both from the Born and from the Kirchhoff approximations to prove the equivalence of these two common approaches. This theoretical study is supplemented with formulas for the method of stationary phase in the time–domain. This research put several known results of seismic transformation theory into a new context and provides new interesting insights.

Finally, I present an application of SDM to the solution of the true amplitude TZO problem in vertically inhomogeneous isotropic media.

TABLE OF CONTENTS

ACKNOWLEDGMENTS

The work presented in this thesis could not have been realized without the help of many individuals. I would like to formally acknowledge them.

First, I would like to thank my thesis advisor, Dr. Norman Bleistein for his great energy and motivation. He was always pushing things forward and getting new insights into the problem. He made of my work an enjoyable experience adding to it lots of knowledge. He taught me how to do asymptotics, and this marked the difference between the way I understood applied mathematics in the past and the way I understand it now. I want to thank Dr. Ken Larner for helping me all these years with all kind of problems. He trusted in me, and he made possible that I could start and finish my studies in the Center for Wave Phenomena. I would also like to acknowledge my other committee members for their support: Dr. Paul Fowler, Dr. Ilya Tsvankin, Dr. Martijn de Hoop, Dr. Alexander Kaufman, Dr. Thomas Boyd and Dr. Martin Tygel. I am indebted also to Dr. Frank Hadsell and Dr. Alfred Balch; they were the people who brought me to this school.

This work would not be possible without the contribution of Marin Tygel, Jörg Schleicher and Peter Hubral. They built the foundations of the Data Mapping problem.

I am also indebted to the following people: Gerardo Garcia, Andreas Rüger, Gabriel Alvarez, Gabriel Perez, Trino Salinas, Pedro Anguiano, Omar Uzcategui, Lan Wang and all the CWP students that gave me support in the difficult times. Jo Ann Fink, Barbara McLenon and Peggy Dunn were always very kind, helpful and supportive.

I would like to dedicate this thesis to Dr. Jack Cohen who passed away. He was always there when I needed him. I would like also to dedicate this work, to my daughters Paula Andrea and Maria Alejandra who were born while I was a student here.

Finally, I would like to thank my father, Alfonso, who passed away and my mother Amparo for their endless support and encouragement. My wife Patricia always believed in me, and never failed to give me the cheers and rest I needed.

Chapter 1

INTRODUCTION

In this introduction, I explain the meaning of Seismic Data Mapping (SDM), its assumptions, limitations, applications, goals and history. Finally I give an outline of the rest of the thesis.

1.1 Basic concepts

We start by making a short description of the reflection seismic experiment. For practical purposes, I describe the earth as consisting of series of layers of rocks. The main target of reflection seismology is to make use of the variation in the properties of different rocks to find oil and gas traps[1]. These variations must be mapped by making use of measurements at or near the surface. The main rock properties of interest in reflection seismology are density and seismic velocity. The reflection seismic experiment is similar to the radar or sonar technique where the backscattered energy is recorded to compute distances to targets. In contrast to radar or sonar, however, in the reflection seismic experiment, the energy travels in a medium that is heterogeneous, laminated, and subject to discontinuities such as those created by unconformities and faults. The elements of the reflection seismic experiment are the sources (dynamite, vibroseis, airguns, etc.), the earth subsurface (rock layers bounded by interfaces that we call reflectors) and receivers (geophones, hydrophones). We record the upward scattered (acoustic or elastic) wavefield by measuring particle velocity (in geophones) and/or pressure (in hydrophones), which generate electric signals that are then amplified, filtered, digitized, and recorded in magnetic tapes. We call these measurements seismic field data. These data or computer–generated simulations thereof, are what I call Seismic Data (SD). The space of all SD is called the Data Space (DS); for completeness I add to the data space all the output from any SDM (not yet defined) process. The signal recorded by each receiver is plotted along the vertical (time axis) as a seismic trace. A seismic trace is uniquely defined by six spatial parameters. Three coordinates for the source (x_s, y_s, z_s) and three coordinates

[1] In fact the technology of reflection seismology is also used in the search for waste–disposal sites, in determining the stability of the ground under proposed industrial facilities, in archaeological investigations, and for study of the deep continental crust down to and below the Moho (Evans, 1997).

for the receiver (x_g, y_g, z_g). This thesis treats processing of SD divided into subsets, such as common–shot, common–offset, etc. Each such subset can be mapped, into a surface parameterized by a two–dimensional parameter $\boldsymbol{\xi} = (\xi_1, \xi_2)$. For example, for a given common–shot gather, fix the three shot coordinates and parameterize the receivers as $[x_g(\xi_1, \xi_2), y_g(\xi_1, \xi_2), z_g(\xi_1, \xi_2)]$.

1.2 Definition

SDM defines a family of processes that convert one set of seismic data into a different set of seismic data after either the source/receiver recording configuration and/or the model parameters have been changed. The processes included in SDM are specifically grounded in an underlying geophysical model as will be explained in more detail later in this section. All processes done under SDM are "true amplitude" in the sense that amplitude variations attributable to the point–source and reflector curvature for the input configuration are mapped into the respectively amplitude variations for the point–source and curvature of the output configuration; therefore the reflection coefficient is preserved in the output data.

To better understand this concept consider a simple example. Figure 1.1 shows a common–offset seismic data set corresponding to a horizontal reflector at a depth of $d = 2$ km, in a homogeneous isotropic medium, with constant velocity $v_1 = 2$ km/s and semi–offset (half the lateral separation between source and receiver) of $h = 1$ km. Figure 1.2 shows a data set in depth after prestack migration is applied to the set in Figure 1.1. Here we see the reflector located at the correct depth. The peak amplitude on this traces represents the reflection coefficient for oblique incidence. Now I apply inverse migration (demigration) to the section in Figure 1.2, to a zero–offset section assuming a subsurface with a new velocity $v_2 = 4$ km/s. The result is shown in Figure 1.3.

Kinematically, inverse migration creates modeled zero–offset traces for the output velocity v_2. Dynamically, inverse migration introduces the geometrical spreading of the zero–offset modeling and preserves the oblique–incidence reflection coefficient.

We want to formulate the SDM problem in a precise way and show how to implement this operator for the solution of a variety of seismic data processing problems.

Given that the cascade of prestack migration and demigration can be expensive for 3D data, we would like to achieve a shortcut for this process. I will refer again to the same example that started with the data in Figure 1.1 and produced the data in Figure 1.3. A shortcut to this cascade of migration and demigration process, can be found. We time shift the data upward by the amount $\Delta t = 2\sqrt{d^2 + h^2}/v_1 - 2\,d/v_2$ and multiply the input amplitude by the ratio of geometrical spreading factors of the second and the first configuration. This ratio will remove the geometrical

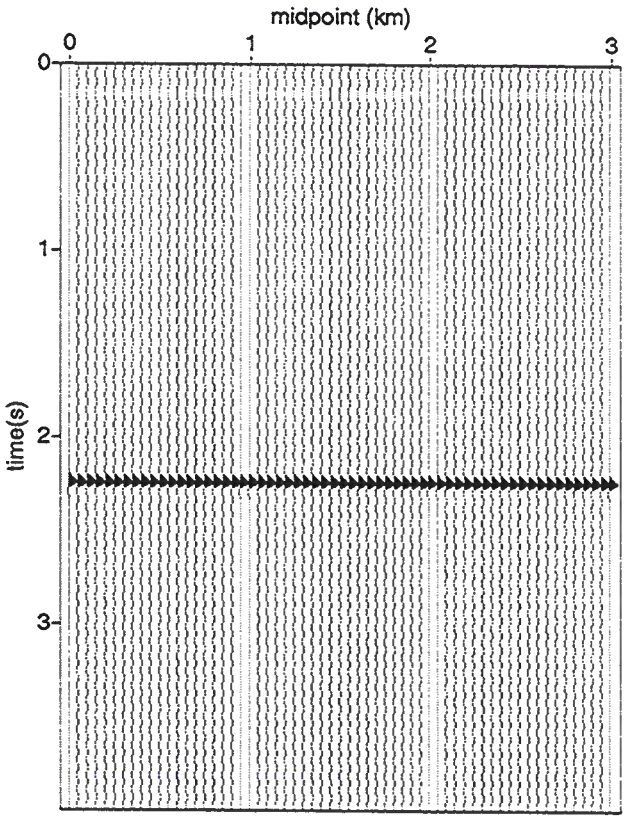

FIG. 1.1. Common–offset section to a reflector in a homogeneous isotropic media. Reflector depth $d = 2$ km, velocity $v_1 = 2$ km/s, semi–offset $h = 1$ km.

spreading from the first experiment and include the geometrical spreading from the second (output configuration) experiment. The shortcut for this simple example illustrates what we expect from SDM. Figure 1.4 shows a sketch of this process. It is precisely a shortcut of the cascade of prestack migration and demigration operators that interests us here. I formulate the problem as the cascade of prestack migration with demigration. In this case, each of these operators is a surface integral. The prestack migration is an integral over a particular subset of SD parameterized by $\boldsymbol{\xi} = (\xi_1, \xi_2)$ and the demigration operator is a surface integral over an isochron (surface of equal travel time from fixed source to receiver positions). Given that our output data should not depend on the earth coordinates, the SDM operator collapses to another surface integral of the data over a given surface (stacking surface). This reduction is done by using the stationary phase method. We will find also that the stationary phase method is good for many possible situations, but it fails in some simple cases (for example offset continuation in constant–velocity media).

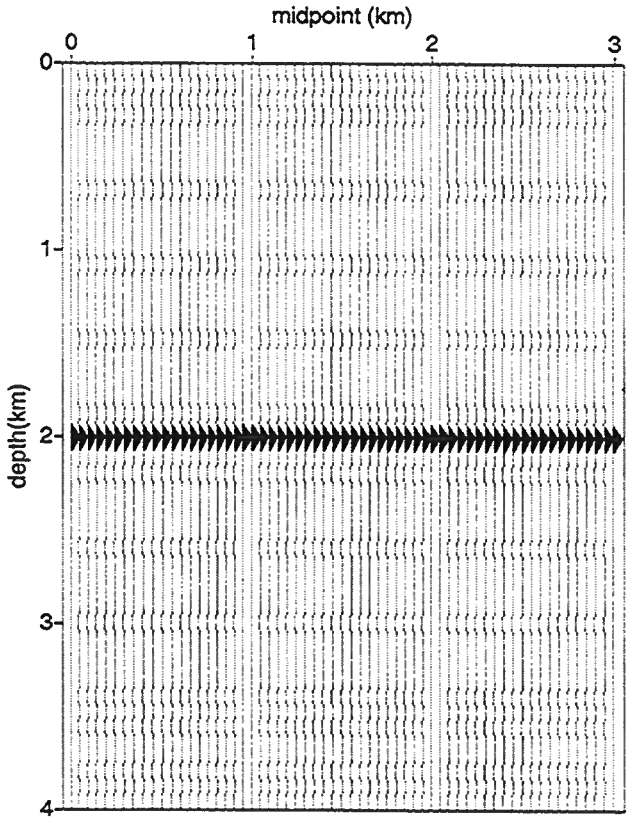

FIG. 1.2. Migrated section corresponding to the data in Figure 1.1.

For the simple case of a horizontal reflector, the prestack imaging step reduces to a combination of geometrical spreading correction, normal moveout and vertical time–to–depth correction. The zero–offset modeling consists of depth–to–time conversion and another geometrical spreading correction. If we keep the velocity v_1 constant throughout, these two steps represent the simple process of normal moveout (NMO) correction. This simplistic example is actually a special case of an important case of SDM. If the combination of constant–offset migration followed by zero–offset modeling is extended to handle all dips, not just horizontal reflectors, the SDM is in this case a Transformation to Zero Offset (TZO) operator. This operator is widely used in seismic data processing. The TZO operator will be examined in much greater detail in Chapters 6 and 8.

For horizontal reflectors, the TZO process takes each input data sample to a single sample in the output data. The full–dip TZO operator provides a better example of the general SDM integral operators, for which each output data point is a line (or a surface) integral over many input data points. I will show that aperture for the

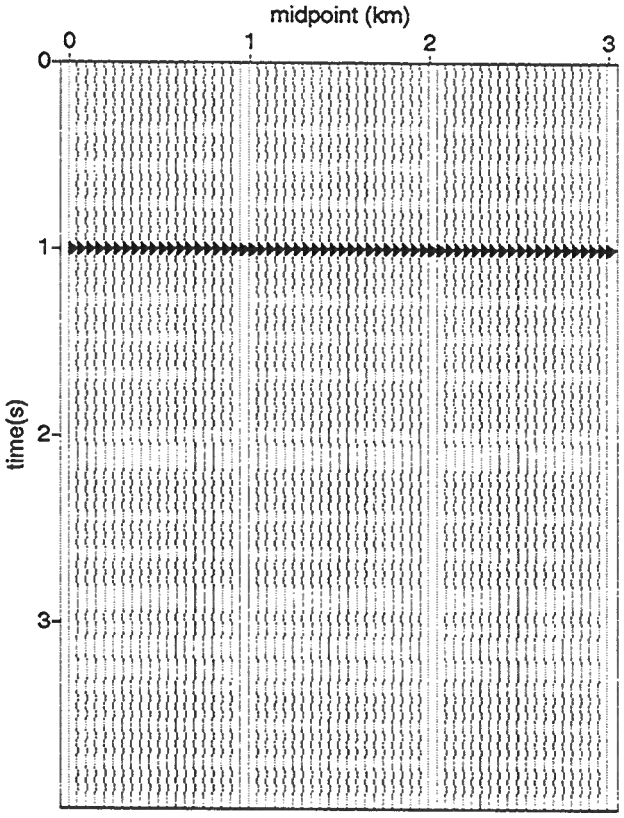

FIG. 1.3. Demigration of the migrated data in Figure 1.2 to a zero–offset section with velocity $v_2 = 4$km/s.

line (or surface) of integration for SDM is smaller than that for prestack migration or modeling. This would translate into computational savings.

In a more rigorous way, SDM is the composition (cascade) of a "true amplitude" prestack migration operator with a "true amplitude" inverse migration (demigration) operator. The prestack migration operator defines the location of the geological structures (reflectors) and weights this with the reflection coefficient, by undoing the defocussing and focussing due to point–source and reflector curvature created during the modeling process; the demigration operator creates reflections according to the new output configuration and weights these reflections with the point–source and geometrical–spreading factors associated with reflector curvature for the output configuration. The reflection coefficient of the input configuration is held fixed in this process.

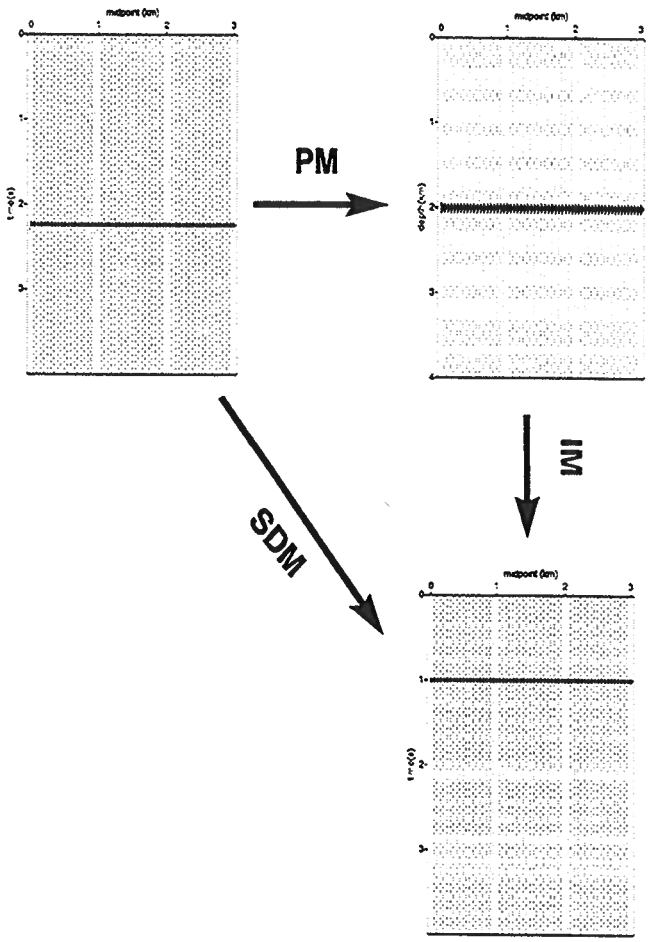

FIG. 1.4. SDM is the cascade of a prestack migration operator with a demigration operator. The main goal of this thesis is to provides shortcuts for this process.

1.3 Properties of SDM operators

The space of SDM operators is a well–defined algebraic structure. The composition of two SDM operators is a new SDM operator. This is clear if we see that each SDM operator is a cascade of migration and demigration operators. The demigration operator from the first SDM operator combined with the migration operator of the second SDM operator will produce the identity operator[2], the composition is then given by the prestack migration of the first SDM operator followed by an identity distribution and the demigration of the second SDM operator. Hence the composition of SDM operators is another SDM operator. The identity function is an SDM operator. If we cascade prestack migration with demigration without changing the source/receiver

[2]Given that our data are band–limited, instead of a pure delta function this identity should be a band–limited delta function, or a sinc function.

configuration and without changing the seismic parameters we should get the identity operator.

The inverse of a SDM operator is another SDM operator. This inverse is obtained by performing prestack migration to the output data with the output seismic parameters and then demigrating the result using the input seismic parameters and input source/receiver configuration.

1.4 Assumptions and limitations

The assumptions in applying an SDM operator are basically those needed to perform prestack migration and demigration. I derive prestack migration and demigration operators in Chapters 3 and 4. The assumptions underlaying these derivations will automatically be inherited by the SDM operator. Some of them are as follows.

- Although the idea of cascading a prestack migration operator with a demigration operator applies as well to anisotropy, here I develop all the mathematical formulation based on scalar wave fields for isotropic media.
- The seismic velocity that properly migrates the input data is assumed to be known.
- Although changes in density could be considered, by choosing appropriate Green functions, I assume constant density everywhere.
- High–frequency approximation. I work with the leading asymptotic term of the asymptotic series expansion of the wavefield, under the assumption of high frequency.
- All operators derived here are integral operators, so they consider the data embedded in a continuous domain. The issues of sampling are not considered until Chapter 8, where an application to TZO is numerically implemented. We assume that the input data are not aliased, and that we can adequately approximate our integral operators via discrete summations for practical implementation.
- The data represent primary scalar upward–scattered data from a single reflector. The superposition principle applies when a set of layers is to be considered.

1.4.1 Applications

Some of the direct applications of SDM are

1. **Offset continuation and Transformation to Zero Offset (TZO).** We can transform data from a given fixed (input) offset to another (output) offset. When the output offset is zero, we have, in particular, TZO (sometimes referred to as dip moveout). Some of the applications for offset continuation are:

   - **Binning.** In practice data, are collected on an irregular grid. For processing purposes I assign a collection of traces around a bin point to that bin. To increase the accuracy it is desired to perform offset continuation so that all the traces correspond to the same bin point.
   - **Reconstruction of missing offsets.** We know that for field data, the near offsets are not recorded. We can reconstruct the near offsets by doing offset continuation from large offsets. The reconstruction of near offsets represents a useful tool for velocity analysis (Ji, 1995) and surface–related multiple elimination (Verschuur, 1991; Verschuur & Berkhout, 1992).
   - **TZO.** Transformation to Zero Offset (TZO) is convenient, since the output data are then in the state that can be stacked and then migrated using a poststack migration algorithm. In this sense, TZO is an imaging tool. TZO also provides tools for doing Amplitude Versus Offset (AVO) analysis.

2. **Amplitude Preserving Azimuthal continuation.** Biondi and Chemingui (1994) introduced a partial–migration operator named Azimuth–Offset Moveout (AMO) that rotates data azimuth and changes the absolute offset. The AMO operator can be seen as an example of SDM by cascading a migration operator with a given offset and azimuth with a demigration operator with different offset and azimuth. Chemingui and Biondi (1995) make the AMO a "true amplitude" process through the cascading of Dip Moveout (DMO) and inverse DMO (IDMO). Note here that both DMO and IDMO are SDM processes, and the cascade of two SDM process is another SDM process. Given that marine data have azimuths that are near zero, the software developed for marine data could be used for land "acoustic" data after the azimuths are rotated to near zero azimuth.

3. **Transforming mode–converted data to unconverted data.** For example, one could map P–S data to P–P data (Chan & Stewart, 1996). In fact the output data are not truly P–P data since the reflection coefficient of the P-S data remains. Many of the processing routines designed for P–P data could be used to process P–S data after the application of this mapping. To perform this process I assume that polarization analysis has been performed on the data so that the P–S scalar wavefield is well separated as input to the SDM process.

4. **Datuming.** This technique is convenient for downward or upward continuing sources and receivers to map an irregular acquisition topography into a planar topography. See Sheaffer and Bleistein (1998).

5. **Mapping data from complex velocity to simpler velocity.** One direct application of this could be layer replacement. Yilmaz (1987) shows how layer replacement can be done by changing the velocity of the overburden by the substratum velocity (layer replacement). The advantage of this process is that it removes the distortions and disruptions of the underlying target reflections due to the raypath bending produced by the complexity of the overburden. We can perform layer replacement also by performing two datuming processes. The first datuming process eliminates the undesired layer and the second introduces the new (desired) layer. The cascade of these two datuming processes is also a SDM process.

6. **Combinations of the above.** Chemingui and Biondi (1995) formulate the amplitude preserving AMO problem as a cascade of DMO and IDMO. Given that DMO is an SDM process and so its inverse, and that the cascade of two SDM process is another SDM process, amplitude preserving AMO is a SDM process. Another example: Traditionally wave–equation datuming (WED) is done in two steps. Downward extrapolating sources and downward extrapolating receivers (Salinas, 1996). We can combine both processes into a single SDM operator.

All the applications named above are SDM operators. Another application that is not an SDM operator but that can be developed by the use of SDM operators is velocity analysis. This could be done in combination with TZO. After all offsets are mapped to zero–offset, events should line up. To the extent that they do not, they provide the same type of information about velocity errors as does a common–trace gather of a suite of prestack migrations/inversions.

1.5 History

Dip Moveout (DMO) is historically an archetypical SDM operator. In some way, the history of DMO is that of SDM. Fabio Rocca (Claerbout, 1985) showed that the DMO impulse response could be constructed by tracing zero–offset rays (forward problem) to the prestack migration impulse response (inverse problem). Later, Jorden (1987) used Rocca's concept to introduce the "true amplitude" DMO as a cascade of two integral operators: zero–offset modeling, cascaded with finite–offset inversion. Hubral et al. (1996) expanded Rocca's idea of doing DMO to a general process that could be used to solve a wealth of imaging problems such as: offset continuation, P–SV converted waves TZO, P–SV to P–P mode conversion and remigration. Their idea was to use a combination of a forward problem and the inverse problem without the restrictions of Rocca's DMO technique. For example, if instead of doing the zero–offset modeling over the prestack migration impulse response, one performs a different finite–offset ray tracing, then the result would be an impulse response for offset con-

tinuation. Tygel et al. (1996) developed the mathematical tools for this general problem based on the concept of Hubral et al. (1996). The mathematical problem is seen as a cascade of integral operators. The forward and inverse operators used by Tygel et al. (1996) are the isochron stack (converted into a demigration operator) and the diffraction stack. An isochron is the geometrical locus of the prestack migration impulse response. Thus, just as a diffraction stack is a summation over the traveltimes predicted for a point scatterer for a given source/receiver configuration and background velocity, the isochron stack is a summation over the equi–traveltime locus for the same source/receiver configuration and background velocity. The cascade of migration and demigration gives birth to the Configuration Transformation (CT) operator. The CT operator is simplified by using the method of stationary phase. CT is then a technique that maps data from any source/receiver configuration into data from a different source/receiver configuration. Seismic Data Mapping (SDM) is an extension of the Configuration Transform (CT) technique found in Hubral et al. (1996) and Tygel et al. (1996). CT assumes that only the recording configuration is modified, while the medium parameters remain unchanged. The CT needs only a single ray tracing. That is, only one eikonal and one transport equation needs to be solved (for all medium diffractors and all possible recording locations). In contrast, SDM might need two ray tracers —one for the input medium parameters and another for the output medium parameters. Nevertheless, the same mathematical formalism used to describe CT is readily extended to the SDM problem.

1.6 Outline

We start (Chapter 2) with the basic physical principles, primarily resting on the foundation of the diffraction theory. This chapter is included to make this document self–contained, and it can be skipped by the reader already familiar with the Kirchhoff and Born modeling formulas. The Born approximative and Kirchhoff approximative formulas are derived from the scalar Helmholtz equation using perturbation theory and linear approximations. Chapter 3 shows the derivation of the isochron stack. The isochron stack is a demigration operator, a modeling (from data) formula that uses migrated data and velocity information as input. No reflectors have to be defined in advance since they are implicit in the migrated data. Some of the applications of demigration and its mathematical treatment are developed here. We show that the demigration operator can be derived both from the Kirchhoff and from the Born approximations. The Kirchhoff approximation does not present the constraint of small perturbations of parameters as opposite to the Born approximation (Burridge *et al.*, 1995).

Chapter 4 shows the derivation of the migration operator. This derivation is performed in the time domain with the help of the plane–wave expansion of the δ function (Gel'fand & Shilov, 1964). This is at the heart of the Generalized Radon Transform

(GRT) inversion.

Chapter 5 introduces the stationary phase analysis in time domain for one and two dimensions. Using the two–dimensional stationary phase formulas, I find the leading order asymptotic terms of the demigration and the migration operators. Here I prove that the operators locate reflections (demigration) and reflectors (migration) properly, and they evaluate the right dynamic weights so as to include (demigration) or remove (migration) the appropriate amplitude variation for point–source and reflector curvature.

Chapter 6 constructs the SDM operator as a cascade of migration and demigration. The chained operator is simplified by the method of stationary phase. This gives rise to a Kirchhoff–type operator. That is an integral over a stacking surface. The weights in this integral are studied for different acquisition geometries and simplified in terms of some curvature factors. Here, I illustrate, an application of the SDM problem to the analytical solution of the 3D TZO problem for a depth–dependent velocity in an isotropic media is illustrated.

In Chapter 7, I derive the 2.5D demigration, migration and SDM operators. Also the weight factor for the 2.5D SDM operator is studied in some detail.

Chapter 8 shows a typical application of SDM for TZO in an isotropic depth–dependent velocity media. This is in a way an extension of the work of Artley (1994) and Artley & Hale (1994). This implementation is in the space–time domain, while Artley's implementation was performed in the wave–number frequency domain.

Finally, chapter 9 shows a numerical demonstration of SDM in the form of constant velocity TZO. The main aspects of SDM, such as kinemtics, point–source and reflector curvature geometrical spreading effecs, and oblique reflection coefficient are illustrated in a numerical demonstration.

Chapter 2

THEORY

Here, I introduce the basic mathematical tools to construct operators that perform practical imaging tasks, such as demigration, migration and Transformation to Zero Offset (TZO), among others. These problems are studied from the point of view of diffraction theory. Scales (1995) presented a unified treatment of the Born and Kirchhoff approximations from the Helmholtz equation after using some perturbation–theory concepts and the second Green's identity. Here, I follow Scales's approach and provide further insights into those approximations.

2.1 Fourier Transforms

Many of the results here make use of Fourier transforms. The forward and inverse Fourier transforms are defined by the relations:

$$\begin{aligned} F(\omega) &= \int_0^\infty dt\, f(t)\, e^{i\omega t} \\ f(t) &= \frac{1}{\pi}\, \mathrm{Re} \int_0^\infty d\omega\, F(\omega)\, e^{-i\omega t}. \end{aligned} \tag{2.1}$$

I will assume below, that all functions $f(t)$ and $F(w)$ are "well–behaved" in the sense that these relations can be used. $F(\omega)$, in the positive real ω-axis $\mathrm{Im}(\omega) = 0$, is seen as an analytic continuation in the upper half complex ω-plane and $f(t)$ in the positive real t-axis $\mathrm{Im}(t) = 0$, is seen as an analytic continuation in the lower half complex t-plane.

2.2 A note on diffraction theory

In this section I find a representation of the scattered wavefield as a superposition of the contributions of volume and surface sources (scatterers). I start with a given reflector surface, S_r (see Figure 2.1, and assume that the velocity $v(\boldsymbol{x})$ is known above S_r. I introduce a "background" wavespeed $c(\boldsymbol{x})$ equal to $v(\boldsymbol{x})$ above the reflector. The acoustic wavefield $u(\boldsymbol{x}, \boldsymbol{x}_s)$ at any point due to a unit impulsive point–source at $\boldsymbol{x}_s$ is

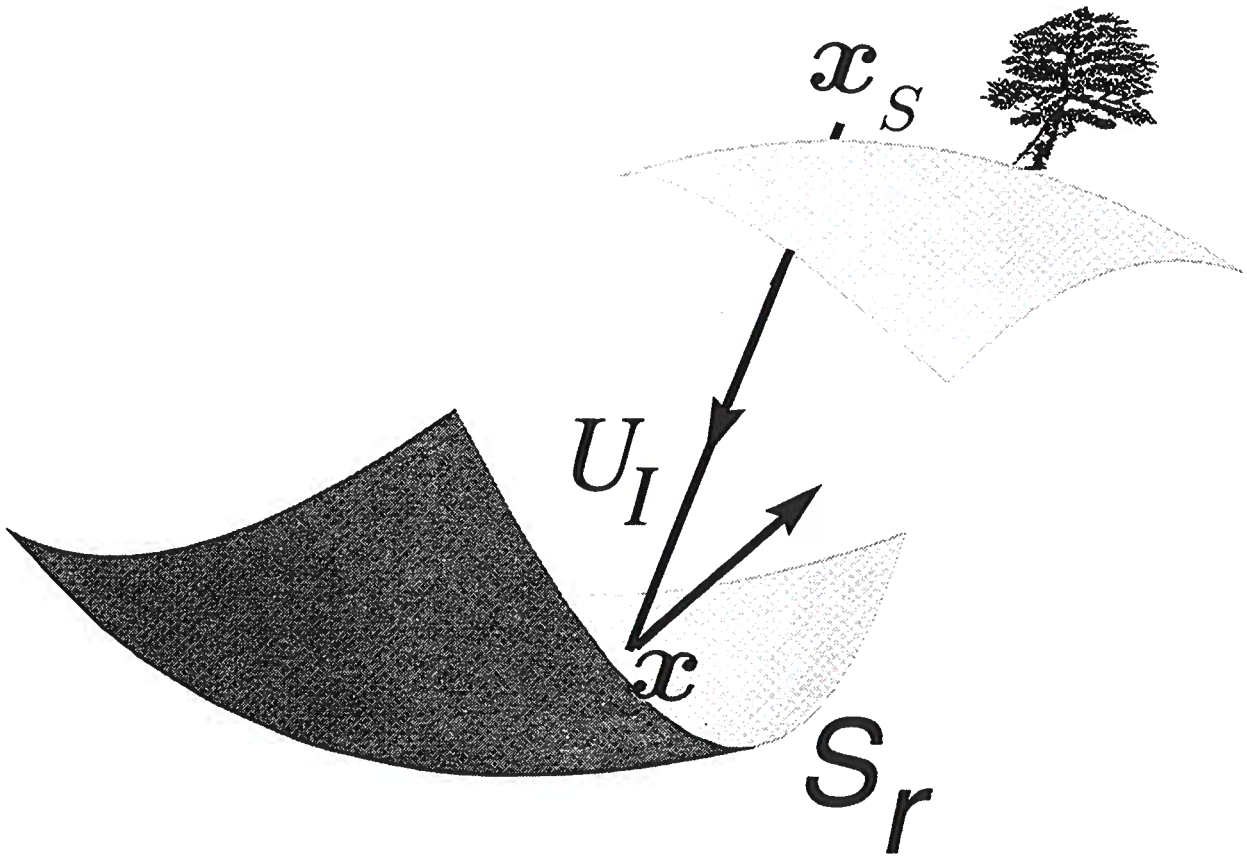

FIG. 2.1. Description of the experiment involving a source and incident wavefield and a scattering (reflecting)surface. S_r is a reflecting surface, $\boldsymbol{x}_s$ represents the source location, u_I the input wavefield and $\boldsymbol{x}$ a scatter in the reflecting surface

governed by the Helmholtz equation with velocity v,

$$\left[\nabla^2 \div \frac{\omega^2}{v^2}\right] u(\boldsymbol{x}, \boldsymbol{x}_s) = -\delta(\boldsymbol{x} - \boldsymbol{x}_s) \tag{2.2}$$

with boundary conditions at infinity

$$r\, u(\boldsymbol{x}, \boldsymbol{x}_s) \quad \text{bounded,} \quad r \left[\frac{\partial u(\boldsymbol{x}, \boldsymbol{x}_s)}{\partial r} \mp \frac{i\omega}{v} u(\boldsymbol{x}, \boldsymbol{x}_s)\right] \to 0, \quad \text{as} \quad r \to \infty, \quad r = |\boldsymbol{x} - \boldsymbol{x}_s|.$$

These are the *Sommerfeld radiation conditions* (Bleistein *et al.*, 1996). Mathematically, these conditions ensure the uniqueness of the solution, and physically they prevent reflections from infinity, in the case of a causal wavefield $(-)$ and allow radiation from infinity in the case of an anticausal wavefield $(\div)$.

The incident wavefield u_I, satisfies the wave equation with the background wavespeed $c(\boldsymbol{x})$

$$\left[\nabla^2 \div \frac{\omega^2}{c^2}\right] u_I(\boldsymbol{x}, \boldsymbol{x}_s) = -F(\omega)\delta(\boldsymbol{x} - \boldsymbol{x}_s).$$

Here $F(\omega)$ corresponds to the band–limited character of the input signal. I will assume that $F(\omega) = 1$.

The total wavefield can be decomposed as

$$u(\boldsymbol{x}, \boldsymbol{x}_s) = u_I(\boldsymbol{x}, \boldsymbol{x}_s) \div u_S(\boldsymbol{x}, \boldsymbol{x}_s),$$

where $u_S(\boldsymbol{x}, \boldsymbol{x}_s)$ is the scattered wavefield at the point $\boldsymbol{x}$ due to a point–source at $\boldsymbol{x}_s$.

Let us introduce a quantity α that represents the perturbation between the background model velocity and the true model velocity:

$$\alpha(\boldsymbol{x}) \equiv \frac{c^2(\boldsymbol{x})}{v^2(\boldsymbol{x})} - 1,$$

so that

$$\frac{\alpha}{c^2} \equiv \frac{1}{v^2} - \frac{1}{c^2}.$$

Since $c = v$ above the reflector, α is zero in this region; clearly α is nonzero below the reflector. I further assume that α decays smoothly to zero with depth. In terms of α, the equation for the scattered wavefield can be written as

$$\left[\nabla^2 \div \frac{\omega^2}{c^2}\right] u_S(\boldsymbol{x}, \boldsymbol{x}_s, \omega) = -\frac{\omega^2}{c^2}\, \alpha\, u(\boldsymbol{x}, \boldsymbol{x}_s, \omega). \tag{2.3}$$

Now let us introduce a Green's function for the background model:

$$\left[\nabla^2 + \frac{\omega^2}{c^2}\right] G(\boldsymbol{x}, \boldsymbol{r}, \omega) = -\delta(\boldsymbol{x} - \boldsymbol{r}), \tag{2.4}$$

where $\boldsymbol{r}$ is an arbitrary point in the volume of scatteres D. Now we multiply equation (2.3) by G and equation (2.4) by u_S and substract them. Then after integrating over the volume D and applying Green's second identity one finds

$$\begin{aligned} \Phi(\boldsymbol{r})\, u_S(\boldsymbol{r}, \boldsymbol{x}_s, \omega) \;=\; & \int_D d^3x\, G(\boldsymbol{x}, \boldsymbol{r}, \omega)\, \frac{\omega^2}{c^2}\, \alpha\, u(\boldsymbol{x}, \boldsymbol{x}_s, \omega) \\ & + \int_S \left[G(\boldsymbol{x}, \boldsymbol{r}, \omega)\, \frac{\partial u_S(\boldsymbol{x}, \boldsymbol{x}_s, \omega)}{\partial n} - u_S(\boldsymbol{x}, \boldsymbol{x}_s, \omega)\, \frac{\partial G(\boldsymbol{x}, \boldsymbol{r}, \omega)}{\partial n} \right] dS. \end{aligned} \tag{2.5}$$

Here $\Phi(\boldsymbol{r})$ is 1 if $\boldsymbol{r}$ is in the interior of D, 1/2 if $\boldsymbol{r}$ is in the boundary of D and 0 if $\boldsymbol{r}$ is outside of D. We further assume that α goes to zero with distance $r = |\boldsymbol{r}|$, fast enough for the volume integral to converge.

This equation represents the monochromatic (for each fixed ω) scattered wavefield at any point of the acoustic space ($\boldsymbol{r}$) of study, due to a point–source at $\boldsymbol{x}_s$. It is a representation of the wavefield in terms of body sources (the volume integral, referred to here as the Born integral) and surface sources (the surface integral, referred to here as the Kirchhoff integral). The surface integral, in turn, is computed as the contribution of monopole sources (first term) and dipole sources (second term).

The scattered wavefield given by equation (2.5) is not uniquely defined. We have still two degrees of freedom over infinite dimensional spaces. One is the Green's function to be picked, and the other is the boundaries of the volume scatterer. Among all possible Green's functions are two important sets —causal and anti–causal Green's functions. A causal Green's function is to be used in forward propagation (modeling), while an anti–causal Green's function should be used for backward propagation of the wavefield (migration or downward continuation). Here the wavefield in the surface integral should be u instead of u_S. The causal Green's functions are appropriate for forward modeling.

At this point, this theory is exact, and no approximations have been made yet. By assuming that we are interested only in high–frequency data, we can exploit leading–order asymptotic analysis. For this purpose I choose the causal WKBJ Green's function for the Helmholtz equation (2.2). This is given by

$$G(\boldsymbol{r}, \boldsymbol{x}_s, \omega) = A(\boldsymbol{r}, \boldsymbol{x}_s) e^{i\omega\tau(\boldsymbol{r}, \boldsymbol{x}_s)}.$$

Here, τ is the traveltime from $\boldsymbol{x}_s$ to $\boldsymbol{r}$ and $A(\boldsymbol{r}, \boldsymbol{x}_s)$ is the corresponding ray-theoretic

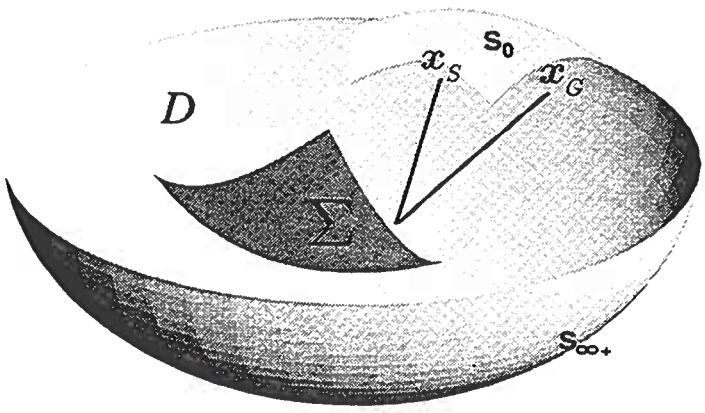

FIG. 2.2. Surface S is the union of the surface S_0 and a spherical cap smoothly joined to S_0 but receding to infinity in the $\div z$ direction. We are interested on the wavefield under the surface S_0.

amplitude, derived by solving the eikonal equation,

$$\nabla\tau \cdot \nabla\tau = \frac{1}{c^2(\boldsymbol{x})}, \qquad \tau(\boldsymbol{x}_s, \boldsymbol{x}_s) = 0, \tag{2.6}$$

and the (first) transport equation

$$2\nabla\tau \cdot \nabla A \div A\nabla^2\tau = 0, \tag{2.7}$$

subject to the condition

$$4\pi A|\boldsymbol{r} - \boldsymbol{x}_s| \to 1, \qquad \text{as} \quad |\boldsymbol{r} - \boldsymbol{x}_s| \to 0.$$

Two fundamental modeling formulas can be derived from equation (2.5) by picking suitable boundaries of the volume of scatterers. One is the Born modeling formula (known as the Born approximation), and the other is the Kirchhoff modeling formula (or Kirchhoff approximation). This is the topic of the next two sections.

2.2.1 The Born approximation

Let us first assume that the boundaries of the body scatterer are $S = S_0 \cup S_{\infty\div}$, where S_0 is an upper bound for the data recording surface and $S_{\infty\div}$ is a spherical cap smoothly joined to S_0, but which recedes to infinity in the $\div z$ direction (see Figure 2.2). Let us discuss why for this particular Green's function, the surface integral in equation (2.5) vanishes.

If we consider the volume surrounded by the surface S_0 and an upper spherical cap

($S_{\infty-}$ not in the figure), we find that the volume integral vanishes since the perturbation $\alpha(\boldsymbol{x})$ is zero there. Now for all points $\boldsymbol{r}$ in the lower volume (the volume of interst) we find that the surface integral in equation (2.5) vanishes (here the surface is $S_0 \cup S_{\infty-}$) given that $\Phi(\boldsymbol{r}) = 0$ there. Due to the Sommerfeld radiation condition, the causality of the wavefield u and the Green's function, the surface integral over that upper spherical cap should vanish. This implies that the integral over S_0 vanishes too.

Now again, due to the Sommerfeld radiation condition, and the causality of the wavefield u and the Green's function, the integral over the surface $S_{\infty+}$ vanishes.

Thus, the integral surface vanishes on the surface $S = S_0 \cup S_{\infty+}$, Therefore we have

$$\begin{aligned} u_S(\boldsymbol{r}, \boldsymbol{x}_s, \omega) &= \int_D d^3x\, G(\boldsymbol{x}, \boldsymbol{r}, \omega)\, \frac{\omega^2}{c^2}\, \alpha\, u_I(\boldsymbol{x}, \boldsymbol{x}_s, \omega) \\ &+ \int_D d^3x\, G(\boldsymbol{x}, \boldsymbol{r}, \omega)\, \frac{\omega^2}{c^2}\, \alpha\, u_S(\boldsymbol{x}, \boldsymbol{x}_s, \omega). \end{aligned} \tag{2.8}$$

Let us characterize the perturbation function α by a small constant parameter $\epsilon > 0$. That is, $\alpha = \epsilon\, \alpha_0$, where α_0 is a bounded by one.

Let us also, identify

$$f = -\int_D d^3x\, G(\boldsymbol{x}, \boldsymbol{r}, \omega)\, \frac{\omega^2}{c^2}\, \alpha_0\, u_I(\boldsymbol{x}, \boldsymbol{x}_s, \omega),$$

$$Tu_s = \int_D d^3x\, G(\boldsymbol{x}, \boldsymbol{r}, \omega)\, \frac{\omega^2}{c^2}\, \alpha_0 u_S(\boldsymbol{x}, \boldsymbol{x}_s, \omega)$$

$u_S = u_S(\boldsymbol{x}, \boldsymbol{x}_s, \omega)$ and $\lambda = 1/\epsilon$. Then equation (2.8) is recast as:

$(T - \lambda I) u_S = f.$

If there are non–zero solutions to this equation when no input wavefield is present ($u_I = 0$, so $f = 0$), then the u_S's are normal modes (eigenfunctions of the operator T) and the λ's are the corresponding eigenvalues. The geometrical series representation of the operator $(T - \lambda I)^{-1}$ is given by the resolvent:

$$R_\lambda(T) = -\lambda^{-1}(I + \lambda^{-1}T + \lambda^{-2}T^2 + ...) = -\epsilon(I + \epsilon T + \epsilon^2 T^2 + ...). \tag{2.9}$$

If this resolvent operator exists (that is, if it is bounded), then one can writes the solution to the integral equation (2.8) as:

$u_S = R_\lambda(T) f = -\epsilon f + O(\epsilon^2).$

This series representation is known as a Neumann series, (Kreyszig, 1978). For the series (2.9) to converge, we need $\epsilon \|T\| < 1$, (Kreyszig, 1978). In Appendix A, I derive

a convergence criterion for the Neumann series, in the case of constant background speed c_0. I found that a sufficient condition for this happen is by choosing:

$$\alpha(\boldsymbol{x}) < \frac{2\,c_0^2}{\omega^2\,R^2}, \tag{2.10}$$

where R is the radius of the smallest ball surrounding the scattering body D. It is interesting, then, to observe that the perturbation magnitude for convergence should be determined from the given frequency (ω), the scatterer body size (say R), and the background speed c_0. The truncation of the Neumman series, so as to make it linear in ϵ, is the so–called Born approximation. Physically, this means that we neglect the scattering wavefield with respect to the incident wavefield. I will refer to the scattered wavefield obtained after the Born approximation as the Born approximation. It is a remarkable fact that the Born approximation works so well in practice[1] while only the leading order term of the Neumman series is considered and the series is not asymptotic. The Born approximation formula is a linear operator in the perturbation α, facilitating the inversion for α. Bleistein et al. (1996) found an inversion formula for $\alpha(\boldsymbol{x})$ by identifying the Born approximation integral with a forward Fourier transform.

To evaluate the Born approximation I will use the WKBJ Green's functions $G(\boldsymbol{r},\boldsymbol{x},\omega)$ and $u_I = F(\omega)\,G(\boldsymbol{x},\boldsymbol{r},\omega)$. Substituting the appropriate Green's functions and neglecting the scattering wavefield contribution to equation (2.8) one obtains:

$$u_S(\boldsymbol{x}_g,\boldsymbol{x}_s,\omega) \approx \omega^2 F(\omega)\int d^3x\,\frac{\alpha(\boldsymbol{x})}{c^2(\boldsymbol{x})}\,a(\boldsymbol{x},\boldsymbol{\xi})\,e^{i\omega\phi(\boldsymbol{x},\boldsymbol{\xi})}, \tag{2.11}$$

where $\boldsymbol{r} = \boldsymbol{x}_g(\boldsymbol{\xi})$

$$\phi(\boldsymbol{x},\boldsymbol{\xi}) = \tau_s + \tau_g \quad a(\boldsymbol{x},\boldsymbol{\xi}) = A(\boldsymbol{x},\boldsymbol{x}_s(\boldsymbol{\xi}))A(\boldsymbol{x}_g(\boldsymbol{\xi}),\boldsymbol{x}). \tag{2.12}$$

Here $\boldsymbol{\xi}$ is a two dimensional vector that parameterizes the measurement surface and

$$\tau_s = \tau(\boldsymbol{x},\boldsymbol{x}_s(\boldsymbol{\xi})), \qquad \tau_g = \tau(\boldsymbol{x}_g(\boldsymbol{\xi}),\boldsymbol{x}).$$

2.2.2 The Kirchhoff approximation

If I now take the volume V to be the volume bounded by the recording surface S_0 and the reflector surface (Σ), then, again, the volume integral vanishes since α is zero in this region. This gives:

$$u_S(\boldsymbol{r},\boldsymbol{x}_s,\omega) = \int_{S_0\cup\Sigma}\left[G(\boldsymbol{x},\boldsymbol{r},\omega)\frac{\partial u_S(\boldsymbol{x},\boldsymbol{x}_s,\omega)}{\partial n} - u_S(\boldsymbol{r},\boldsymbol{x}_s,\omega)\frac{\partial G(\boldsymbol{x},\boldsymbol{r},\omega)}{\partial n}\right]dS. \tag{2.13}$$

[1] As it is remarkable that, after all, we see useful images of the interior of the earth assuming that earth is isotropic and the rock density and seismic propagation velocity are constant!

The integral over S_0 is zero, for the same reasons explained above. Then:

$$u_S(\boldsymbol{r}, \boldsymbol{x}_s, \omega) = \int_\Sigma \left[G(\boldsymbol{x}, \boldsymbol{r}, \omega) \frac{\partial u_S(\boldsymbol{x}, \boldsymbol{x}_s, \omega)}{\partial n} - u_S(\boldsymbol{r}, \boldsymbol{x}_s, \omega) \frac{\partial G(\boldsymbol{x}, \boldsymbol{r}, \omega)}{\partial n} \right] d\Sigma.$$

New approximations emerge here. The incident wavefield in the surface will be approximated by the WKBJ Green's function $u_I = F(\omega) G(\boldsymbol{x}, \boldsymbol{x}_S, \omega)$. For the scattered wavefield, I use the Kirchhoff approximation:

$$u_s = R u_I, \qquad \frac{\partial u_S}{\partial n} = -R \frac{\partial u_I}{\partial n} \tag{2.14}$$

where $R = R(\boldsymbol{x}, \boldsymbol{x}_s)$ is the geometrical-optics reflection coefficient

$$R(\boldsymbol{x}, \boldsymbol{x}_s) = \frac{\left| \frac{\partial}{\partial n} \tau(\boldsymbol{x}, \boldsymbol{x}_s) \right| - \left\{ 1/c_-^2(\boldsymbol{x}) - 1/c^2(\boldsymbol{x}) + \left[\frac{\partial}{\partial n} \tau(\boldsymbol{x}, \boldsymbol{x}_s) \right]^2 \right\}^{1/2}}{\left| \frac{\partial}{\partial n} \tau(\boldsymbol{x}, \boldsymbol{x}_s) \right| + \left\{ 1/c_-^2(\boldsymbol{x}) - 1/c^2(\boldsymbol{x}) + \left[\frac{\partial}{\partial n} \tau(\boldsymbol{x}, \boldsymbol{x}_s) \right]^2 \right\}^{1/2}}. \tag{2.15}$$

Here, $c_-(\boldsymbol{x})$ is the propagation speed below the reflector. The reflection coefficient is computed by assuming continuity of the wavefield and its normal derivative across the reflecting interface (Bleistein, 1984). The normal derivatives are

$$\frac{\partial G}{\partial n} = i\omega \hat{\boldsymbol{n}} \cdot \nabla \tau(\boldsymbol{x}, \boldsymbol{x}_s, \omega) A(\boldsymbol{x}, \boldsymbol{x}_s, \omega) e^{i\omega\tau(\boldsymbol{x}, \boldsymbol{x}_s, \omega)}$$

and

$$\frac{\partial u_S}{\partial n} = -i\omega F(\omega) \hat{\boldsymbol{n}} \cdot \nabla \tau(\boldsymbol{x}, \boldsymbol{x}_s, \omega) A(\boldsymbol{x}, \boldsymbol{x}_s, \omega) e^{i\omega\tau(\boldsymbol{x}, \boldsymbol{x}_s, \omega)}.$$

Here, only leading asymptotic order is taken into account.

For data recorded in a surface parameterized by the two dimensional vector $\boldsymbol{\xi}$ and for $\boldsymbol{r} = \boldsymbol{x}_g$ one finds then:

$$u_S(\boldsymbol{x}_g(\boldsymbol{\xi}), \boldsymbol{x}_s(\boldsymbol{\xi}), \omega) \sim i\omega F(\omega) \int_\Sigma R(\boldsymbol{x}, \boldsymbol{x}_s) a(\boldsymbol{x}, \boldsymbol{\xi}) (\hat{\boldsymbol{n}} \cdot \nabla_x \phi(\boldsymbol{x}, \boldsymbol{\xi})) \, e^{i\omega\phi(\boldsymbol{x}, \boldsymbol{\xi})} dS. \tag{2.16}$$

Here, ϕ and a are defined by equation (2.12); the unit normal $\hat{\boldsymbol{n}}$ points upward and $\partial/\partial n = \hat{\boldsymbol{n}} \cdot \nabla_x$. Figure 2.3 illustrates the different symbols defined above.

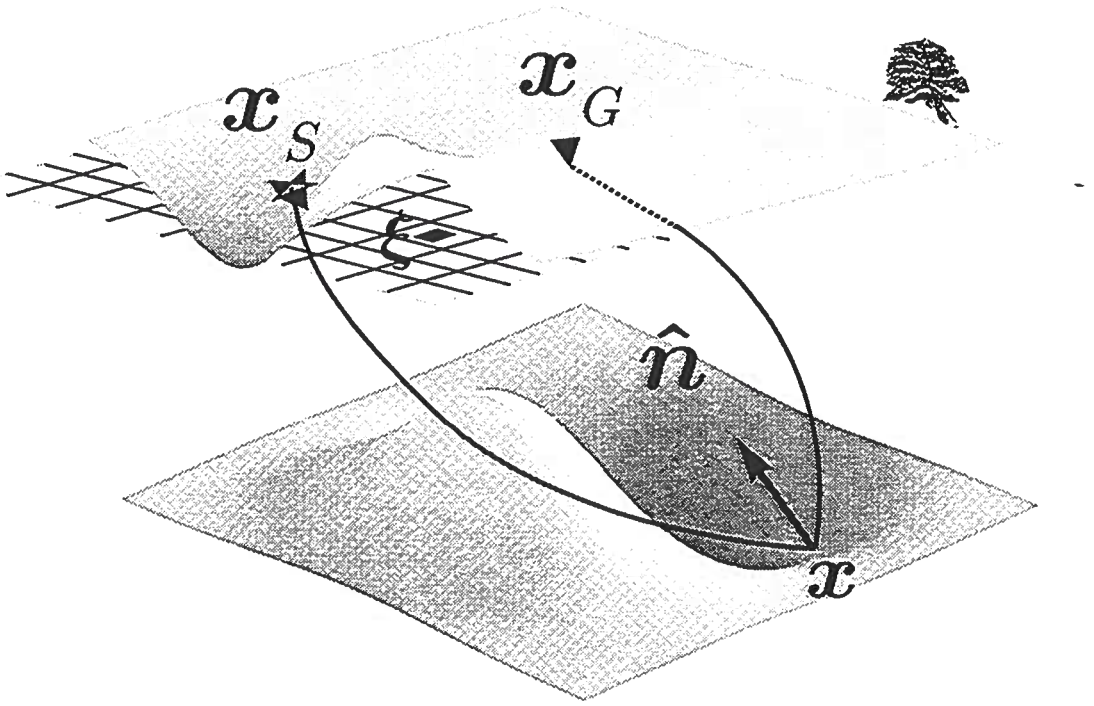

FIG. 2.3. Description of symbols involved in the Kirchhoff modeling formula. Here x_s represents the source position, x_G the receiver position, x a reflector point and $\hat{n}$ a normal vector to the reflecting surface at x.

Chapter 3

THE ISOCHRON STACK

The purpose of this section is to derive and study the true–amplitude, inverse–migration operator from the inverse scattering point of view. Seismic data are band–limited. Thus, below, when using full–bandwidth distributions —Dirac delta functions, for example— I am describing only the "most singular part" or high–frequency part of the solution. By using the Dirac delta function, we are able to take advantage of the theory of distributions, carry out asymptotic approximations easily by recognizing the smooth and sharp operators (especially when taking derivatives, or introducing factors under the integral sign) and also by exploiting results from the Generalized Radon Transform (GRT) theory. Only after I obtain the final result will I introduce a filter on the data. This is a valid argument, since convolution is a linear and commutative process. Band–limiting amounts to multiplication by a frequency domain filter or convolution with a time–domain wavelet. This process commutes with all of the previous processes that I shall have employed.

3.1 Modeling versus inverse migration

Before studying the operators, let us see some subtle differences between modeling and inverse migration processes.

- Seismic modeling maps acoustic, earth–model parameters to data along a recording surface with a prescribed measurement configuration.
- Seismic imaging maps the recorded data from the surface to the discontinuity surfaces or singular functions of the modeling parameters (reflectors).
- Seismic inversion maps the recorded data back into the earth–model parameters.
- Seismic true amplitude migration maps the recorded data into imaged data. The peak amplitude, of these data images, should be the value corresponding to the oblique–incidence specular reflection coefficient.
- Seismic inverse migration (or demigration) maps true amplitude migrated data into data that would be recorded for a given set of earth model parameters and a defined measurement configuration along the recording surface. The

amplitude of these data has the right geometrical spreading factors but preserves the reflection coefficient of the input data.

From the above, the output section of a modeling algorithm and an inverse migration algorithm should be the same; however the input section for the inverse migration algorithm consists of output data traces with format identical to that of the recorded data, while the input of a modeling algorithm is an earth model. From the seismic data processing point of view, the use of cascaded migration and demigration algorithms to solve practical problems such as DMO or offset continuation is preferred to the use of cascaded inversion and modeling algorithms. The reason for this is that the output of a migration program is ready to be used as input for a demigration program, while the output traces of an inversion program have to be pre–processed (travel times and amplitudes should be picked) before going into the modeling program. This pre–processing is not only tedious but a major source of human errors. Mathematically, there is no fundamental difference between cascading modeling and inversion operators or cascading demigration and migration operators for solution of imaging problems. The input and output data of the two cascading processes are the same. The intermediate data differ from one another but these data are used only while deriving the final composed operator. They will not be of any use after that.

3.2 The isochron stack as seen from the Born approximation

Here, I show how to recast the Born approximation in 3D – a volume integral – into an isochron stack – an integral over an equi–travel–time surface– plus an integral normal to the isochron, or in the direction of increasing time. Let us assume that a given reflecting surface is described by the equation $\Sigma_R(\boldsymbol{x}) = 0$. The perturbation α associated with that surface can be written as $\alpha(\boldsymbol{x})\ H(\Sigma_R(\boldsymbol{x}))$ where H is the step function; H is equal to zero above $\Sigma_R(\boldsymbol{x})$ and equal to unity below. For simplicity in our discussion, I assume here that the surface is of infinite extent, dividing all of our three dimensional space into two regions. The Born approximation (2.11) is rewritten as

$$D_B(\boldsymbol{\xi},\omega) \sim \omega^2 F(\omega) \int_D d^3x\, \frac{\alpha(\boldsymbol{x})}{c^2(\boldsymbol{x})}\, H(\Sigma_R(\boldsymbol{x}))\, a(\boldsymbol{x},\boldsymbol{\xi}) e^{i\omega\phi(\boldsymbol{x},\boldsymbol{\xi})}. \tag{3.1}$$

Here, D stands for Demigration or Data, and I will use the B for Born, and K for Kirchhoff, below.

The WKBJ amplitude factor a, consistent with the wave phenomena that we study, can be written as

$$a(\boldsymbol{x},\boldsymbol{\xi}) = |a(\boldsymbol{x},\boldsymbol{\xi})|\, e^{i\,\mathrm{sgn}(\omega)\,\varphi}. \tag{3.2}$$

We now apply the inverse Fourier transform, as given by the second line of equation (2.1), to equation (3.1). We find

$$D_B(\boldsymbol{\xi},t) \sim \int_D d^3x \frac{\alpha(\boldsymbol{x})\,|a(\boldsymbol{x},\boldsymbol{\xi})|\,H(\Sigma_R(\boldsymbol{x}))}{c^2(\boldsymbol{x})} \frac{1}{\pi}\,\mathrm{Re}\int_0^\infty d\omega\,\omega^2\,e^{i\,\mathrm{sgn}(\omega)\,\varphi}\,e^{-i\omega[t-\phi(\boldsymbol{x},\boldsymbol{\xi})]}. \tag{3.3}$$

The second integral, by the convolution theorem for Fourier integrals, can be written as $-w_\varphi(t) * \delta''(t-\phi(\boldsymbol{x},\boldsymbol{\xi}))$, where the φ–phase shift wavelet $w_\varphi(t)$ is given by

$$w_\varphi(t) = \frac{1}{\pi}\mathrm{Re}\int_0^\infty d\omega\,e^{i\,\mathrm{sgn}(\omega)\,\varphi}\,e^{-i\omega t} = \mathrm{Re}\,e^{i\varphi}\,\triangle\,(t) \tag{3.4}$$

with

$$\begin{aligned}\triangle(t) = \frac{1}{\pi}\int_0^\infty d\omega\,e^{-i\omega t} &= \frac{1}{2\,\pi}\int_{-\infty}^\infty d\omega\,2H(\omega)e^{-i\omega t} \\ &= \frac{1}{2\pi}\int_{-\infty}^\infty d\omega\,(1+\mathrm{sgn}\,\omega)e^{-i\omega t} \\ &= \delta(t) - \mathcal{H}\,[\delta(t)]\end{aligned} \tag{3.5}$$

being the one–side (analytic) delta distribution. Here $\mathcal{H}$ is the Hilbert transform operator defined by

$$\mathcal{H}\,[f(t)] = \frac{1}{\pi}\int_{-\infty}^\infty \frac{f(\tau)}{\tau - t}d\tau, \tag{3.6}$$

(Bracewell, 1986). With this, equation (3.3) becomes

$$D_B(\boldsymbol{\xi},t) \sim \int_D d^3x \frac{\alpha(\boldsymbol{x})\,|a(\boldsymbol{x},\boldsymbol{\xi})|\,H(\Sigma_R(\boldsymbol{x}))}{c^2(\boldsymbol{x})}\,\delta''(t-\phi(\boldsymbol{x},\boldsymbol{\xi})) * w_\varphi(t). \tag{3.7}$$

For the moment I will ignore the convolution with the wavelet $w(t)$ and perform this convolution at the end. We will work then only with the left term, which I call

$$D_L(\boldsymbol{\xi},t) = \int_D d^3x \frac{\alpha(\boldsymbol{x})\,|a(\boldsymbol{x},\boldsymbol{\xi})|\,H(\Sigma_R(\boldsymbol{x}))}{c^2(\boldsymbol{x})}\,\delta''(t-\phi(\boldsymbol{x},\boldsymbol{\xi})). \tag{3.8}$$

Let us proceed. We pick u, a parameter running along a given direction specified by the unit vector $\boldsymbol{u}$, such that $\partial\phi/\partial u \neq 0$, then

$$\delta''(t-\phi) = -\frac{d\delta'(t-\phi)}{d\phi} = -\frac{\partial\delta'(t-\phi)/\partial u}{\partial\phi/\partial u} = \frac{-\boldsymbol{u}\cdot\nabla_x\delta'(t-\phi)}{\boldsymbol{u}\cdot\nabla_x\phi}, \tag{3.9}$$

where ∇_x means gradient with respect to $\boldsymbol{x}$. The substitution of this result in (3.8),

yields

$$D_L(\boldsymbol{\xi},t) = \int_D d^3x\, \frac{\alpha(\boldsymbol{x})\,|a(\boldsymbol{x},\boldsymbol{\xi})|\,H(\Sigma_R(\boldsymbol{x}))}{c^2(\boldsymbol{x})}\, \frac{\boldsymbol{u}\cdot\nabla_x\delta'(t-\phi)}{\boldsymbol{u}\cdot\nabla_x\phi}.$$

For the moment, let us think of the integration variables as one coordinate along $\boldsymbol{u}$, and the other two orthogonal to $\boldsymbol{u}$. Then, integrate by parts in the $\boldsymbol{u}$ direction and keep only the most singular term. The result is

$$D_L(\boldsymbol{\xi},t) = \int_D d^3x\, \frac{\alpha(\boldsymbol{x})}{c^2(\boldsymbol{x})}|a(\boldsymbol{x},\boldsymbol{\xi})|\,\boldsymbol{u}\cdot\nabla_x H(\Sigma_R(\boldsymbol{x}))\, \frac{\delta'(t-\phi)}{\boldsymbol{u}\cdot\nabla_x\phi}. \tag{3.10}$$

Now, I rewrite

$$\nabla_x H(\Sigma_R(\boldsymbol{x})) = H'(\Sigma_R(\boldsymbol{x}))\nabla_x\Sigma_R(\boldsymbol{x}) = \delta(\Sigma_R(\boldsymbol{x}))\nabla_x\Sigma_R(\boldsymbol{x}). \tag{3.11}$$

I remind the reader that H represents the step function. If one uses equation (3.9), but this time with only a first order derivative of the delta distribution on the left side, and a unit vector $\boldsymbol{v}$ instead of $\boldsymbol{u}$, one finds that

$$\delta'(t-\phi) = \frac{-\boldsymbol{v}\cdot\nabla_x\delta(t-\phi)}{\boldsymbol{v}\cdot\nabla_x\phi}. \tag{3.12}$$

Here again I pick $\boldsymbol{v}$ such that $\boldsymbol{v}\cdot\nabla_x\phi \neq 0$. Using these results, one can rewrite equation (3.10) as

$$D_L(\boldsymbol{\xi},t) = -\int_D d^3x\, \frac{\alpha(\boldsymbol{x})}{c^2(\boldsymbol{x})}|a(\boldsymbol{x},\boldsymbol{\xi})|\delta(\Sigma_R(\boldsymbol{x}))\,\boldsymbol{u}\cdot\nabla_x\Sigma_R(\boldsymbol{x})\, \frac{\boldsymbol{v}\cdot\nabla_x\delta(t-\phi)}{(\boldsymbol{v}\cdot\nabla_x\phi)(\boldsymbol{u}\cdot\nabla_x\phi)}. \tag{3.13}$$

As I did before, let us think of the integration variables as having one coordinate directed along $\boldsymbol{v}$, and the others orthogonal to $\boldsymbol{v}$. Then, I integrate by parts and keep only the most singular term. The result is

$$\begin{aligned} D_L(\boldsymbol{\xi},t) \;=\; & -\int_D d^3x\, \frac{\alpha(\boldsymbol{x})}{c^2(\boldsymbol{x})}|a(\boldsymbol{x},\boldsymbol{\xi})|\boldsymbol{v}\cdot\nabla_x\delta(\Sigma_R(\boldsymbol{x}))\,\boldsymbol{u}\cdot\nabla_x\Sigma_R(\boldsymbol{x}) \\ & \times \quad \frac{\delta(t-\phi)}{(\boldsymbol{v}\cdot\nabla_x\phi)(\boldsymbol{u}\cdot\nabla_x\phi)}. \end{aligned} \tag{3.14}$$

Now it is appropriate to collapse the volume integral into a surface integral over the support of the delta distribution. For this purpose I use the identity

$$\int d^3x.....\delta(t-\phi) = \int .....\frac{d\Sigma_I}{|\nabla_x\phi|}\bigg|_{t=\phi(\boldsymbol{x},\boldsymbol{\xi})}, \tag{3.15}$$

where Σ_I is the locus of all $\boldsymbol{x}$ points such that $t=\phi(\boldsymbol{x},\boldsymbol{\xi})$, for each fixed t and fixed source receiver configuration dictated by $\boldsymbol{\xi}$. The proof of this identity is easily seen by writing the volume integral as a surface integral over the surface Σ_I times an integral

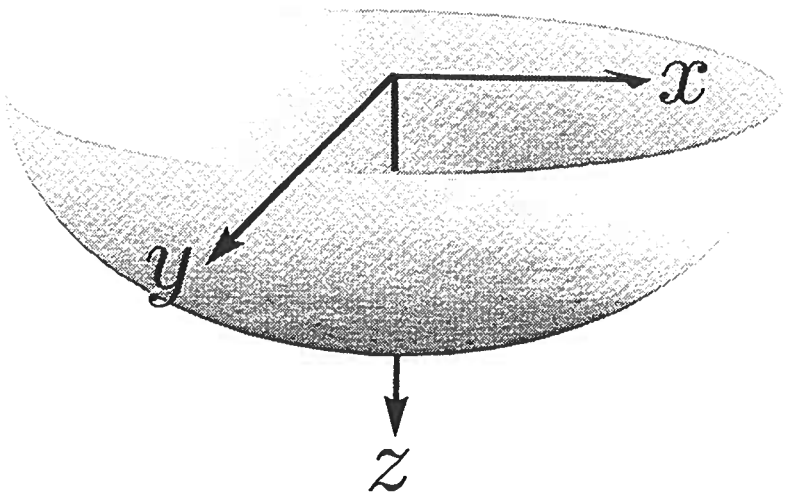

FIG. 3.1. Isochron for a finite offset source/receiver configuration in a constant velocity medium.

along the normal to that surface. Then, I use

$$\delta(t-\phi) = \frac{\delta(u_3)}{|\partial(t-\phi)/\partial u_3|} = \frac{\delta(u_3)}{|\nabla_x \phi|},$$

where u_3 is the coordinate along the normal to the surface Σ_I.

The set

$$\Sigma_I = \{\boldsymbol{x} : t = \phi(\boldsymbol{x}, \boldsymbol{\xi})\} \tag{3.16}$$

represents the isochron (t–level surface) in the $\boldsymbol{x}$–domain for each fixed t and $\boldsymbol{\xi}$. Figure 3.1 shows a typical isochron for a constant–velocity medium. Applying identity (3.15) to equation (3.14) one finds

$$D_L(\boldsymbol{\xi}, t) = -\int_{\Sigma_I} d\Sigma_I \, \frac{\alpha(\boldsymbol{x})}{c^2(\boldsymbol{x})} \frac{|a(\boldsymbol{x}, \boldsymbol{\xi})|}{|\nabla_x \phi|}$$

$$\boldsymbol{v} \cdot \nabla_x \delta(\Sigma_R(\boldsymbol{x})) \, \frac{\boldsymbol{u} \cdot \nabla_x \Sigma_R(\boldsymbol{x})}{(\boldsymbol{v} \cdot \nabla_x \phi)(\boldsymbol{u} \cdot \nabla_x \phi)} \Big|_{t=\phi(\boldsymbol{x},\boldsymbol{\xi})}.$$

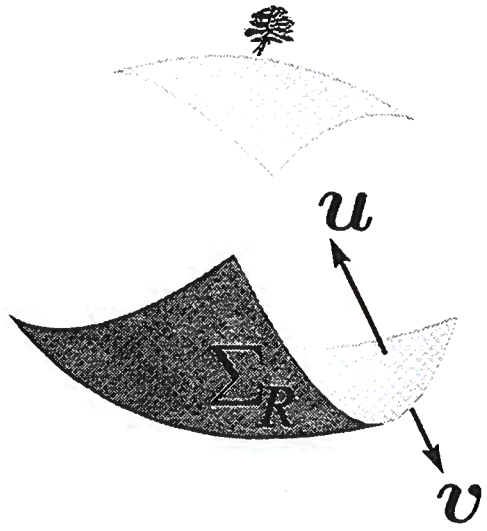

FIG. 3.2. Sketch of the selected normal vectors to the reflecting surface.

At this moment, we have freedom in picking $\boldsymbol{u}$ and $\boldsymbol{v}$ as long as they are not orthogonal to $\nabla_x\phi$. I pick $\boldsymbol{u}$ as the upward unit vector normal to the surface Σ_R, and I pick $\boldsymbol{v}$ as the normal to the isochron Σ_I, that is, along $\nabla_x\phi$; Figure 3.2 illustrates this. The integral is dominated by the stationary, value of $\Sigma_R(\boldsymbol{x})$ on the isochron Σ_I. One can show that, at stationarity, $\boldsymbol{v} = -\boldsymbol{u} = \hat{\boldsymbol{n}}$. Thus, to leading order, one can modify the integrand as follows:

$$
\begin{aligned}
D_L(\boldsymbol{\xi},t) &= \int_{\Sigma_I} d\Sigma_I \, \frac{\alpha(\boldsymbol{x})}{c^2(\boldsymbol{x})} \frac{|a(\boldsymbol{x},\boldsymbol{\xi})|}{|\nabla_x\phi)|^3} \frac{\partial\delta(\Sigma_R(\boldsymbol{x}))}{\partial n} \, |\nabla_x\Sigma_R(\boldsymbol{x})| \, \Big|_{t=\phi(\boldsymbol{x},\boldsymbol{\xi})} \\
&= \int_{\Sigma_I} d\Sigma_I \, \frac{\alpha(\boldsymbol{x})}{c^2(\boldsymbol{x})|\nabla_x\phi|^2} \, \frac{a(\boldsymbol{x},\boldsymbol{\xi})}{|\nabla_x\phi|} \frac{\partial}{\partial n} \{\delta(\Sigma_R(\boldsymbol{x})) \, |\nabla_x\Sigma_R(\boldsymbol{x})|\} \, \Big|_{t=\phi(\boldsymbol{x},\boldsymbol{\xi})} .,
\end{aligned}
$$

where $\partial/\partial n$ means normal derivative along $\hat{\boldsymbol{n}}$.

The function,

$$\gamma(\boldsymbol{x}) \sim \delta(\Sigma_R(\boldsymbol{x})) \, |\nabla_x\Sigma_R(\boldsymbol{x})|, \tag{3.17}$$

is the singular function of the reflecting surface as defined in Bleistein (1987). Figure 3.3 shows an illustration of $\gamma(\boldsymbol{x})$. This function is a delta of a single argument, normal distance to the reflector, peaking at the reflecting surface and plotted in band–limited form along a normal line to the reflector. After using the singular function γ one finds

$$D_L(\boldsymbol{\xi},t) = \int_{\Sigma_I} d\Sigma_I \, \frac{\alpha(\boldsymbol{x})}{c^2(\boldsymbol{x})|\nabla_x\phi|^2} |a(\boldsymbol{x},\boldsymbol{\xi})| \frac{\partial\gamma(\boldsymbol{x})}{\partial n} . \, \Big|_{t=\phi(\boldsymbol{x},\boldsymbol{\xi})} . \tag{3.18}$$

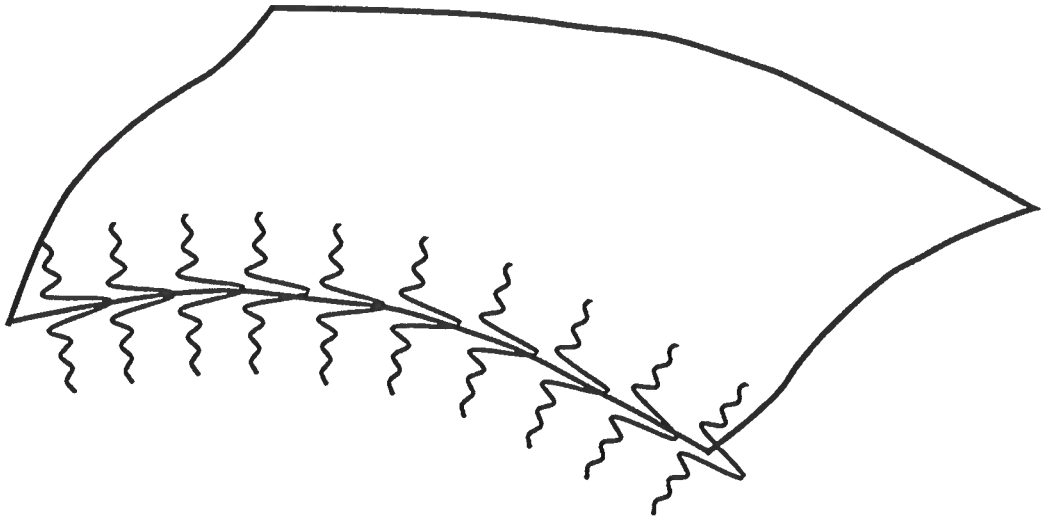

FIG. 3.3. Sketch of the singular function of a given surface. As seen here the singular function is a collection of band–limited delta functions plotted along a normal line to the surface.

Now, using the result

$$\begin{aligned} |\nabla_x\phi|^2 = |\nabla_x\tau_s + \nabla_x\tau_g|^2 &= |\nabla_x\tau_s|^2 + |\nabla_x\tau_g|^2 + 2\nabla_x\tau_s \cdot \nabla_x\tau_g \\ &= \frac{2}{c^2(\boldsymbol{x})} + \frac{2\cos 2\theta}{c^2(\boldsymbol{x})} \\ &= \frac{4\cos^2\theta}{c^2(\boldsymbol{x})}. \end{aligned}$$

Here, θ is half the angle between the slowness vectors $\nabla_x\tau_s$ and $\nabla_x\tau_g$; [τ_s and τ_g are as in equation (2.13)]. Figure 3.4 illustrate these terms. Then, in place of equation (3.18), one finds

$$D_L(\boldsymbol{\xi}, t) = \int_{\Sigma_I} d\Sigma_I \, \frac{\alpha(\boldsymbol{x})}{4\cos^2\theta} \frac{|a(\boldsymbol{x}, \boldsymbol{\xi})|}{|\nabla_x\phi|} \frac{\partial\gamma(\boldsymbol{x})}{\partial n} \Bigg|_{t=\phi(\boldsymbol{x},\boldsymbol{\xi})}.$$

The coefficient,

$$R_B = \frac{\alpha(\boldsymbol{x})}{4\cos^2\theta}, \tag{3.19}$$

is the linearized Born reflection coefficient. The interpretation of R_B as a reflection coefficient is explained in Appendix A, where the Kirchhoff–approximate formula is derived from the Born–approximate formula by replacing R_B by R_K. With this

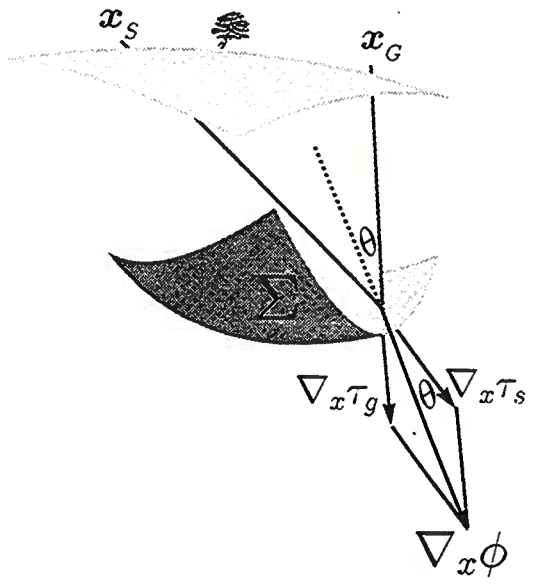

FIG. 3.4. Illustration of the vectors $\nabla_x \phi$, $\nabla_x \tau_s$, $\nabla_x \tau_g$ and the angle θ.

representation of the reflection coefficient, equation (3.19) becomes

$$D_L(\boldsymbol{\xi}, t) = \int_{\Sigma_I} d\Sigma_I \, R_B \frac{|a(\boldsymbol{x}, \boldsymbol{\xi})|}{|\nabla_x \phi|} \frac{\partial \gamma(\boldsymbol{x})}{\partial n} \Big|_{t=\phi(\boldsymbol{x},\boldsymbol{\xi})}. \tag{3.20}$$

From Beylkin (1990), the linearized Born reflection coefficient is given by

$$R(\boldsymbol{x}, \theta_s) = \frac{f(\boldsymbol{x}, 2\theta_s)}{4\cos^2\theta_s},$$

where θ_s is the angle between the normal and the ray connecting the source with the point $\boldsymbol{x}$, and

$$f(\boldsymbol{x}, \theta) = \frac{\kappa'(\boldsymbol{x})}{\kappa^0(\boldsymbol{x})} + \frac{\sigma'(\boldsymbol{x})}{\sigma^0(\boldsymbol{x})} \cos\theta$$

is the amplitude radiation pattern. Here $\kappa(\boldsymbol{x}) = \sigma(\boldsymbol{x})/c(\boldsymbol{x})^2$, is the compressibility (reciprocal of bulk modulus), where $c(\boldsymbol{x})$ is the sound speed, and $\sigma(\boldsymbol{x})$ (reciprocal of density ρ), is the specific volume. We have also

$$\begin{aligned}
\kappa' &= \kappa - \kappa^0 = \frac{1}{v^2} - \frac{1}{c^2} = \frac{\alpha}{c^2} \\
\sigma' &= \sigma - \sigma^0 = \frac{1}{\rho} - \frac{1}{\rho} = 0 \\
\kappa^0 &= \frac{1}{c^2}.
\end{aligned}$$

We find then that:

$$R(\boldsymbol{x},\theta_s) = \frac{\alpha(\boldsymbol{x})}{4\cos^2\theta_s}$$

and this is precisely the linearized Born reflection coefficient R_B found above. If I define $\beta_B(\boldsymbol{x}) = R_B\ \gamma(\boldsymbol{x})$ and introduce the reflection coefficient into the derivative sign (which asymptotically is a valid step), then one finds

$$D_L(\boldsymbol{\xi},t) = \int_{\Sigma_I} \frac{|a(\boldsymbol{x},\boldsymbol{\xi})|}{|\nabla_x\phi|}\frac{\partial}{\partial \boldsymbol{n}}\beta_B(\boldsymbol{x})\Big|_{t=\phi(\boldsymbol{x},\boldsymbol{\xi})}.$$

At this point we are ready to introduce the wavelet $w_\varphi(t)$ into the Born demigration operator D_B. We see that the dependence of time, on the right hand side, is through the evaluation $|_{t=\phi(\boldsymbol{x},\boldsymbol{\xi})}$. From equation (3.7) one can see that

$$D_B((\xi,t) \sim D_L(\boldsymbol{\xi},t) * w_\varphi(t) \tag{3.21}$$

so

$$D_B((\xi,t) \sim \int_{\Sigma_I} \frac{|a(\boldsymbol{x},\boldsymbol{\xi})|}{|\nabla_x\phi|}\frac{\partial}{\partial \boldsymbol{n}}\beta_B(\boldsymbol{x})\Big|_{t=\phi(\boldsymbol{x},\boldsymbol{\xi})} * w_\varphi(t) \tag{3.22}$$

applying equations (3.2) and (3.4) one finds

$$D_B((\xi,t) \sim \mathrm{Re}\int_{\Sigma_I} \frac{a(\boldsymbol{x},\boldsymbol{\xi})}{|\nabla_x\phi|}\frac{\partial}{\partial \boldsymbol{n}}\beta_B(\boldsymbol{x})\Big|_{t=\phi(\boldsymbol{x},\boldsymbol{\xi})} * \triangle(t). \tag{3.23}$$

The real part was moved outside of the integral given that all factors on its left are real numbers. The phase φ was incorporated into the WKBJ amplitude factor a. We also used the fact that in our formalism $\mathrm{sgn}\,\omega = 1$.

This is an isochron stack and represents a mapping from the Born reflectivity data $\beta_B(\boldsymbol{x})$ to the Born modeled data $D_B(\boldsymbol{\xi},t)$.

3.2.1 Comparison with Tygel et al., demigration operator

Tygel et al. (1996) developed a formula to do demigration. Their formula was derived by assuming that the demigration operator has the form of a Kirchhoff integral over the source–receiver isochron for each recording time t. The weight in this integral was an unknown. This weight was found by doing stationary phase analysis to their Kirchhoff–type integral and by knowing the expected zero–order ray–theory, primary–reflected wave–field. The matching of these two results at the stationary phase point provided a way to find the weight. A constraint imposed into their demigration operator is that the isochron is parameterized as $z = z_I(x,y,t)$. In this sense I want to obtain a formula that converts prestack depth migrated data into recorded data.

Prestack depth–migrated data are represented as vertical traces in depth. Therefore, I specialize equation (3.20) by projecting it into the depth (z) direction.

Let us introduce $\sqrt{g}$ as the metric correction factor for geological dip (reflector dip) [1] when I describe Σ in x, y with $z = z_\Sigma(x, y, t)$; that is, $\sqrt{g}\, dx\, dy = d\Sigma$. At stationarity, both the geological dip and the isochron dip coincide, so $\sqrt{g}$ is the same for both. We have,

$$\sqrt{g} = \frac{1}{\hat{\boldsymbol{n}} \cdot \hat{\boldsymbol{n}}_z} = \frac{\partial z}{\partial n} = \frac{|\nabla_x \phi|}{\partial \phi / \partial z}, \tag{3.24}$$

where $\hat{\boldsymbol{n}}_z = (0, 0, 1)$, and $\hat{\boldsymbol{n}}$ is a unit vector in the direction of $\nabla_x \phi$. It then follows that

$$d\Sigma_I = \sqrt{g}\, dx\, dy = \frac{|\nabla_x \phi|}{\partial \phi / \partial z} dx\, dy, \tag{3.25}$$

$$\frac{\partial}{\partial n} = \frac{\partial z}{\partial n}\frac{\partial}{\partial z} = \sqrt{g}\,\frac{\partial}{\partial z} = \frac{|\nabla_x \phi|}{\partial \phi / \partial z}\frac{\partial}{\partial z}, \tag{3.26}$$

$$\gamma(\boldsymbol{x}) \sim \sqrt{g}\,\delta(z - z_{\Sigma_R}) = \frac{|\nabla_x \phi|}{\partial \phi / \partial z}\delta(z - z_{\Sigma_R}). \tag{3.27}$$

We use these results to replace $\partial\gamma/\partial n$ in equation (3.20) as follows.

$$\begin{aligned} R\frac{\partial \gamma}{\partial n} &\sim R\,|\nabla_x \phi|\,\frac{\partial}{\partial z}\frac{\delta(z - z_{\Sigma_R})}{\partial \phi / \partial z} \\ &\sim R\,|\nabla_x \phi|\,\frac{\partial}{\partial z}\delta\left\{\frac{\partial \phi}{\partial z}(z - z_{\Sigma_R})\right\}. \end{aligned} \tag{3.28}$$

Now, equation (3.20) can be rewritten as

$$D_L(\boldsymbol{\xi}, t) \sim \int dx\, dy\, \frac{a(\boldsymbol{x}, \boldsymbol{\xi})\,|\nabla_x \phi|^2}{(\partial \phi / \partial z)^2}\,\frac{\partial}{\partial z} R_B\,\delta(m_D(z - z_{\Sigma_R}))\Big|_{z = z_I(x,y,t)}, \tag{3.29}$$

where $z_I = z_I(x, y, t)$ is the depth coordinate of the isochron, and

$$m_D = \partial \phi / \partial z \tag{3.30}$$

is called the migration stretching factor by Tygel et al. (1994). Again, as I did above, D_B should be computed by convolving with the wavelet $w_\varphi(t)$. This would produce the following result

$$D_B(\boldsymbol{\xi}, t) \sim \mathrm{Re} \int dx\, dy\, w_D(\boldsymbol{x}, \boldsymbol{\xi})\,\frac{\partial}{\partial z} M_B(\boldsymbol{x})\Big|_{z = z_I(x,y,t)} * \Delta(t), \tag{3.31}$$

[1] g is the discriminant of the first fundamental form of the differential geometry (Kreyszig, 1991).

where I introduce the notation,

$$w_D(\boldsymbol{x},\boldsymbol{\xi}) = \frac{a(\boldsymbol{x},\boldsymbol{\xi})\,|\nabla_x\phi|^2}{(\partial\phi/\partial z)^2}, \tag{3.32}$$

and, following Tygel et al. (1996), I define

$$M_B(\boldsymbol{x}_g) \sim R_B\delta(m_D(z-z_S)) \tag{3.33}$$

as the white (full–spectrum) migrated data.

Now consider the structure of this isochron stack formula. It has two factors and a convolution with the one–side delta distribution. The factors are

- The weighting factor (w_D) corrects for geometrical spreading, source–directivity, and stretching and

- the migrated data, $M_B(\boldsymbol{x})$, are the true–amplitude migration data, correctly positioned at the reflector location, stretched by the stretching factor, m_D, and weighted by the oblique–incidence linearized Born reflection coefficient, R_B, but with no limits in spectra.

Equation (3.31) would match the Tygel et al. (1996) demigration operator if one multiplies their weight by $\cos^2\beta_R$ where β_R is the reflector dip at the stationary phase point. The differences on the weight are, as explained before, due to errors in Tygel et al. (1996) as shown in Jaramillo et al. (1997).

The integration surface corresponding to the demigration operator is an isochron Σ_I for each fixed time t and source/receiver parameter $\boldsymbol{\xi}$. This explains the name *isochron stack* . It is unfortunate, however, that we are not getting the true reflection coefficient, but only an approximation that is good only for small contrast α. It is evident that one cannot account for post–critical reflections, since R_B is a real number, while the post–critical reflection coefficient is complex. We are tempted to change the formula by replacing the linearized Born reflection coefficient R_B by the Kirchhoff reflection coefficient R_K defined in equation (2.15), and then extend the range of validity of this formula. However, instead of doing this I will derive the isochron stack formula directly from the Kirchhoff approximation. Thereby, I will confirm that the change from Born to Kirchhoff reflection coefficient is a natural action to take.

3.3 The isochron stack as seen from the Kirchhoff approximation

We now derive the isochron stack equation based on the Kirchhoff approximation, equation (2.16),

$$D_K(\boldsymbol{\xi},\omega) \;\sim\; i\omega \int_{\Sigma_R} R(\boldsymbol{x},\boldsymbol{x}_s)a(\boldsymbol{x},\boldsymbol{\xi})(\hat{\boldsymbol{n}}\cdot\nabla_x\phi(\boldsymbol{x},\boldsymbol{\xi}))e^{i\omega\phi(\boldsymbol{x},\boldsymbol{\xi})}\,d\Sigma_R. \tag{3.34}$$

Similar to the Born approach, $D_K = u_S$, also the source signature $F(\omega) = 1$ is assumed. The first objective is to recast this surface integral as a volume integral. To do this, let us introduce the singular function, $\gamma(\boldsymbol{x})$, as defined in equation(3.17). Then, I can rewrite the right side of equation(3.34), as

$$D_K(\boldsymbol{\xi},\omega) \;\sim\; i\omega \int d^3x\, R(\boldsymbol{x},\boldsymbol{x}_s)a(\boldsymbol{x},\boldsymbol{\xi})(\hat{\boldsymbol{n}}\cdot\nabla_x\phi(\boldsymbol{x},\boldsymbol{\xi}))\,\gamma(\boldsymbol{x})\,e^{i\omega\phi(\boldsymbol{x},\boldsymbol{\xi})}. \tag{3.35}$$

As in the discussion of Born–approximate data, I take the inverse Fourier transform from frequency (ω) to time (t), to obtain

$$D_K(\boldsymbol{\xi},t) \;\sim\; -\int d^3x\, R(\boldsymbol{x},\boldsymbol{x}_s)|a(\boldsymbol{x},\boldsymbol{\xi})|(\hat{\boldsymbol{n}}\cdot\nabla_x\phi(\boldsymbol{x},\boldsymbol{\xi}))\,\gamma(\boldsymbol{x})\,\delta'(t-\phi(\boldsymbol{x},\boldsymbol{\xi})) \tag{3.36}$$

$$* \quad w_\varphi(t).$$

The use of identity (3.12) with $\boldsymbol{v} = \hat{\boldsymbol{n}}$ yields

$$D_K(\boldsymbol{\xi},t) \;\sim\; \int d^3x\, R(\boldsymbol{x},\boldsymbol{x}_s)|a(\boldsymbol{x},\boldsymbol{\xi})|\,\gamma(\boldsymbol{x})\,\hat{\boldsymbol{n}}\cdot\nabla_x\delta(t-\phi(\boldsymbol{x},\boldsymbol{\xi}))*w_\varphi(t). \tag{3.37}$$

Integrating by parts along $\hat{\boldsymbol{n}}$, and keeping the most singular term, yields

$$D_K(\boldsymbol{\xi},t) \;\sim\; \int d^3x\, R(\boldsymbol{x},\boldsymbol{x}_s)|a(\boldsymbol{x},\boldsymbol{\xi})|\,\frac{\partial\gamma(\boldsymbol{x})}{\partial n}\delta(t-\phi(\boldsymbol{x},\boldsymbol{\xi}))*w_\varphi(t). \tag{3.38}$$

After using identity (3.15) and relations (3.2) and (3.4) in this equation, one finds

$$D_K(\boldsymbol{\xi},t) \;\sim\; \mathrm{Re}\int d\Sigma_I\, R(\boldsymbol{x},\boldsymbol{x}_s)\frac{a(\boldsymbol{x},\boldsymbol{\xi})}{|\nabla_x\phi|}\,\frac{\partial\gamma(\boldsymbol{x})}{\partial n}\bigg|_{t=\phi(\boldsymbol{x},\boldsymbol{\xi})} * \triangle(t). \tag{3.39}$$

In Bleistein (1987), the stationary value of $R(\boldsymbol{x},\boldsymbol{x}_S)\,\gamma(\boldsymbol{x})$ was called the *reflectivity function* and denoted by $\beta(\boldsymbol{x})$. Since I am using only leading–order asymptotics here, let us use this replacement and further rewrite the previous result as

$$D_K(\boldsymbol{\xi},t) \sim \mathrm{Re}\int d\Sigma_I\,\frac{a(\boldsymbol{x},\boldsymbol{\xi})}{|\nabla_x\phi|}\,\frac{\partial\beta(\boldsymbol{x},\boldsymbol{x}_S)}{\partial n}\bigg|_{t=\phi(\boldsymbol{x},\boldsymbol{\xi})} * \triangle(t). \tag{3.40}$$

We interpret this demigration operator as a mapping function from the reflectivity data to modeled data.

We recognize that equation (3.40) is analogous to equation (3.20), with the only difference being the form of the reflection coefficient. The reflection coefficient $R(\boldsymbol{x}, \boldsymbol{x}_s)$ is the Kirchhoff reflection coefficient defined in equation (2.15), while the reflection coefficient R_B in equation (3.20) is the linearized Born reflection coefficient. It is known that the Kirchhoff approximation, using the geometrical optics reflection coefficient provides an accurate representation of the reflected wavefield, up to and beyond the critical angle of reflection (Burridge *et al.*, 1995), while the linearized Born reflection coefficient is restricted to a narrow range of incidence angles near normal incidence. Thus, I have extended the apparent range of validity of our problem, just by working with the Kirchhoff modeling (approximate) formula instead of the Born approximation formula. Another point that supports use of the Kirchhoff formula (2.16) is that this is a surface integral, while the Born approximation formula (2.11) is itself a volume integral. The transformation of the Born formula into a surface integral is equivalent (after using the Kirchhoff reflection coefficient) to Kirchhoff modeling. Therefore, I abandon the Born approach and use only a Kirchhoff–type approach. We also drop the subscript K, below.

3.3.1 Comparison with Tygel et al., demigration operator

As above, I will project the previous equation along the vertical z–direction. We start with the migrated data defined in equation (3.33) as

$$M(\boldsymbol{x}) \sim R(\boldsymbol{x}, \boldsymbol{x}_s)\delta(m_D(z - z_\Sigma)). \tag{3.41}$$

The isochron stack is then represented by the equation:

$$D(\boldsymbol{\xi}, t) \sim \mathrm{Re} \int dx\, dy\, w_D(\boldsymbol{x}, \boldsymbol{\xi}) \frac{\partial}{\partial z} M(\boldsymbol{x}) \Big|_{z=z_I(x,y,t)} * \triangle t \tag{3.42}$$

As in Born modeling, here the integrand has only two factors. The factor $w_D(\boldsymbol{x}, \boldsymbol{\xi})$ in(3.32), compensates for geometrical spreading and obliquity of migrating the data. The other factor is the derivative of the white–reflectivity data, positioned at the right location, stretched with the correct stretching factor and weighted with the Kirchhoff–approximate reflection coefficient. This formula corresponds to the demigration formula derived by Tygel et al. (1996). However, the weight derived by Tygel et al. (1996), would have to be multiplied by $\cos^2 \beta_R$ where β_R is the reflector dip at the stationary phase point, to obtain the weight $w_D(\boldsymbol{x}, \boldsymbol{\xi})$ in 3.32. The differences in the weights are, as explained before, due to errors in Tygel et al. (1996) as shown in Jaramillo et al. (1997).

In this and the previous section, then, I have provided simplified derivations of the more global results of de Hoop and Bleistein (1996). We have converted the Born and Kirchhoff modeling formulas into a demigration from data formula and also I showed that for the particular parameterization of the isochron as $z = z_I(x, y)$, that formula

reduces to Tygel et al. (1996) demigration formula.

Chapter 4

THE DIFFRACTION STACK

4.1 Introduction

In this section I find an expression for the migration operator as a diffraction stack. This diffraction stack operator coincides with the reflectivity function in Bleistein (1987).

At the end of the chapter I discuss dualities between migration, demigration, as well as isochron surfaces and diffraction surfaces. For example, an alternative representation of the migration operator is found by using the superposition principle. Here, I can migrate by smearing input energy along an isochron (isochron superposition) instead of summing amplitudes along a diffraction response (diffraction stack). The idea of smearing energy along an isochron, to do migration, was introduced by Schneider (1971). Hubral et al. (1996) extended Schneider's idea to consider the case of demigration. They show that demigration can be done by summing energy along an isochron or smearing energy along a diffraction. Here I give precise mathematical formulation for those statements.

4.2 Previous work

It is a generally accepted principle that seismic migration can be carried out by stacking amplitudes along a diffraction curve and mapping its result into the corresponding diffractor location. See, for example, Hagedoorn (1954), Lindsey and Hermann (1985), Rockwell (1971), Schneider (1978), and Schleicher et al. (1993). This problem has been studied in a more formal way from the point of view of inverse–scattering theory by using the Generalized Radon Transform (GRT), starting with Norton and Linzer (1981), who treated ultrasonic experiments in medical imaging, and followed by Miller et al. (1984), Beylkin (1985) and others. Bleistein (1987) introduces the inverse scattering solution by using the Fourier transform instead of the GRT. An extension to general anisotropic media is obtained by Burridge et al. (1995).

4.3 Diffraction stack as inverse of the isochron stack

In this section I derive the diffraction stack operator as the asymptotic inverse of the isochron stack operator in the time domain by using the plane wave expansion of the δ function (Gel'fand & Shilov, 1964). This is at the heart of the GRT inversion.

To start, I rewrite equation (3.36) as

$$D(\boldsymbol{\xi},t) \;\sim\; \int d^3x\, \beta(\boldsymbol{x})\, |a(\boldsymbol{x},\boldsymbol{\xi})|\, |\nabla_x \phi(\boldsymbol{x},\boldsymbol{\xi})|\; \delta'(t-\phi(\boldsymbol{x},\boldsymbol{\xi})) * w_\varphi(t), \tag{4.1}$$

where $\beta(\boldsymbol{x}) = R(\boldsymbol{x}_s,\boldsymbol{x})\gamma(\boldsymbol{x})$ and I used the fact that at stationarity the unit normal vector to the reflector $\hat{\boldsymbol{n}}$ and the vector of $\nabla_x\phi$ are opposite. That is,

$$\hat{\boldsymbol{n}} \cdot \nabla_y \phi(\boldsymbol{y},\boldsymbol{\xi}) \sim -|\nabla_y \phi(\boldsymbol{y},\boldsymbol{\xi}|. \tag{4.2}$$

By direct convolution it is easy to show that the convolutional inverse of $w_\varphi(t)$ is given by

$$w_\varphi(t)^{-1} = \mathrm{Re}\, e^{-i\varphi}\, \triangle \tag{4.3}$$

Now after convolving both sides of equation (4.1) with $w_\varphi(t)^{-1}$ and taking the time derivative one finds

$$\mathrm{Re}\, \frac{\partial}{\partial t}\, e^{-i\varphi}\, D(\boldsymbol{\xi},t) * \triangle \;\sim\; \int d^3x\, \beta(\boldsymbol{x})\, |a(\boldsymbol{x},\boldsymbol{\xi})|\, |\nabla_x \phi(\boldsymbol{x},\boldsymbol{\xi})|\; \delta''(t-\phi(\boldsymbol{x},\boldsymbol{\xi})). \tag{4.4}$$

The equation, $t = \phi(\boldsymbol{y},\boldsymbol{\xi})$, defines the t–isochron for a fixed source–receiver configuration dictated by $\boldsymbol{\xi}$. Let us pick a point $\boldsymbol{x}$ close to the isochron and denote by $\boldsymbol{y}$ the points on the isochron. Now, for points $\boldsymbol{y}$ near $\boldsymbol{x}$, expand ϕ in a Taylor series,

$$\phi(\boldsymbol{x},\boldsymbol{\xi}) = \phi(\boldsymbol{y},\boldsymbol{\xi}) + \nabla_y \phi(\boldsymbol{y},\boldsymbol{\xi}) \cdot (\boldsymbol{x}-\boldsymbol{y}) + \ldots \;.$$

When considering full bandwidth data in the frequency domain or, equivalently, when considering the "most singular part" of the modeling and inversion output, the support of the delta function in the previous equation is the isochron itself. For high frequency data, one can say that $\boldsymbol{x}$ should be close to $\boldsymbol{y}$, in order to obtain some contribution from the integral. Based on this, we can assume the linear approximation,

$$t - \phi(\boldsymbol{x},\boldsymbol{\xi}) = \phi(\boldsymbol{y},\boldsymbol{\xi}) - \phi(\boldsymbol{x},\boldsymbol{\xi}) \approx \nabla_y \phi(\boldsymbol{y},\boldsymbol{\xi}) \cdot (\boldsymbol{y}-\boldsymbol{x}), \tag{4.5}$$

so that

$$\begin{aligned} \delta''(t-\phi) &\approx \delta''(\nabla_y\phi \cdot (\boldsymbol{x}-\boldsymbol{y})) \\ &= \delta''(\,|\nabla_y\phi|\, \boldsymbol{\nu} \cdot (\boldsymbol{x}-\boldsymbol{y})) \\ &= |\nabla_y\phi|^{-3}\, \delta''(\boldsymbol{\nu} \cdot (\boldsymbol{x}-\boldsymbol{y})), \end{aligned} \tag{4.6}$$

where $\boldsymbol{\nu} = \boldsymbol{\nu}(\boldsymbol{y})$ is a unit vector normal to the isochron. I remark that for fixed $\boldsymbol{x}$ and $\boldsymbol{y}$, the vector $\boldsymbol{\nu}$ can be varied (over a hemisphere) by varying the source/receiver location through variations in $\boldsymbol{\xi}$. Substituting equation (4.6) into equation (4.4) yields

$$\mathrm{Re}\,\frac{\partial}{\partial t}\, e^{-i\varphi}\, D(\boldsymbol{\xi},t) * \Delta(t)\Big|_{t=\phi(\boldsymbol{y},\boldsymbol{\xi})} \sim \int d^3x\, \beta(\boldsymbol{x})\, |a(\boldsymbol{x},\boldsymbol{\xi})|\, |\nabla_y \phi|^{-2}\, \delta''(\boldsymbol{\nu}\cdot(\boldsymbol{x}-\boldsymbol{y})). \tag{4.7}$$

For each output image point $\boldsymbol{y}$, let us consider, for the moment, only those $\boldsymbol{\nu}$'s in the lower hemisphere (this would exclude migration dips larger than 90 degrees, imaged by turning rays). The reason for this will be explained below. I then multiply the previous equation by

$$|\nabla_y \phi|^2 / |a(\boldsymbol{y},\boldsymbol{\xi})| \tag{4.8}$$

and integrate over all $\boldsymbol{\nu}'s$ to obtain

$$\begin{aligned} &\mathrm{Re}\int d\boldsymbol{\nu}\, \frac{|\nabla_y \phi|^2}{a(\boldsymbol{y},\boldsymbol{\xi})} \frac{\partial}{\partial t}\, D(\boldsymbol{\xi},t) * \Delta(t)\Big|_{t=\phi(\boldsymbol{y},\boldsymbol{\xi})} \sim \\ &\int d\boldsymbol{\nu} \frac{|\nabla_y \phi|^2}{a(\boldsymbol{y},\boldsymbol{\xi})} \int d^3x\, \frac{\beta(\boldsymbol{x})\, a(\boldsymbol{x},\boldsymbol{\xi})}{|\nabla_y \phi|^2}\, \delta''(\boldsymbol{\nu}\cdot(\boldsymbol{x}-\boldsymbol{y})). \end{aligned} \tag{4.9}$$

At this point I can use the plane wave expansion representation of the delta function:

$$\delta(\boldsymbol{x}-\boldsymbol{y}) = \frac{(-1)^{\frac{n-1}{2}}}{2(2\pi)^{n-1}} \int \delta^{(n-1)}((\boldsymbol{x}-\boldsymbol{y})\cdot\boldsymbol{\nu}) d\boldsymbol{\nu}, \tag{4.10}$$

where n is an odd number representing the dimension of the space (Gel'fand & Shilov, 1964). After substituting equation (4.10) for $(n=3)$ into equation (4.9), one finds

$$-\mathrm{Re}\int d\boldsymbol{\nu}\, \frac{|\nabla_x \phi|^2}{a(\boldsymbol{y},\boldsymbol{\xi})}\, \frac{\partial}{\partial t} D(\boldsymbol{\xi},t) * \Delta(t)\Big|_{t=\phi(\boldsymbol{y},\boldsymbol{\xi})} \sim 4\pi^2 \beta(\boldsymbol{y}). \tag{4.11}$$

The factor 4 in the right hand side comes from the fact that we are integrating only in half of the sphere; for the full sphere, this factor would be 8. One finds then,

$$\beta(\boldsymbol{y}) \sim -\mathrm{Re}\,\frac{1}{4\pi^2}\int d\boldsymbol{\nu}\, \frac{|\nabla_x \phi|^2}{a(\boldsymbol{y},\boldsymbol{\xi})}\, \frac{\partial}{\partial t} D(\boldsymbol{\xi},t) * \Delta(t)\Big|_{t=\phi(\boldsymbol{y},\boldsymbol{\xi})}. \tag{4.12}$$

At this point we have an inversion formula in terms of an integral over all directions in the lower hemisphere. To derive the inversion formula in terms of an integration over the recording surface parameterized by $\boldsymbol{\xi}$, we should map the lower hemisphere into the recording surface. This can be done through the following Jacobian relations:

$$d\boldsymbol{\nu} = \sqrt{g_\xi}\, d\boldsymbol{\xi} \;=\; \Big|\frac{\partial \boldsymbol{\nu}}{\partial \xi_1} \times \frac{\partial \boldsymbol{\nu}}{\partial \xi_2}\Big|\, d\boldsymbol{\xi}$$

$$
\begin{aligned}
&= \left|\boldsymbol{\nu} \cdot \frac{\partial \boldsymbol{\nu}}{\partial \xi_1} \times \frac{\partial \boldsymbol{\nu}}{\partial \xi_2}\right| d\boldsymbol{\xi} \\
&= \left|\nabla_y \phi\right|^{-3} \left|\boldsymbol{p} \cdot \frac{\partial \boldsymbol{p}}{\partial \xi_1} \times \frac{\partial \boldsymbol{p}}{\partial \xi_2}\right| d\boldsymbol{\xi},
\end{aligned}
\tag{4.13}
$$

Here I used the fact that $\boldsymbol{p} \cdot \boldsymbol{p} \times \partial \boldsymbol{p}/\partial \xi_i = 0$ with $\boldsymbol{p} = \nabla_y \phi(\boldsymbol{y}, \boldsymbol{\xi})$, to eliminate parts of the triple scalar product arising from differentiation of $\boldsymbol{\nu} = \boldsymbol{p}/|\boldsymbol{p}|$. Substituting equation (4.13) into equation (4.12) yields

$$
\beta(\boldsymbol{y}) \sim -\mathrm{Re}\, \frac{1}{4\pi^2} \int d\boldsymbol{\xi} \frac{h_B(\boldsymbol{y}, \boldsymbol{\xi})}{a(\boldsymbol{y}, \boldsymbol{\xi}) \left|\nabla_y \phi(\boldsymbol{y}, \boldsymbol{\xi})\right|} \frac{\partial}{\partial t} D(\boldsymbol{\xi}, t) * \triangle(t) \Big|_{t=\phi(\boldsymbol{y}, \boldsymbol{\xi})}. \tag{4.14}
$$

where,

$$
h_B(\boldsymbol{y}, \boldsymbol{\xi}) = \det \begin{bmatrix} \nabla_y \phi(\boldsymbol{y}, \boldsymbol{\xi}) \\ \frac{\partial}{\partial \xi_1} \nabla_y \phi(\boldsymbol{y}, \boldsymbol{\xi}) \\ \frac{\partial}{\partial \xi_2} \nabla_y \phi(\boldsymbol{y}, \boldsymbol{\xi}) \end{bmatrix}, \tag{4.15}
$$

is the Beylkin determinant (Beylkin, 1985; Bleistein *et al.*, 1996).

I have a two–fold reason for choosing the integration of migration dips ($\boldsymbol{\nu}'s$) on the lower hemisphere. Since we allow both positive and negative frequencies (ω), we will have a maximum angular aperture of 360 degrees, which is consistent with the physics of the problem. That is, for any $\boldsymbol{\nu}$ direction between $-\pi/2$ and $\pi/2$, we have, for negative frequencies, directions between $\pi/2$ and $3\pi/2$. This sweeps the whole sphere once. On the other hand, it can be shown that the Beylkin determinant h changes sign at horizontal migration dips. In other words, the mapping from the unit sphere to the recording surface parameter is singular. The meaning of this is that we will have to split the data set into two data sets, depending on whether the migration dips are smaller or larger than 90 degrees. Each data set can be processed with the same formula (4.14).

The set

$$
\Sigma_I = \{(\xi_1, \xi_2, t) : t = \phi(\boldsymbol{y}, \boldsymbol{\xi})\} \tag{4.16}
$$

defines a diffraction surface. That is the reason for name diffraction stack in equation (4.14). Figure 4.1 shows a typical diffraction surface for a constant velocity medium.

To find the frequency–domain counterpart of equation (4.14), I rewrite that equation

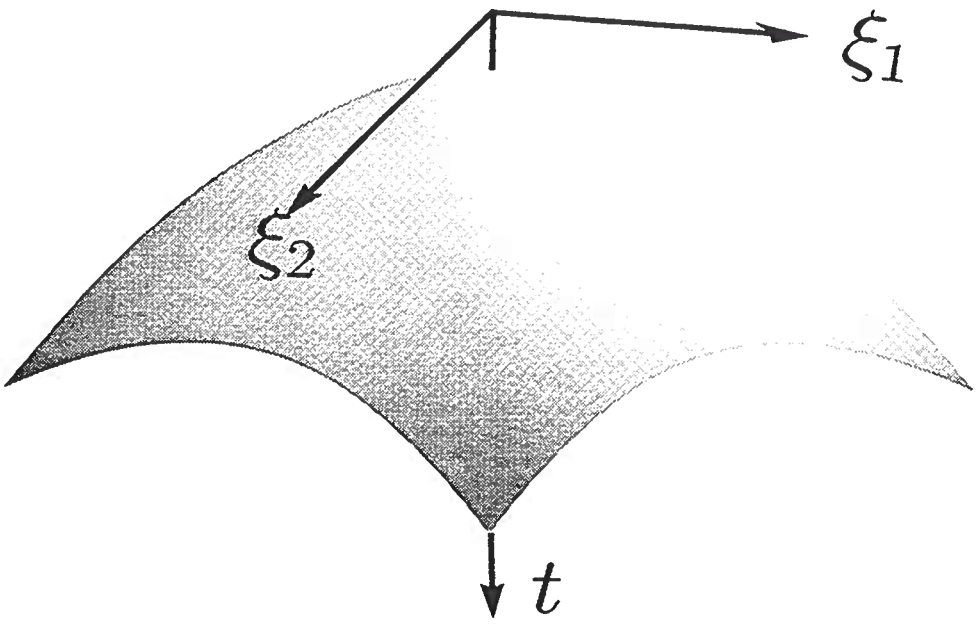

FIG. 4.1. Diffraction surface for a finite offset source/receiver configuration in a constant velocity medium.

as

$$\beta(\boldsymbol{y}) \sim -\mathrm{Re}\frac{1}{4\pi^2}\int d\boldsymbol{\xi}\, dt \frac{h_B(\boldsymbol{y},\boldsymbol{\xi})}{a(\boldsymbol{y},\boldsymbol{\xi})\,|\nabla_y\phi(\boldsymbol{y},\boldsymbol{\xi})|}\frac{\partial}{\partial t}D(\boldsymbol{\xi},t) * \triangle(t)\;\delta(t-\phi(\boldsymbol{y},\boldsymbol{\xi})). \qquad (4.17)$$

Now, I use the two–side frequency representation of the delta function given by [1].

$$\delta(t-\phi) = \frac{1}{2\pi}\int_{-\infty}^{\infty} d\omega\; e^{i\omega(t-\phi)}.$$

Then

$$\begin{aligned}\beta(\boldsymbol{y}) &\sim -\mathrm{Re}\frac{1}{8\pi^3}\int d\boldsymbol{\xi} dt\, \frac{h_B(\boldsymbol{y},\boldsymbol{\xi})}{a(\boldsymbol{y},\boldsymbol{\xi})\,|\nabla_y\phi(\boldsymbol{y},\boldsymbol{\xi})|}\,\frac{\partial}{\partial t}D(\boldsymbol{\xi},t) * \triangle(t)\,\int_{-\infty}^{\infty} d\omega\; e^{i\omega(t-\phi)} \\ &\sim -\mathrm{Re}\,\frac{1}{8\pi^3}\int d\boldsymbol{\xi}\frac{h_B(\boldsymbol{y},\boldsymbol{\xi})}{a(\boldsymbol{y},\boldsymbol{\xi})\,|\nabla_y\phi(\boldsymbol{y},\boldsymbol{\xi})|}\int_{-\infty}^{\infty} d\omega\; e^{-i\omega\phi}\int dt\frac{\partial}{\partial t}D(\boldsymbol{\xi},t) * \triangle\; e^{i\omega t}\end{aligned}$$

[1] While the convention used in this dissertation is consistent with the one–side delta distribution, I am choosing here the two-side delta distribution so I can compare this result with a well known formula from Bleistein (1987).

$$\sim \quad \mathrm{Re}\,\frac{1}{8\pi^3}\int d\boldsymbol{\xi}\frac{h_B(\boldsymbol{y},\boldsymbol{\xi})}{a(\boldsymbol{y},\boldsymbol{\xi})\,|\nabla_y\phi(\boldsymbol{y},\boldsymbol{\xi})|}\int_{-\infty}^{\infty} d\omega\, i\omega\,(1+i\,\mathrm{sgn}(\omega))\,e^{-i\omega\phi}\hat{D}(\boldsymbol{\xi},\omega), \tag{4.18}$$

where $\hat{D}(\boldsymbol{\xi},\omega)$ is the Fourier transform function of $D(\boldsymbol{\xi},t)$. For real WKBJ amplitude $a(\boldsymbol{y},\boldsymbol{\xi})$ and $F(\omega)=1$, Equation (4.18) corresponds to equation (4) in Bleistein (1987).

4.4 Comparison with Tygel et al. (1996)

In order to rewrite equation (4.14) in the notation of Tygel et al. (1996), I recast our distributional representation in terms of a distribution in z, as follows. Set

$$\begin{aligned}\beta(\boldsymbol{y})\sim R(\boldsymbol{y},\boldsymbol{x}_s)\,\gamma(\boldsymbol{y}) \quad &\sim \quad R(\boldsymbol{y},\boldsymbol{x}_s)\,\sqrt{g}\,\delta(z-z_\Sigma)\\ &\sim \quad R(\boldsymbol{y},\boldsymbol{x}_s)\frac{|\nabla_y\phi|}{\partial\phi/\partial z}\,\delta(z-z_\Sigma)\\ &\sim \quad |\nabla_y\phi|\,R(\boldsymbol{y},\boldsymbol{x}_s)\,\delta(m_D(z-z_\Sigma)).\end{aligned} \tag{4.19}$$

Here g is as introduced above (3.24). Also I use the fact that the geological dip and the isochron dip coincide at stationarity, so that $\sqrt{g}=|\nabla_y\phi|/(\partial\phi/\partial z)$. The factor m_D is defined by equation (3.30). Now from equations (3.41), (4.14), and (4.19) one finds that

$$M(\boldsymbol{y})\sim\frac{\beta(\boldsymbol{y})}{|\nabla_y\phi(\boldsymbol{y},\boldsymbol{\xi})|} \tag{4.20}$$

or

$$M(\boldsymbol{y}) \quad \sim \quad -\mathrm{Re}\,\frac{1}{4\pi^2}\int d\boldsymbol{\xi}\frac{h_B(\boldsymbol{y},\boldsymbol{\xi})}{a(\boldsymbol{y},\boldsymbol{\xi})\,|\nabla_y\phi|^2}\,\frac{\partial}{\partial t}D(\boldsymbol{\xi},t)*\Delta(t)\Big|_{t=\phi(\boldsymbol{x},\boldsymbol{\xi})}. \tag{4.21}$$

Let us now define

$$w_M=-\frac{1}{4\pi^2}\frac{h_B(\boldsymbol{y},\boldsymbol{\xi})}{a(\boldsymbol{y},\boldsymbol{\xi})\,|\nabla_x\phi|^2},$$

so that,

$$M(\boldsymbol{y})\sim\mathrm{Re}\int d\boldsymbol{\xi}\;w_M(\boldsymbol{y},\boldsymbol{\xi})\;\frac{\partial}{\partial t}D(\boldsymbol{\xi},t)*\Delta(t)\Big|_{t=\phi(\boldsymbol{y},\boldsymbol{\xi})}. \tag{4.22}$$

This is the diffraction–stack operator as derived by Tygel, et al. (1996). Again, the difference in the weight is due to errors that are being documented in Jaramillo et al. (1997). This operator represents a weighted (with weight w_M) stack of data along

diffraction curves $t = \phi(\boldsymbol{y}, \boldsymbol{\xi})$ for each output point x. The output is a true–amplitude migrated image corresponding to the reflecting model.

4.5 Discussion

4.5.1 The stacking (summing) approach

The isochron stack operator, (3.42),

$$D(\boldsymbol{\xi}, t) \sim \mathrm{Re} \int dxdy\, w_D(\boldsymbol{x}, \boldsymbol{\xi})\, \frac{\partial}{\partial z} M(\boldsymbol{x}) * \triangle(t) \Big|_{z=z_I(x,y,t)}, \tag{4.23}$$

and the diffraction stack operator, (4.22),

$$M(\boldsymbol{x}) \sim \mathrm{Re} \int d\boldsymbol{\xi}\, w_M(\boldsymbol{x}, \boldsymbol{\xi})\, \frac{\partial}{\partial t} D(\boldsymbol{\xi}, t) * \triangle(t) \Big|_{t=\phi}, \tag{4.24}$$

constitute an asymptotic transform pair between the space of seismic reflectors and the space of seismic reflections. The duality of these spaces is studied in Tygel et al. (1996). By back–substituting the isochron stack (3.42) into the diffraction stack (4.22) one can study the resolution operator for the inverse process. Due to limitations in aperture, this operator differs asymptotically from the identity operator. The resolution operator express how well the reconstruction can be accomplished within the framework of the linear theory. If we do the back–substitution in the other direction (substituting the diffraction stack operator into the isochron operator) we can study the resolution in the data space. These types of substitutions could be introduced by modifying the configuration in one of the two operators. For example, zero–offset data can be obtained from finite–offset data, by cascading finite–offset (prestack) migration, which is a modified version of zero–offset migration (poststack), with zero–offset modeling. Thus, I could obtain "resolution" operators in the image space (reflectors) and in the data space (reflections). In this general context, processes such as remigration (Tygel *et al.*, 1996) can be seen as a "resolution" operator in the image space and TZO could be seen as a "resolution" operator in the data space. Being resolution operators close to the identity, their spatial support should be small with respect to the support of their corresponding forward or inverse operators.

4.5.2 The convolutional (smearing) approach

A different and more geometrical approach, to do demigration and migration, can be derived from the diffraction stack and isochron stack operators as follows. Both the diffraction stack and the isochron stack operators are linear. Thus, if we derive impulse responses for these operators, then, by applying the superposition principle,

we can derive inversion operators from these impulse responses. Interestingly, they will turn out to be slightly different from those derived above, as we will see below.

Let us assume that $D(\boldsymbol{\xi},t)=\delta(\boldsymbol{\xi}-\boldsymbol{\xi}_0,t-t_0)$, and find the migration impulse response by inserting these data into the diffraction stack operator (4.22). Then,

$$\begin{aligned} M_\delta(\boldsymbol{x};\boldsymbol{\xi}_0,t_0) &\sim \int d\boldsymbol{\xi} w_M(\boldsymbol{x},\boldsymbol{\xi})\,\frac{\partial\delta(\boldsymbol{\xi}-\boldsymbol{\xi}_0,t-t_0)}{\partial t}\Big|_{t=\phi(\boldsymbol{x},\boldsymbol{\xi})} \\ &\sim \int d\boldsymbol{\xi}\frac{w_M(\boldsymbol{x},\boldsymbol{\xi})}{m_D(\boldsymbol{x},\boldsymbol{\xi})}\,\frac{\partial\delta(\boldsymbol{\xi}-\boldsymbol{\xi}_0,t-t_0)}{\partial z}\Big|_{t=\phi(\boldsymbol{x},\boldsymbol{\xi})} \\ &\sim -\int d\boldsymbol{\xi}\,\frac{\partial}{\partial z}\frac{w_M(\boldsymbol{x},\boldsymbol{\xi})}{m_D(\boldsymbol{x},\boldsymbol{\xi})}\delta(\boldsymbol{\xi}-\boldsymbol{\xi}_0,t-t_0)\Big|_{t=\phi(\boldsymbol{x},\boldsymbol{\xi})} \\ &\sim -\frac{\partial}{\partial z}\frac{w_M(\boldsymbol{x},\boldsymbol{\xi}_0)}{m_D(\boldsymbol{x},\boldsymbol{\xi}_0)}\Big|_{t_0=\phi(\boldsymbol{x},\boldsymbol{\xi}_0)}. \end{aligned} \tag{4.25}$$

For each fixed $\boldsymbol{\xi}_0$ and t_0, the equation $t_0=\phi(\boldsymbol{x},\boldsymbol{\xi}_0)$ defines an isochron. That is, the support of a migration impulse response is an isochron; so, migration can be carried out as a superposition of this impulse response over isochrons. To see how this works, let us write the data $\mathbf{D}(\boldsymbol{\xi},t)$ as a superposition of impulses in the following way:

$$D(\boldsymbol{\xi},t)=\int d\boldsymbol{\xi}_0\,dt_0\;\delta(\boldsymbol{\xi}-\boldsymbol{\xi}_0,t-t_0)\,D(\boldsymbol{\xi}_0,t_0),$$

so after applying the migration operator to these data and using linearity of the migration operator and equation 4.25 yields

$$M(\boldsymbol{x})\sim\int d\boldsymbol{\xi_0}\,dt_0\,M_\delta(\boldsymbol{x};\boldsymbol{\xi}_0,t_0)\,D(\boldsymbol{\xi_0},t_0).$$

Schneider (1971) shows how migration can be done as a superposition of isochrons or as a summation along a diffraction surface. His approach is qualitative. Here I showed the mathematical justification for his statements.

On the other hand, if we assume an impulsive migrated section defined by $M(\boldsymbol{x})\sim\delta(\boldsymbol{x}-\boldsymbol{x}_0)$, then the inverse migration impulse response will be

$$\begin{aligned} D_\delta(\boldsymbol{\xi};\boldsymbol{t},\boldsymbol{x}_0) &\sim \int dxdy\;w_D(\boldsymbol{x},\boldsymbol{\xi})\frac{\partial\delta(\boldsymbol{x}-\boldsymbol{x}_0)}{\partial z}\Big|_{z=z_I(x,y,\boldsymbol{\xi},t)} \\ &\sim -\int dxdy\,\frac{\partial}{\partial z}w_D(\boldsymbol{x},\boldsymbol{\xi})\delta(\boldsymbol{x}-\boldsymbol{x}_0)\Big|_{z=z_I(x,y,\boldsymbol{\xi},t)} \\ &\sim -\frac{\partial}{\partial z}w_D(\boldsymbol{x}_0,\boldsymbol{\xi})\Big|_{z_0=z_I(x_0,y_0,\boldsymbol{\xi},t)}. \end{aligned} \tag{4.26}$$

For each fixed $\boldsymbol{x}_0$ the equation $z_0 = z_I(x_0, y_0, \boldsymbol{\xi}, t)$ defines a diffraction surface. That is, the support of the inverse migration impulse response is a diffraction surface; so inverse migration can be done as a superposition of these impulse responses over diffraction surfaces according to the formula:

$$D(\boldsymbol{\xi}, t) \sim \int d\boldsymbol{x}_0 D_\delta(\boldsymbol{\xi}; \boldsymbol{t}, \boldsymbol{x}_0) M(\boldsymbol{x}_0).$$

This formula is obtained in the same way as the migration formula 4.26. That is, by writing the migration image as a superposition of spikes. Hubral (1996) shows that demigration can be done by superposition of diffraction surfaces or by stacking along an isochron. Here I showed the mathematical justification of his statements.

A simple geometrical interpretation of the equivalence between the diffraction stack and the isochron superposition is sketched in Figure 4.2. Here, for simplicity, the velocity is assumed to be $v = 2$ km/s, and the offset is $h = 0$, so the time and depth plots coincide. Also, I display only the in–line direction of the experiment. The isochrons are concave semi–circles and the diffraction curves are hyperbolas. The illustration corresponds to the migration response of a point input that is an isochron (or semi–circle in this case) and to the migration response of a diffraction surface input (or hyperbola in this case), which is a point. A similar interpretation follows for the inverse migration process by interchanging the words superposition and stacking. When stacking is performed along diffraction surfaces we are doing migration, but when superposition is done with diffraction surfaces we are doing inverse migration. In this sense stacking along curves is the inverse process of superposition of those curves. Similarly, when stacking is performed along diffraction surfaces we are doing migration, but when stacking is performed along isochrons we are doing inverse migration. In this sense diffraction surfaces and isochrons are duals of each other. The following table shows a summary of these conclusions.

	stack	**superpose**
demig	isochron	diffraction
mig	diffraction	isochron

If the purpose is to migrate a limited subset of input data, then the isochron superposition is preferred. For example, if a file contains the picked reflections, then the isochron for each picked event is superposed to obtain the migrated data. On the other hand if the user wants to obtain a migrated section of a limited output subset, then the diffraction stack is more convenient. For example, if we want to obtain only a section in the in–line direction, we stack only on those diffraction surfaces corresponding to points in the in–line direction. An extreme case, would be that of migrating a single diffractor. It would be more appropriate to sum along the only diffraction surface corresponding to the diffractor, than to superpose *all* the isochrons that touch the diffractor. These remarks apply in a similar way to the inverse migration process, by interchanging the words isochron and diffraction surfaces. In practice it is

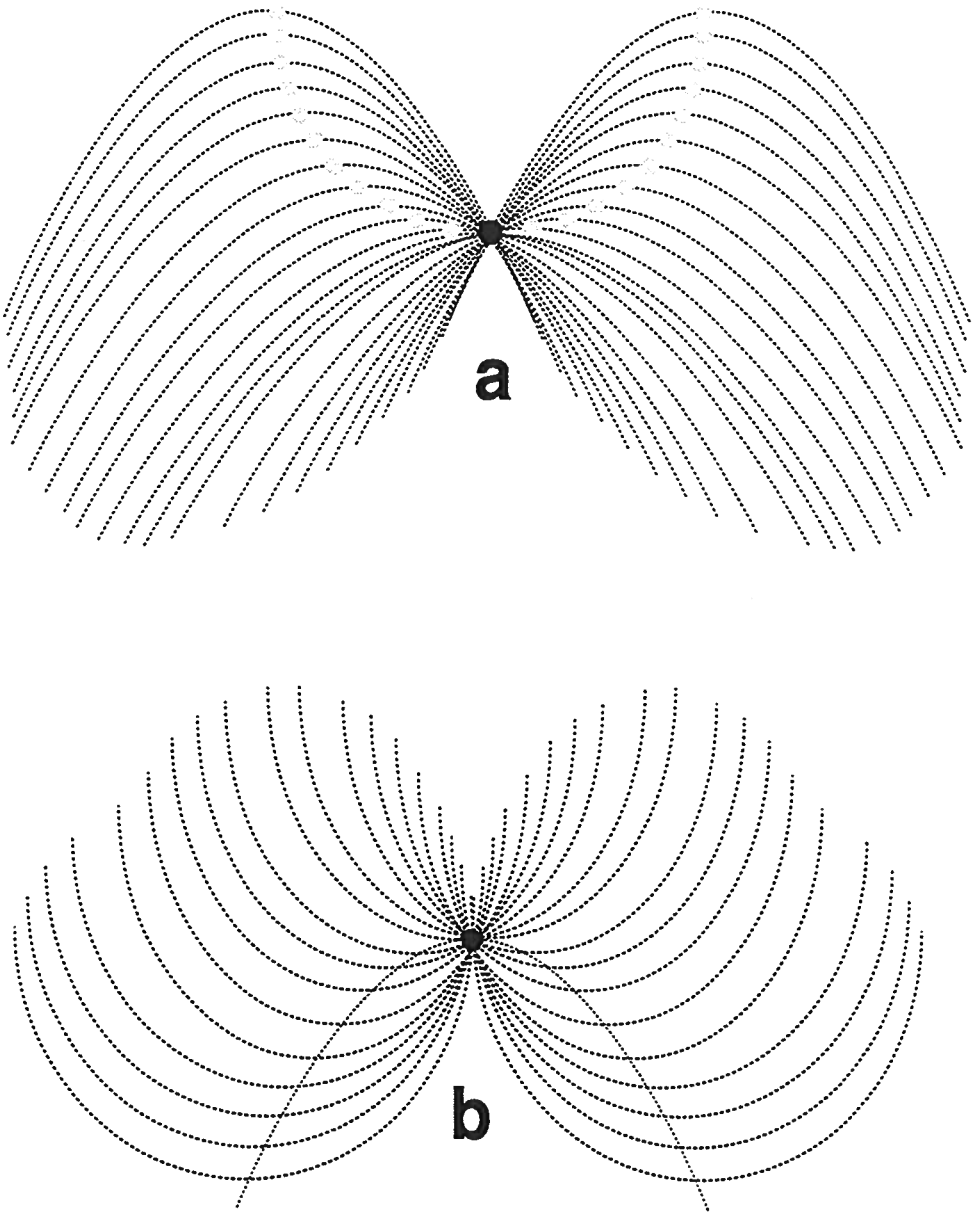

FIG. 4.2. (a) The input data are represented by a point (black) and the migration response is an upward concave semi–circle that can be constructed as i) a superposition of semi–circles (only one is needed, and here is represented by the gray dots) or ii) as a diffraction stack where each hyperbola smears the input point to its apex. (b) The output image is a point (black), and it can be computed i) as a superposition of semi–circles going through the output image point and with their minimum point sitting on a hyperbola(only one hyperbola is needed), or ii) as a diffraction stack,where each point along the hyperbola is summed into its apex.

common to find migrated picked events for interpretation purposes. These data sets can be used to create superposition of diffractions to demigrate the data for different purposes.

Chapter 5

ASYMPTOTIC ANALYSIS OF THE DEMIGRATION AND MIGRATION OPERATORS

In this chapter, I compute the leading–order asymptotic term of the demigration and migration operators by using the time domain stationary phase method.

I show that asymptotically, the migration operator places reflectors in the correct location and weights them with the proper oblique (source/receiver) reflection coefficient. In the same way, demigration maps reflectors into seismic reflections according to a given source/receiver configuration geometry and given model parameters. The amplitude on the demigrated data should account for the proper geometrical spreading due to a point–source and reflector curvature, and it should preserve the reflection coefficient embedded in the imaged data. I refer to the amplitude treatment under these processes, as *true amplitude.*

5.1 Preliminary analysis

To find the time domain asymptotic representation of the demigration and migration operators, I will use the Bleistein et al. (1996) frequency–domain stationary phase analysis formula. Consistent with our Fourier transforms convention (2.1), I only consider the use of positive frequencies ($\omega > 0$). An advantage of the use of only positive frequencies is explained in below. One of the factors of Bleistein's stationary phase formula is $\exp\{i\,\mathrm{sgn}(\omega)\,\mathrm{sgn}(\Phi)\,\pi/4\}$. For the 3D problem, we will need a 2D stationary phase formula. Here Φ would be a 2x2 Hessian matrix. For any positive or negative frequency, there are two choices of $\mathrm{sgn}(\omega)$. The signature of the matrix, defined as the number of positive eigenvalues minus the number of negative eigenvalues, has three possibilities. These are $\mathrm{sgn}(\Phi) = 0, -1, 1$. Given that I want to transform this back into the time domain; I would have to consider six combinations (according to the signature of Φ and $\mathrm{sgn}(\omega)$). If we restrict our frequencies to be positive only we could get a more compact expression that would be valid for "only" three combinations.

I want to find explicit stationary phase formulas in the time domain. The integrations

that we will deal with here are all of the form,

$$\hat{f}(t) = \int d\sigma_1 d\sigma_2 \, f(\boldsymbol{\sigma}) \; \triangle' \left(t - \phi(\boldsymbol{\sigma})\right), \tag{5.1}$$

where, $\boldsymbol{\sigma} = (\sigma_1, \sigma_2)$, is a vector that parameterizes a given surface (isochron, diffraction stack, reflector or recording surface). If $\nabla_\sigma \phi \neq 0$ then the integral can be recast in terms of lower order boundary contributions. These contributions do not correspond to specular reflections, but to undesired edge effects due to insufficient spatial aperture. They are tails of deterministic noise that can be suppressed by introducing a neutralizer (test function, or tapering filter) into the integral. We then can think of all our integral operators as truly distributional, where the test functions are implicitly assumed. I further assume that there is only one stationary point. That is, there is only one $\boldsymbol{\sigma}_0$ such that

$$\nabla_\sigma \phi = 0 \qquad \text{at} \qquad \boldsymbol{\sigma} = \boldsymbol{\sigma}_0 \tag{5.2}$$

and $\Phi = (\phi_{,ij})$ at $\boldsymbol{\sigma} = \boldsymbol{\sigma}_0$ where $\phi_{,ij} = \partial^2 \phi / \partial \sigma_i \partial \sigma_j$ are elements of a non–singular matrix. That is $\det \Phi \neq 0$. If there are a finite number of stationary points, the integral operator can be divided in several parts each one having only one stationary point. To avoid edge effects as above, appropriate neutralizer functions should be chosen. In our context, the presence of several stationary points indicates the existence of multiple reflections associated with the same source–receiver parameter $\boldsymbol{\xi}$ in the case of the demigration operator. This means the existence of an isochron that is tangent to a reflecting surface in several places. One example is found in synclinal structures, where even triplications can occur, giving bow–tie–shaped reflections. The worse possible case is given by a reflector that coincides with the isochron in a continuous set. This creates a focusing with high amplitudes. Here the stationary phase analysis fails. In the case of the migration operator, several source–receiver combinations correspond to the same reflection point as happens for diffractors or geological corners (pinchouts, faults etc). If the primaries reflection–data coincide with a diffraction surface for a continuous set of source–receiver parameters $\boldsymbol{\xi}$, then we have another type of focusing. Figure 5.1 sketches some examples of this. Here also the stationary phase method fails. It is interesting to observe that the stationary phase method would not work for migration in the midpoint domain, where all reflection strips are seen as diffractions associated with the midpoint. If $\det \Phi = 0$, then higher–order stationary phase analysis or more sophisticated techniques are required. As mentioned above, in order to keep this analysis simple I will assume that there is only one stationary phase point.

Stationary phase analysis of these type of integrals for the small parameter $t > 0$ in a general n–dimensional space is a rather complicated problem. Gel'fand and Shilov (1964) show the asymptotic series expansion of $\hat{f}(t)$ (for Re $\triangle \, (t - \phi)$) in terms of the small parameter $t > 0$. They find what the leading order should be for any $n \geq 1$, and kth derivative ($k = 1, 2, ..$) of the most singular function Re $\triangle(t - \phi)$. For

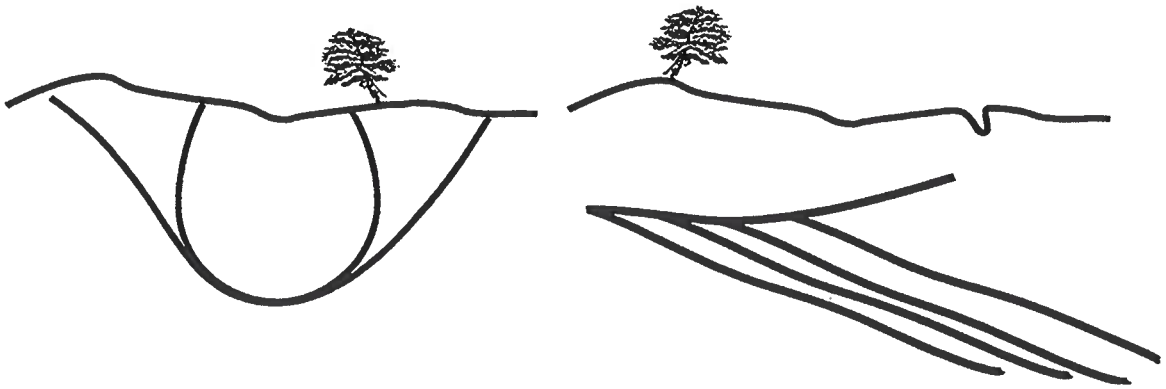

FIG. 5.1. Left: A synclinal structure is locally coincident with an isochron. The difference of curvatures along the continuous contact path breaks the method of stationary phase for doing modeling. Right: The corners on the geological structure produce diffractions which will coincide with the diffraction stacking path. The amplitude to perform migration using the stationary phase analysis approach, increases without bounds as the two diffraction curves get closer.

$n = 2$ ($\boldsymbol{\sigma} \in \mathbb{R}^2$) and $k = 1$, the analysis becomes rather simple by using the one–side frequency domain representation of the analytic delta distribution. Let us start:

$$\triangle(t - \phi) = \frac{1}{\pi} \int_{\omega>0} d\omega e^{-i\omega(t-\phi)} \tag{5.3}$$

so

$$\begin{aligned} \int d\sigma_1\, d\sigma_2\ \triangle'(t-\phi) f(\boldsymbol{\sigma}) &= -\int d\sigma_1\, d\sigma_2\, \frac{f(\boldsymbol{\sigma})}{\pi} \int_{\omega>0} d\omega\ (i\omega)\ e^{-i\omega(t-\phi(\boldsymbol{\sigma})} \\ &= -\frac{1}{\pi} \int_{\omega>0} d\omega\ i\omega\, e^{-i\omega t} \int d\sigma_1 d\sigma_2\ f(\boldsymbol{\sigma}) e^{i\omega\phi(\boldsymbol{\sigma})}. \end{aligned} \tag{5.4}$$

The appropriate stationary phase formula used here (Bleistein *et al.*, 1996) is

$$\int d\sigma_1 d\sigma_2\ f(\boldsymbol{\sigma})\ e^{i\omega\phi(\boldsymbol{\sigma})} \sim \frac{2\pi}{\omega} \frac{f(\boldsymbol{\sigma_0}) e^{i\omega\phi(\boldsymbol{\sigma_0})} e^{i\,\mathrm{sgn}(\Phi)\frac{\pi}{4}}}{\sqrt{|\det \Phi|}}, \tag{5.5}$$

so

$$\begin{aligned} \int d\sigma_1\, d\sigma_2\ \triangle'(t-\phi) f(\boldsymbol{\sigma}) &\sim \frac{-2f(\boldsymbol{\sigma_0})\, e^{i\frac{\pi}{2}(1+\frac{\mathrm{sgn}(\Phi)}{2})}}{\sqrt{|\det \Phi|}} \int_{\omega>0} d\omega\ e^{i\omega\phi(\boldsymbol{\sigma_0})}\, e^{-i\omega t} \\ &\sim \frac{-2\pi f(\boldsymbol{\sigma_0})\, e^{i\frac{\pi}{2}(1+\frac{\mathrm{sgn}(\Phi)}{2})}}{\sqrt{|\det \Phi|}} \frac{1}{\pi} \int_{\omega>0} d\omega e^{-i\omega(t-\phi(\boldsymbol{\sigma_0}))}. \end{aligned} \tag{5.6}$$

Finally, we have the asymptotic result

$$\int d\sigma_1\, d\sigma_2\ \triangle'\,(t-\phi) f(\boldsymbol{\sigma}) \ \sim\ \frac{-2\pi\, f(\boldsymbol{\sigma_0})\, e^{i\frac{\pi}{2}(1+\frac{\mathrm{sgn}(\Phi)}{2})}}{\sqrt{|\det\Phi|}}\ \triangle'\,(t-\phi(\boldsymbol{\sigma_0})). \tag{5.7}$$

In some cases the data are collected along one line of point sources. The appropriate *thought experiment* is one where the propagation speed and other earth parameters are independent of the transverse direction. In these cases I want to evaluate the contributions from the integral along that transverse direction (cross–line) by doing stationary phase analysis. This gives rise to the so called 2.5D experiment.

I will then perform the integration in equation (5.1) along just the direction σ_2 by using the method of stationary phase. We have then

$$\int d\sigma_1 d\sigma_2\, f(\boldsymbol{\sigma})\, e^{i\omega\phi(\boldsymbol{\sigma})} \sim \sqrt{\frac{2\pi}{\omega}} \int d\sigma_1 \frac{f(\boldsymbol{\sigma_0}) e^{i\omega\phi(\boldsymbol{\sigma_0})} e^{i\,\mathrm{sgn}(\Phi_2)\frac{\pi}{4}}}{\sqrt{|\Phi_2|}} \tag{5.8}$$

where $\boldsymbol{\sigma_0} = (\sigma_1, \sigma_{20}(\sigma_1))$, $\sigma_{20}(\sigma_1)$ is solution to the stationary phase equation $\partial\phi/\partial\sigma_2 = 0$ and $\Phi_2 = \partial^2\phi/\partial\sigma_2^2\,|_{\sigma_2=\sigma_{20}}$. By substituting equation (5.8) into equation (5.4) one finds

$$\begin{aligned}\int d\sigma_1\, d\sigma_2\ \triangle'\,(t-\phi) f(\boldsymbol{\sigma}) \ \sim\ & -\sqrt{\frac{2}{\pi}} \int d\sigma_1 \frac{f(\boldsymbol{\sigma_0})}{\sqrt{|\Phi_2|}} \\ & \times \int_{\omega>0} d\omega\ i\sqrt{\omega}\, e^{i\,\mathrm{sgn}(\Phi_2)\frac{\pi}{4}}\, e^{-i\omega(t-\phi(\boldsymbol{\sigma_0}))}.\end{aligned} \tag{5.9}$$

Now

$$i\sqrt{\omega} = e^{\frac{i\pi}{2}}\sqrt{\omega}\, e^{-\frac{i\pi}{4}}\, e^{\frac{i\pi}{4}} = -\sqrt{-i\omega}\, e^{-\frac{i\pi}{4}} \tag{5.10}$$

so equation (5.9) becomes

$$\begin{aligned}\int d\sigma_1\, d\sigma_2\ \triangle'\,(t-\phi) f(\boldsymbol{\sigma}) \ \sim\ & \sqrt{\frac{2}{\pi}} \int d\sigma_1 \frac{f(\boldsymbol{\sigma_0})}{\sqrt{|\Phi_2|}} \\ & \times \int_{\omega>0} d\omega\ \sqrt{-i\omega}\, e^{-i\omega(t-\phi(\boldsymbol{\sigma_0}))}\, e^{\frac{i\pi}{4}(\mathrm{sgn}(\Phi_2)-1)}.\end{aligned} \tag{5.11}$$

That is,

$$\int d\sigma_1\, d\sigma_2\ \triangle'\,(t-\phi) f(\boldsymbol{\sigma}) \sim \sqrt{2\pi} \int d\sigma_1 \frac{e^{i\frac{\pi}{4}(\mathrm{sgn}(\Phi_2)-1)}}{\sqrt{|\Phi_2|}}\, f(\boldsymbol{\sigma_0})\ \triangle_{\frac{1}{2}}\,(t-\phi(\boldsymbol{\sigma_0})). \tag{5.12}$$

Here, $\triangle_{\frac{1}{2}}(t-\boldsymbol{\sigma_0})$ is the fractional derivative of the analytic delta distribution, defined

through the relation:

$$\triangle_{\frac{1}{2}}(t-\sigma_0) = \delta_{\frac{1}{2}}(t-\sigma_0) - i\,\mathcal{H}\left[\delta_{\frac{1}{2}}((t-\sigma_0)\right]. \tag{5.13}$$

In Appendix C, I show that the definition of fractional derivatives of the Fractional Calculus agrees with that shown here. That is a $q-$fractional derivative of a causal function can be identified with a multiplication in the frequency domain by $(-i\omega)^q$. This fact has not previously been shown to be equivalent in the context of the Fractional Calculus. Fractional derivatives as operators of the type $(-i\omega)^q$ are known to be valid only for causal functions. In general, the Hilbert transform of a causal function produces a noncausal function. Thus, one cannot apply the fractional calculus to the Hilbert transform of a causal function. Rather, one must apply the fractional derivative to the causal function, first, and then apply the Hilbert transform to the result. In the frequency domain, this amounts to multiplication of filters, which is a commutative operation. In the time domain, we are performing convolutions, but with functions that could be not well–defined.

The theory of pseudo–differential operators seems to be a good alternative, to understand this problem, given that the operator $(-i\omega)^q$ is well defined and associated to fractional derivatives, for causal and (or) non causal functions [1].

Deregowski and Brown (1983) show that for causal functions

$$\frac{1}{2\pi}\int_{-\infty}^{\infty} d\omega\,\sqrt{-i\omega}\,e^{-i\omega t} = \frac{1}{\sqrt{\pi}}\left(\frac{\delta(t)}{\sqrt{t}} - \frac{1}{2}\frac{H(t)}{t^{3/2}}\right); \tag{5.14}$$

so that half–differentiation can be obtained by convolution with the operator

$$d_{1/2}(t) = \frac{1}{\sqrt{\pi}}\left(\frac{\delta(t)}{\sqrt{t}} - \frac{1}{2}\frac{H(t)}{t^{3/2}}\right). \tag{5.15}$$

In particular,

$$\delta_{\frac{1}{2}}(t-\phi(\sigma_0)) = \frac{1}{\sqrt{\pi}}\left(\frac{\delta(t-\phi(\sigma_0))}{\sqrt{(t-\phi(\sigma_0))}} - \frac{1}{2}\frac{H(t-\phi(\sigma_0))}{(t-\phi(\sigma_0))^{3/2}}\right). \tag{5.16}$$

In conclusion, I derived time–domain stationary phase formulas to evaluate integrals of the type shown in equation 5.1. These integrals represent a weighted summation over a surface, of data in the three–dimensional space. These type of operations are typical in seismic data processes such as Kirchhof migration, demigration and TZO. Equation (5.7) is used to solve the 3D demigration, migration and SDM problems, while equation (5.12) is used to solve the 2.5D demigration, migration and SDM problems. These time–domain stationary phase formulas were derived from their counterpart frequency–domain formulas found in Bleistein (1984).

[1] Ahmed I. Zayed, 1997. Electronic mail communication

5.2 Asymptotic evaluation of the demigration operator

In this section, I will find the leading order asymptotic term of the demigration operator, by using the stationary phase analysis formula derived in the previous section. I show that asymptotically demigration maps reflectors into seismic reflections according to a given source/receiver configuration geometry and given model parameters. The amplitude on the demigrated data should account for the proper geometrical spreading due to a point–source and reflector curvature, and it should preserve the reflection coefficient embedded in the imaged data.

I start by rewriting the demigration operator as in the formula (3.39)

$$D(\boldsymbol{\xi},t) \;\sim\; \mathrm{Re}\int d\Sigma_I\, R(\boldsymbol{x},\boldsymbol{x}_s)\frac{a(\boldsymbol{x},\boldsymbol{\xi})}{|\nabla_x\phi|}\,\frac{\partial\gamma(\boldsymbol{x})}{\partial n}\bigg|_{t=\phi(\boldsymbol{x},\boldsymbol{\xi})} * \triangle(t). \tag{5.17}$$

Here $t=\phi(\boldsymbol{x},\boldsymbol{\xi})$, for fixed t and $\boldsymbol{\xi}$, defines the isochron surface Σ_I. The singular function of the reflecting surface is given by

$$\gamma(\boldsymbol{x}) = \delta(\phi-\tau_R)|\nabla_x\phi|, \tag{5.18}$$

where $\tau_R(\boldsymbol{\xi})$ corresponds to the reflection time (Bleistein, 1987). Also, $\partial/\partial n = \boldsymbol{n}\cdot\nabla$; therefore,

$$\frac{\partial}{\partial n}\delta(\phi-\tau_R) = \boldsymbol{n}\cdot\nabla_x\delta(\phi-\tau_R) = -\delta'(\phi-\tau_R)|\nabla_x\phi| \tag{5.19}$$

at stationarity. The minus sign comes from the fact that at stationarity, the normal vector to the surface $\boldsymbol{n}$ points upwards while the gradient vector $\nabla_x\phi$ points downward. Then, equation (5.17) can be written as

$$D(\boldsymbol{\xi},t) \;\sim\; -\mathrm{Re}\int d\Sigma_I\, R(\boldsymbol{x},\boldsymbol{x}_s)a(\boldsymbol{x},\boldsymbol{\xi})|\nabla_x\phi|\,\delta'(\phi-\tau_R)\Big|_{t=\phi(\boldsymbol{x},\boldsymbol{\xi})} * \triangle(t). \tag{5.20}$$

That is

$$D(\boldsymbol{\xi},t) \;\sim\; -\mathrm{Re}\int d\Sigma_I\, R(\boldsymbol{x},\boldsymbol{x}_s)a(\boldsymbol{x},\boldsymbol{\xi})|\nabla_x\phi|\;\triangle'\left(\phi-\tau_R\right)\Big|_{t=\phi(\boldsymbol{x},\boldsymbol{\xi})}. \tag{5.21}$$

Let us now parameterize the isochron surface Σ_I using coordinates $\boldsymbol{\sigma}=(\sigma_1,\sigma_2)$, where the parameters σ_1 and σ_2 define an orthogonal coordinate system along the plane tangent to the isochron at the stationary phase point. I represent the isochron as $[\sigma_1,\sigma_2,\tilde{x}_3(\sigma_1\sigma_2)]$, where $\tilde{x}_3$ is plotted along the normal direction to $\sigma_1\sigma_2$.

The stationary phase condition is described by

$$\nabla_\sigma\left[\,\phi\left(\boldsymbol{x}(\boldsymbol{\sigma}),\boldsymbol{\xi}\right)-\tau_R(\boldsymbol{\xi})\,\right]=0, \tag{5.22}$$

so one can rewrite equation (5.21) as

$$D(\boldsymbol{\xi},t) \;\sim\; -\mathrm{Re}\int d\boldsymbol{\sigma}\,\sqrt{g}\;R(\boldsymbol{x},\boldsymbol{x}_s)a(\boldsymbol{x},\boldsymbol{\xi})\;|\nabla_x\phi|\;\triangle'\left(\phi-\tau_R\right) \tag{5.23}$$

where g is the determinant of the first fundamental form of differential geometry.

Now, since, at the stationary point, $\partial\tilde{x}_3/\partial\sigma_k = 0$, for the specific chosen parameterization, then $\partial x_l/\partial\sigma_k = \delta_{lk}$, $l = 1..3$, $k = 1,2$ where the Kronecker delta is defined by

$$\delta_{ij} = \begin{cases} 1 & \text{if } i = j \\ 0 & \text{if } i \neq j \end{cases} . \tag{5.24}$$

Now the metric tensor g_{ij}, for this surface, is found as follows

$$g_{ij} = \frac{\partial x_k}{\partial\sigma_i}\,\frac{\partial x_k}{\partial\sigma_j} = \delta_{ik}\,\delta_{jk} = \delta_{ij}, \tag{5.25}$$

so that $g = 1$.

Stationary phase formula (5.7) produces

$$D(\boldsymbol{\xi},t) \sim \mathrm{Re}\,\frac{4\pi\;R(\boldsymbol{x}_0,\boldsymbol{x}_s)\,a(\boldsymbol{x}_0,\boldsymbol{\xi})\;\cos\theta}{c\,(\boldsymbol{x}_0)\sqrt{\det|\Phi|}}\;e^{i\frac{\pi}{2}(1-\frac{\mathrm{sgn}(\Phi)}{2})}\;\;\triangle\left(t-\tau_R(\boldsymbol{\xi})\right)\Big|_{t=\phi(\boldsymbol{x}_0,\boldsymbol{\xi})} . \tag{5.26}$$

Here, $\boldsymbol{x}_0 = \boldsymbol{x}(\boldsymbol{\sigma}_0)$ is the reflection point, $c\,(\boldsymbol{x}_0)$ is the P–wave speed of the layer just above $\boldsymbol{x}_0$, θ is half the angle between the source and receiver rays at $\boldsymbol{x}_0$. The matrix Φ, to within a sign, represents the second–derivative matrix of the reflection time $\phi(\boldsymbol{x}(\boldsymbol{\sigma}),\boldsymbol{\xi})$ with respect to the coordinates of an (arbitrarily oriented) 2–D local Cartesian coordinate system (σ_1,σ_2), within the plane tangent to the reflector at $\boldsymbol{x}_0(\boldsymbol{\sigma})$. In other words, Φ is just the Fresnel matrix H_F, introduced by Tygel et al. (1995). Given that at stationarity the tangent plane to the isochron is the same as the tangent plane of the reflector, one needs no further rotation to find the Fresnel matrix. The relation $\mathrm{sgn}(\Phi) = -\,\mathrm{sgn}(H_F)$ is due to the fact that the orientation of the tangent plane with respect to the isochron is opposite to that with respect to the reflector, since the normal vectors are opposite to each other at stationarity. Tygel et al. (1995) define the Fresnel geometrical spreading factor $\mathcal{L}_F(\boldsymbol{x}_0)$ as

$$\mathcal{L}_F(\boldsymbol{x}_0) = \frac{\cos\theta}{c\,(\boldsymbol{x}_0)}\,\frac{e^{i\frac{\pi}{2}(1-\frac{\mathrm{sgn}(H_F)}{2})}}{\sqrt{\det|H_F|}}. \tag{5.27}$$

In terms of $\mathcal{L}_F(\boldsymbol{x}_0)$ one has

$$D(\boldsymbol{\xi},t) \;\sim\; \mathrm{Re}\;4\pi R(\boldsymbol{x}_0,\boldsymbol{x}_s)a(\boldsymbol{x}_0,\boldsymbol{\xi})\mathcal{L}_F(\boldsymbol{x}_0)\;\triangle\left(t-\tau_R(\boldsymbol{\xi})\right). \tag{5.28}$$

The amplitude term $a(\boldsymbol{x}_0, \boldsymbol{\xi})$ can be written in the form $a(\boldsymbol{x}_0, \boldsymbol{\xi}) = \mathcal{A}(\boldsymbol{x}_0, \boldsymbol{\xi})/\mathcal{L}_S\mathcal{L}_G$, where $\mathcal{L}_S$ and $\mathcal{L}_G$ are the geometrical spreading factors from source and receiver, respectively, and $\mathcal{A} = \mathcal{A}(\boldsymbol{x}_0, \boldsymbol{\xi})$ is the total loss in amplitude due to transmission across all interfaces along the ray. For a complete treatment of amplitudes along the ray, the reader is referred to Červený (1995). After these considerations, equation (5.28) turns out to be

$$D(\boldsymbol{\xi}, t) \sim \text{Re } 4\pi \frac{\mathcal{A}}{\mathcal{L}_S\mathcal{L}_G} \mathcal{L}_F(\boldsymbol{x}_0) R(\boldsymbol{x}_0, \boldsymbol{x}_s) \triangle (t - \tau_R(\boldsymbol{\xi})). \tag{5.29}$$

Now, using $\mathcal{L}_{SG} = \mathcal{L}_S\mathcal{L}_G/\mathcal{L}_F$ (Tygel *et al.*, 1995), where $\mathcal{L}_{SG}$ represents the geometrical–spreading factor for the combined source–receiver event, one finds that

$$D(\boldsymbol{\xi}, t) \sim \text{Re } 4\pi \frac{\mathcal{A} R(\boldsymbol{x}_0, \boldsymbol{x}_s)}{\mathcal{L}_{SG}} \triangle (t - \tau_R(\boldsymbol{\xi})). \tag{5.30}$$

This is precisely the zero–order ray term corresponding to a reflected event with reflecting time given by τ_R, transmission amplitude loss given by $\mathcal{A}$, source–receiver geometrical–spreading factor given by $\mathcal{L}_{SG}$, reflection coefficient given by $R(\boldsymbol{x}_0, \boldsymbol{x}_s)$ and isotropic source radiation pattern represented by the constant 4π.

5.3 Asymptotic evaluation of the diffraction stack

Here, I find the leading–order asymptotic term of the diffraction stack operator.

I start by rewriting equation (4.14)

$$\beta(\boldsymbol{x}) \sim -\frac{1}{4\pi^2} \int d\boldsymbol{\xi} \frac{h_B(\boldsymbol{x}, \boldsymbol{\xi})}{a(\boldsymbol{x}, \boldsymbol{\xi}) \left| \nabla_x \phi(\boldsymbol{x}, \boldsymbol{\xi}) \right|} \frac{\partial}{\partial t} D(\boldsymbol{\xi}, t) * \triangle(t) \Big|_{t=\phi(\boldsymbol{x}, \boldsymbol{\xi})}, \tag{5.31}$$

and insert, the analytical data

$$D(\boldsymbol{\xi}, t) * \triangle(t) \sim 4\pi \frac{\mathcal{A} R(\boldsymbol{x}_0, \boldsymbol{x}_s)}{\mathcal{L}_{SG}} \triangle (t - \tau_R(\boldsymbol{\xi})). \tag{5.32}$$

Taking the real part of the resulting equation, yields

$$\begin{aligned} \beta(\boldsymbol{x}) &\sim -\text{Re} \frac{1}{\pi} \int d\boldsymbol{\xi} \frac{\mathcal{A} R(\boldsymbol{x}, \boldsymbol{x}_s)}{\mathcal{L}_{SG}} \frac{h_B(\boldsymbol{x}, \boldsymbol{\xi})}{a(\boldsymbol{x}, \boldsymbol{\xi}) \left| \nabla_x \phi(\boldsymbol{x}, \boldsymbol{\xi}) \right|} \triangle' (\phi(\boldsymbol{x}, \boldsymbol{\xi}) - \tau_R(\boldsymbol{\xi})) \\ &\sim \text{Re} \frac{1}{\pi} \int d\boldsymbol{\xi} \frac{\mathcal{A} R(\boldsymbol{x}, \boldsymbol{x}_s)}{\mathcal{L}_{SG}} \frac{h_B(\boldsymbol{x}, \boldsymbol{\xi})}{a(\boldsymbol{x}, \boldsymbol{\xi}) \left| \nabla_x \phi(\boldsymbol{x}, \boldsymbol{\xi}) \right|} \triangle' (\tau_R(\boldsymbol{\xi}) - \phi(\boldsymbol{x}, \boldsymbol{\xi})), \end{aligned} \tag{5.33}$$

since $\triangle'$ is antisymmetric (odd) in its argument. Here $\beta(\boldsymbol{x})$ is a migration operator.

I extend this formula as a time continuation operator in the following way:

$$\beta(\boldsymbol{x},t) \sim \mathrm{Re}\frac{1}{\pi}\int d\boldsymbol{\xi}\,\frac{\mathcal{A}R(\boldsymbol{x},\boldsymbol{x}_s)}{\mathcal{L}_{SG}}\,\frac{h_B(\boldsymbol{x},\boldsymbol{\xi})}{a(\boldsymbol{x},\boldsymbol{\xi})\,|\nabla_x\phi(\boldsymbol{x},\boldsymbol{\xi})|} \times \quad \triangle'\left(t-(\phi(\boldsymbol{x},\boldsymbol{\xi})-\tau_R(\boldsymbol{\xi}))\right). \tag{5.34}$$

The "imaging condition" $t=0$ makes of $\beta(\boldsymbol{x},t=0)$ the migration operator defined in equation (5.33). Formula (5.34) is already in the form of formula (5.1). The time domain stationary phase analysis yields

$$\beta(\boldsymbol{x},t) \sim -\mathrm{Re}\frac{2\,\mathcal{A}\,R(\boldsymbol{x},\boldsymbol{x}_s)\,h_B(\boldsymbol{x},\boldsymbol{\xi}_0)}{\mathcal{L}_{SG}\,a(\boldsymbol{x},\boldsymbol{\xi}_0)\,|\nabla_x\phi(\boldsymbol{x},\boldsymbol{\xi})|}\,\frac{e^{i\frac{\pi}{2}(1+\mathrm{sgn}(\frac{\Phi}{2}))}}{\sqrt{|\det\Phi|}} \times \quad \triangle\left(t-(\phi(\boldsymbol{x},\boldsymbol{\xi})-\tau_R(\boldsymbol{\xi}))\right). \tag{5.35}$$

Here $\Phi_{ij}=\frac{\partial^2}{\partial\xi_i\xi_j}(\phi(\boldsymbol{x},\boldsymbol{\xi})-\tau_R(\boldsymbol{\xi}))\Big|_{\boldsymbol{\xi}=\boldsymbol{\xi}_0}$; the evaluation at, $\boldsymbol{\xi}=\boldsymbol{\xi}_0$, corresponds to the two–dimensional parameter that identifies $\boldsymbol{x}_s(\boldsymbol{\xi}_0)$ and $\boldsymbol{x}_g(\boldsymbol{\xi}_0)$ as the source–receiver combination that selects the specular ray reflecting at point $\boldsymbol{x}$. The stationary phase condition implies that the diffraction surface corresponding to the diffractor point $\boldsymbol{x}$ and the equation $t=\phi(\boldsymbol{x},\boldsymbol{\xi})$ is tangent to the primaries surface $t=\tau_R(\boldsymbol{\xi})$. The point of tangency is $[\boldsymbol{\xi}_0,\phi(\boldsymbol{x},\boldsymbol{\xi}_0)=\tau_R(\boldsymbol{\xi}_0)]$.

Going back to $t=0$ one finds

$$\beta(\boldsymbol{x},t=0) \sim -\mathrm{Re}\frac{2\,\mathcal{A}\,R(\boldsymbol{x},\boldsymbol{x}_s)\,h_B(\boldsymbol{x},\boldsymbol{\xi}_0)}{\mathcal{L}_{SG}\,a(\boldsymbol{x},\boldsymbol{\xi}_0)\,|\nabla_x\phi(\boldsymbol{x},\boldsymbol{\xi})|}\,\frac{e^{i\frac{\pi}{2}(1+\mathrm{sgn}(\frac{\Phi}{2}))}}{\sqrt{|\det\Phi|}} \times \quad \triangle\left(\phi(\boldsymbol{x},\boldsymbol{\xi}_0)-\tau_R(\boldsymbol{\xi}_0)\right). \tag{5.36}$$

Now from,

$$\mathcal{L}_{SG}=\frac{\mathcal{L}_S\mathcal{L}_G}{\mathcal{L}_F} \qquad \text{and} \qquad a=\frac{\mathcal{A}}{\mathcal{L}_S\mathcal{L}_G}, \tag{5.37}$$

follows

$$\beta(\boldsymbol{x},t=0) \sim -\mathrm{Re}\frac{2\,R(\boldsymbol{x},\boldsymbol{x}_s)\,h_B(\boldsymbol{x},\boldsymbol{\xi}_0)\,\mathcal{L}_F(\boldsymbol{x})}{|\nabla_x\phi(\boldsymbol{x},\boldsymbol{\xi}_0)|}\,\frac{e^{i\frac{\pi}{2}(1+\mathrm{sgn}(\frac{\Phi}{2}))}}{\sqrt{|\det\Phi|}} \times \quad \triangle\left(\phi(\boldsymbol{x},\boldsymbol{\xi}_0)-\tau_R(\boldsymbol{\xi}_0)\right). \tag{5.38}$$

Now, Tygel et al. (1995) [2] show that

$$\mathcal{L}_F(\boldsymbol{x}) = \frac{m_D \cos\theta}{h_B(\boldsymbol{x},\boldsymbol{\xi}_0)c(\boldsymbol{x})\cos\beta_R} |\det\Phi|^{\frac{1}{2}} e^{i\frac{\pi}{2}(1-\mathrm{sgn}(\frac{\Phi}{2}))}. \tag{5.39}$$

Here, θ is half the angle between the rays from $\boldsymbol{x}$ to the source and to the receiver, β_R is the reflector dip and m_D is the stretching factor defined in equation (3.30). We further observe that

$$m_D = \partial\phi/\partial z = \nabla_x\phi \cdot \boldsymbol{n}_z = |\nabla_x\phi| \cos\beta_R. \tag{5.40}$$

The substitution of equations (5.39) and (5.40) into equation (5.38) produces

$$\beta(\boldsymbol{x}, t=0) \sim \mathrm{Re}\frac{2\cos\theta}{c(\boldsymbol{x})} R(\boldsymbol{x},\boldsymbol{x}_s)\ \triangle\left(\phi(\boldsymbol{x},\boldsymbol{\xi}_0) - \tau_R(\boldsymbol{\xi}_0)\right). \tag{5.41}$$

At stationarity

$$|\nabla_x\phi| = \frac{2\cos\theta}{c(\boldsymbol{x})} \tag{5.42}$$

so that equation (5.41) can be written as

$$\beta(\boldsymbol{x}, t=0) \sim \mathrm{Re}\,|\nabla_x\phi(\boldsymbol{x},\boldsymbol{\xi}_0)|\, R(\boldsymbol{x},\boldsymbol{x}_s)\ \triangle\left(\phi(\boldsymbol{x},\boldsymbol{\xi}_0) - \tau_R(\boldsymbol{\xi}_0)\right). \tag{5.43}$$

Since, for the leading order approximation, we need the reflection coefficient $R(\boldsymbol{x},\boldsymbol{x}_s)$ to be real, we have that

$$\beta(\boldsymbol{x}, t=0) \sim |\nabla_x\phi(\boldsymbol{x},\boldsymbol{\xi}_0)| R(\boldsymbol{x},\boldsymbol{x}_s)\,\delta(\phi(\boldsymbol{x},\boldsymbol{\xi}_0) - \tau_R(\boldsymbol{\xi}_0)), \tag{5.44}$$

and using equation (5.18) one finds

$$\beta(\boldsymbol{x}) \sim R(\boldsymbol{x},\boldsymbol{x}_s)\,\gamma(\boldsymbol{x}). \tag{5.45}$$

This is the asymptotic approximation of the reflectivity function derived in Bleistein (1987).

[2] This is their equation (24). We identify Φ with H_{DS}. I want to remark that Tygel et al. left the term $\cos\beta_R$ out when coming from their equation (19a). I made the appropriate correction here.

Chapter 6

SEISMIC DATA MAPPING

6.1 Introduction

Here I give a precise mathematical definition of the SDM operator along with a simplified form obtained from the use of the method of stationary phase.

By defining SDM as a cascade of migration and demigration I am defining a process that takes seismic data from any prescribed source/receiver configuration and model parameters to data that would be collected under a different source/receiver configuration and/or model parameters. Processes such as offset continuation (and in particular TZO), re–datuming, transformation of P–SV mode–converted data to P–P data, AMO, any combination of the previous processes, can be seen as examples of SDM. SDM is an extension of the technique described by Hubral et al. (1996) as Configuration Transform (CT).

The space of SDM operators has a well defined algebraic structure. Given that demigration is the (asymptotic) inverse of prestack migration I find that the composition (cascade) of two SDM operators is another SDM operator, the inverse of an SDM operator is an SDM operator and the identity[1] function is an SDM operator (resulting from cascading prestack migration and demigration without changes in the model). These properties show that space of SDM operators has the algebraic structure of a group.

The mathematical formula of an SDM operator, based on the cascaded of a migration with a demigration operator represents a four–fold integral. This formula is collapsed to a two–fold integral (integral over a surface) operator by the use of the method of stationary phase. The simplified operator is of the type of Kirchhoff migration operator, but with smaller aperture. I compare my SDM formula with the CT formula derived by Tygel et al. (1996). Both formulas agree in their common domain of application. I do the analysis in terms of curvatures of the input and output configuration isochrons, and finally develop a simplified formula in terms of second derivatives of the stacking path (geometrical locus of the inverse impulse response for the SDM operator) and the Huygens diffraction surfaces.

[1] The identity distribution is a delta function with zero lag. Due to band–limiting issues I associate the identity with a sinc function.

As a direct application of the SDM operator I develop an analytic formulation of TZO in a depth–dependent linear velocity medium.

6.2 The chained operator

Here I will derive an expression for the SDM operator, as a composition of the demigration and the migration operator.

In order to apply the time–domain stationary phase method, we need to rewrite the normal derivative of the migration operator (4.14) in terms the time derivative $\partial/\partial t$.

I start from equations (5.18) and (5.45), so

$$\beta(\boldsymbol{x}) = R(\boldsymbol{x},\boldsymbol{x}_s)\,\delta(t-\tau_R)\,|\nabla_x\phi|\,\Big|_{t=\phi}. \tag{6.1}$$

Now from (5.19) one finds

$$\frac{\partial\beta(\boldsymbol{x})}{\partial n} \sim -R(\boldsymbol{x},\boldsymbol{x}_s)\,\delta'(\phi-\tau_R)\,|\nabla_x\phi|^2 \sim -|\nabla_x\phi|\,\frac{\partial}{\partial t}\beta(\boldsymbol{x})\Big|_{t=\phi}. \tag{6.2}$$

Let us now rewrite the migration operator (4.14):

$$\beta(\boldsymbol{x}) \sim -\mathrm{Re}\,\frac{1}{4\pi^2}\int d\boldsymbol{\xi}\,\frac{h_B(\boldsymbol{x},\boldsymbol{\xi})}{a(\boldsymbol{x},\boldsymbol{\xi})\,|\nabla_x\phi(\boldsymbol{x},\boldsymbol{\xi})|}\frac{\partial}{\partial t}D(\boldsymbol{\xi},t)*\triangle(t)\Big|_{t=\phi(\boldsymbol{x},\boldsymbol{\xi})}, \tag{6.3}$$

so that

$$\frac{\partial}{\partial t}\beta(\boldsymbol{x}) \sim -\mathrm{Re}\frac{1}{4\pi^2}\int d\boldsymbol{\xi}\,\frac{h_B(\boldsymbol{x},\boldsymbol{\xi})}{a(\boldsymbol{x},\boldsymbol{\xi})\,|\nabla_x\phi(\boldsymbol{x},\boldsymbol{\xi})|}\,\frac{\partial^2}{\partial t^2}D(\boldsymbol{\xi},t)*\triangle(t)\Big|_{t=\phi(\boldsymbol{x},\boldsymbol{\xi})}, \tag{6.4}$$

where the partial derivative operator was introduced under the integral sign and only the leading asymptotic term retained.

The demigration operator (3.40), after introducing equation (6.2) becomes

$$D(\tilde{\xi},\tilde{t}) \sim -\mathrm{Re}\int d\Sigma_0\,\tilde{a}(\boldsymbol{x},\tilde{\boldsymbol{\xi}})\,\frac{\partial\beta(\boldsymbol{x})}{\partial t}\Big|_{\tilde{t}=\tilde{\phi}(\boldsymbol{x},\tilde{\boldsymbol{\xi}})} * \triangle(t). \tag{6.5}$$

Note that I introduced the tilde character to indicate output variables since they will play that role in the SDM chained operator. Here, Σ_0 is the output configuration isochron. I parameterize the output isochron as $\Sigma_0(\sigma_1,\sigma_2)$ in the following way:

$$\Sigma_0 = \left\{\boldsymbol{x}(\boldsymbol{\sigma}) : \tilde{t} = \tilde{\phi}(\boldsymbol{x}(\boldsymbol{\sigma}),\tilde{\boldsymbol{\xi}})\right\}, \tag{6.6}$$

where $\boldsymbol{x}(\boldsymbol{\sigma}) = (x(\sigma_1, \sigma_2), y(\sigma_1, \sigma_2), z(\sigma_1, \sigma_2))$. I then rewrite equation (6.5) as

$$D(\tilde{\boldsymbol{\xi}}, \tilde{t}) \sim -\mathrm{Re} \int d\boldsymbol{\sigma}\, \sqrt{g}\, \tilde{a}(\boldsymbol{x}, \tilde{\boldsymbol{\xi}})\, \frac{\partial \beta(\boldsymbol{x}, \boldsymbol{x}_S)}{\partial t} \Big|_{\tilde{t}=\tilde{\phi}(\boldsymbol{x}, \tilde{\boldsymbol{\xi}})} * \triangle(\tilde{t}), \tag{6.7}$$

where $\sqrt{g}$ is the metric correction associated with the parameterization of the surface Σ_0 in terms of the two dimensional vector $\boldsymbol{\sigma}$.

The chained operator is obtained by substituting equation (6.4) into equation (6.7). This results in

$$\begin{aligned} D(\tilde{\boldsymbol{\xi}}, \tilde{t}) \;\sim\; & \mathrm{Re} \frac{1}{4\pi^2} \int d\boldsymbol{\sigma}\, \sqrt{g}\, \tilde{a}(\boldsymbol{x}, \tilde{\boldsymbol{\xi}}) \\ & \times \int d\boldsymbol{\xi}\, \frac{h_B(\boldsymbol{x}, \boldsymbol{\xi})}{a(\boldsymbol{x}, \boldsymbol{\xi}) |\nabla_x \phi(\boldsymbol{x}, \boldsymbol{\xi})|} \frac{\partial^2}{\partial t^2} D(\boldsymbol{\xi}, t) * \triangle(t) \Big|_{t=\phi(\boldsymbol{x}, \boldsymbol{\xi})} \Big|_{\tilde{t}=\tilde{\phi}(\boldsymbol{x}, \tilde{\boldsymbol{\xi}})} * \triangle(\tilde{t}) \end{aligned} \tag{6.8}$$

This is a four–fold integral that maps input data $D(\boldsymbol{\xi}, t)$ into output data $D(\tilde{\boldsymbol{\xi}}, \tilde{t})$. That explains the name Seismic Data Mapping (SDM). I want to simplify this operator by using the method of stationary phase on the integration over $\boldsymbol{\sigma}$; that is, on the integral over the output isochron surface Σ_0.

6.3 Stationary phase analysis

In this section I find the leading–order asymptotic approximation of the SDM operator.

The analytic zero–order asymptotic analytic ray data can be represented as

$$D(\boldsymbol{\xi}, t) * \triangle(t) \sim A_0(\boldsymbol{\xi})\, \triangle\left(t - \tau_R(\boldsymbol{\xi})\right) \tag{6.9}$$

where the amplitude and phase terms A_0 and $\tau_R(\boldsymbol{\xi})$ are shown in equation (5.30). By using these analytical data in the chained operator (6.8) and interchanging the order of integration one obtains

$$D(\tilde{\boldsymbol{\xi}}, \tilde{t}) \sim \mathrm{Re} \int d\boldsymbol{\xi}\, A_0(\boldsymbol{\xi}) \int d\boldsymbol{\sigma}\; w_{CC}(\boldsymbol{x}, \boldsymbol{\xi}, \tilde{\boldsymbol{\xi}})\; \triangle''\left(\phi(\boldsymbol{x}, \boldsymbol{\xi}) - \tau_R(\boldsymbol{\xi})\right) \Big|_{\tilde{t}=\tilde{\phi}(\boldsymbol{x}, \tilde{\boldsymbol{\xi}})}, \tag{6.10}$$

where the cascaded weight w_{CC} is given by

$$w_{CC}(\boldsymbol{x}, \boldsymbol{\xi}, \tilde{\boldsymbol{\xi}}) = \frac{1}{4\pi^2} \sqrt{g}\, \frac{\tilde{a}(\boldsymbol{x}, \tilde{\boldsymbol{\xi}})}{a(\boldsymbol{x}, \boldsymbol{\xi})}\, \frac{h_B(\boldsymbol{x}, \boldsymbol{\xi})}{|\nabla_x \phi(\boldsymbol{x}, \boldsymbol{\xi})|}. \tag{6.11}$$

At this point we recognize that the inner integral in equation (6.10) is an isochron stack over the output isochron. I will apply the stationary phase formula (5.7) to this

inner integral. The stationary phase conditions are given by

$$\frac{\partial}{\partial \sigma_i}\left[\phi(\boldsymbol{x}(\boldsymbol{\sigma}),\boldsymbol{\xi}) - \tau_R(\boldsymbol{\xi})\right] = \frac{\partial \phi(\boldsymbol{x}(\boldsymbol{\sigma}),\boldsymbol{\xi})}{\partial \sigma_i} = \frac{\partial \phi(\boldsymbol{x},\boldsymbol{\xi})}{\partial x_j}\frac{\partial \tilde{x}_j(\boldsymbol{\sigma})}{\partial \sigma_i} = 0, \quad i = 1,2, \tag{6.12}$$

where the tilde character in x_j is just to emphasize that the derivative is taking over the output isochron. Here, I assume summation over the repeated indices. The point, $\boldsymbol{\sigma} = \boldsymbol{\sigma}_0$, such that equation (6.12) is satisfied, is the stationary point. I assume that there exists one stationary point. It was showed in Chapter 5 that this assumption is violated in some simple (and important) cases. I also show below examples where this assumption is violated. Formula (6.12) tells us that, at the stationary point, the source–scatterer–receiver vector $(\nabla_x \phi)$ [2] is perpendicular to the output isochron tangent plane. This means that the corresponding source–scatterer-receiver ray represents a specular reflection on the isochron; in other words, it satisfies Snell's law along any reflector tangent to the isochron. Figure 6.1 illustrates this. The interpretation of the stationary phase condition is then that the point $\boldsymbol{x}(\boldsymbol{\sigma}_0) = \boldsymbol{x}_0(\tilde{\boldsymbol{\xi}},\tilde{t})$ belongs to the output configuration [3] isochron and serves as a specular reflection point determined by the parameter $\boldsymbol{\xi}$ in the input configuration. That is, the triplet $(\boldsymbol{x}_s(\boldsymbol{\xi}), \boldsymbol{x}_0(\tilde{\boldsymbol{\xi}},\tilde{t}), \boldsymbol{x}_g(\boldsymbol{\xi}))$ represents a source–reflector–receiver specular ray on the output isochron. I then define the mapping:

$$\begin{aligned} \boldsymbol{x}_0(\tilde{\boldsymbol{\xi}},\tilde{t}) : \mathrm{S} \subseteq \mathbb{R}^2 &\longrightarrow \mathbb{R}^3 \\ \boldsymbol{\xi} &\longmapsto \boldsymbol{x}_0(\tilde{\boldsymbol{\xi}},\tilde{t})(\boldsymbol{\xi}), \end{aligned} \tag{6.13}$$

where S is the set of all unique parameters $\boldsymbol{\xi}$ such that $\boldsymbol{x}_0(\tilde{\boldsymbol{\xi}},\tilde{t})$ is a specular reflection point in the output isochron defined by the equation $\tilde{t} = \tilde{\phi}(\boldsymbol{x},\tilde{\boldsymbol{\xi}})$. This specular reflection is identified with the triplet $(\boldsymbol{x}_s(\boldsymbol{\xi}), \boldsymbol{x}_0(\tilde{\boldsymbol{\xi}},\tilde{t}), \boldsymbol{x}_g(\boldsymbol{\xi}))$. S is then the domain of integration of the SDM stack operator. I can then justify the representation $\boldsymbol{x}_0 = \boldsymbol{x}_0(\boldsymbol{\xi},\tilde{\boldsymbol{\xi}},\tilde{t})$. This physical interpretation of the stationary phase condition (6.12) gives us an algorithm to compute the SDM stacking surface (support of the SDM stacking operator). The SDM stacking surface is the locus of all (input) points $(t,\boldsymbol{\xi})$ corresponding to specular reflections in the output isochron. In other words, to compute the SDM stacking surface, we need to do a ray tracing to the output configuration isochron with the input recording configuration. The mathematical definition of the SDM stacking surface is given by:

$$\Sigma_{SDM} = \left\{(t,\boldsymbol{\xi}) \mid t = \tau_s(\boldsymbol{x}_s(\boldsymbol{\xi}), \boldsymbol{x}_0(\boldsymbol{\xi},\tilde{\boldsymbol{\xi}},\tilde{t})) \div \tau_g(\boldsymbol{x}_g(\boldsymbol{\xi}), \boldsymbol{x}_0(\boldsymbol{\xi},\tilde{\boldsymbol{\xi}},\tilde{t}))\right\}, \tag{6.14}$$

where τ_s and τ_g are the traveltimes from the source and receiver positions to the point $\boldsymbol{x}_0$, respectively. Figure 6.3 show the inline portion of the stacking surface for the case of a TZO experiment in constant velocity. This curve is constructed as the envelope of Huygens curves corresponding to points in the output configuration isochron.

[2] This is the sum of the slowness vector from the source and the slowness vector from the receiver.

[3] Here the output (input) configuration means both output (input) recording configuration and output (input) model parameters.

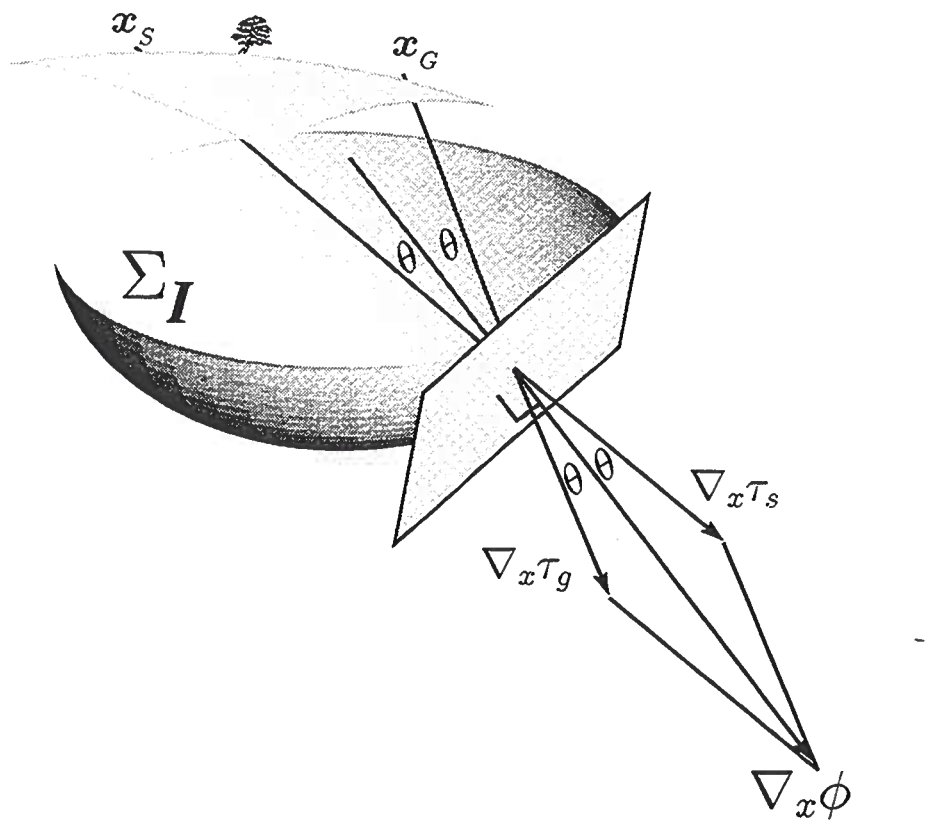

FIG. 6.1. Here I illustrate how the stationary phase condition implies Snell's law. The stationary phase condition requires that the slowness vector $\nabla_x \phi$ be perpendicular to the tangent reflector. Now the angles that this slowness vector makes with the source and receiver slowness vectors are equal to θ. This is because both, the source and receiver, vectors have the same magnitude of $1/c(\boldsymbol{x})$, where $c(\boldsymbol{x})$ is the wavespeed at the reflecting point.

Kinematically speaking, the SDM could be numerically implemented as a Kirchhoff prestack migration algorithm where the diffraction surfaces are replaced by the SDM stacks defined in equation (6.14). To have the dynamics right, we should proceed further with the stationary phase analysis. I apply the stationary phase formula (5.7) to the inner integral in equation (6.10) and find

$$D(\tilde{\xi},\tilde{t}) \sim \text{Re} \int d\xi \; w_{SDM}(\xi,\tilde{\xi},\tilde{t}) \; A_0(\xi) \; \Delta' \left(\phi_{SDM}(\xi,\tilde{\xi},\tilde{t}) - \tau_R(\xi)\right), \tag{6.15}$$

where

$$w_{SDM}(\xi,\tilde{\xi},\tilde{t}) = -2\pi \, w_{CC}\left(\boldsymbol{x}_0(\xi,\tilde{\xi},\tilde{t}) \, , \, \xi \right) \frac{e^{\frac{i\pi}{2}(1+\text{sgn}(\Phi)/2)}}{\sqrt{|\det \Phi(\xi,\tilde{\xi},\tilde{t})|}}, \tag{6.16}$$

$$\phi_{SDM}(\xi,\tilde{\xi},\tilde{t}) = \phi\,(\,\boldsymbol{x}_0(\xi,\tilde{\xi},\tilde{t})\,,\,\xi\,), \tag{6.17}$$

and

$$\Phi(\xi,\tilde{\xi},\tilde{t}) = \left(\frac{\partial^2\phi(\boldsymbol{x}(\sigma),\xi)}{\partial\sigma_i\sigma_j}\right)\Bigg|_{\boldsymbol{x}=\boldsymbol{x}_0(\xi,\tilde{\xi},\tilde{t})}. \tag{6.18}$$

Now, equation (6.15) can be written as

$$D(\tilde{\xi},\tilde{t}) \sim \mathrm{Re}\int d\xi\;\; w_{SDM}(\xi,\tilde{\xi},\tilde{t})\,\frac{\partial}{\partial t}\,D(\xi,t)*\triangle(t)\Big|_{t=\phi_{SDM}(\xi,\tilde{\xi},\tilde{t})}, \tag{6.19}$$

where the real part of the complex integral evaluation is taken to be consistent with the physics of the problem. The weight w_{SDM} is a compound of many factors that relate the input data with the output data. These factors include the following: geometrical spreading factors from both input and output configurations (a,$\tilde{a}$), Beylkin determinant h and stretching factors (g) that come with the particular chosen parameterization. The factors that arise from the stationary phase analysis (Φ and $\mathrm{sgn}(\Phi)$) account for ray caustics at the reflector interface and the difference in isochron curvatures that are part of the Fresnel geometrical–spreading factor (Tygel *et al.*, 1995).

Discussion

In the same way that I computed the impulse responses for the demigration and migration operators I could compute the impulse response for the SDM stack operator here. Once that impulse response is computed we can again apply the superposition principle to find a different representation of the SDM operator that we can call the SDM superposition operator. While the SDM stack operator can be constructed by ray–tracing to the output isochron with the input configuration, the SDM superposition operator can be constructed by ray–tracing to the input isochron with the output isochron configuration. Claerbout (1985) shows how Rocca's DMO operator is constructed exactly in this way. That is, the DMO superposition operator is found by doing zero–offset ray tracing (output recording configuration) into a finite–offset isochron (input isochron). Let me mention that Hubral et al. (1996) use the word, "inplanat", for a stack–type operator in their CT problem. My guess is that the reason for this word is that the operator belongs to the input data space. In a similar fashion the word, "outplanat", in the above reference, means a superposition–type operator in a CT problem. (This operator belongs to the output data space). I would like to borrow these terms to describe any stack–type [4] operators and any superposition–type operators [5].

[4]Generalized Radon transform–like operators. They are integrals over an $n-1$ dimensional surface in the input data space.

[5]Superposition integrals. They are volume integrals in the n–dimensional output data space.

6.4 Relation between the Hessian matrix Φ, and the curvature of the difference between the output and input isochrons

The determinant of the Hessian matrix Φ as it is defined here is of little utility both from the analytical and from the numerical point of view. I want to transform this determinant into a more useful expression, both from the computational and from the theoretical point of view. The first step is to transform the determinant of the Hessian matrix Φ into an expression in terms of the Gaussian curvature (Laugwitz, 1965) of the difference of the output and the input isochron surfaces. This expression not only tells us more about the physics of the problem but becomes handy for analytical computations. In a latter section, this Gaussian curvature is used to compute the weights that will go into a 3D TZO operator for the case of a medium with linear velocity distribution with depth. A second step is to transform the Gaussian curvature of the difference between the output and input isochrons into a second derivative matrix between the difference of the stacking surface S and the Huygens diffraction surface tangent to S at the stationary phase point $\boldsymbol{x}_0$.

In Appendix D, I show that

$$\det \Phi = |\nabla_x \phi|^2 K. \tag{6.20}$$

where K is the Gaussian curvature of the difference between the output and the input isochrons. I find also that If L_{ij} is the second fundamental tensor for the difference between the output and input configuration isochron surfaces, then $\operatorname{sgn} \Phi = \operatorname{sgn} L_{ij}$. The reader is referred to appendix D and Laugwitz (1965) for the description of the Gaussian curvature and the second fundamental tensor of a given surface.

I now re–write the weight w_{SDM} in terms of the Gaussian curvature K of the difference between the output and input configuration isochron surfaces. This turns out to be

$$w_{SDM}(\xi, \tilde{\xi}, \tilde{t}) = -\frac{1}{2\pi} \frac{\tilde{a}(\boldsymbol{x}, \tilde{\boldsymbol{\xi}})}{a(\boldsymbol{x}, \boldsymbol{\xi})} \frac{h_B(\boldsymbol{x}, \boldsymbol{\xi})}{|\nabla_x \phi(\boldsymbol{x}, \boldsymbol{\xi})|^2 \sqrt{|K|}} e^{\frac{i\pi}{2}(1 - \operatorname{sgn}(L_{ij})/2)}. \tag{6.21}$$

Appendix D also shows that this weight is independent of any coordinate system used in the representation of the isochron surfaces.

Figure 6.2 shows an illustration, for the differences of curvature, in the case of a TZO experiment in constant velocity. For simplicity only the inline direction is shown. The output isochron is a circle and the input isochrons at each point of the circle are ellipses. The square root of the positive difference of curvature between the circles and the ellipses at each point of the circle is reciprocal to the amplitude. We now are prepared to derive an alternative representation of the weight w_{SDM}, which simplifies the numerical computations of the SDM operator. This simplification can be obtained using a formula derived by Tygel et al. (1995).

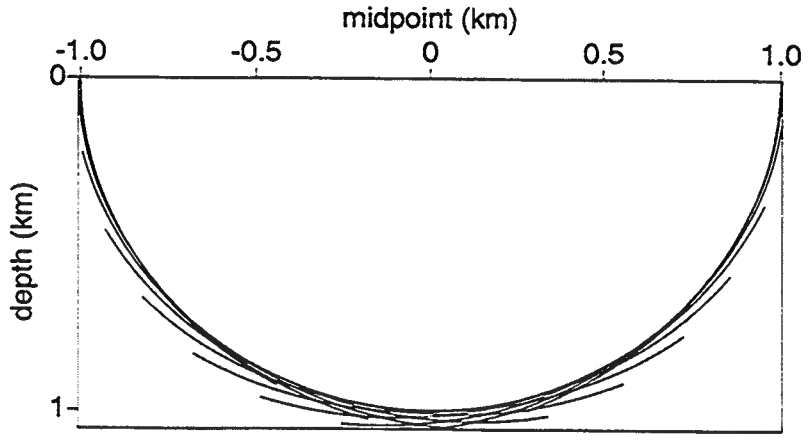

FIG. 6.2. The inline output isochron for a TZO experiment in a constant velocity medium is a circle. The inline input isochrons for the same experiment are ellipses. The stationary phase condition requires that those ellipses be tangent to the input output isochron (circle). The square root of the absolute value difference of curvatures between output and input isochrons is reciprocal to the TZO weigth.

Let us begin. I consider the Hessian matrices $\boldsymbol{H}_D$ and $\boldsymbol{H}_R$ defined by

$$\boldsymbol{H}_D = \left[\frac{\partial^2 \phi}{\partial \xi_i \, \partial \xi_j} \right], \tag{6.22}$$

and

$$\boldsymbol{H}_R = \left[\frac{\partial^2 \phi_{SDM}}{\partial \xi_i \, \partial \xi_j} \right]. \tag{6.23}$$

$\boldsymbol{H}_D$ represents a matrix of second derivatives of the diffraction time surface. More specifically, this diffraction surface is the support of the data generated by a scatter located at the stationary phase point, using the input configuration geometry. $\boldsymbol{H}_R$ is a matrix of second derivatives of the time in the SDM stacking surface defined by equation 6.14.

Tygel et al. (1995) (equations 25a and 25b) showed that the determinant of the difference between these two matrices is related to the Gaussian curvature K by the formula

$$\det(\boldsymbol{H}_D - \boldsymbol{H}_R) = - \left[\frac{c(\boldsymbol{x}_0)}{2 \cos\theta} \right]^4 \frac{h_B^2}{K}, \tag{6.24}$$

and

$$\operatorname{sgn}(\boldsymbol{H}_D - \boldsymbol{H}_R) = -\operatorname{sgn}(\Phi). \tag{6.25}$$

Here, $\boldsymbol{x}_0$ is the stationary phase point and θ is half the angle between the source and receiver rays at $\boldsymbol{x}_0$. Using equations (6.24) and (6.25) in (6.21) yields

$$w_{SDM}(\xi, \tilde{\xi}, \tilde{t}) = \frac{1}{2\pi} \frac{\tilde{a}(\boldsymbol{x}, \tilde{\xi})}{a(\boldsymbol{x}, \xi)} \sqrt{|\det(\boldsymbol{H}_D - \boldsymbol{H}_R)|}\, e^{\frac{i\pi}{2}(1-\operatorname{sgn}(\boldsymbol{H}_D - \boldsymbol{H}_R)/2)}. \tag{6.26}$$

This representation of the SDM weight is desirable for numerical computations. The weight is more simplified than the representation 6.21, also the matrix $\boldsymbol{H}_R$ can be computed directly from the SDM stacking surface that is computed as a first step in the evaluation of the SDM output. The matrix $\boldsymbol{H}_D$ should be computed from raytracing traveltime tables. The representation 6.21 is good for theoretical purposes. For example, while there is not an analytical expression for the SDM stacking surface, in the case of TZO for a model with linear velocity gradient with depth, there are analytical expressions for the both the zero–offset and the finite–offset isochrons.

Figure 6.3 shows an illustration, for the differences of second derivative matrices, in the case of a TZO experiment in constant velocity. For simplicity only the inline direction is shown. The sets of Huygens diffraction curves are the double root equations for each of the points on the input isochron. The envelope of these curves is the the stationary phase path. I integrate along that path. The Square root of the positive difference of second derivatives between this stacking path and the Huygens diffraction curves is (asymptotically) proportional to the SDM amplitude. Figure 6.4 shows a construction of the inline stacking path for the same experiment of Figure 6.3 but this time with band–limited signals.

6.5 Some special cases of input data

The SDM weight w_{SDM}, in equation(6.21), admits some simplifications in some particular input geometries. I give some examples below.

6.5.1 Common–shot (receiver) gather

For a common–shot gather, Bleistein et al. (1996) showed that

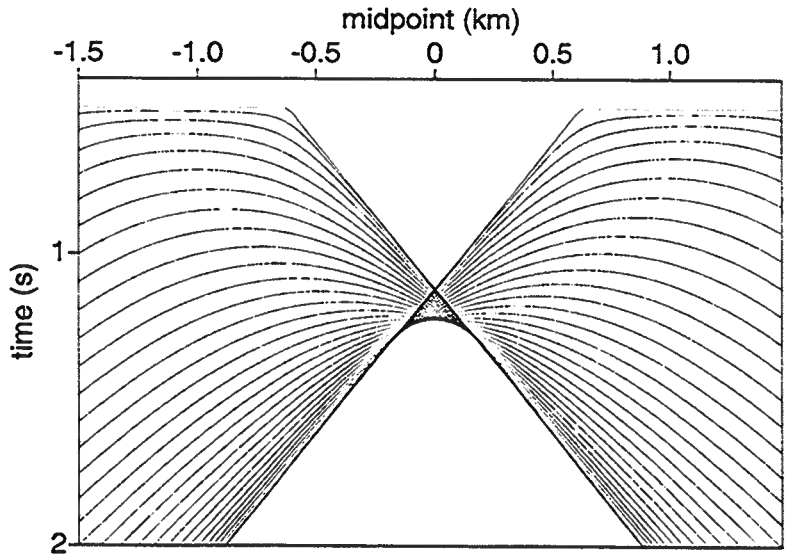

FIG. 6.3. Huygens diffractions (double square root paths) corresponding to the points of tangency between the circle and the ellipses in figure 6.2. The envelope corresponds to the stationary phase path (or surface for a full 3D experiment). The square root of the positive difference between the second derivatives of these paths and the envelope is proportional to the weigth of the SDM operator.

$$h_B(\boldsymbol{x},\boldsymbol{\xi}) = 2\cos^2\theta \ \det \begin{bmatrix} \boldsymbol{p}_g \\ \dfrac{\partial \boldsymbol{p}_g}{\partial \xi_1} \\ \dfrac{\partial \boldsymbol{p}_g}{\partial \xi_2} \end{bmatrix} \equiv 2\cos^2\theta \ h_g(\boldsymbol{x},\boldsymbol{\xi}). \tag{6.27}$$

Here $\boldsymbol{p}_g(\boldsymbol{x},\boldsymbol{\xi}) = \nabla_x \tau_g(\boldsymbol{x},\boldsymbol{\xi})$, and θ is the half angle between the source and receiver rays at $\boldsymbol{x}$. Now, given that $|\nabla_x \phi(\boldsymbol{x},\boldsymbol{\xi})|^2 = 4\cos^2\theta/c^2(\boldsymbol{x})$, one obtains for (6.21) the more simplified weight

$$w_{SDM}(\boldsymbol{\xi},\tilde{\boldsymbol{\xi}},\tilde{t}) = -\frac{1}{4\pi}\ \frac{\tilde{a}(\boldsymbol{x},\tilde{\boldsymbol{\xi}})}{a(\boldsymbol{x},\boldsymbol{\xi})}\ \frac{c^2(\boldsymbol{x})\ h_g(\boldsymbol{x},\boldsymbol{\xi})}{\sqrt{|K|}}\ e^{\frac{i\pi}{2}(1-\mathrm{sgn}(L_{ij})/2}. \tag{6.28}$$

For the common–receiver configuration, the mathematics is the same, but all subscripts "$_g$" (for receiver) should be replace with subscripts "$_s$" (for source).

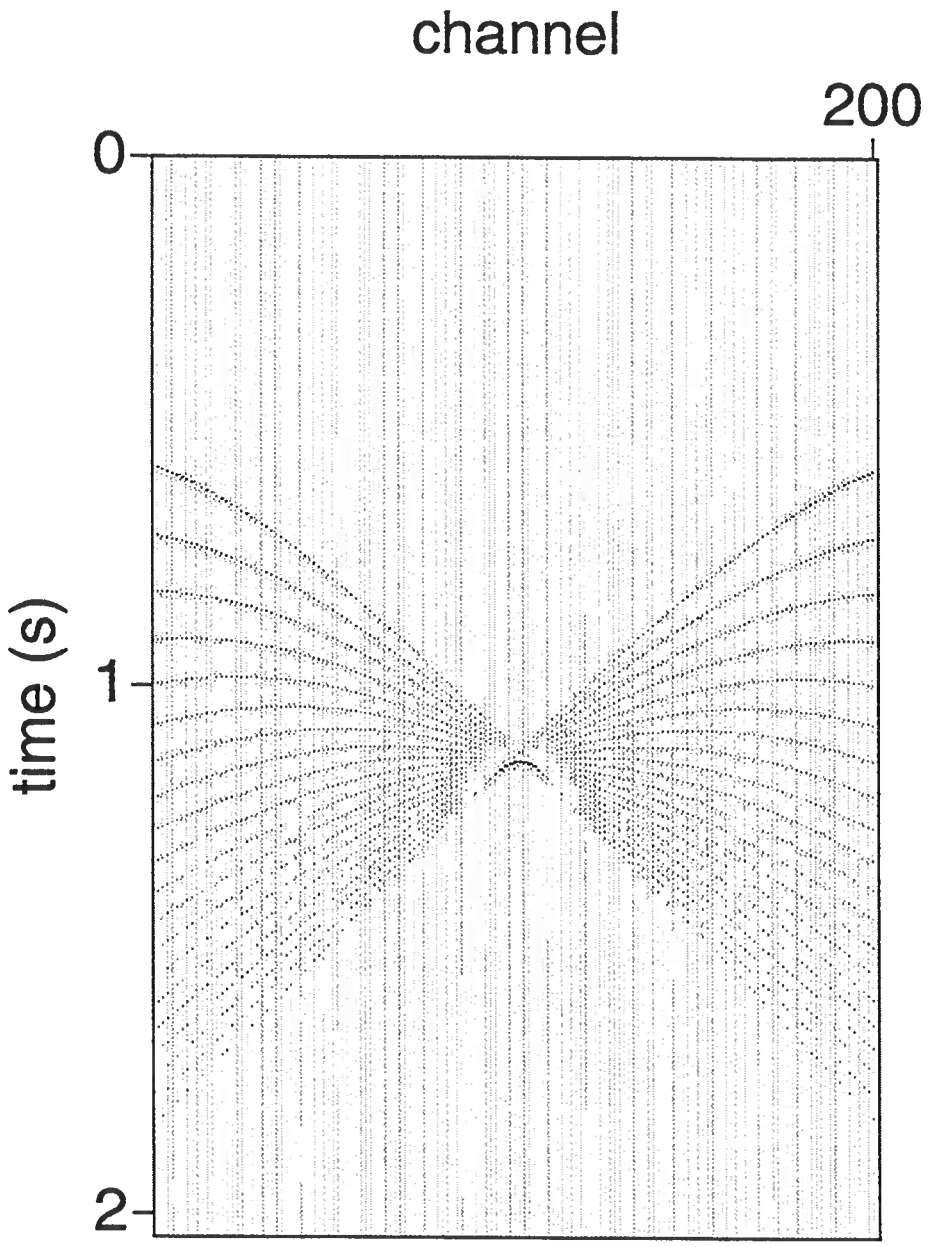

FIG. 6.4. The superposition of many Huygens diffraction curves corresponding to points along an output isochron, generate the stacking (stationary phase) path. I sampled the output configuration isochron as a set of coarsely distributed diffractors, so that the Huygens diffraction curves could be distinguished. A fine spacing of diffractors on the output configuration isochron would show only the stacking path. The stationary phase principle guarantees constructive interference along the envelope of the Huygens diffraction curves.

6.5.2 Zero–offset data

If input data are in the zero–offset domain, then $|\nabla_x \phi(\boldsymbol{x}, \boldsymbol{\xi})|^2 = 4/c^2(\boldsymbol{x})$ and

$$h_B(\boldsymbol{x}, \boldsymbol{\xi}) = 8 \det \begin{bmatrix} \boldsymbol{p} \\ \dfrac{\partial \boldsymbol{p}}{\partial \xi_1} \\ \dfrac{\partial \boldsymbol{p}}{\partial \xi_2} \end{bmatrix} \equiv 8\, h_0(\boldsymbol{x}, \boldsymbol{\xi}), \tag{6.29}$$

where $\boldsymbol{p} = \nabla_x \phi$. One then finds

$$w_{SDM}(\boldsymbol{\xi}, \tilde{\boldsymbol{\xi}}, \tilde{t}) = -\frac{1}{\pi} \frac{\tilde{a}(\boldsymbol{x}, \tilde{\boldsymbol{\xi}})}{a(\boldsymbol{x}, \boldsymbol{\xi})} \frac{c^2(\boldsymbol{x})\, h_0(\boldsymbol{x}, \boldsymbol{\xi})}{\sqrt{|K|}}\, e^{\frac{i\pi}{2}(1 \div \mathrm{sgn}(L_{ij})/2)}. \tag{6.30}$$

6.5.3 Common–offset (constant velocity c) gather

Bleistein et al. (1996) showed that for a constant velocity medium, common–offset configuration, with a flat recording surface

$$h_B(\boldsymbol{x}, \boldsymbol{\xi}) = 2 \cos^2 \theta\, \frac{z}{c^3} \left[\frac{(r_s \div r_g)\,(r_s^2 \div r_g^2)}{r_s^3\, r_g^3} \right], \qquad a(\boldsymbol{x}, \boldsymbol{\xi}) = \frac{1}{16\pi^2\, r_s\, r_g}. \tag{6.31}$$

Here $r_s = |\boldsymbol{x}_s(\boldsymbol{\xi}) - \boldsymbol{x}|$, $r_g = |\boldsymbol{x}_g(\boldsymbol{\xi}) - \boldsymbol{x}|$ are the lengths of the source and receiver rays in the input configuration respectively. The SDM weight is then transformed into

$$w_{SDM}(\boldsymbol{\xi}, \tilde{\boldsymbol{\xi}}, \tilde{t}) = -\frac{z}{64\pi^3}\; \tilde{a}(\boldsymbol{x}, \tilde{\boldsymbol{\xi}}) \left[\frac{(r_s \div r_g)\,(r_s^2 \div r_g^2)}{c\, r_s^4\, r_g^4 \sqrt{|K|}} \right] e^{\frac{i\pi}{2}(1 \div (\mathrm{sgn}(L_{ij})/2)}. \tag{6.32}$$

I will show that in the particular case of offset continuation, $K = 0$, and the stationary phase solution is not appropriate anymore. If, further, the output data correspond to a constant–velocity experiment, then

$$w_{SDM}(\boldsymbol{\xi}, \tilde{\boldsymbol{\xi}}, \tilde{t}) = -\frac{z}{4\pi}\; \tilde{r}_s \tilde{r}_g \left[\frac{(r_s \div r_g)\,(r_s^2 \div r_g^2)}{c\, r_s^4\, r_g^4 \sqrt{|K|}} \right] e^{\frac{i\pi}{2}(1 \div \mathrm{sgn}(L_{ij})/2)}. \tag{6.33}$$

Here $\tilde{r}_s = |\boldsymbol{x}_s(\tilde{\boldsymbol{\xi}}) - \boldsymbol{x}|$, $\tilde{r}_g = |\boldsymbol{x}_g(\tilde{\boldsymbol{\xi}}) - \boldsymbol{x}|$ are the lengths of the source and receiver rays in the output configuration, respectively.

6.6 Reduction to the Tygel et al. CT formula

The derivation of the weight in Tygel et al. (1996) CT formula is based on the parameterization of the input and output configuration isochrons in the form $z = z(x, y)$. Tygel et al. use then z as the preferred direction.

Thus, here I select z as the preferred direction to parameterize the input and output isochrons. This is $\tilde{z} = \tilde{z}(\tilde{\boldsymbol{\xi}}, \tilde{t}, \boldsymbol{\rho})$ and $z = z(\boldsymbol{\xi}, t, \boldsymbol{\rho})$. Here, $\boldsymbol{\rho} = (x_1, x_2) = (x, y)$.

From equations (D.1) and (D.3) it follows that the stationary phase condition is equivalent to the fact that at the stationary point $\boldsymbol{x}_0$,

$$\frac{\partial z}{\partial x} = \frac{\partial \tilde{z}}{\partial x} = -\frac{\partial \phi / \partial x}{\partial \phi / \partial z}, \tag{6.34}$$

and

$$\frac{\partial z}{\partial y} = \frac{\partial \tilde{z}}{\partial y} = -\frac{\partial \phi / \partial y}{\partial \phi / \partial z}. \tag{6.35}$$

Let us, further define the matrices Z and $\tilde{Z}$ as

$$\tilde{\boldsymbol{Z}} = \left(\frac{\partial^2 \tilde{z}(\tilde{\boldsymbol{\xi}}, \tilde{t}, \boldsymbol{\rho})}{\partial x_i x_j} \right) \quad \text{and} \quad \boldsymbol{Z} = \left(\frac{\partial^2 z(\boldsymbol{\xi}, t, \boldsymbol{\rho})}{\partial x_i x_j} \right). \tag{6.36}$$

From equation (D.9) we see that, for $\sigma_1 = x$ and $\sigma_2 = y$,

$$\sqrt{|\det \Phi_z|} = |\nabla_x \phi| \sqrt{|\det(\hat{Z} - Z)|}, \tag{6.37}$$

where I used the index z to denote that we are looking the surface in a horizontal (xy) plane.

After using equation (D.18), in the coordinates $x, y, z(x, y)$ one can write [6]

$$|\nabla_x \phi| \sqrt{|\det(\hat{Z} - Z)|} = \sqrt{g\,|\det \Phi|}. \tag{6.38}$$

[6] Note that equation (D.18) was derived by assuming that the coordinates σ_1 and σ_2 were sitting on the common-tangent plane to the input and output configuration isochrons at the stationary phase point. However, thanks to equations (6.34) and (6.35), this equation also applies for those coordinates sitting in a horizontal plane. What makes the difference between the two different parameterizations is the factor g_d that comes later in that process.

Then by using equation (D.14), where $g_d = g$ we see that

$$\sqrt{K} = \frac{\sqrt{|\det \Phi|}}{\sqrt{g\,|\nabla_x \phi|^2}} = \frac{\sqrt{|\det(\hat{Z} - Z)|}}{g} = \frac{m_D^2}{|\nabla_x \phi|^2}\sqrt{\det(\hat{Z} - Z)|}, \tag{6.39}$$

where I used the definition of $m_D = \partial\phi/\partial z$ given by equation (3.30). Substitution of equation (6.39) in equation (6.21) yields

$$w_{SDM} = -\frac{1}{2\pi}\mathcal{K}_{CT}\frac{e^{\frac{i\pi}{2}(1+\mathrm{sgn}(\tilde{Z}-Z)/2)}}{\sqrt{|\det(\tilde{Z} - Z)|}}. \tag{6.40}$$

Here I used $\mathrm{sgn}(L_{ij}) = \mathrm{sgn}(\tilde{Z} - Z)$, coming from the fact that rotation matrix does not change the signature of the operator it acts on. Also the weight $\mathcal{K}_{CT}$ is given by

$$\mathcal{K}_{CT} = \frac{\tilde{a}(\boldsymbol{x}, \tilde{\boldsymbol{\xi}})}{a(\boldsymbol{x}, \boldsymbol{\xi})}\,\frac{h_B(\boldsymbol{x}, \boldsymbol{\xi})}{m_D^2(\boldsymbol{x}, \boldsymbol{\xi})}. \tag{6.41}$$

The weight $\mathcal{K}_{CT}$ coincides with the one derived by Tygel et al. (1996). The latter is seen to be the same as the result here, except for the specific parameterizations of the two.

6.7 Offset continuation in a constant–velocity medium: An ill–posed problem?

While the SDM simplified operator seems to be a general and robust tool, it might have some deficiencies in some of its simplest uses. These deficiencies are introduced by the 2D stationary phase analysis as will be seen below. The way to get around this problem is by starting again with the full four–fold integral (6.8). In this section, I explain the problem and propose a solution.

By offset continuation, I mean a process that transforms data from one fixed offset $\boldsymbol{h} = (h_1, h_2)$ to another fixed offset $\tilde{\boldsymbol{h}} = \alpha\boldsymbol{h}$, with constant scalar α, thereby preserving the source–receiver line orientation. The case, $\alpha = 0$, represents the TZO process. We do not lose generality by assuming $h_2 = 0$. The general case of arbitrary h_2 is obtained by working in a new Cartesian coordinate system after rotating the old Cartesian coordinate system by an angle ϕ such that $\sin\phi = h_2/\sqrt{h_1^2 + h_2^2}$. Let us then parameterize the input configuration data offset vector by the single parameter h and the output configuration data offset vector by the single parameter $\tilde{h}$.

For a constant velocity isotropic medium, the source–reflector, receiver–reflector and the zero–offset rays lie in the same plane defined by the source position $\boldsymbol{x}_s$, the receiver position $\boldsymbol{x}_g$ and the reflection point $\boldsymbol{x}$. To see this, recall that the slowness vector corresponding to the zero–offset ray has the direction of sum of the slowness vectors

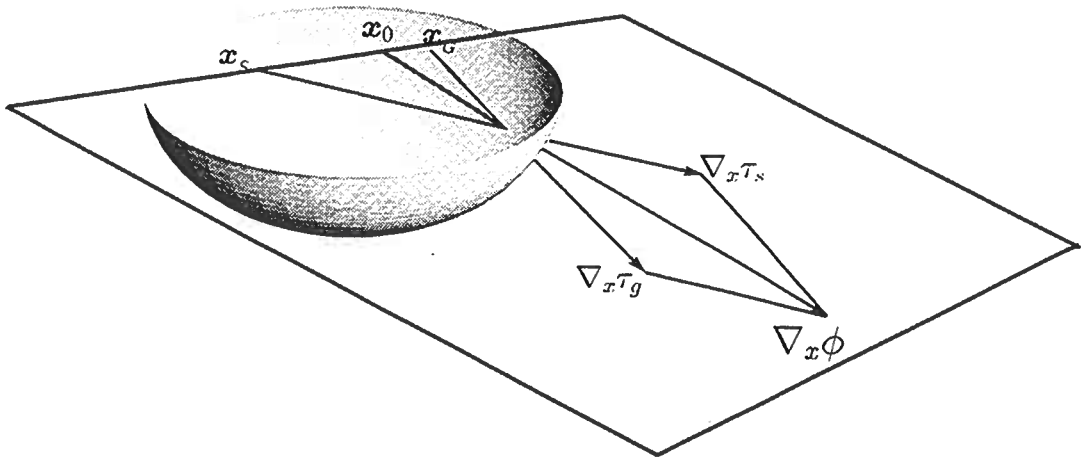

FIG. 6.5. Here the plane that contains the vectors $\boldsymbol{p}_s = \nabla_x \tau_s$ and $\boldsymbol{p}_g = \nabla_x \tau_g$ goes through the source $\boldsymbol{x}_s$, the receiver $\boldsymbol{x}_g$ and the zero–offset location $\boldsymbol{x}_0$ on the earth's surface.

from the source–reflector and receiver–reflector rays, so the slowness vectors are all in the same plane. Since the velocity is constant, all rays are straight lines in the direction of the slowness vectors. This confirms our claim. Now if we move (continue) to a different offset along the same source–receiver line, corresponding to the same surface arrival point (the zero–offset point in the surface), and reflector point $\boldsymbol{x}$, it is obvious that the rays all stay in the same plane. What I am saying is that the support (domain of definition) of the offset–continuation operator stays in the source–receiver line, which is the intersection of *all* planes, having the source, the receiver and any point $\boldsymbol{x}$ in the 3D earth model. Figure 6.5 shows a sketch of the plane that goes through the source, receiver and zero–offset locations. As shown in the figure this plane contains the source and receiver slowness vectors $\boldsymbol{p}_x$ and $\boldsymbol{p}_g$ respectively.

What I have just proved is that the offset continuation operator for a constant velocity isotropic medium is, in essence, a 2D operator with its domain of definition in the source–receiver line. This degeneration translates into lots of savings for the kinematic process, since it is a 2D instead of a 3D process. On the other hand, we have to be careful in the dynamic (amplitude computations) problem due to degeneration of the experiment by losing one dimension. Furthermore, we will see that the 2D stationary phase analysis fails due to the fact that the stationary points are not isolated. They are found along a continuous circular path, creating focusing along the cross–line direction. These facts violate the assumptions made in the previous section about the stationary phase method. This does not mean that the SDM is an unstable process. It is unstable if we do it through the method of 2D stationary phase. One special thing about stationary phase analysis, is that it enhances the specular reflections by constructive interference (a Huygens principle type process). Since the imaging algorithms that we use are based on specular reflections, we can say that, as in the

stationary phase analysis approach, we still have a 2D operator for this 3D experiment. One way to simplify this problem is by acquiring the data along the line of maximum dip. These are the type of data that Bleistein (1986) call 2.5D data. Here the data are independent of the cross–line direction, and the integration along this direction can be performed analytically. Fortunately, the demigration and migration operators do not present this instability problem (except for the special cases illustrated in Chapter 5). We can, then, reduce the 3D demigration and migration operators to 2.5D operators by using the method of stationary phase along the cross–line direction and then cascade the resulting operators to find a simplified SDM operator. This operator can be further simplified by using the 1D stationary phase method along the inline direction for the dummy variable σ_1. This is the topic of next Chapter. Here, I explain the instability of the 2D stationary–phase analysis method for the 3D SDM approach in a constant–velocity medium.

To see the problem in a quantitative way, let us define the midpoint of the input configuration as $\boldsymbol{\xi} = (\xi_1, \xi_2)$ and that of the output configuration as $\tilde{\boldsymbol{\xi}} = (\tilde{\xi}_1, \tilde{\xi}_2)$. Then

$$\boldsymbol{x}_s = (\xi_1 - h, \xi_2, 0), \boldsymbol{x}_g = (\xi_1 + h, \xi_2, 0), \tilde{\boldsymbol{x}}_s = (\tilde{\xi}_1 - \tilde{h}, \tilde{\xi}_2, 0), \tilde{\boldsymbol{x}}_g = (\tilde{\xi}_1 + \tilde{h}, \tilde{\xi}_2, 0),$$

where the tildes are used for the output configuration variables and, for simplicity, a horizontal ($z = 0$) acquisition surface is assumed. I further assume that $\boldsymbol{x}$ is the stationary phase point for the SDM problem.

Since the velocity is constant, the source and receiver slowness vectors for the input and output configurations are represented by

$$\begin{aligned} \boldsymbol{p}_s &= \lambda_s(\boldsymbol{x} - \boldsymbol{x}_s) \\ \boldsymbol{p}_g &= \lambda_g(\boldsymbol{x} - \boldsymbol{x}_g) \\ \tilde{\boldsymbol{p}}_s &= \tilde{\lambda}_s(\boldsymbol{x} - \tilde{\boldsymbol{x}}_s) \\ \tilde{\boldsymbol{p}}_g &= \tilde{\lambda}_g(\boldsymbol{x} - \tilde{\boldsymbol{x}}_g), \end{aligned} \tag{6.42}$$

where the λ's are positive scalars that depend on the corresponding ray lengths and the medium velocity c. Let us assume that there exist two planes: P_1 having the points $\boldsymbol{x}_s$, $\boldsymbol{x}$ and $\boldsymbol{x}_g$ and P_2 having the points $\tilde{\boldsymbol{x}}_s$, $\boldsymbol{x}$ and $\tilde{\boldsymbol{x}}_g$. I will prove that this cannot happen. For this purpose let us make use of two simple facts. First, since, at the stationary point $\boldsymbol{x}$, both the input and the output configuration isochrons are tangent, they share the same normal direction line; that is

$$\boldsymbol{p}_s + \boldsymbol{p}_g = \lambda\,(\tilde{\boldsymbol{p}}_s + \tilde{\boldsymbol{p}}_g), \tag{6.43}$$

for some scalar λ. Second, given that

$$\boldsymbol{x}_g - \boldsymbol{x}_s = (2\,h, 0, 0) = \frac{h}{\tilde{h}}(2\,\tilde{h}, 0, 0) = \frac{h}{\tilde{h}}(\tilde{\boldsymbol{x}}_g - \tilde{\boldsymbol{x}}_s), \tag{6.44}$$

then, by using equation (6.42) in equation (6.44) one finds

$$\frac{\boldsymbol{p}_s}{\lambda_s} - \frac{\boldsymbol{p}_g}{\lambda_g} = \frac{h}{\tilde{h}}\left[\frac{\tilde{\boldsymbol{p}}_s}{\tilde{\lambda}_s} - \frac{\tilde{\boldsymbol{p}}_g}{\tilde{\lambda}_g}\right]. \tag{6.45}$$

From equation (6.43) it follows that the vector $\boldsymbol{p}_s + \boldsymbol{p}_g$ belongs to the planes P_1 and P_2, and from equation (6.45) one can see that the vector $\boldsymbol{p}_s/\lambda_s - \boldsymbol{p}_g/\lambda_g$ also belongs to both planes P_1 and P_2. Now given that these two vectors are linearly independent (since $\lambda_s > 0$ and $\lambda_g > 0$), the two planes are coincident.

As a first consequence, one finds that $\xi_2 = \tilde{\xi}_2$ =constant, hence $d\,\xi_2 = 0$. The meaning of this result, is that a stationary phase argument in the inner part (integral over space variables) of the integral (6.10) implies degeneracy in the outer integral (integral over data coordinates).

Another complication that is present in this SDM problem is the fact that there is a continuum of stationary points along a circle in the cross–line direction. To show this, I proceed as follows.

As is well known, the finite–offset isochron for an isotropic homogeneous medium is an ellipsoid of revolution. This can be seen in the following simple manner. By definition, an isochron is a locus of points that are of equal total traveltimes to a fixed source and receiver (foci) positions. Since the velocity is constant, equal total traveltime translates into equal total distance ($v\,t$). Let us first construct the isochron in the vertical plane. This would be an ellipse with semi–axes $a = v\,t/2$ and $b = \sqrt{a^2 - h^2}$. Given that the velocity is constant, this experiment remains exactly the same under any rotation of the 3D space with respect to the source–receiver line. That means that the vertical ellipse generates an ellipsoid of revolution which is the locus of points of equal distance $v\,t$ to the fixed source, receiver (foci) points. Since the velocity is constant and the medium homogeneous, there are no multi–pathing issues, so there are not multi–sheets on this isochron. Therefore, this surface is *the* input configuration isochron. The input configuration isochron is then described, in global Cartesian coordinates, by the equation

$$\frac{(x-\xi_1)^2}{a^2} + \frac{(y-d)^2}{b^2} + \frac{z^2}{b^2} = 1, \tag{6.46}$$

or alternatively,

$$(y-d)^2 + z^2 = b^2\left[1 - \frac{(x-\xi_1)^2}{a^2}\right], \tag{6.47}$$

Here $y = d$ represents the in–line. Figure 6.6 shows the isochron computed with velocity $v = 2$ km/s, time $t = 1$ s and semi–offset $h = 0.5$ km. Only the part of geophysical interest ($z > 0$) for positive midpoints is displayed. Observe that the cross–section is a circle and for a the center midpoint this circle has radius $r = b$.

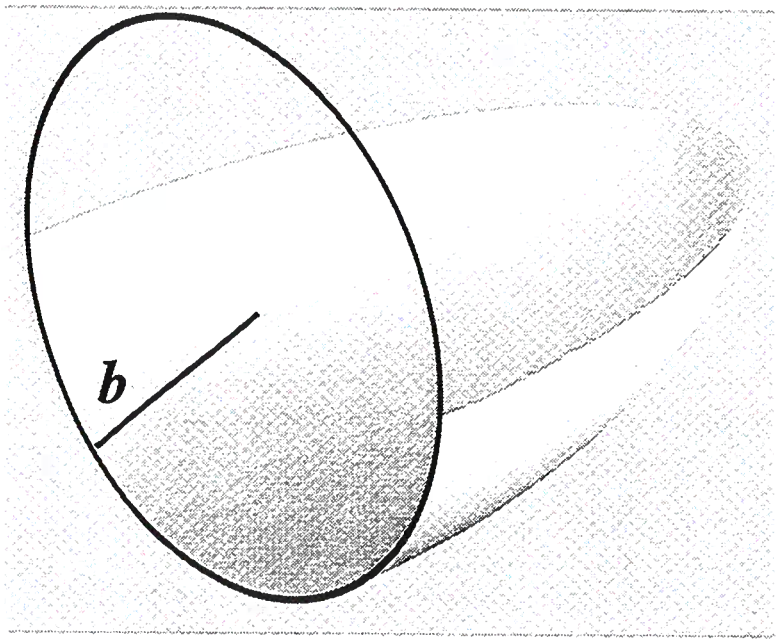

FIG. 6.6. Input isochron for a constant velocity medium $v = 2$ km/s, semi-offset $h = 1$ km and time $t = 1$ s. The cross-sections of this ellipsoid are circles. The circle for the midpoint between source and receiver has radius $r = b$.

On the other hand, the output configuration isochron is described by

$$\frac{(x-\tilde{\xi}_1)^2}{\tilde{a}^2} + \frac{(y-d)^2}{\tilde{b}^2} + \frac{z^2}{\tilde{b}^2} = 1, \tag{6.48}$$

or alternatively,

$$(y-d)^2 + z^2 = \tilde{b}^2\left[1 - \frac{(x-\tilde{\xi}_1)^2}{\tilde{a}^2}\right]. \tag{6.49}$$

Here, $\tilde{a}^2 = v^2\tilde{t}^2/4$ and $\tilde{b}^2 = \tilde{a}^2 - \tilde{h}^2$, where $\tilde{t}$ is the output time.

Let us now assume that there is an stationary point $\boldsymbol{x}_0 = (x_0, y_0, z_0)$, for the SDM (here, offset continuation) process. This would mean that for this point and from equations (6.47) and (6.49)

$$b^2\left[1 - \frac{(x_0-\xi_1)^2}{a^2}\right] = \tilde{b}^2\left[1 - \frac{(x_0-\tilde{\xi}_1)^2}{\tilde{a}^2}\right] = \sigma_0^2. \tag{6.50}$$

It is obvious that any point in the circle

$$C = \left\{(x_0, y, z) \;\middle|\; (y-d)^2 + z^2 = \sigma_0^2\right\}, \tag{6.51}$$

belongs to both the input and the output configuration isochrons. Figure 6.7 illus-

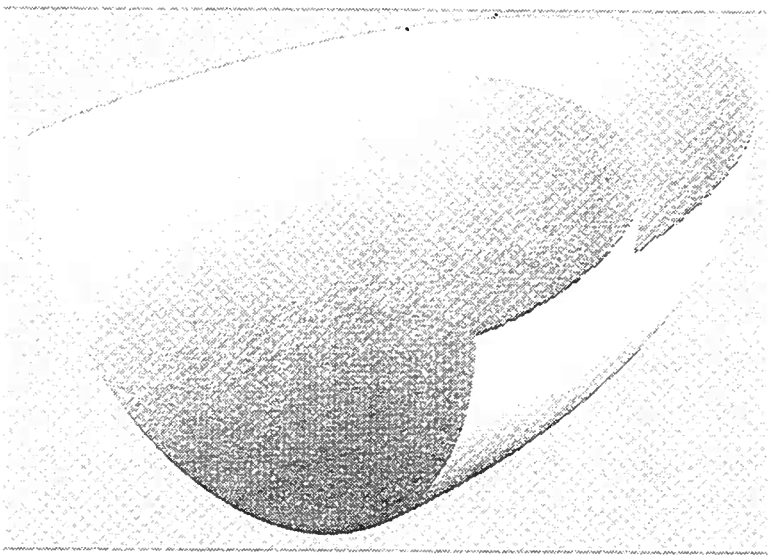

FIG. 6.7. Input (piece of ellipse) and output (piece of sphere) configuration isochrons for a horizontal reflector in a constant velocity medium with $v = 2$ km/s. The parameters semi–offset $h = 1.7$ km for the input isochron and total traveltime of $t = 2$ s were used. Observe that both isochrons have a common circle at the cutting edge $x_0 = 0$.

trates this fact for a medium with velocity $v = 2$ km/s. Here an offset of $h = 1.7$ km and a total traveltime of $t = 2$ s is assumed, also the two isochrons refer to a horizontal reflector. We observe that both isochrons share the same circle at $x_0 = 0$ (where we cut the two surfaces).

Let us now parameterize the input isochron as $z = z(x, y)$ and the output isochron as $z = \tilde{z}(x, y)$. Taking implicit partial derivatives in equations (6.47) and (6.49), yields the stationary point $\boldsymbol{x}_0$

$$\frac{\partial z}{\partial y} = -\frac{y-d}{z} \qquad \text{and} \qquad \frac{\partial \tilde{z}}{\partial y} = -\frac{y-d}{\tilde{z}}. \tag{6.52}$$

Given that $z = \tilde{z}$ along circle C, the partial derivatives with respect to the cross–line direction y agree along the circle. This is a geometrically obvious fact since, given two coincident circles, they should share the same tangent vectors. On the other hand, at the stationary point $\boldsymbol{x}_0$ one has

$$\frac{\partial z}{\partial x} = \frac{\partial \tilde{z}}{\partial x} = -\frac{b^2}{a^2}\,\frac{(x_0 - \xi_1)}{z} = -\frac{\tilde{b}^2}{\tilde{a}^2}\,\frac{(x_0 - \tilde{\xi}_1)}{\tilde{z}} = f(x_0). \tag{6.53}$$

By direct calculation it is clear that at any point of the circle C,
$\partial z/\partial x = \partial \tilde{z}/\partial x = f(x_0)$.

I have shown that the input and output configuration isochrons share the same partial

derivatives along the circle C and so, if the stationary condition is satisfied by one point ($\boldsymbol{x}_0$) on the circle C, then it is also satisfied by every point on the circle C. The physical explanation, is that if the point $\boldsymbol{x}_0$ represents a specular reflection, so any rotation of the 3D space with respect to the source–receiver line would not change the experiment (since the medium is homogeneous and isotropic). The tip of the source (receiver)–reflector ray at the point $\boldsymbol{x}_0$ is rotated, drawing the circle C. Therefore, all these points are then also specular reflection points. Figure 6.7 illustrates this facts.

In the previous chapter I mentioned that the stationary phase method, as applied here, would fail if a continuum of points satisfies the stationary phase condition. I now describe this breakdown of the method.

The weight corresponding to the problem that we are dealing with here is the one defined by equation (6.33). The only cause of instability can be produced when $K \to 0$. Let us show that this is the case here. Recall that K is the Gaussian curvature of the difference between the output and the input isochrons. I claim that, along the circle C, this difference and all its partial derivatives are zero. This means that the surface difference is flat along the cross–line (y) direction, or is of a cylindrical type. The Gaussian curvature of these type of surfaces is zero. Let us see this in a more mathematical way.

After taking implicit partial derivatives in equation (6.46) one finds that for the input configuration isochron

$$\frac{\partial^2 z}{\partial x\,\partial y} = -\frac{(\partial z/\partial x)\,(\partial z/\partial y)}{z} \tag{6.54}$$

and

$$\frac{\partial^2 z}{\partial y^2} = -\frac{1 \div (\partial z/\partial y)^2}{z}. \tag{6.55}$$

In exactly the same way, from equation (6.48) one finds

$$\frac{\partial^2 \tilde{z}}{\partial x\,\partial y} = -\frac{(\partial \tilde{z}/\partial x)\,(\partial \tilde{z}/\partial y)}{\tilde{z}}, \tag{6.56}$$

and

$$\frac{\partial^2 \tilde{z}}{\partial y^2} = -\frac{1 \div (\partial \tilde{z}/\partial y)^2}{\tilde{z}}. \tag{6.57}$$

Now, using equations (6.34) and (6.35) and the fact that at stationarity $z = \tilde{z}$ yields

$$\frac{\partial^2 (\tilde{z} - z)}{\partial x\,\partial y} = \frac{\partial^2 (\tilde{z} - z)}{\partial y\,\partial x} = 0, \tag{6.58}$$

and

$$\frac{\partial^2(\tilde{z}-z)}{\partial^2 y}=0. \tag{6.59}$$

The previous equations imply that $\det(\partial^2(z-\tilde{z})/\partial\sigma_i\partial\sigma_j)=0$. Using equation (6.39), I show that $K=0$. This completes the proof.

I found here that the simplified SDM operator, for constant velocity, have problems if the method of stationary phase to be used. Those problems are illustrated specifically for the case of offset continuation. The way to get around this problem is to integrate along the in–line direction using the stationary phase analysis and along the cross-line analytically. What we should find is that the integral along the cross-line direction should be a band–limited delta function. The reason for this is that the demigration operator smears the energy along a circular trajectory and the migration operator collapses back this energy into a point. Due to aperture limitations that point is a band–limited delta function. The amplitude of the input and output samples should asymptotically equivalent The amplitude of the input and output samples should asymptotically equivalent.

6.8 Common–shot TZO in a medium with linear velocity gradient in the vertical direction: An example.

In this section, I study the SDM weight for the case of a TZO operator in a medium with velocity function

$$c(\boldsymbol{x})=v(z)=v_0+kz, \tag{6.60}$$

where v_0 is the velocity at the earth's surface and k is the vertical velocity gradient. The input data $D(\boldsymbol{\xi},t)$ are assumed to be a $P-P$ shot gather.

Without loss of generality I can assume that the shot position is at the center of the Cartesian coordinate system ($\boldsymbol{x}_s=(0,0,0)$). For simplicity in the computations I pick the receiver at an arbitrary location $\boldsymbol{x}_r=(\xi_1,\xi_2,0)$ on a horizontal datum $z=0$. Given a fixed output point $(\tilde{\boldsymbol{\xi}},\tilde{t})$, one finds $\boldsymbol{x}_0(\boldsymbol{\xi},\tilde{\boldsymbol{\xi}},t)$ under the mapping (6.13). For convenience in notation I define $\tilde{\boldsymbol{\xi}}=\boldsymbol{\xi}_0$ and $\tilde{t}=t_0$.

The traveltime from the source $\boldsymbol{x}_s$ to any point ($\boldsymbol{x}=(x,y,z)$) in the media is given by the equation:

$$\tau_s(\boldsymbol{x}_s,\boldsymbol{x})=\frac{1}{k}\cosh^{-1}\left[\frac{k^2(x^2+y^2)+(v_0+kz)^2+v_0^2}{2\,v_0\,(v_0+kz)}\right] \tag{6.61}$$

and the traveltime from $\boldsymbol{x}_g$ to the point $\boldsymbol{x}$ is given by

$$\tau_g(\boldsymbol{x}, \boldsymbol{x}_g(\xi_1, \xi_2)) = \frac{1}{k} \cosh^{-1} \left[\frac{k^2(x-\xi_1)^2 + (y-\xi_2)^2 + (v_0 + kz)^2 + v_0^2}{2\, v_0\, (v_0 + kz)} \right], \tag{6.62}$$

(Slotnick, 1959; Dietrich & Cohen, 1993).

For the purpose of computing the TZO weight in this particular case, I will start by using the weight given by equation (6.28).

6.8.1 The geometrical–spreading factors.

I write

$$\frac{\tilde{a}(\boldsymbol{x}, \tilde{\boldsymbol{\xi}})}{a(\boldsymbol{x}, \boldsymbol{\xi})} = \frac{\mathcal{A}_s(\boldsymbol{x}, \tilde{\boldsymbol{\xi}}) \mathcal{A}_g(\boldsymbol{x}, \tilde{\boldsymbol{\xi}})}{\mathcal{L}_s(\boldsymbol{x}, \tilde{\boldsymbol{\xi}}) \mathcal{L}_g(\boldsymbol{x}, \tilde{\boldsymbol{\xi}})} \frac{\mathcal{L}_s(\boldsymbol{x}, \boldsymbol{\xi}) \mathcal{L}_g(\boldsymbol{x}, \boldsymbol{\xi})}{\mathcal{A}_s(\boldsymbol{x}, \boldsymbol{\xi}) \mathcal{A}_g(\boldsymbol{x}, \boldsymbol{\xi})}. \tag{6.63}$$

Here, $\mathcal{A}$s represent transmission losses from source (receiver) to scatter point $\boldsymbol{x}$, under the output (input) configuration, according to their corresponding notation. The $\mathcal{L}$ terms are the geometrical–spreading factors from source (receiver) to scatter point $\boldsymbol{x}$, under the output (input) configurations. For a smooth background velocity, as I have chosen here, there are no transmission losses. We then have the formula

$$\frac{\tilde{a}(\boldsymbol{x}, \tilde{\boldsymbol{\xi}})}{a(\boldsymbol{x}, \boldsymbol{\xi})} = \frac{\mathcal{L}_s(\boldsymbol{x}, \boldsymbol{\xi}) \mathcal{L}_g(\boldsymbol{x}, \boldsymbol{\xi})}{\mathcal{L}_s(\boldsymbol{x}, \tilde{\boldsymbol{\xi}}) \mathcal{L}_g(\boldsymbol{x}, \tilde{\boldsymbol{\xi}})}. \tag{6.64}$$

After making all the $\mathcal{A}$s equal to one.

Dietrich and Cohen (1993) found an expression for the right hand side of equation (6.64). This is given by their equation (33). I use their result and find

$$\frac{\tilde{a}(\boldsymbol{x}, \tilde{\boldsymbol{\xi}})}{a(\boldsymbol{x}, \boldsymbol{\xi})} = \frac{\cosh kt - \cosh k(\tau_s - \tau_g)}{\cosh kt_0 - 1}. \tag{6.65}$$

$\tau_s = \tau_s(\boldsymbol{x}_s, \boldsymbol{x})$ and $\tau_g = \tau_g(\boldsymbol{x}, \boldsymbol{x}_g(\boldsymbol{\xi}))$ are defined in equations (6.61) and (6.62) respectively. If the data are already zero–offset, then $t = t_0$, $\tau_s = \tau_g = t/2$ and the geometrical corrections reduce to unity as expected.

The geometrical correction factor for finite offset, ($k = 0$), can be computed by taking the limit of equation 6.65.

$$\frac{\tilde{a}(\boldsymbol{x}, \tilde{\boldsymbol{\xi}})}{a(\boldsymbol{x}, \boldsymbol{\xi})} = \lim_{k \to 0} \frac{\cosh kt - \cosh k(\tau_s - \tau_g)}{\cosh kt_0 - 1} \tag{6.66}$$

$$= \frac{t^2 - (\tau_s - \tau_g)^2}{t_0^2}.$$

Here, L'Hopital's rule has been applied twice. From the previous formula it is easy to see that for horizontal reflectors ($\tau_s = \tau_g$) the geometrical correction is given by the factor t^2/t_0^2. If we use the fact that $t = \tau_s + \tau_g$ and that $\tau_s = r/v_0$, $\tau_s = r_\xi/v_0$, where $r = \sqrt{x^2 + y^2 + z^2}$ and $r_\xi = \sqrt{(x-\xi_1)^2 + (y-\xi_2)^2 + z^2}$, then equation (6.66) turns out to be

$$\frac{\tilde{a}(\boldsymbol{x}, \tilde{\boldsymbol{\xi}})}{a(\boldsymbol{x}, \boldsymbol{\xi})} = \frac{r\, r_\xi}{r_0^2}. \tag{6.67}$$

Here, $r_0 = v_0 t_0/2$.

6.8.2 The Beylkin determinant.

Here one needs only compute h_g as defined in equation (6.27). After some algebra we find that:

$$h_g(\boldsymbol{x}, \boldsymbol{\xi}) = \frac{4(k r_\xi^2 + 2v_0 z)}{r_\xi^3 v (k^2 r_\xi^2 + 4v_0 v)^{\frac{3}{2}}}. \tag{6.68}$$

Again, the reduction to constant velocity is obtained by taking the limit as $k \to 0$. Taking this limit yields

$$h_g(\boldsymbol{x}, \boldsymbol{\xi}) = \frac{z}{r_\xi^3 v_0^3}. \tag{6.69}$$

6.8.3 The curvature factor

Here I present the main results about the curvature factor in the TZO operator. As we already know, the curvature factor K represents the Gaussian curvature of the difference between the output and input isochron at the stationary point $\boldsymbol{x}_0$. Here are the main facts about the curvatures. The proofs for these statements are shown in Appendix E.

- The output (zero–offset) isochron is a sphere with radius

  $$r = \hat{z}_0 \sinh(k\, t_0/2) \tag{6.70}$$

  and curvature

  $$\tilde{\kappa} = -\frac{1}{\hat{z}_0 \sinh(k\, t_0/2)}. \tag{6.71}$$

Here $\hat{z}_0 = v_0/k$.

- The input (finite–offset) isochron is given by the formula

$$z = z_I(\boldsymbol{\xi}, t, \boldsymbol{\rho}) = \sqrt{\frac{-b \div \sqrt{b^2 - 4ac}}{2a}} - \hat{z}_0, \tag{6.72}$$

where

$$a = 2\cosh k\,t - 2, \tag{6.73}$$

$$b = b(x,y) = 2\cosh k\,t\,(\rho^2 \div \rho_\xi^2 \div 2\hat{z}_0^2) - 2\,(\rho^2 \div \rho_\xi^2) - 4\,\hat{z}_0^2\,\cosh^2 k\,t, \tag{6.74}$$

$$c = c(x,y) = 2\cosh k\,t\,(\rho^2 \div \hat{z}_0^2)(\rho_\xi^2 \div \hat{z}_0^2) - (\rho^2 \div \hat{z}_0^2)^2 - (\rho_\xi^2 \div \hat{z}_0^2)^2, \tag{6.75}$$

$$\rho = \sqrt{x^2 \div y^2} \qquad \rho_\xi = \sqrt{(x-\xi_1)^2 \div (y-\xi_2)^2} \tag{6.76}$$

and $\boldsymbol{\rho} = (x, y)$.

- The Gaussian curvature of the difference between the output and input configuration isochrons is given by

$$K = \tilde{K} - 2\,H\tilde{\kappa} \div K_I, \tag{6.77}$$

where

$$\begin{aligned}
\tilde{K} &= \tilde{\kappa}^2 \\
2\,H &= \frac{(1 \div z_{,1}{}^2)\,z_{,22} - 2\,z_{,1}\,z_{,12}\,z_{,2} \div (1 \div z_{,2}{}^2)\,z_{,11}}{(1 \div z_{,1}{}^2 \div z_{,2}{}^2)^{\frac{3}{2}}} \\
K_I &= \frac{z_{,11}\,z_{,22} - z_{,12}{}^2}{(1 \div z_{,1}{}^2 \div z_{,2}{}^2)^2}.
\end{aligned}$$

Here $z_{,i} = \partial z/\partial x_i$ and $z_{,ij} = \partial z/\partial x_i \partial x_j$

- If $k = 0$ then the Hessian matrix Φ has a singularity and the stationary phase technique fails to give the right result. If $k \neq 0$, then we find that the signature of the Hessian is $\mathrm{sgn}(\Phi) = -2$, for points above a certain depth $z^{\div}$. These are elliptic points. For points below $z^{\div}$ the $\mathrm{sgn}(\Phi) = -2$, and at $z = z^{\div}$ the method of stationary phase fails.

Discussion The DMO problem for a 3D variable velocity media is a 3D problem. That is, the impulse response is a surface in the 3D space with finite measure domain in the $\mathbb{R}^2$ space (Dietrich & Cohen, 1993; Jaramillo & Fowler, 1997). We ask now if the SDM stack operator (TZO stack) is a 3D or a 2D operator. From the 3D DMO

problem in $v(z)$ velocity media, we know that the up–dip zero–offset reflections fall inside the source–receiver line, while the zero–offset out–of–plane reflections fall outside the source–receiver line. That is, the trio of rays determined by the zero–offset ray and the rays from source to reflector and from reflector to receiver hit the surface at points that are not collinear, given that the reflection corresponds to an out–of–plane reflection. Since, the TZO stack is constructed by doing a finite–offset ray tracing into a zero–offset isochron, then the support of the TZO operator has a is a 2D set. There are points along a given source–receiver line (in–plane or up–dip reflections) and points outside the source–receiver line (out-of–plane reflections). Figure 6.8 illustrates the case of an isochron and DMO impulse response, for a medium with linear velocity with depth. The dots represent rays that hit the isochron normally. What I am saying is that the 3D TZO stacking surface for the difference between the output and input configuration isochrons, in a $v(z)$ media is not degenerate. The difference on Gaussian curvatures along the cross–line vanishes for a certain depth $(z^{\mp})$, dividing the signature of the Hessian matrix Φ in two branches. If we consider more complexities in the media, such as converted waves or anisotropy, then it is expected that while the analytic work cannot be carried out this far, the numerical implementations should be stable in the domain where the isochrons are well–defined convex surfaces.

I found an operator to transform seismic modeled data into other data that would be modeled under different conditions. This operator has a wide range of applications but we should be careful about the possible instability problems that it might generate, when using the method of stationary phase. These problems arise when we want to take into account the curvatures from the isochrons into the weights of the operator. Assuming a fixed value of curvature would cure all the stability problems but it would corrupt the amplitudes. The kinematics of the problem agrees with the kinematics of the problems being solved in routine seismic data processing, such as DMO or offset continuation or any other process to transform data.

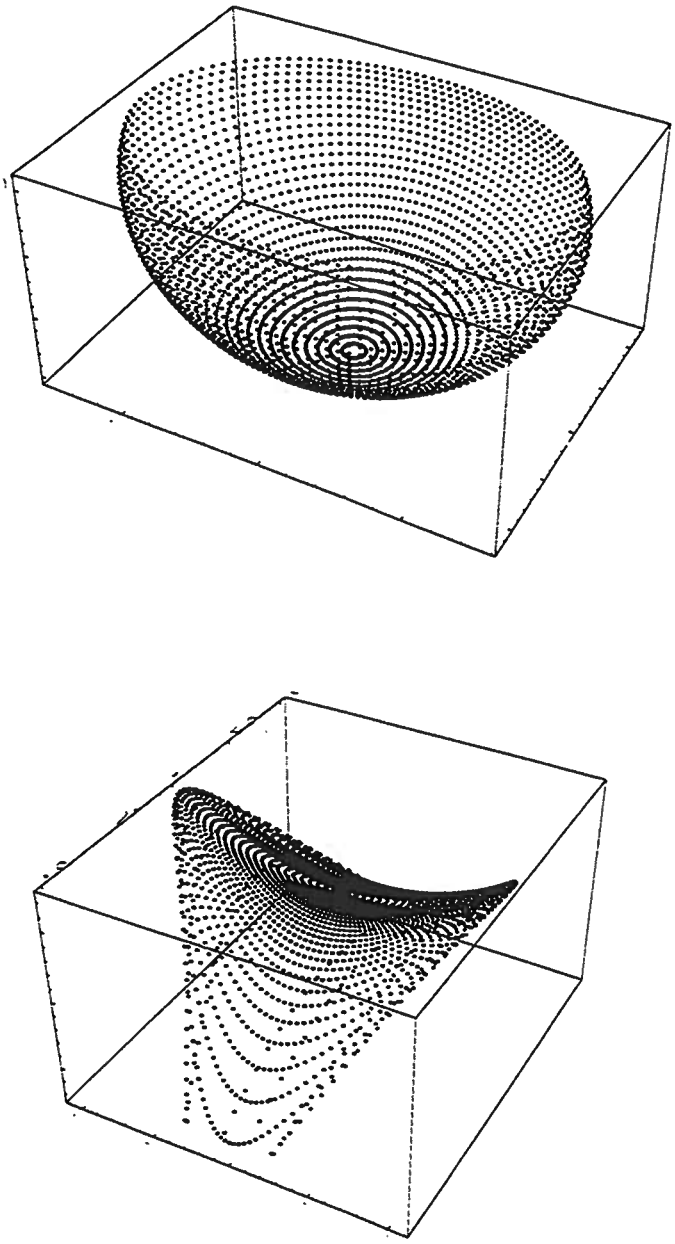

FIG. 6.8. Top: a finite offset isochron for a depth–dependent medium with constant velocity gradient. Here I consider a surface velocity of $v_0 = 2$ km/s , a gradient of $k = 0.6\text{s}^{-1}$ and a source–receiver offset of 2 km. Bottom the DMO impulse response is generated by computing the traveltime from each dot in the isochron to the zero–offset location at the earth's (flat) surface. The three coordinates of each point represent the surface location (two coordinates) and the zero–offset traveltime.

Chapter 7

2.5D

The objective of this Chapter is to derive 2.5D leading–order asymptotic formulas for the demigration, the migration, and the SDM operators. We will assume, for all geological models, a background velocity of the form $c(\boldsymbol{x}) = v(x,z)$. The meaning of 2.5D is married to geological models that are invariant in the cross–line direction. Figure 7.1 shows a sketch of one of those models. The data are assumed to be collected along the line of maximum dip with no out–of–plane reflections. While the model and the data are 2D I assume a point–source, so the 3D geometrical spreading of a point–source is taken into account. The methodology used here is to start with the 3D demigration and migration operators derived in Chapters 3 and 4 and, by using the one–dimensional stationary phase method along the cross–line direction, arrive at 2.5D operators for these processes. Then, by chaining those operators, a 2.5D SDM operator would be constructed. This operator can be further simplified by one–dimensional stationary phase analysis along the (dummy) depth variable.

Let us start with the demigration operator.

7.1 The demigration operator

In this section I find the leading asymptotic order term of the 2.5D demigration operator.

We start with formula (5.21), that I rewrite as

$$D(\boldsymbol{\xi},t) \;\sim\; -\,\mathrm{Re}\int d\Sigma_I\, R(\boldsymbol{x},\boldsymbol{x}_s)\, a(\boldsymbol{x},\boldsymbol{\xi})\, |\nabla_x\phi|\; \triangle'\left(t-\tau_R\right)\Big|_{t=\phi(\boldsymbol{x},\boldsymbol{\xi})}. \tag{7.1}$$

Let us parameterize the isochron surface as $z = z_I(\sigma_1, y)$. Here, σ_1 is a parameter along the in–line direction. For example, this could be arc length s or the Cartesian coordinate x; y is a parameter along the cross–line direction. Here, for simplicity we take y as the Cartesian coordinate along the cross–line direction. One has then,

$$d\Sigma_I = d\sigma_1\, dy\sqrt{g}. \tag{7.2}$$

If s denotes arclength along the isochron in the inline direction, then $\sqrt{g} = ds/d\sigma_1$ assumes the role of the determinant of the first fundamental tensor (metric tensor)

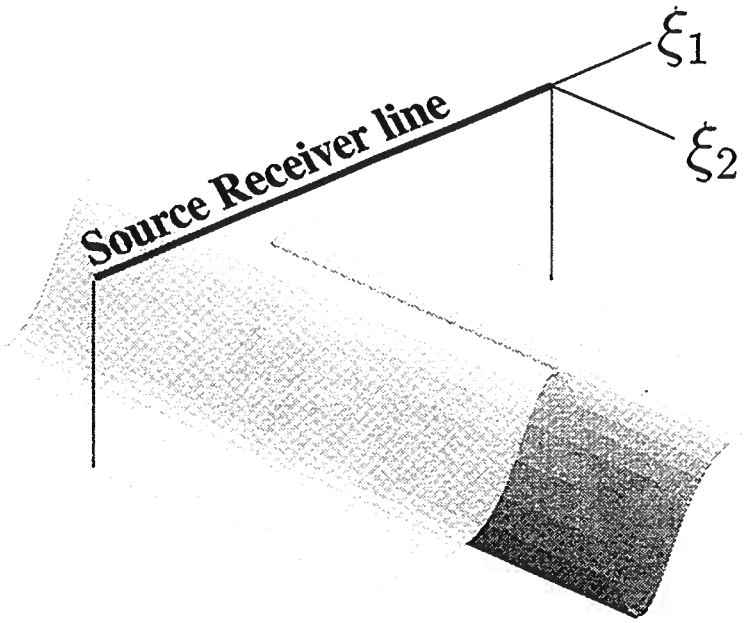

FIG. 7.1. A layer model and the acquisition geometry for the 2.5D experiment. Observe that the collected data along any line parallel to the source/receiver line would be identical.

for the surface Σ_I. Equation (7.1) becomes

$$D(\boldsymbol{\xi},t) \;\sim\; -\,\mathrm{Re}\int d\sigma_1 dy\,\sqrt{g}\,R(\boldsymbol{x},\boldsymbol{x}_s)\,a(\boldsymbol{x},\boldsymbol{\xi})\,|\nabla_x\phi|\;\Delta'\,(t-\tau_R)\Big|_{t=\phi(\boldsymbol{x},\boldsymbol{\xi})}. \tag{7.3}$$

I will perform stationary phase analysis along the cross–line (y) direction. The stationary phase condition is given by

$$\frac{\partial\phi}{\partial y}=0, \tag{7.4}$$

where I use the fact that the reflection data strip $\tau_R=\tau_R(\boldsymbol{\xi})$ does not depend on y. The meaning of the stationary phase condition is that $\nabla_x\phi$ is a vector in the vertical x-z plane. If, in addition, the medium velocity is given by $c(\boldsymbol{x})=v(x,z)$ then the ray is a plane ray (has zero torsion); that is, the ray stays in the plane in which it started (Červený, 1995). The only plane having the source–receiver line and satisfying the stationary phase condition (no source–reflector–receiver slowness component in the cross-line direction) is the vertical plane through the source–receiver line. This statement implies that the stationary phase condition is married to reflections directly under the source–receiver line for a medium with $v(x,z)$ velocity distribution. That is, no out–of–plane reflections would be handled in this case. The ideal data for this type of processing, are these acquired along the maximum dip direction. These are

data that have no variation in the cross–line direction. The experiment is then a 2D experiment, but we will acknowledge point sources with 3D geometrical spreading. Bleistein, (1986) named these type of experiments as 2.5D. We then assume that the data are acquired along the line of maximum dip. Although this assumption is restrictive, for many years 2D seismic data have been acquired and processed this way. Still, today many data sets can be re–processed with improved 2.5D techniques. Without loss in generality we will assume, from now on, that $y = 0$. Before I proceed further into the analysis of the demigration operator, I will present some important notes in ray–tracing, which are needed for further development of the demigration, migration and SDM operators.

7.1.1 Ray–tracing for inhomogeneous isotropic media

All processes studied so far require ray–tracing algorithms. We need to compute travel times as well as geometrical spreading factors among other things, before I can correctly evaluate any process such as demigration, migration or SDM. Červený (1995), derives the characteristic equations for ray–tracing for an arbitrary number of parameters along the ray. In particular if the parameter along the ray is the travel–time τ. The characteristic equations are

$$\frac{dx_i}{d\tau} = v^2\, p_i, \quad \frac{dp_i}{d\tau} = -\frac{\partial \ln v}{\partial x_i}. \tag{7.5}$$

Here, x_i is the i-th coordinate of the ray and p_i, the i-th coordinate of the slowness vector $\boldsymbol{p}$.

The initial data for the system (7.5) can be written as

$$\begin{aligned} \boldsymbol{x}(0) &= \boldsymbol{\xi}, \\ \boldsymbol{p}(0) &= 1/v(\boldsymbol{\xi})\,(\cos\alpha\sin\phi, \sin\alpha\sin\phi, \cos\phi), \\ \tau(0) &= 0. \end{aligned} \tag{7.6}$$

See that $\boldsymbol{p}(0) = (p_1(0), p_2(0), p_3(0))$ is characterized by its polar spherical coordinates. Here α is the azimuthal angle and ϕ the polar angle of the initial direction of the ray. Figure 7.2 shows these angles.

Now let us return to our 2.5D assumptions and apply them to the ray–tracing system (7.5). Given that the velocity is independent of the out of plane (x_2) direction, then

$$\frac{dp_2}{d\tau} = -\frac{\partial \ln v}{\partial x_2} = 0 \tag{7.7}$$

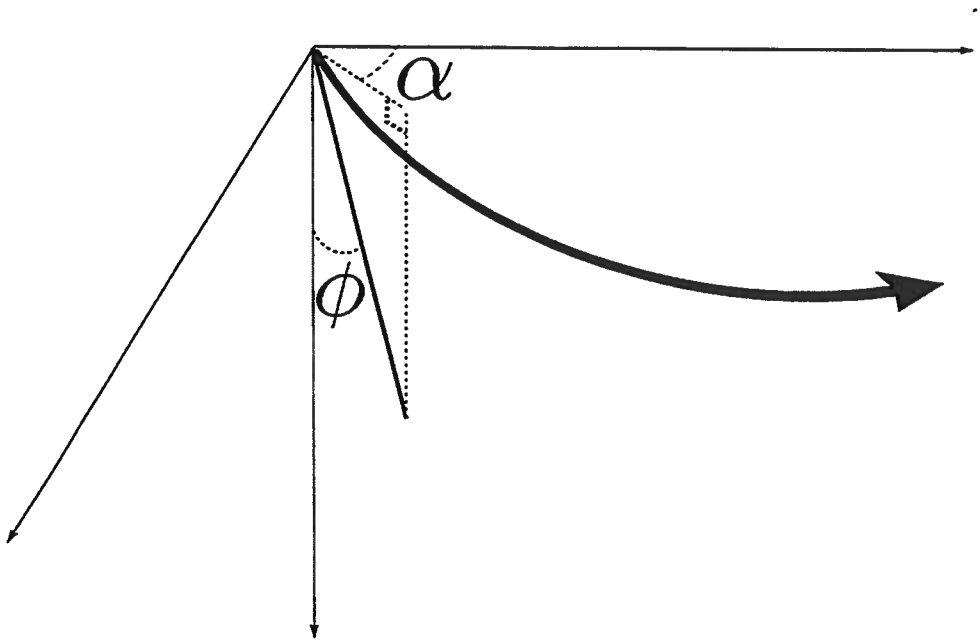

FIG. 7.2. Azimuthal angle α and polar angle ϕ for the initial direction of the ray.

so that p_2 is constant and equal to its initial value, that is

$$p_2 = \frac{1}{v(\boldsymbol{\xi})} \sin\alpha \sin\phi. \tag{7.8}$$

Then integrating the first of equations (7.5) and using the first and third initial conditions in equation (7.6) one obtains

$$x_2 = p_2 \int_0^\tau v^2[\boldsymbol{x}(t)]\, dt + \xi_2, \tag{7.9}$$

where t is the traveltime along the ray, from the source to the point $\boldsymbol{x}$.

Following Bleistein (1986), let us define

$$\sigma = \int_0^\tau v^2[x(t)]dt, \tag{7.10}$$

then using the first and third initial condition in equation (7.6) one obtains

$$x_2 = p_2\,\sigma + \xi_2 = \sigma \frac{\sin\alpha\, \sin\phi}{v(\boldsymbol{\xi})} + \xi_2. \tag{7.11}$$

So, for the inline direction, we have $\alpha = 0$, $x_2 = 0$ and $p_2 = 0$.

I now take again the stationary phase condition (7.4) and write it as

$$\frac{\partial\phi}{\partial x_2} = \frac{\partial\tau_s}{\partial x_2} + \frac{\partial\tau_g}{\partial x_2} = p_{s2} + p_{g2} = 0, \tag{7.12}$$

where I used the relation $\phi = \tau_s + \tau_g$. Here τ_s is the travel time from the source to the scatterer, τ_g the travel time from the receiver to the scatterer, p_{s2} is the out–of–plane ray parameter for the source–scatter ray and p_{g2} the out–of–plane ray parameter for the receiver–scatter ray. All of these, are evaluated at the stationary phase point $\boldsymbol{x}_0$. Given that the rays are all in the vertical plane that contains the source and receiver, $p_{s2} = p_{g2} = 0$. So, the stationary phase condition agrees with the physics of the problem. We are now interested on finding the second derivative of the phase. This is given by

$$\begin{aligned} \Phi_2 &= \frac{\partial^2 \phi}{\partial x_2} \\ &= \frac{\partial p_{s2}}{\partial x_2} + \frac{\partial p_{g2}}{\partial x_2} \end{aligned} \tag{7.13}$$

at $x_2 = \xi_2$. Differentiating (7.11) implicitly with respect to x_2 and yields

$$1 = \frac{\partial p_2}{\partial x_2}\sigma + p_2 \frac{\partial \sigma}{\partial x_2}. \tag{7.14}$$

At $p_2 = 0$, one finds

$$\frac{\partial p_2}{\partial x_2} = \frac{1}{\sigma}. \tag{7.15}$$

Applying this equation for the source–scatter ray and the receiver–scatter ray in equation (7.13) yields

$$\Phi_2 = \frac{1}{\sigma_s} + \frac{1}{\sigma_g}. \tag{7.16}$$

Thus, after using the stationary phase formula (5.12) in equation (7.1) one finds

$$D(\boldsymbol{\xi}, t) \sim -\mathrm{Re}\sqrt{2\pi} \int d\sigma_1 \sqrt{g}\, \frac{R(\boldsymbol{x}_0, \boldsymbol{x}_s)\, a(\boldsymbol{x}_0, \boldsymbol{\xi}) |\nabla_x \phi|}{\sqrt{1/\sigma_s + 1/\sigma_g}}\, d_{\frac{1}{2}}\, \triangle\,(t - \tau_R)\Big|_{t=\phi(\boldsymbol{x}_0, \boldsymbol{\xi})}. \tag{7.17}$$

Given that $\beta(\boldsymbol{x}) \sim R(\boldsymbol{x}, \boldsymbol{x}_s)\, |\nabla_x \phi|\, \delta(\phi - \tau_R)$ and using the results of Appendix C, we can say that

$$|\nabla_x \phi|\, R(\boldsymbol{x}, \boldsymbol{x}_s)\, \delta_{\frac{1}{2}}(\phi - \tau_R) \sim \delta_{\frac{1}{2}} \beta(\boldsymbol{x}_0). \tag{7.18}$$

I rewrite equation (7.17) as

$$D(\boldsymbol{\xi}, t) \sim -\mathrm{Re}\sqrt{2\pi} \int d\sigma_1 \sqrt{g}\, \frac{a(\boldsymbol{x}_0, \boldsymbol{\xi})}{\sqrt{1/\sigma_s + 1/\sigma_g}}\, d_{\frac{1}{2}}\, \hat{\beta}(\boldsymbol{x}_0)\Big|_{t=\phi(\boldsymbol{x}_0, \boldsymbol{\xi})}, \tag{7.19}$$

where now $d_{\frac{1}{2}} \hat{\beta}(\boldsymbol{x}_0) = |\nabla_x \phi|\, R(\boldsymbol{x}, \boldsymbol{x}_s)\, \triangle_{\frac{1}{2}}\, (\phi - \tau_R)$. The relationship of β to the half

derivative operator $d_{\frac{1}{2}}$ is not clear at this point. The filter $\sqrt{-i\omega}$ suggests that this is a time derivative, however the function $\beta(\boldsymbol{x})$ does not show any apparent dependence on time. The relation of $\beta(\boldsymbol{x})$ to time is seen through the evaluation at the end of equation(7.19). To get a better insight into this, let us define

$$\beta_t(\boldsymbol{x}, t) = R(\boldsymbol{x}, \boldsymbol{x}_s)\, |\nabla_x \phi|\, \delta(t - \tau_R). \tag{7.20}$$

We then have that $\beta(\boldsymbol{x}) = \beta_t(\boldsymbol{x}, \phi)$. Let us now take the forward Fourier transform from $\beta_t(\boldsymbol{x}, t)$ into $\beta_\omega(\boldsymbol{x}, \omega)$, then multiply by the half–derivative filter $\sqrt{-i\omega}$. After this, we take the inverse Fourier transform (over $\omega > 0$, with the use of the $2\,H(\omega)$ factor) and replace t by ϕ.

To implement the demigration formula (7.19) in a computer, we can proceed as follows. The reflectivity function operates on points, $\boldsymbol{x} = (x, z)$ (since $y = 0$). Now we can process the demigration formula (7.19) on a trace–by–trace basis. Let us fix the source–receiver position by choosing a fixed vector $\boldsymbol{\xi}$. Afterwards we fix the coordinate x (this coordinate should have a known one–to–one relation with σ_1). For each depth z, there is a total traveltime t to the source $\boldsymbol{x}_s(\boldsymbol{\xi})$ and receiver $\boldsymbol{x}_g(\boldsymbol{\xi})$. If we consider a uniform sampling in z, in general we would have a non–uniform sampling on t. The function that relates z to t is a one–to–one, monotonically increasing function. We can resample by interpolating the times t and then construct the function $\beta_t(x, t)$, where the variable t takes the place of the variable z. This function is Fourier Transformed into the ω domain, scaled by $2\,H(\omega)$, half–derivative filtered, and taken back into the time domain. We will not need to do any further interpolation, since the new function $d_{\frac{1}{2}}\hat{\beta}(x, t)$ is already in a form that can be used to process equation (7.19).

Equation (7.19) represents the 2.5D demigration operator. Now, I show the 2.5D demigration operator for two commonly used parameters. If $\sigma_1 = s$ then $\sqrt{g} = 1$ and

$$D(\boldsymbol{\xi}, t) \sim -\mathrm{Re}\sqrt{2\pi} \int ds\, \frac{a(\boldsymbol{x}_0, \boldsymbol{\xi})}{\sqrt{1/\sigma_s + 1/\sigma_g}}\, d_{\frac{1}{2}}\, \hat{\beta}(\boldsymbol{x}_0)\Big|_{t=\phi(\boldsymbol{x}_0, \boldsymbol{\xi})}. \tag{7.21}$$

If instead $\sigma_1 = x$ then

$$\sqrt{g} = \frac{1}{\cos\alpha} = \frac{|\nabla_x \phi|}{\partial\phi/\partial z} \tag{7.22}$$

so

$$D(\boldsymbol{\xi}, t) \sim -\mathrm{Re}\sqrt{2\pi} \int dx\, \frac{a(\boldsymbol{x}_0, \boldsymbol{\xi})\, |\nabla_x \phi|}{\sqrt{1/\sigma_s + 1/\sigma_g}\; \partial\phi/\partial z}\, d_{\frac{1}{2}}\, \hat{\beta}(\boldsymbol{x}_0)\Big|_{t=\phi(\boldsymbol{x}_0, \boldsymbol{\xi})}. \tag{7.23}$$

7.2 The migration operator

Here, I derive a formula for the 2.5D migration operator in the time domain.

I start with equation (4.14)

$$\beta(\boldsymbol{x}) \sim -\mathrm{Re}\,\frac{1}{4\pi^2}\int d\boldsymbol{\xi}\frac{h_B(\boldsymbol{x},\boldsymbol{\xi})}{a(\boldsymbol{x},\boldsymbol{\xi})\,|\nabla_y\phi(\boldsymbol{x},\boldsymbol{\xi})|}\frac{\partial}{\partial t}D(\boldsymbol{\xi},t)*\triangle(t)\Big|_{t=\phi(\boldsymbol{x},\boldsymbol{\xi})}. \tag{7.24}$$

After using the asymptotic representation of the analytic data as given in equation (6.9)

$$D(\boldsymbol{\xi},t)*\triangle(t) \sim A_0(\boldsymbol{\xi})\ \triangle\left(t-\tau_R(\boldsymbol{\xi})\right), \tag{7.25}$$

one finds

$$\hat{\beta}(\boldsymbol{x}) \sim -\frac{1}{4\pi^2}\int d\boldsymbol{\xi}\ \frac{h_B(\boldsymbol{x},\boldsymbol{\xi})A_0(\boldsymbol{\xi})}{a(\boldsymbol{x},\boldsymbol{\xi})\,|\nabla_y\phi(\boldsymbol{x},\boldsymbol{\xi})|}\ \triangle'\left(t-\tau_R(\boldsymbol{\xi})\right)\Big|_{t=\phi(\boldsymbol{x},\boldsymbol{\xi})}. \tag{7.26}$$

The hat in $\hat{\beta}$ defines the complex reflectivity function.

At this point I want to perform the integration along the ξ_2 direction by using the stationary phase formula (5.12). Then

$$\hat{\beta}(\boldsymbol{x}) \sim \frac{1}{(2\pi)^{\frac{3}{2}}}\int d\xi_1\,\frac{h_B(\boldsymbol{x},\boldsymbol{\xi}_0)A_0(\boldsymbol{\xi}_0)e^{i\frac{\pi}{4}(\mathrm{sgn}\,\Phi-1)}}{a(\boldsymbol{x},\xi)\,|\nabla_x\phi(\boldsymbol{x},\boldsymbol{\xi}_0)|\sqrt{|\Phi|}}\,d_{\frac{1}{2}}\triangle\left(t-\tau_R(\boldsymbol{\xi}_0)\right)\Big|_{t=\phi(\boldsymbol{x}_0,\boldsymbol{\xi})}, \tag{7.27}$$

where $\boldsymbol{\xi}_0$ is a solution of the stationary phase condition,

$$\frac{\partial\phi(\boldsymbol{x},\boldsymbol{\xi})}{\partial\xi_2}=0. \tag{7.28}$$

I used the fact that $\tau_R(\boldsymbol{\xi})$ is independent of ξ_2. Also

$$\Phi=\frac{\partial^2\phi(\boldsymbol{x},\boldsymbol{\xi})}{\partial\xi_2^2}\Big|_{\boldsymbol{\xi}=\boldsymbol{\xi}_0}. \tag{7.29}$$

Following the same steps done to find an expression for the second derivative of the phase term, one can enumerate the following results:

- The stationary phase condition (7.28) implies that $\xi_2 = y = 0$.

- $\Phi = 1/\sigma_s + 1/\sigma_g$

- $h_B(x,\xi) = -\Phi H(\boldsymbol{x},\xi)$, where $\xi = \xi_1$ and

$$H(\boldsymbol{x},\xi) \;=\; \det\begin{bmatrix} \nabla_x\phi(\boldsymbol{x},\xi) \\ \frac{\partial}{\partial\xi}\nabla_x\phi(\boldsymbol{x},\xi) \end{bmatrix}. \tag{7.30}$$

The last item is derived by Bleistein et al. (1996). I now rewrite equation (7.27) as

$$\begin{aligned} \hat{\beta}(\boldsymbol{x}) \;&\sim\; \frac{1}{(2\pi)^{\frac{3}{2}}}\int d\xi\, \frac{H(\boldsymbol{x},\xi)A_0(\xi)\sqrt{\Phi}}{a(\boldsymbol{x},\xi)\,|\nabla_x\phi(\boldsymbol{x}_0,\xi)|}\, d_{\frac{1}{2}}\,\triangle\,(t-\tau_R(\xi)\Big|_{t=\phi(\boldsymbol{x}_0,\xi)} \\ &\sim\; \frac{1}{(2\pi)^{\frac{3}{2}}}\int d\xi\, \frac{H(\boldsymbol{x},\xi)\sqrt{\Phi}}{a(\boldsymbol{x},\xi)\,|\nabla_x\phi(\boldsymbol{x},\xi)|}\, d_{\frac{1}{2}}\hat{D}(\xi,t)\Big|_{t=\phi(\boldsymbol{x}_0,\xi)}, \end{aligned} \tag{7.31}$$

The hat in $\hat{D}$ defines the analytic data. Here, I applied the homogeneity property of the fractional differentiation,

$$A_0(\xi)\, d_{\frac{1}{2}}\,\triangle\,(t-\tau_R(\xi)) = d_{\frac{1}{2}}\, A_0(\xi)\,\triangle\,(t-\tau_R(\xi)) \tag{7.32}$$

illustrated in Appendix C.

A different representation of the migration operator can be achieved by writing equation (7.31) as

$$\hat{\beta}(\boldsymbol{x}) \;\sim\; \frac{1}{(2\pi)^{\frac{3}{2}}}\int dt\, d\xi\, \frac{H(\boldsymbol{x},\xi)\sqrt{\Phi}}{a(\boldsymbol{x},\xi)\,|\nabla_x\phi(\boldsymbol{x},\xi_0)|}\, d_{\frac{1}{2}}\hat{D}(\xi,t)\,\delta(t-\phi(\boldsymbol{x}_0,\xi)), \tag{7.33}$$

and using the two–side representation of the delta function given by

$$\delta(t-\phi) = \frac{1}{2\pi}\int_{-\infty}^{\infty} d\omega\; e^{i\omega(t-\phi)}.$$

Then

$$\begin{aligned} \hat{\beta}(\boldsymbol{x}) \;&\sim\; \frac{1}{(2\pi)^{\frac{5}{2}}}\int d\xi\, dt\, \frac{H(\boldsymbol{x},\xi)\sqrt{\Phi}}{a(\boldsymbol{x},\xi)\,|\nabla_x\phi(\boldsymbol{x},\xi)|}\, d_{\frac{1}{2}}\hat{D}(\xi,t)\int_{-\infty}^{\infty} d\omega\, e^{i\omega(t-\phi)} \\ &\sim\; \frac{1}{(2\pi)^{\frac{5}{2}}}\int d\xi\, \frac{H(\boldsymbol{x},\xi)\sqrt{\Phi}}{a(\boldsymbol{x},\xi)\,|\nabla_x\phi(\boldsymbol{x},\xi)|}\int_{-\infty}^{\infty} d\omega\, e^{-i\omega\,\phi}\int dt\; d_{\frac{1}{2}}\hat{D}(\xi,t)e^{i\omega\,t} \\ &\sim\; \frac{1}{(2\pi)^{\frac{5}{2}}}\int d\xi\, \frac{H(\boldsymbol{x},\xi)\sqrt{\Phi}}{a(\boldsymbol{x},\xi)\,|\nabla_x\phi(\boldsymbol{x},\xi)|}\int_{-\infty}^{\infty} d\omega\, e^{-i\omega\,\phi}\,\sqrt{-i\omega}\,\hat{D}(\xi,\omega)e^{i\omega\,t}. \end{aligned} \tag{7.34}$$

Here, $\sqrt{-i\omega} = \sqrt{|\omega|}\,\exp\left(-i\,\mathrm{sgn}(\omega)\,\pi/4\right)$ corresponds to the frequency representation of the half differentiation, and $\hat{D}(\xi,\omega)$ is the frequency representation of the analytic input data. Equation (7.34) corresponds to the 2.5D reflectivity function in Bleistein

et al. (1996).

7.3 The 2.5 SDM operator

In this section, I present 2.5D SDM as a chain of the migration and demigration operators. I further simplify the operator by using the method of stationary phase.

I rewrite equation (7.19) as

$$D(\tilde{\xi},\tilde{t}) \sim -\mathrm{Re}\sqrt{2\pi}\int d\sigma_1\,\sqrt{g}\,\frac{a(\boldsymbol{x},\tilde{\xi})}{\sqrt{1/\tilde{\sigma}_s \div 1/\tilde{\sigma}_g}}\,d_{\frac{1}{2}}\,\hat{\beta}(\boldsymbol{x})\Big|_{\tilde{t}=\phi(\boldsymbol{x},\tilde{\xi})}. \tag{7.35}$$

Here, $\tilde{\xi}$ is a one–dimensional output parameter that specifies the source–receiver configuration and $\tilde{t}$ is the output time. I assume $\xi_2 = 0$, $\boldsymbol{x} = (x,0,z)$. Now, from equation (7.31)

$$\begin{aligned} d_{\frac{1}{2}}\hat{\beta}(\boldsymbol{x}) &\sim \frac{1}{(2\pi)^{\frac{3}{2}}}\int d\xi\,\frac{H(\boldsymbol{x},\xi)\sqrt{\Phi}}{a(\boldsymbol{x},\xi)\,|\nabla_x\phi(\boldsymbol{x},\xi)|}\,d_{\frac{1}{2}}\,d_{\frac{1}{2}}\hat{D}(\xi,t)\Big|_{t=\phi(\boldsymbol{x},\xi)} \\ &\sim \frac{1}{(2\pi)^{\frac{3}{2}}}\int d\xi\,\frac{H(\boldsymbol{x},\xi)\sqrt{\Phi}}{a(\boldsymbol{x},\xi)\,|\nabla_x\phi(\boldsymbol{x},\xi)|}\,\frac{\partial}{\partial t}\hat{D}(\xi,t)\Big|_{t=\phi(\boldsymbol{x},\xi)}, \end{aligned} \tag{7.36}$$

where I introduced the half–derivative into the integral sign and used the composition rule $d_{\frac{1}{2}}\,d_{\frac{1}{2}} = \partial/\partial t$ (see the homogeneity property for fractional derivatives in Appendix C).

Now, I chain the operators (7.36) and (7.35) by introducing (7.36) into (7.35). Using the fact that $\Phi = 1/\sigma_s \div 1/\sigma_g$ yields

$$\begin{aligned} D(\tilde{\xi},\tilde{t}) &\sim -\mathrm{Re}\,\frac{1}{2\pi}\int d\sigma_1\,d\xi\sqrt{g}\,\frac{\tilde{a}(\boldsymbol{x},\tilde{\xi})}{a(\boldsymbol{x},\xi)} \\ &\times \frac{H(\boldsymbol{x},\xi)\,\mu(\boldsymbol{x},\xi,\tilde{\xi})}{|\nabla_x\phi(\boldsymbol{x},\xi)|}\,\frac{\partial}{\partial t}\hat{D}(\xi,t)\Big|_{t=\phi(\boldsymbol{x},\xi)}\Big|_{\tilde{t}=\phi(\boldsymbol{x},\tilde{\xi})}. \end{aligned} \tag{7.37}$$

Here,

$$\mu(\boldsymbol{x},\xi,\tilde{\xi}) = \sqrt{\frac{\tilde{\sigma}_s\,\tilde{\sigma}_g(\sigma_s \div \sigma_g)}{\sigma_s\,\sigma_g(\tilde{\sigma}_s \div \tilde{\sigma}_g)}}. \tag{7.38}$$

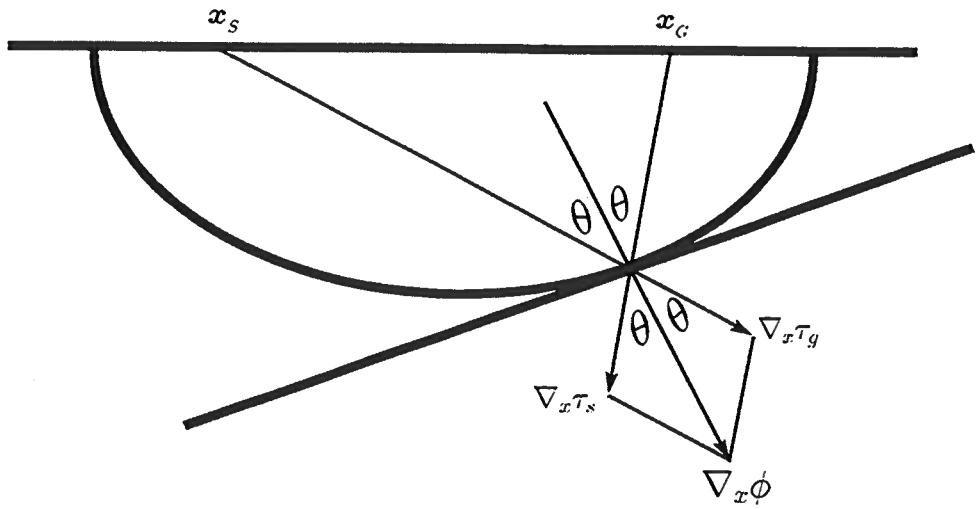

FIG. 7.3. Here I illustrate how the stationary phase condition implies Snell's law. The stationary phase condition requires that the slowness vector $\nabla_x \phi$ be perpendicular to the tangent reflector. Now the angles that this slowness vector makes with the source and receiver slowness vectors are equal to θ. This is because both, the source and receiver, vectors have the same magnitude of $1/c(\boldsymbol{x})$, where $c(\boldsymbol{x})$ is the wavespeed at the reflecting point.

Let us now introduce the analytic data

$$\hat{D}(\xi, t) = A_0(\xi) \triangle (t - \tau_R(\xi)). \tag{7.39}$$

With this, equation (7.37) becomes

$$\begin{aligned} D(\tilde{\xi}, \tilde{t}) \sim & -\mathrm{Re}\, \frac{1}{2\pi} \int d\xi A_0(\boldsymbol{\xi}) \\ & \int d\sigma \sqrt{g}\, \frac{\tilde{a}(\boldsymbol{x}, \tilde{\xi})}{a(\boldsymbol{x}, \xi)}\, \frac{H(\boldsymbol{x}, \xi)\, \mu(\boldsymbol{x}, \xi, \tilde{\xi})}{|\nabla_x \phi(\boldsymbol{x}, \xi)|}\, \triangle' (\phi(\boldsymbol{x}, \xi) - \tau_R(\xi)) \Big|_{\tilde{t} = \phi(\boldsymbol{x}, \tilde{\xi})}. \end{aligned} \tag{7.40}$$

Let us perform stationary phase analysis to the second integral. The stationary phase condition is given by

$$\frac{\partial \phi}{\partial \sigma} = \nabla_x \phi \cdot \left(\frac{\partial x_i}{\partial \sigma} \right) = 0. \tag{7.41}$$

I call σ_0 the solution of the stationary phase condition, and $\boldsymbol{x}_0 = (x(\sigma_0), z(\sigma_0))$. Formula (7.41) tells us that, at the stationary point, the source–scatterer–receiver slowness vector $(\nabla_x \phi)$ is perpendicular to the output isochron tangent line. This means that the corresponding source–scatterer-receiver ray represents a specular reflection or; in other words, it satisfies Snell's law. Figure 7.3 illustrates this fact. The interpretation of the stationary phase condition is then that the point $\boldsymbol{x}(\sigma_0) = \boldsymbol{x}_0(\tilde{\xi}, \tilde{t})$

belongs to the output configuration isochron and serves as a specular reflection point determined by the parameter ξ in the input configuration. That is, the triplet $(\boldsymbol{x}_s(\xi), \boldsymbol{x}_0(\tilde{\xi}, \tilde{t}), \boldsymbol{x}_g(\xi))$ represents a source–reflector–receiver specular ray on the output isochron. I then define the mapping

$$\begin{aligned} \boldsymbol{x}_0(\tilde{\xi}, \tilde{t}) : \mathcal{C} \subseteq \mathbb{R} &\longrightarrow \mathbb{R}^2 \\ \xi &\longmapsto \boldsymbol{x}_0(\tilde{\xi}, \tilde{t})(\xi), \end{aligned} \tag{7.42}$$

where $\mathcal{C}$ is the set of all unique parameters ξ such that $\boldsymbol{x}_0(\tilde{\xi}, \tilde{t})$ is a specular reflection point in the output isochron defined by the equation $\tilde{t} = \tilde{\phi}(\boldsymbol{x}, \tilde{\xi})$. This specular reflection is identified with the triplet $(\boldsymbol{x}_s(\xi), \boldsymbol{x}_0(\tilde{\xi}, \tilde{t}), \boldsymbol{x}_g(\xi))$. $\mathcal{C}$ is then the domain of integration of the SDM stack operator. We can then justify the representation $\boldsymbol{x}_0 = \boldsymbol{x}_0(\xi, \tilde{\xi}, \tilde{t})$. This physical interpretation of the stationary phase condition (7.41) gives us an algorithm to compute the SDM stacking curve (support of the SDM stacking operator). The SDM stacking curve is the locus of all (input) points (t, ξ) corresponding to specular reflections in the output isochron. In other words, to compute the SDM stacking curve we need to do a ray–tracing to the output configuration isochron with the input recording configuration. The mathematical definition of the SDM stack curve is given by

$$\mathcal{S} = \left\{ (t, \xi) \mid t = \tau_s(\boldsymbol{x}_s(\xi), \boldsymbol{x}_0(\xi, \tilde{\xi}, \tilde{t})) + \tau_g(\boldsymbol{x}_g(\xi), \boldsymbol{x}_0(\xi, \tilde{\xi}, \tilde{t})) \right\}, \tag{7.43}$$

where τ_s and τ_g are the travel times from the source and receiver positions to the point $\boldsymbol{x}_0$, respectively. Kinematically speaking, the SDM could be numerically implemented as a Kirchhoff prestack migration algorithm where the diffraction curves are replaced by the SDM stacks defined in equation (7.43). To have the dynamics right, we should proceed further with the stationary phase analysis. We apply the stationary phase formula (5.12) to the inner integral in equation (7.40) and find

$$\begin{aligned} D(\tilde{\xi}, \tilde{t}) \sim & -\mathrm{Re} \frac{1}{\sqrt{2\pi}} \int d\xi \sqrt{g}\, A_0(\xi) \frac{\tilde{a}(\boldsymbol{x}_0, \tilde{\xi})}{a(\boldsymbol{x}_0, \xi)} \frac{H(\boldsymbol{x}_0, \xi)\, \mu(\boldsymbol{x}_0, \xi, \tilde{\xi})}{\sqrt{|\Phi|}\, |\nabla_x \phi(\boldsymbol{x}_0, \xi)|} \\ & \times \quad e^{i \frac{\pi}{4} (\operatorname{sgn} \Phi - 1)} \, \triangle_{\frac{1}{2}} \, (\Phi_{SDM}(\xi, \tilde{\xi}, \tilde{t}) - \tau_R(\xi)). \end{aligned}$$

Here

$$\Phi(\xi, \tilde{\xi}, \tilde{t}) = \left. \frac{\partial^2 \phi}{\partial \sigma_1^2} \right|_{\sigma_1 = \sigma_0},$$

and Φ_{SDM} is equal to t in equation (7.43). We can reintroduce the amplitude factor $A_0(\xi)$ into the half derivative operator (see Appendix C) and find that

$$D(\tilde{\xi}, \tilde{t}) \sim -\mathrm{Re} \frac{1}{\sqrt{2\pi}} \int_S d\xi \sqrt{g} \frac{\tilde{a}(\boldsymbol{x}_0, \tilde{\xi})}{a(\boldsymbol{x}_0, \xi)} \frac{H(\boldsymbol{x}_0, \xi)\, \mu(\boldsymbol{x}_0, \xi, \tilde{\xi})}{|\nabla_x \phi(\boldsymbol{x}, \xi)| \sqrt{|\Phi|}} \tag{7.44}$$

$$\times \qquad e^{i\frac{\pi}{4}(\operatorname{sgn}\Phi-1)}\,\hat{D}_{\frac{1}{2}}(t,\xi).$$

The summation is taken along $\mathcal{S}$.

Let us now study the isochron curvature. For exposition purposes, I will omit the arguments of the function ϕ. In any case, ϕ is the total traveltime of the source–scatterer–receiver ray, but in some cases this traveltime is taken with respect to the input configuration isochron and in other cases with respect to the output configuration isochron. To distinguish between these two choices, I use the tilde for the coordinates of the output configuration isochron. Also, for convenience, I again use Einstein summation convention.

Let us begin by rewriting the stationary phase condition:

$$\frac{\partial\phi}{\partial\sigma_1} = \frac{\partial\phi}{\partial x_l}\,\frac{\partial\tilde{x}_l}{\partial\sigma_1} = 0. \tag{7.45}$$

By using twice the chain rule for derivatives, one has that

$$\frac{\partial^2\phi}{\partial\sigma_1^2} = \frac{\partial^2\phi}{\partial x_l\partial x_k}\,\frac{\partial\tilde{x}_l}{\partial\sigma_1}\,\frac{\partial\tilde{x}_k}{\partial\sigma_1} + \frac{\partial\phi}{\partial x_l}\,\frac{\partial^2\tilde{x}_l}{\partial\sigma_1^2}. \tag{7.46}$$

where $l = 1,3$ and $k = 1,3$. Now let us take the input isochron defined by $t = \phi(\boldsymbol{x}(\boldsymbol{\sigma}),\xi)$. Given that t is constant along the isochron,

$$\frac{\partial t}{\partial\sigma_1} = \frac{\partial\phi}{\partial x_l}\,\frac{\partial x_l}{\partial\sigma_1} = 0, \tag{7.47}$$

and

$$\frac{\partial^2 t}{\partial\sigma_1^2} = \frac{\partial^2\phi}{\partial x_l\partial x_k}\,\frac{\partial x_l}{\partial\sigma_1}\,\frac{\partial x_k}{\partial\sigma_1} + \frac{\partial\phi}{\partial x_l}\,\frac{\partial^2 x_l}{\partial\sigma_1^2} = 0. \tag{7.48}$$

From equations (7.45) and (7.47), and the fact that the point $\boldsymbol{x}_0$ belongs both to the input and to the output isochron, we find that both isochrons share the same tangent line at the point $\boldsymbol{x}_0$. Also there exists a constant c such that

$$\frac{\partial x_l}{\partial\sigma_1} = c\,\frac{\partial\tilde{x}_l}{\partial\sigma_1} \tag{7.49}$$

Let us use the same parameter σ_1 for both the input and the output configuration isochrons. Without loss of generality, we also can say that both isochrons share the same abscissa, that is $x_1(\sigma_1) = \tilde{x}_1(\sigma_1)$. So that the first derivatives of those abscissas respect to the parameter σ_1 are also equal. This implies that $c = 1$ in equation (7.49).

Now substract equation (7.48) from equation (7.46); then using equation (7.49) with

$c = 1$ one finds

$$\frac{\partial^2 \phi}{\partial \sigma_1^2} = \frac{\partial \phi}{\partial x_l} \frac{\partial^2 (\tilde{x}_l - x_l)}{\partial \sigma_1^2}. \tag{7.50}$$

I now apply the chain rule for $\partial \tilde{x}_l / \partial \sigma_1$ by introducing the arclength s, and obtain

$$\frac{\partial^2 \tilde{x}_l}{\partial \sigma_1^2} = \frac{\partial^2 \tilde{x}_l}{\partial s^2} \left(\frac{\partial s}{\partial \sigma} \right)^2 + \frac{\partial s}{\partial \sigma_1} \frac{\partial}{\partial s} \left(\frac{\partial s}{\partial \sigma_1} \right) \frac{\partial \tilde{x}_l}{\partial s}. \tag{7.51}$$

Performing the same procedure for $\partial x_l / \partial \sigma_1$, and then subtracting the result from equation 7.51 yields

$$\frac{\partial^2 \phi}{\partial \sigma_1^2} = \frac{\partial \phi}{\partial x_l} \frac{\partial^2 (\tilde{x}_l - x_l)}{\partial s^2} \left(\frac{ds}{d\sigma_1} \right)^2. \tag{7.52}$$

Here I used the fact that $\partial \tilde{x}_l / \partial s = \partial x_l / \partial s$.

The vector $\boldsymbol{\kappa} = \partial^2((\tilde{x}_l - x_l)/\partial s^2$ represents the difference in curvature between the output and input isochrons and is directed in the normal direction to both isochrons at the stationary point $\boldsymbol{x}_0$. Therefore, it is either pointing in the same or in opposite direction as $\nabla_x \phi = (\partial \phi / \partial x_l)$. So

$$\Phi = \frac{\partial^2 \phi}{\partial \sigma_1^2} = \operatorname{sgn} (\nabla_x \phi \cdot \boldsymbol{\kappa}) \, |\nabla_x \phi| \, (\kappa_o - \kappa_i) \left(\frac{ds}{d\sigma_1} \right)^2. \tag{7.53}$$

where κ_o is the curvature of the output configuration isochron and κ_i is the curvature of the input configuration isochron.

So, equation (7.44) turns out to be

$$\begin{aligned} D(\tilde{\xi}, \tilde{t}) \sim -\mathrm{Re} \frac{1}{\sqrt{2\pi}} \int_S d\xi \, \frac{\tilde{a}(\boldsymbol{x}_0, \tilde{\xi})}{a(\boldsymbol{x}_0, \xi)} \frac{H(\boldsymbol{x}_0, \xi) \, \mu(\boldsymbol{x}_0, \xi, \tilde{\xi})}{\sqrt{|\kappa_i - \kappa_o| |\nabla_x \phi|^{3/2}}} \\ \times \quad e^{i \frac{\pi}{4} [\operatorname{sgn} (\nabla_x \phi \cdot \boldsymbol{\kappa}) (\kappa_o - \kappa_i) - 1]} \, \hat{D}_{\frac{1}{2}}(t, \xi) \end{aligned} \tag{7.54}$$

Let us now derive an alternative form for the SDM operator along the same lines of the derivation of the 3D SDM weight. This alternative weight is useful for numerical purposes, as explained before.

Let us define the second derivative of the diffraction curve, corresponding to the stationary point, with respect to the parameter ξ as

$$H_D = \frac{\partial^2 \phi}{\partial \xi^2}, \tag{7.55}$$

and the second derivative of the time in the stacking path, with respect to the pa-

rameter ξ as

$$H_R = \frac{\partial^2 \phi_{SDM}}{\partial \xi^2}. \tag{7.56}$$

Tygel et al. (1995) found the following relation between the difference of input and output isochron curvatures $\kappa_i - \kappa_0$ and the difference $H_D - H_I$:

$$H_D - H_R = -\left[\frac{c(\boldsymbol{x}_0)}{2\cos\theta}\right]^3 \frac{H^2}{\kappa_i - \kappa_o}. \tag{7.57}$$

Here θ is half the angle between the source and receiver rays at the stationary phase point $\boldsymbol{x}_0$. Using equation (7.57) in (7.54) yields

$$\begin{aligned} D(\tilde{\xi},\tilde{t}) \sim -\mathrm{Re}\,\frac{1}{\sqrt{2\pi}} \int_{\mathcal{S}} d\xi\, \frac{\tilde{a}(\boldsymbol{x}_0,\tilde{\xi})}{a(\boldsymbol{x}_0,\xi)}\, \mu(\boldsymbol{x}_0,\xi,\tilde{\xi})\, \sqrt{|H_D - H_R|} \\ \times \quad e^{i\frac{\pi}{4}[\mathrm{sgn}(\nabla_x\phi\cdot\boldsymbol{\kappa})(H_R - H_D) - 1]}\, \hat{D}_{\frac{1}{2}}(t,\xi). \end{aligned} \tag{7.58}$$

The reader is referred to Figure 6.2 and Figure 6.3 for explanation of the curvature factors involve in the SDM weights.

In conclusion, I found 2.5D versions of the demigration and migration operators in the time domain, by applying the stationary phase method to their 3D counterpart. I chained the 2.5D demigration and migration operators to obtain a 2.5 SDM operator that was also simplified using the method of stationary phase. The SDM operator is derived, first, in terms of curvatures of difference of isochrons, and second in terms of second derivatives of phase functions. These phase functions are a Huygens diffraction curve and the integration path. The first method gives a formula that is good for theoretical purposes, while the second gives us a method which is easier to implement numerically as will be shown in the next chapter.

Chapter 8

COMMON–OFFSET 2.5 TZO IN VERTICALLY INHOMOGENEOUS MEDIA

This chapter illustrates a direct application of the SDM problem. I use the SDM operator to build a TZO operator for 2.5D vertically inhomogeneous media. A numerical implementation of the TZO operator is performed in the space–time domain.

8.1 Theory

TZO can be seen as SDM under the following conditions

- The model parameters are not changed in the transformation.
- The input data configuration is finite–offset.
- The output data configuration is zero–offset.

We rewrite the 2.5D data mapping formula (7.58) by replacing the tilde character by a "0" subscript.

$$D(\xi_0,t_0) \sim -\mathrm{Re}\,\frac{1}{\sqrt{2\pi}}\int_{\mathcal{S}} d\xi\,\frac{a_0(\boldsymbol{x}_0,\xi_0)}{a(\boldsymbol{x}_0,\xi)}\,\mu(\boldsymbol{x}_0,\xi,\xi_0)\,\sqrt{|H_D-H_R|} \times \quad e^{i\frac{\pi}{4}[\mathrm{sgn}(\nabla_x\phi\cdot\boldsymbol{\kappa})(H_R-H_D)-1]}\,\hat{D}_{\frac{1}{2}}(t,\xi) \tag{8.1}$$

Let us recall the meaning of the symbols involved in this expression. ξ_0 is the zero–offset position (at the recording line), t_0 is the zero–offset time, $\mathcal{S}$ is the path of integration (locus of the impulse response for the inverse TZO operator), ξ determines the finite–offset (input) location, a_0 is product of the WKBJ zero–offset amplitudes, which are solution of the transport equation (2.7), a is the product of the WKBJ finite–offset amplitudes, which also are solutions of the transport equation (2.7), H_D is the second derivative of the diffraction curve, corresponding to the stationary point, with respect to the parameter ξ and defined by equation 7.55; H_R is the second derivative of the (time) integration path, with respect to the parameter ξ and defined by equation 7.56, μ, defined by equation (7.38), is a weight that accounts for out–of–plane

geometrical spreading, $\boldsymbol{x}_0$ is the stationary phase point defined in equation (7.42), $\boldsymbol{\kappa}$ is the difference of curvatures between the zero–offset and finite–offset isochrons and is directed in the normal direction to both isochrons at the stationary phase point $\boldsymbol{x}_0$. Finally, $D(\xi_0, t_0)$ represents the output analytic data and $\hat{D}_{\frac{1}{2}}(\xi, t)$ represents the input analytic data after a half derivative filter is applied. Here t is two–way traveltime to the source–receiver input configuration, from the stationary phase point $\boldsymbol{x}_0$. In this chapter the configuration parameter ξ represents the midpoint y and the configuration parameter ξ_0 the zero–offset surface location x_0.

Notice that

$$\operatorname{sgn}\left(\nabla_x \phi \cdot \boldsymbol{\kappa}\right)\left(H_R - H_D\right) = 1, \tag{8.2}$$

for the case of TZO.

By equation 7.57 we see that $\operatorname{sgn}\left(H_R - H_D\right) = \operatorname{sgn}(\kappa_o - \kappa_i)$. The zero offset isochron is tangential and totally inside the finite offset isochron, so $\operatorname{sgn}(\nabla_x \phi \cdot \boldsymbol{\kappa}) = \operatorname{sgn}(\kappa_o - \kappa_i)$. This proofs the statement.

Equation 8.1 turns out to be

$$D(\xi_0, t_0) \sim -\operatorname{Re} \frac{1}{\sqrt{2\pi}} \int_{\mathcal{S}} d\xi \, \frac{a_0(\boldsymbol{x}_0, \xi_0)}{a(\boldsymbol{x}_0, \xi)} \, \mu(\boldsymbol{x}_0, \xi, \xi_0) \sqrt{|H_D - H_R|} \, \hat{D}_{\frac{1}{2}}(t, \xi). \tag{8.3}$$

8.2 Numerics

In this section I describe the algorithm to evaluate integral (8.3). I will split the algorithm in three main parts. Kinematics, Basic Dynamics and True amplitude Dynamics.

8.2.1 Kinematics

The kinematics of the whole process is based on computation of the traveltimes from any scatterer to all source–receiver combinations. These times also influence the dynamics, as well, in several ways. The path of integration is determined entirely from the computation of the traveltimes, and the weights in the integral (8.3) are also computed from these traveltimes and their partial derivatives.

The TZO stacking path To evaluate the integral (8.3) for the computation of the TZO process, we need first to find the integration path $\mathcal{S}$. This path is given by

equation (7.43)

$$\mathcal{S} = \{(t,\xi) \mid t = \tau_s(\boldsymbol{x}_s(\xi), \boldsymbol{x}_0(\xi,\xi_0,t_0)) + \tau_g(\boldsymbol{x}_g(\xi), \boldsymbol{x}_0(\xi,\xi_0,t_0))\}, \tag{8.4}$$

The path is found by performing finite–offset kinematic ray tracing to the output (zero–offset isochron). One way to represent this path is by a parametric curve

$$\begin{aligned} y &= y(p) \\ t &= t(p), \end{aligned} \tag{8.5}$$

where $p = 2\sin\phi/v(z)$ is the zero–offset ray parameter and ϕ is the reflector dip. Let us illustrate this TZO path in the case of constant velocity.

Constant velocity. Figure 8.1 shows the geometry of the experiment. The output isochron corresponding to a given fixed point (x_0, t) is a circle of radius $v\,t_0/2$. With no loss in generality, we can assume $x_0 = \xi_0 = 0$. Also note that zero–offset rays are radii of the circle. The source position is at $y - h$ and the receiver position is at $y + h$. By applying the law of sines in the triangle defined by the source position, the zero–offset location and the reflecting point, one finds:

$$\frac{h-y}{\sin\theta} = \frac{v\,t_0}{2\,\sin(\pi/2-\theta-\phi)}. \tag{8.6}$$

In the same way, the application of law of sines to the triangle defined by the receiver position, the zero–offset location and the reflecting point yields

$$\frac{h+y}{\sin\theta} = \frac{v\,t_0}{2\,\sin(\pi/2-\theta+\phi)}. \tag{8.7}$$

The solution of the system given by equation (8.6) and equation (8.7) for the unknowns θ and y is found to be

$$\theta = \arctan\frac{\cot\phi}{2\,h\,p}\left[\sqrt{t_0^2 + 4\,h^2p^2} - t_0\right] \tag{8.8}$$

and

$$y = -\frac{\sqrt{t_0^2 + 4\,h^2p^2} - t_0}{2\,p}. \tag{8.9}$$

To compute the traveltime I refer back to Figure 8.1. This time I use the large gray triangle, to obtain the relation

$$\sin\theta = \frac{2\,h\,\cos\phi}{L}, \tag{8.10}$$

where L is the length of the hypotenuse. After some algebraic manipulation of the

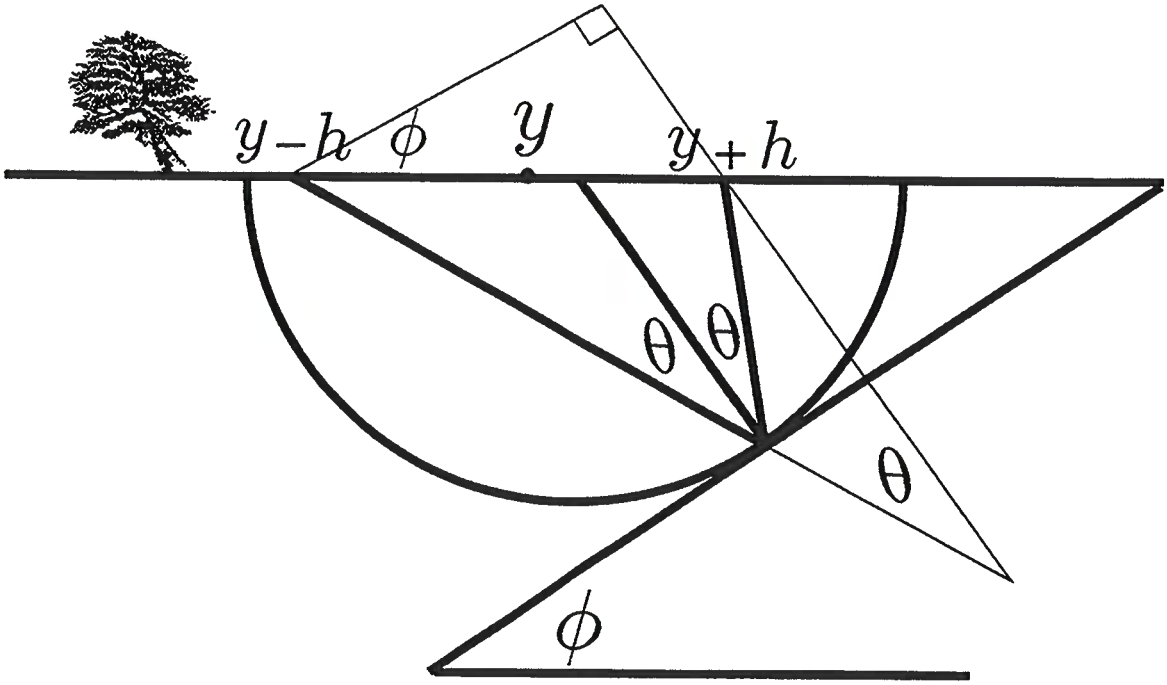

FIG. 8.1. Geometry of the TZO stacking path search. A finite–offset modeling over a zero–offset isochron reflecting surface.

previous formulas on the figure, I derived the following equation:

$$t = \frac{2\,h}{v}\sqrt{1 + \frac{v^2\,(\sqrt{t_0^2 + 4\,h^2p^2} + t_0)^2}{16\,h^2} - \frac{v^2\,p^2}{4}}. \tag{8.11}$$

After expanding the square binomial and collecting terms one finds

$$t = \frac{2\,h}{v}\sqrt{1 + \frac{v^2\,t_0}{8\,h^2}(t_0 + \sqrt{t_0^2 + 4\,h^2p^2}\,)}. \tag{8.12}$$

This equation corresponds to equation E–6 in Bleistein et al. (1997), after noting that L here is $2L$ there. Equations (8.9) and (8.12) parameterize the TZO stacking path. This representation is appropriate for $\omega - k$ algorithms given that in the Fourier domain $p = k/\omega$. Figure 8.2 shows the TZO stacking path for the parameters $v = 2$ km/s, $h = 0.5$ m and $t_0 = 1$ s, and for the zero–offset ray parameter $-\infty \leq p \leq \infty$. The thick bold line corresponds to zero–offset ray parameters $-2/v \leq p \leq 2/v$; that is, to reflected energy, while the thin line assumes $\sin\phi > 1$. That implies evanescent energy. We should then limit the aperture of our TZO stacking path to avoid evanescent energy. The range of non–evanescent midpoints is given by the

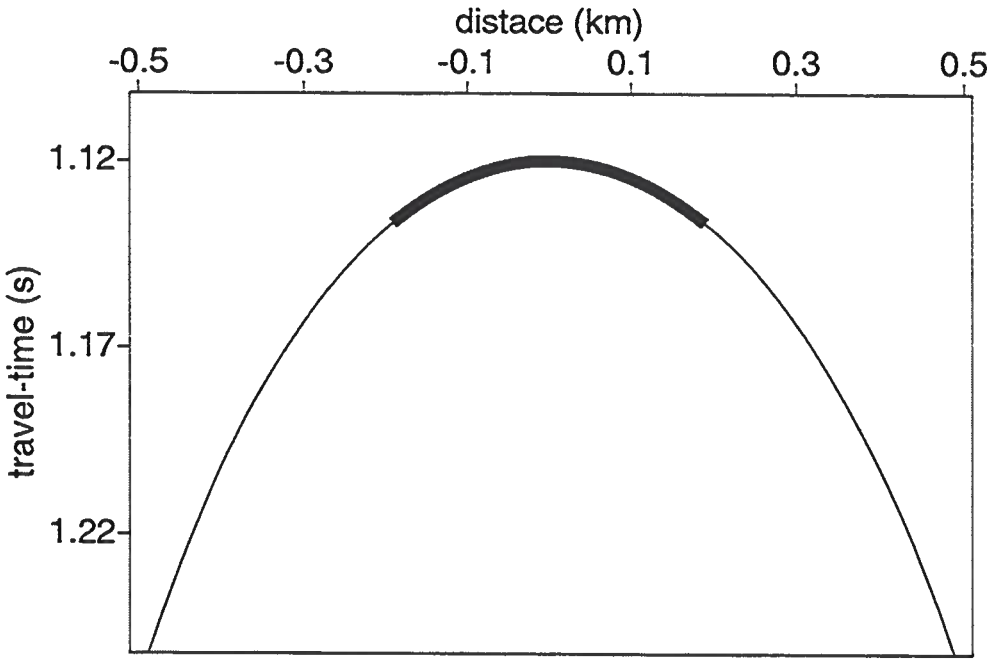

FIG. 8.2. TZO stacking path for the parameters $v = 2$ km/s, $h = 0.5$ km and $t_0 = 1$s. The thick bold part corresponds to reflected energy while the thin part corresponds to evanescent energy.

inequality.

$$|y| \leq \frac{\sqrt{v^2 t_0^2 + 16 h^2} - v t_0}{4}. \tag{8.13}$$

A different representation of the TZO stacking path for the constant velocity case can be obtained by eliminating p from equations (8.9) and (8.12). We find

$$t = \frac{2h}{v} \sqrt{1 + \frac{v^2 t_0^2}{4(h^2 - y^2)}}. \tag{8.14}$$

While this expression is compact, it is not sufficient to derive the aperture of the TZO stacking path.

If, instead of assuming $x_0 = \xi_0 = 0$, I would have started with an arbitrary x_0, the previous formula would be transformed into

$$t = \frac{2h}{v} \sqrt{1 + \frac{v^2 t_0^2}{4\left[h^2 - (y - x_0)^2\right]}}. \tag{8.15}$$

This equation was derived by Tygel et al. (1995a).

Let us now define the Normal MoveOut (NMO) time as

$$t_n = \sqrt{t^2 - \frac{4h^2}{v^2}}. \tag{8.16}$$

By squaring equation (8.15) and using the NMO time t_n, one finds:

$$\frac{t_0^2}{t_n^2} + \frac{(y - x_0)^2}{h^2} = 1. \tag{8.17}$$

Instead of having (x_0, t_0) as input parameters and (y, t) as dependent and independent variables, we reverse roles, so that (y, t) are now (input) parameters and (x_0, t_0) are running (output) variables. Then equation (8.17) represents the well known (velocity independent) DMO ellipse (Hale, 1992). That is, the equation that represents the convolutional (forward) path is algebraically equivalent to the equation that represents the stacking (inverse) path. Going from one to the other is a matter of interchanging input and output variables. This is true not only for TZO but for any SDM process.

Depth–dependent velocity. For the case of depth–dependent velocity, no analytic close forms, analogous to the results above, exist and numerical ray tracing must be used. To better understand this problem, I will include some of the work done by Artley & Hale, (1994) on the TZO forward problem. My goal, here is to find a kinematic inverse TZO operator, since that represents the stacking path $\mathcal{S}$.

We need to perform ray tracing from all scatterers in the medium to all source–receiver points. Given that there are no lateral changes in velocity, we could pick a reference point (we pick midpoint $y = 0$ for the forward TZO problem and zero–offset point $x_0 = 0$ for the inverse TZO problem) and compute all our travel times relative to that point. All travel times relative to different points are obtained by knowing that the rays are shifted versions of those relatives to the reference point $y = 0$ (or $x_0 = 0$). The traveltimes and amplitude weights are stored in ray tables that will be used, first, for the computation of the TZO stacking path $\mathcal{S}$ and, second, for the evaluation of the stacking integral (8.3). I will use Slotnick (1959) to find the table of *two–way* traveltimes, $\tau(p, t)$, lateral traveled distance by the rays $x(p, t)$ and the propagation angle $\theta(p, t)$. Here, p is the ray parameter or vertical slowness. From the traveltime table, I use a non–linear system of five equations with five unknowns. The solution of that system provides, among other things, the stacking curve $\mathcal{S}$. The construction of the tables follows closely the work of Artley and Hale, (1994). They found a system of non–linear equations, from which the DMO impulse response is computed. That system is given by

$$\begin{aligned} 0 &= x(p_g, 2\,t_g) - x\left[p_s, 2\,(t_{sg} - t_g)\right] + 2\,h \\ 0 &= x(p_g, 2\,t_g) - x(p_0, t_0) + h - x_0 \end{aligned}$$

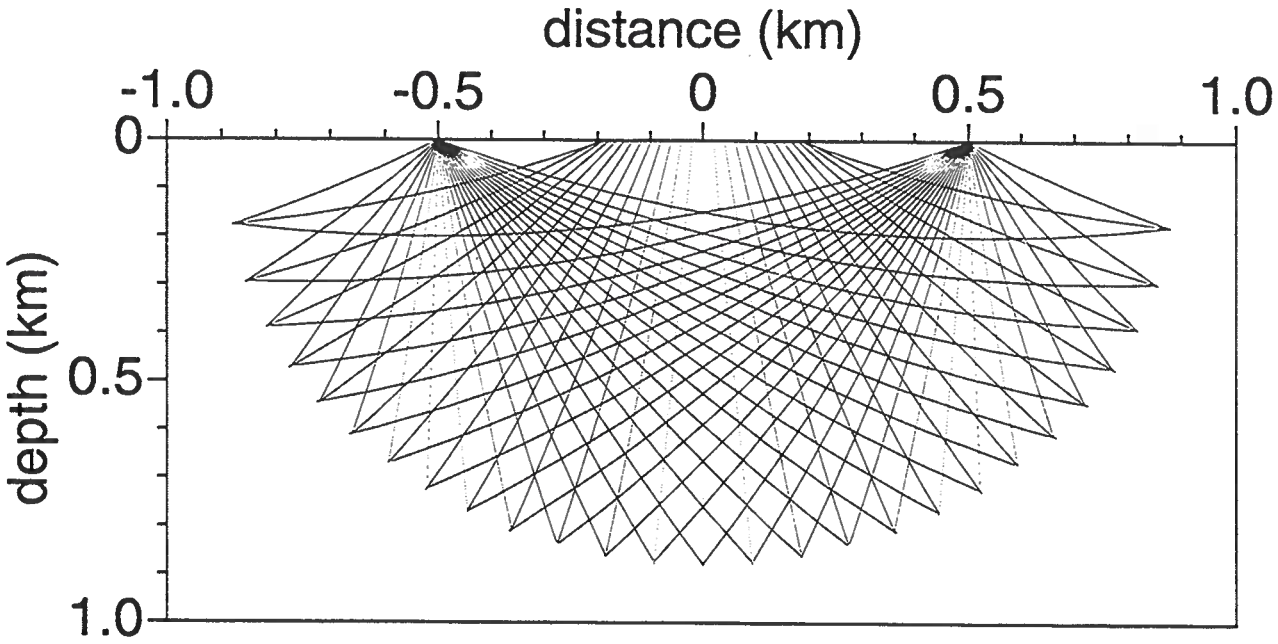

FIG. 8.3. Trios of rays over the finite–offset (input) isochron The computation parameters are: velocity gradient $k = 0.6\,\mathrm{s}^{-1}$, surface velocity $v_0 = 1.5\,\mathrm{km/s}$, NMO time $t_n = 1.0$ s and semi–offset $h = 0.5$ km. Here the source is located at -0.5 km and the receiver at 0.5 km. The midpoint is fixed at 0.

$$\begin{aligned} 0 &= \tau(p_g, 2\,t_g) - \tau\,[p_s, 2\,(t_{sg} - t_g)] \\ 0 &= \tau(p_g, 2\,t_g) - \tau(p_0, t_0) \\ 0 &= \theta(p_s, 2\,tsg - t_g) - \theta(p_g, 2\,t_g) - 2\,\theta(p_0, t_0). \end{aligned} \tag{8.18}$$

Here, $t = t_{sg} = t_s \div t_g$, with t_s and t_g, being the traveltimes from scatter to source and receiver respectively; p_s, p_g, p_0 are the vertical slowness components for the source, receiver, and zero–offset slowness vectors and $x_0 = \xi_0$ is the zero–offset arrival position at the surface. The reader is referred to Artley, (1994) for an insightful discussion of the derivation of this system of equations and its numerical implementation.

The non–linear system of equations (8.18) describes the conditions under which a trio of rays (source ray, receiver ray and zero–offset ray) is realized. The construction of the kinematic DMO impulse response is achieved by selecting the zero–offset rays from all trios which have their tips at the finite–offset isochron. Figure 8.3 shows a set of those trios for the case of a medium with linear velocity distribution with depth. The computation parameters are: velocity gradient $k = 0.6\,\mathrm{s}^{-1}$, surface velocity $v_0 = 1.5\,\mathrm{km/s}$, NMO time $t_n = 1.0$ s and semi–offset $h = 0.5$ km. Note that the tips of the rays draw the finite–offset isochron. Figure 8.4 shows three kinematic impulse

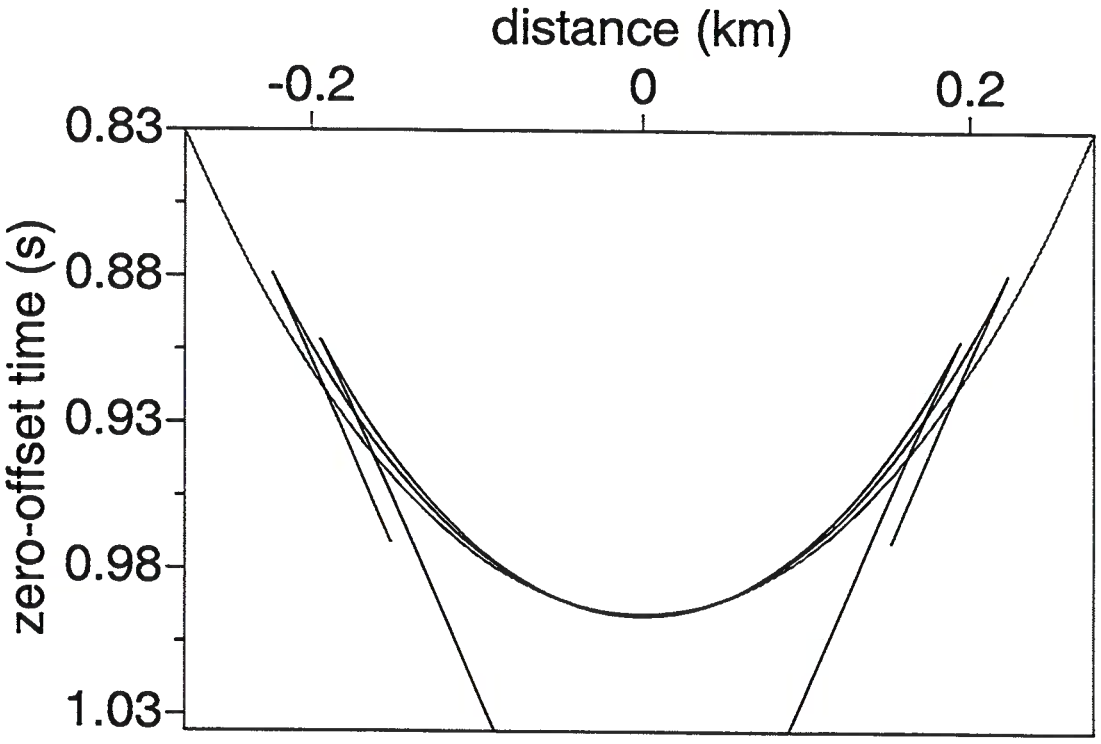

FIG. 8.4. Kinematic TZO impulse responses for a inhomogeneous media with constant velocity gradients $k = 0\,\mathrm{s}^{-1}$ (outer most), $k = 0.3\,\mathrm{s}^{-1}$ (central) and $k = 0.6\,\mathrm{s}^{-1}$ (inner most). Here the surface velocity is $v_0 = 1.5\,\mathrm{km/s}$ and the semi–offset is $h = 0.5$ km. All impulses have the same NMO time $t_n = 1.0$ s.

responses corresponding to the same parameters: surface velocity $v_0 = 1.5\,\mathrm{km/s}$, semi–offset $h = 0.5$ km, NMO time $t_n = 1.0$ s. The velocity gradients for the three curves are $k = 0\,\mathrm{s}^{-1}$ (outer most), $k = 0.3\,\mathrm{s}^{-1}$ (central) and $k = 0.6\,\mathrm{s}^{-1}$ (inner most). The effect of increasing the gradient is to squeeze the operator. One can see from formula (8.13) that for the constant velocity case the increase in velocity reduces the length of midpoint ranges. An increase in gradient implies increase in RMS velocity, so, in a way, this squeezing for the depth–dependent velocity is consistent with the earlier result for constant velocity.

Equation (8.3), however, does not represent a superposition–type operator but a stacking–type operator. Instead of the kinematic impulse response for the direct (TZO) problem, we want to compute the kinematic (path) impulse response for the inverse (TZO) problem. As I explained in Chapter 6, this operator is constructed by doing a finite–offset ray–tracing to the zero–offset isochron. This means that we should select the trios that have their tips on a zero–offset isochron, and from those trios we should pick the finite–offset rays. In this way we find the stacking path $\mathcal{S}$.

One can see, however, that y is not present in the system (8.18). The reason for this is that this system is built assuming that the midpoint, y is zero. Since we need the explicit occurrence of y, we then map x_0 into $y + x_0$. In this way we account for an arbitrary midpoint y. The new system of equations becomes

$$\begin{aligned}
0 &= x(p_g, 2\,t_g) - x\left[p_s, 2\,(t - t_g)\right] + 2\,h \\
0 &= x(p_g, 2\,t_g) - x(p_0, t_0) + h - y - x_0 \\
0 &= \tau(p_g, 2\,t_g) - \tau\left[p_s, 2\,(t - t_g)\right] \\
0 &= \tau(p_g, 2\,t_g) - \tau(p_0, t_0) \\
0 &= \theta(p_s, 2\,t - t_g) - \theta(p_g, 2\,t_g) - 2\,\theta(p_0, t_0).
\end{aligned} \tag{8.19}$$

Now we are ready to define the unknowns and the parameters in this system. We have the five unknowns y, p_s, p_g, t_s, t and the parameters x_0, t_0, p_0, h.

The numerical technique used to solve system (8.19) is the multi–dimensional Newton–Raphson iteration (Press *et al.*, 1986).

The strategy to compute the stacking path $\mathcal{S}$ is as follows. The input parameters (t_0, x_0) and the half–offset h, determine a unique zero–offset (output) isochron. We do not need to compute that isochron explicitly. We use those input parameters and the system (8.19) to find the stacking path $\mathcal{S}$ parameterized in terms of the reflector dip, through the zero–offset vertical slowness p. That is,

$$\mathcal{S} = \left\{(t(p), y(p)), -2/v_0 \leq p \leq 2/v_0\right\}. \tag{8.20}$$

Here, v_0 is the minimum medium speed. Figure 8.5 shows the trios of rays reflecting on the zero–offset isochron. Here the model parameters used are velocity gradient $k = 0.6\,\mathrm{s}^{-1}$, surface velocity $v_0 = 1.5\,\mathrm{km/s}$, semi–offset $h = 0.5$ km and NMO time $t_n = 1.0$ s. Figure 8.6 shows the stacking paths for the same model parameters and three different gradients: $k = 0\,\mathrm{s}^{-1}$ (bottom), $k = 0.3\,\mathrm{s}^{-1}$ (central) and $k = 0.6\,\mathrm{s}^{-1}$ (top). These figures are the loci of points representing the support of the impulse response for the inverse TZO problem.

8.2.2 Basic Dynamics

I define basic dynamics as the evaluation of the integral (8.3), where the weight function is set to unity. The integral should be evaluated in the midpoint ($\xi = y$) domain. The path $\mathcal{S}$ is computed as a parametric curve where the parameter $p = 2\sin\phi/v(z)$ is the zero–offset ray parameter. We perform linear interpolation to reposition the points so that they are located at actual midpoints. Figure 8.7 shows the TZO stacking path corresponding to the model parameters $k = 0.6\,\mathrm{s}^{-1}$, $v_0 = 1.5$ km/s, $h = 0.5$ km and NMO time $t_n = 1.0$ s. The stars represent the midpoint linearly interpolated values.

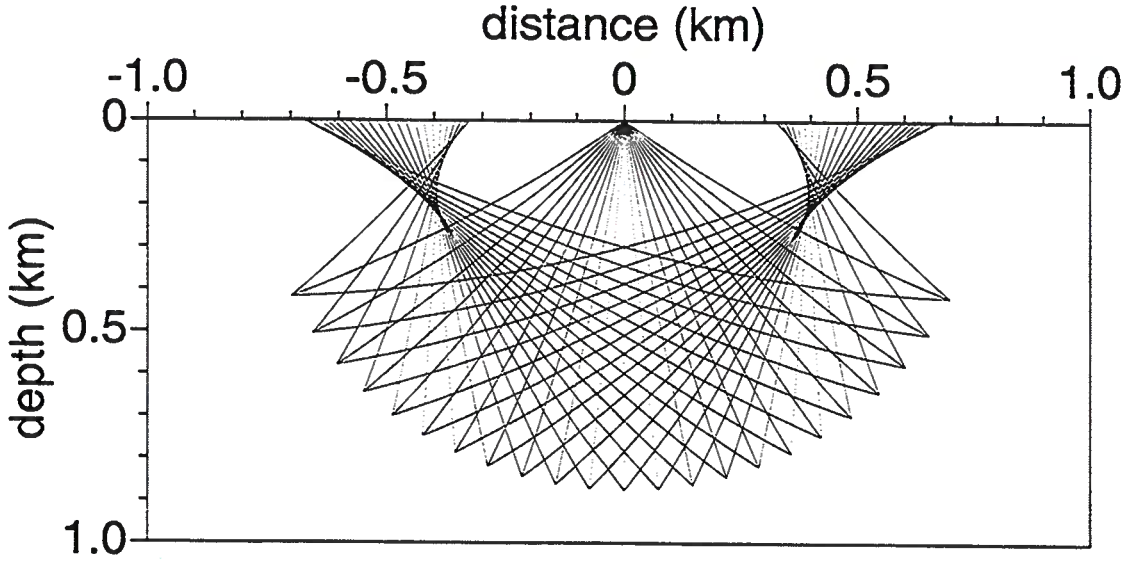

FIG. 8.5. Trios of rays reflecting at the zero–offset (output) isochron surface(curve). The zero–offset location is at zero (center), the source rays are on the left and the receiver on the right. The model parameters for this experiment are: velocity gradient $k = 0.6\,\mathrm{s}^{-1}$, surface velocity $v_0 = 1.5\,\mathrm{km/s}$, semi–offset $h = 0.5$ km and NMO time $t_n = 1$ s.

The TZO impulse response In order to design an accurate algorithm, a detailed study of the unit impulse response will be carried out. Figure 8.8 shows the dynamic impulse response of the basic dynamics for the integral operator (8.3). In the computer implementation, the unit impulse support is given by a single grid cell with amplitude 1, while all other grid cells have amplitude 0. A value of 1 is added to the result (output) each time the TZO stacking path intersects this particular grid. The next obvious test is to band–limit the input spike. A trapezoidal filter of 10, 20, 60, 70 (percentages of the Nyquist frequency) was applied to a spike with an input (and also output) temporal sampling interval of 2 ms and spatial sampling interval of 0.02 km. Figure 8.9 shows the band–limited impulse response, before (top) and after (bottom) the time half–derivative is applied to the data. The half–derivative filter has an overall effect a small phase shift. This effect is more notorious in the border traces due to the constructive interference of two close wavelets. Also, it is apparent from this figure that the operator is spatially aliased. The next task is then to design an antialias filter for the TZO operator.

Operator aliasing In this section, I explain the design of an spatial anti–alias filter for the TZO operator. We need at least two samples per cycle (spatial wavelength) to avoid spatial aliasing. Generally speaking, in a data set we have fixed spatial sampling

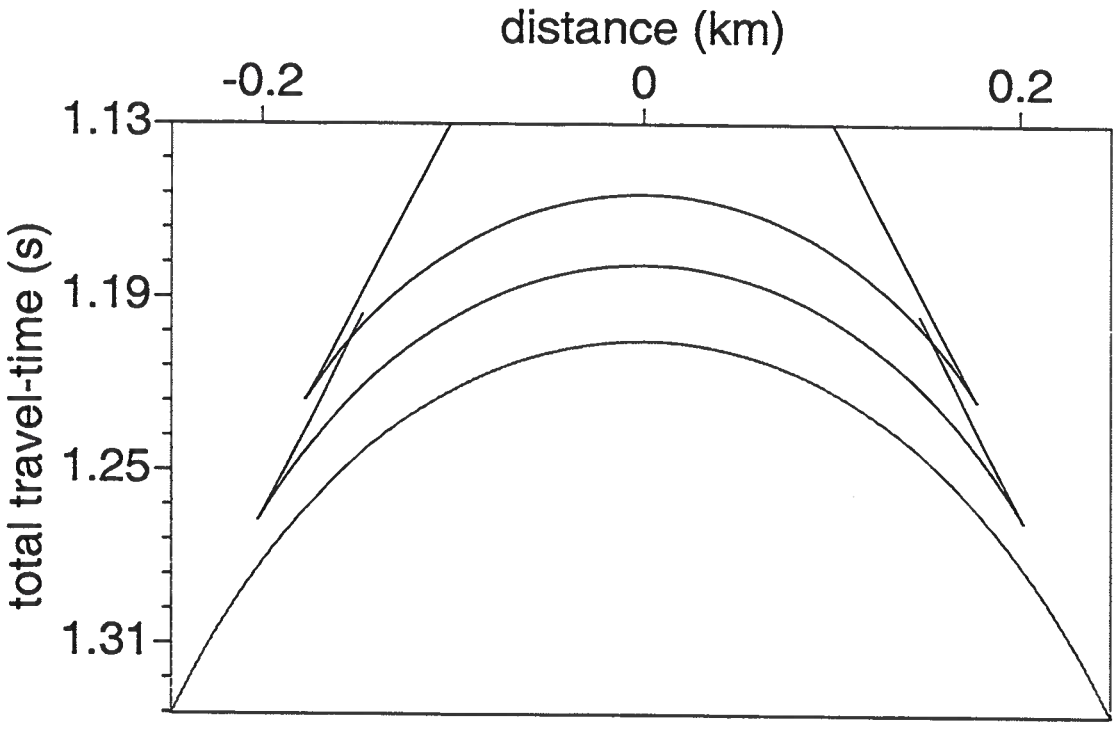

FIG. 8.6. Stacking paths for a TZO operator in a medium with velocity gradients $k = 0\,\mathrm{s}^{-1}$ (bottom), $k = 0.3\,\mathrm{s}^{-1}$ (central) and $k = 0.6\,\mathrm{s}^{-1}$ (top). Here also the surface velocity is $v_0 = 1.5\,\mathrm{km/s}$ and the semi-offset is $h = 0.5$ km. All impulses have the same NMO time $t_n = 1.0$ s.

(Δy) and fixed temporal sampling (Δt). The operator (stacking path) slope, however, is changing along the data. If the dip of the operator is large, we could need a smaller spatial sampling rate (Δy_{new}) or a larger temporal sampling (Δt_{new}). This implies two things. We would have to spatially resample the input data by interpolating new data traces at a higher storage and speed cost, or either low–pass filter the traces at the cost of resolution loss. Let me be more specific here.

I assume a data set with spatial sampling rate Δy and temporal sampling rate Δt. I call $f_c = 1/\Delta t_c$ the maximum temporal frequency that we can handle before spatial aliasing takes place. If a given data point the operator has a slope $p = dt/dy$ then the spatial moveout for the period Δt_c is given by

$$\begin{aligned} \Delta y_m &= \Delta t_c \frac{dy}{dt} \\ &= \frac{1}{f_c p}. \end{aligned} \tag{8.21}$$

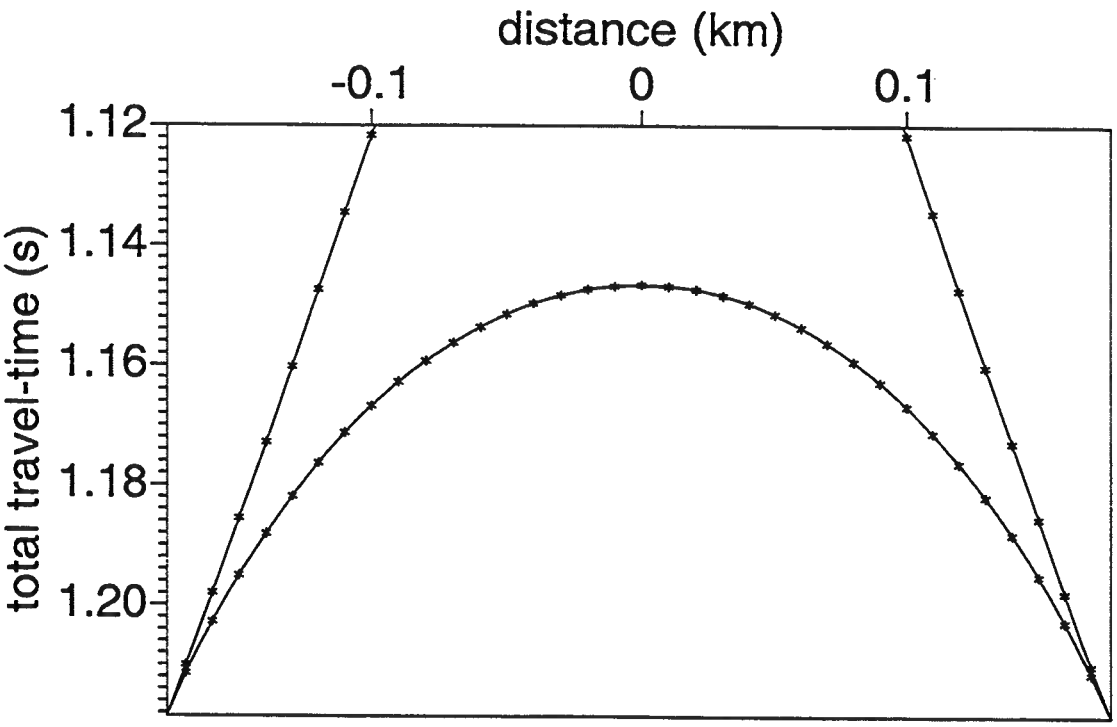

FIG. 8.7. Interpolated values of the stacking path $\mathcal{S}$, for the parameters $k = 0.6\,\mathrm{s}^{-1}$, the surface velocity $v_0 = 1.5\,\mathrm{km/s}$, semi–offset is $h = 0.5\,\mathrm{km}$ and NMO time $t_n = 1.0\,\mathrm{s}$. The solid line is computed from numbers which represent a uniform sampling in ray parameter p. We perform linear interpolation to re–locate those numbers uniformly over midpoint positions. The stars show the points sitting in a midpoint position.

We want 2 spatial samples per cycle, that is, $\Delta y_m \geq 2\Delta y$. In other words,

$$f_c \leq \frac{1}{2\,p\,\Delta y}. \tag{8.22}$$

All frequencies f such that $f_c \leq f \leq f_N = 1/(2\,\Delta t)$ would be spatially aliased.

Let us illustrate this concept with a numerical example. We assume a data set with time sampling rate $\Delta t = 2$ ms and space sampling rate $\Delta y = 0.02$ km. The TZO stacking curve can get close to the maximum $p = 2/v(z)$ for steep reflectors. Let us assume $p = 2/v(z)$ and a velocity at depth z of $v(z) = 2$ km/s. We compute

$$f_c \leq 25\,Hz = 0.1\,f_N. \tag{8.23}$$

This is certainly a strong high cut filter relative to the Nyquist frequency f_N. A different alternative is to interpolate traces so that the spatial sampling rate is smaller.

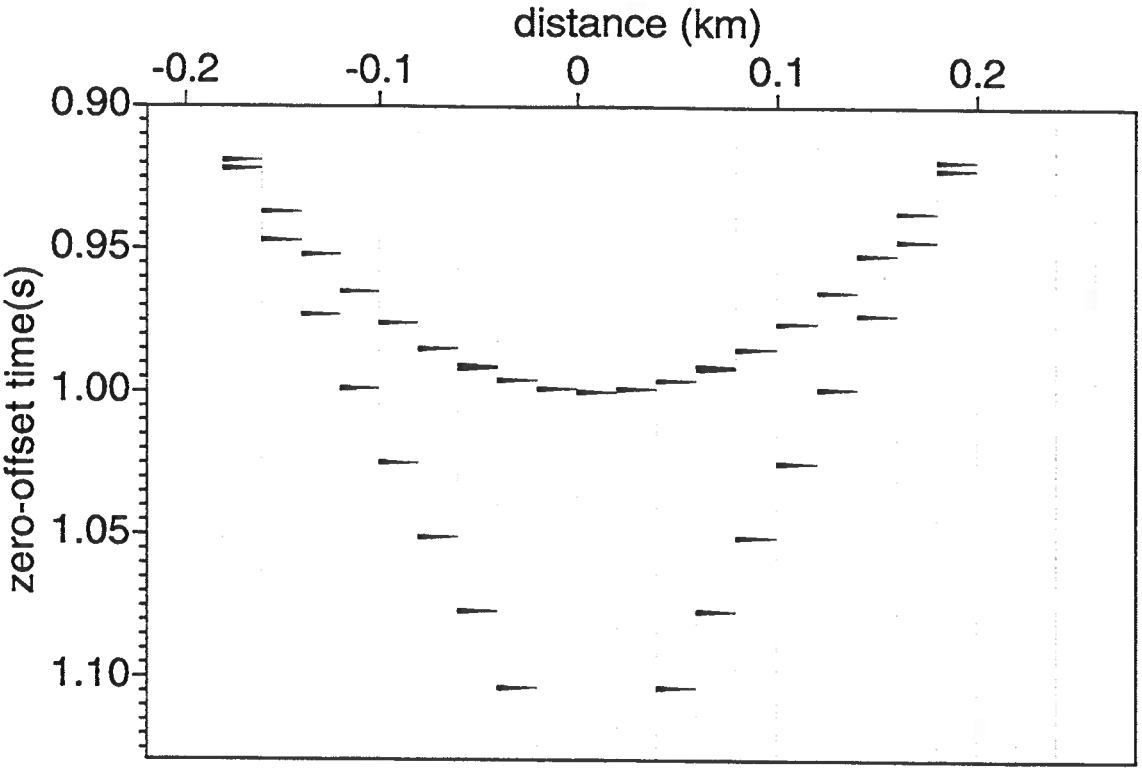

FIG. 8.8. Dynamic impulse response. All spikes are of equal amplitude 1. The parameters for this impulse are $k = 0.6\,\mathrm{s}^{-1}$, the surface velocity $v_0 = 1.5\,\mathrm{km/s}$, semi-offset is $h = 0.5$ km and NMO time $t_n = 1.0\,\mathrm{s}$.

Let us say $\Delta y_{new} = 2$ m. We would then arrive to the inequality

$$f_c \leq f_N. \tag{8.24}$$

We then can broad the working spectrum at the expenses of high memory storage and computational–time requirements.

An alternative to avoid aliasing is to mute the operator for steep dips. This would be a problem for near vertical structures. Gray (1992) proposed a technique where several copies of input data should be filtered to use according to the maximum non alias frequency f_c. Hale (1991) proposed a method to anti–alias dip moveout operators in the time domain. Hale's method applies a sequence of time shifts to each input seismogram. For nearest–neighbor interpolation, this method implies a boxcar averaging of the input trace values along the time direction. Here, I will use a technique described by Lumley et al. (1994). This technique uses a triangle filter in time. Given that we know the maximum unaliased frequency f_c at each point along the TZO stacking path, we need to lowpass filter the seismic data in order to satisfy

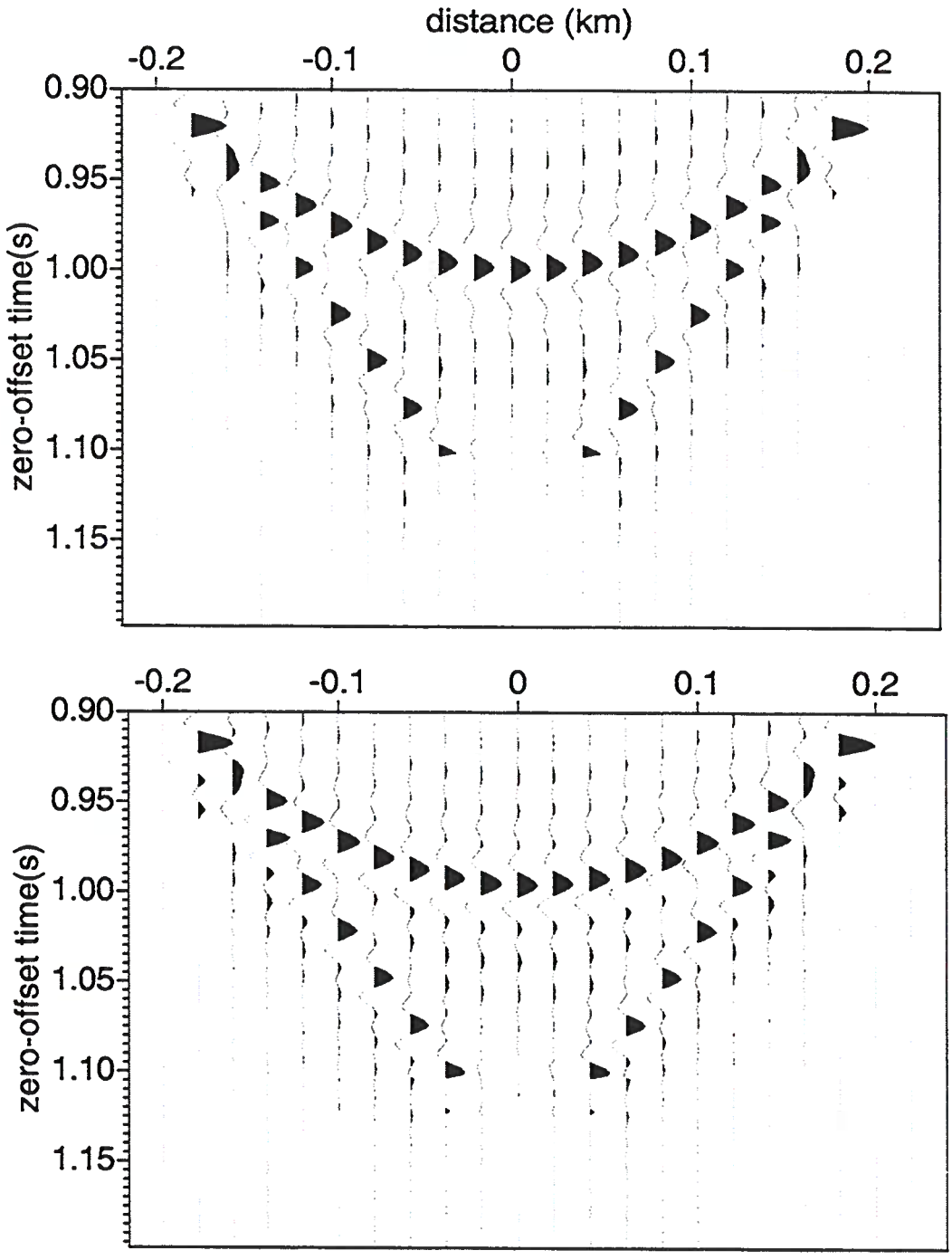

FIG. 8.9. Top: before the half–derivative filter is applied. Bottom: after the half–derivative filter is applied. Dynamic band–limited impulse response. The parameters for this impulse are $k = 0.6\,\mathrm{s}^{-1}$, the surface velocity $v_0 = 1.5\,\mathrm{km/s}$, semi–offset is $h = 0.5$ km and NMO time $t_n = 1.0\,\mathrm{s}$. Temporal sampling interval of 2 ms and spatial sampling rate of 0.02 km are used. Note the aliasing on the steep events.

the aliasing criterion (8.22).

The Z–transform representation of an arbitrary N–point triangle filter can be expressed as

$$g(z) = \frac{-z^{-k-1} + 2 - z^{k+1}}{\alpha(1-z)(1-z^{-1})}. \tag{8.25}$$

Here the triangle length is given by $N = 2k + 1$. The filter scaling coefficient $\alpha = (k+1)^2$ is a normalization factor designed in a way that the area of the wavelet is preserved. We are interested in the preservation of the peak amplitude under filtering, for inversion purposes.

The amplitude spectrum of the triangle filter is then

$$A(\omega) = \frac{\sin^2(\omega\,\Delta t\,N/2)}{\alpha\,\sin^2(\omega\,\Delta t/2)}, \tag{8.26}$$

[1] We want to use the first notch of this filter as the maximum non aliased frequency f_c. Then, the appropriate anti-aliasing triangle operator length N should be

$$N \geq 4p\frac{\Delta y}{\Delta t}, \tag{8.27}$$

where I used equation (8.22). Figure 8.10 shows an illustration of a triangular filter with N=7 (k=3) points, and its frequency domain representation. We see that this triangular filter is a low pass filter. Its high cut frequency f_c is located at the first notch of the filter. I mentioned above that we are interested in preserving the peak value of the wavelet instead of its area. We want to have as an output peak value an amplitude independent of any scaling produced by any filtering not explicitly implied by equation (8.3). We should then normalize the anti–aliasing operator. This is done by dividing it by the area of the filter shown in equation (8.26). The area of the filter would be given by the formula

$$\sum_{j=0}^{nw-1} A(j\,\Delta\omega)\,\Delta\omega \tag{8.28}$$

where $nw = 2.0\,\pi/(nfft * dt)$, $ntfft$ is the total number of frequencies after padding the frequency trace with zeroes and A is defined by the equation,

$$A(j\Delta\omega) = \frac{\sin^2(j\Delta\omega\,\Delta t\,N/2)}{\alpha\,\sin^2(j\Delta\omega\,\Delta t/2)}. \tag{8.29}$$

[1]Note that the factor α is missing in Lumley et al.'s paper.

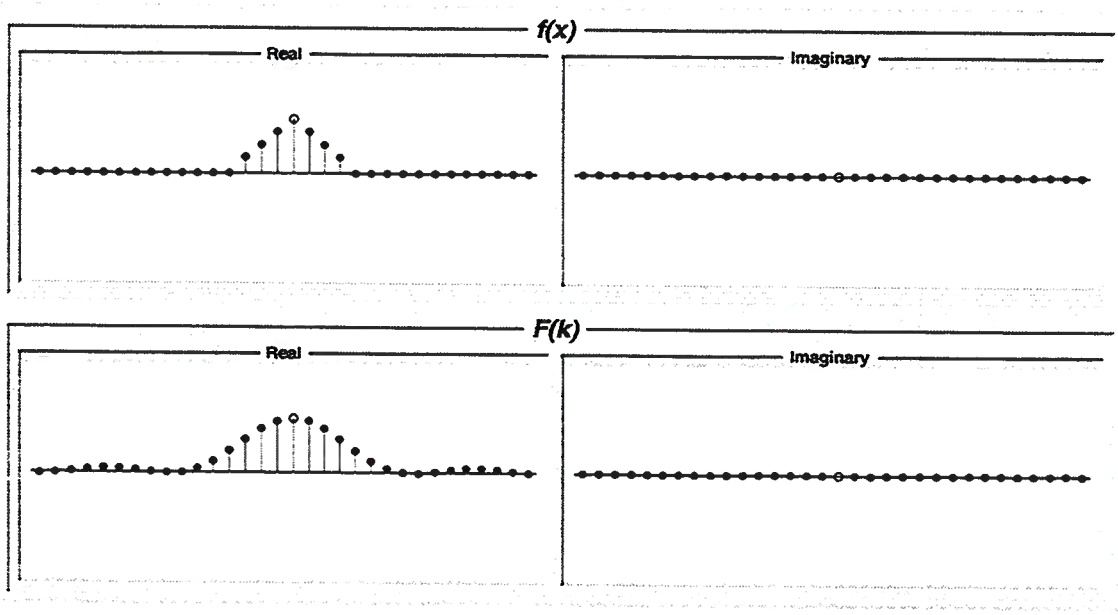

FIG. 8.10. Illustration of a 7 point triangular filter and its frequency domain representation. Plot created with the application FFTLAB written by Dave Hale.

One advantage of this method is that, while being better behaved than the box car filter, it is still inexpensive and can be computed on the fly. The numerical algorithm to compute this filter is split in two parts. First, the trace is integrated twice (causal and anticausal integration representing the denominator of the operator g in equation (8.25)). Then, while the summation over the stacking path is performed, a second derivative–type 3 point filter is applied (the numerator of operator g in equation (8.25)). Figure 8.11 shows an impulse response with the same parameters as the previous impulse responses after the antialias filter was applied.

8.3 True amplitude TZO

This section explains how to numerically compute the different contributions of all factors involved in equation (8.3) to the total weight of the TZO stack. For exposition purposes, I will divide this section into subsections corresponding to individual factors of the TZO integral.

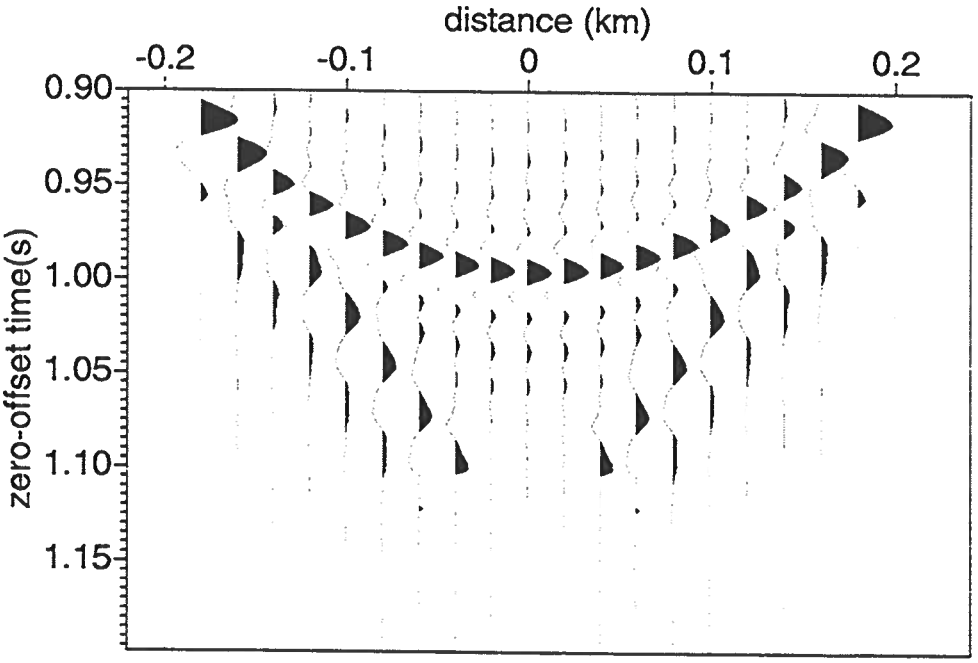

FIG. 8.11. Impulse response after half derivative and antialias filtering. I used the same parameters here as in the previous impulse responses.

8.3.1 The out–of–plane amplitude compensation

The out–of–plane amplitude compensation is given by equation (7.38). For the specific problem that we are dealing with, this expression is

$$\mu(\boldsymbol{x}_0, y) = \sqrt{\frac{\sigma_0(\sigma_s \div \sigma_g)}{2\,\sigma_s\,\sigma_g}} \tag{8.30}$$

The diffent σ values should be computed by integrating directly equation 7.10, for the source, receiver and zero offset rays.

8.3.2 The $H_D - H_R$ contribution

Here we compute the second derivatives of the stacking path and Huygens curve with respect to the midpoint y at the stationary phase point $\boldsymbol{x}_0$. We already know the stacking path, and so we can compute the second derivatives by using a finite difference approximation.

To compute the time corresponding to the Huygens diffraction curve we need to perform two–point ray–tracing from the stationary phase point $\boldsymbol{x}_0$ to the points $(y_0 - \delta y - h, 0)$ and $(y_0 - \delta y \div h, 0)$ as well as to the points $y_0 \div \delta y - h$ and $y_0 \div \delta y \div h$. Here y_0 is the midpoint corresponding to the zero–offset ray through the stationary phase point $\boldsymbol{x}_0$.

The finite difference operator to be computed is

$$H_D - H_R = \frac{\phi_{D-R}(\boldsymbol{x}_0, y_0 - \delta y) \div \phi_{D-R}(\boldsymbol{x}_0, y_0 \div \delta y)}{(\delta y)^2}. \tag{8.31}$$

Here ϕ_{D-R} is the difference on time between the Huygens diffraction curve and the stacking path. Note that the term in the middle of the central difference operator is missing. This is due to the fact that both curves are tangent at that point, so their difference is zero there. H_R can be found by taking the finite difference operator over the stacking path which is already known. To find H_D we should use a travel–time table from all scatters to a fixed source located at zero. See that the time from any source to any scatterer is given only by the lateral distance and depth along the ray due to the lateral invariance of the velocity field.

8.3.3 The WKBJ amplitudes

The WKBJ amplitudes are previously computed by a ray–tracing algorithm and stored in a table; the same is done for a travel–time table. Figure 8.12 shows the $v(z)$ dynamic impulse response with the same parameters used in the previous impulse responses. Although the amplitude distribution seams reasonable (for example, consider the high amplitude in the casps), we unfortunately have no way to quantitatively test the dynamics. For a model of this complexity, there is no closed–form analytical representation of the amplitudes along this operator. The design of further tests that teach us about the amplitude behavior of TZO impulse responses in a medium with varying velocity with depth, is left as future task.

Unlike the $v(z)$ case, for a medium with constant velocity we can find analytical representations that can help us to demonstrate the kinematics and dynamics of the SDM process. In the next chapter I will show a model that illustrates the properties of a canonical SDM operator.

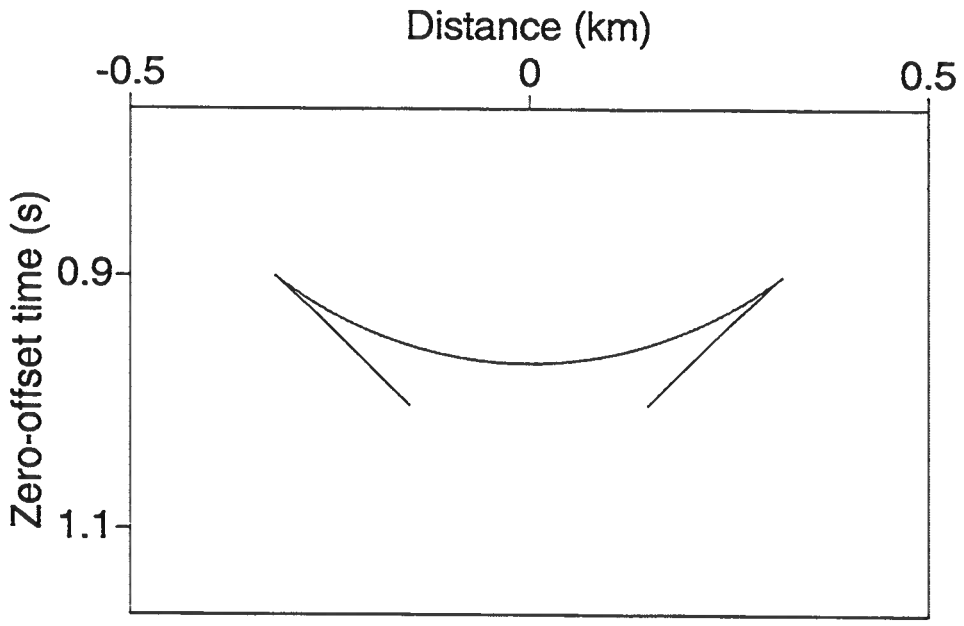

FIG. 8.12. Dynamic TZO impulse response. I used the same parameters here as in the previous impulse responses. The amplitudes at the cusps are clipped for display purposes.

Chapter 9

A NUMERICAL DEMONSTRATION

The main physical properties of SDM are that it produces the kinematics, point–source and reflector curvature geometrical spreading effects of the output configuration and/or model parameters while it preserves the oblique incidence reflection coefficient embedded in the input data.

The canonical example of SDM is TZO. I will illustrate the main properties of SDM based on a model for which we know the asymptotic SDM analytical response. We compare this analytic solution with a numerical computation using an implementation of TZO in a constant velocity medium.

9.1 The model

Let us consider a circular reflector in form of a circular cylinder, with center at a depth of 2 km and a radius of $\rho = 1$ km. (see Figure 9.1). Here $h = 0.5$ km is the semioffset, $\boldsymbol{x}_s = (y - h, 0, 0)$ is the source location, $\boldsymbol{x}_g = (y + h, 0, 0)$ is the receiver location, $\boldsymbol{x}_m = (y, 0, 0)$ is the midpoint location and $\boldsymbol{x}_0 = (x_0, 0, 0)$ is the zero–offset location. r_s denotes the length of the source–to–reflector ray, r_0 is the length of the zero–offset ray, r_g is the length of the receiver–to–reflector ray. $H = 1$ km describes the depth at the top of the cylinder, ρ is radius of the cylinder, ϕ is the reflector dip at the reflection point and θ is the angle that the source (or receiver) ray makes with the normal to the reflector.

Below, I will model a common offset section and then apply TZO to this section in the common offset domain.

9.1.1 The kinematics

Here I present a collection of formulas, that describe the kinematics of this experiment. They can be derived from the plane geometry in Figure 9.1. The reader is referred to Bleistein et al. (1997) for more insight into these formulas.

$$\phi = \arctan \frac{x_0}{H + \rho}, \tag{9.1}$$

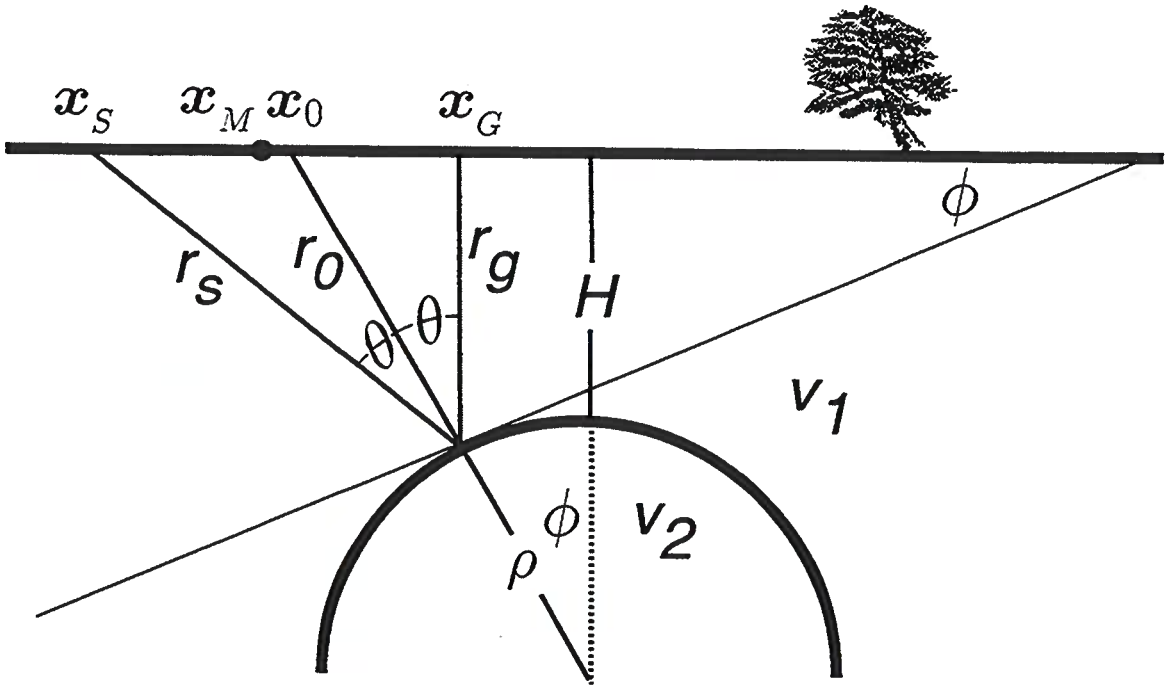

FIG. 9.1. Model of a cylindrical reflector in a constant velocity medium.

$$y = x_0 \div \frac{2\,h^2 \sin\phi}{\sqrt{\left[\rho - (H \div \rho)\sec\phi\right]^2 \div 4h^2} - \left[\rho - (H \div \rho)\sec\phi\right]}, \tag{9.2}$$

$$r_0 = \sqrt{(H \div \rho)^2 \div x_0^2} - \rho, \tag{9.3}$$

$$L = \frac{r_s \div r_g}{2} = \sqrt{(y - x_0 \div r_0)^2 \sin^2\phi \div h^2 \cos^2\phi}, \tag{9.4}$$

and

$$\cos\theta = \frac{\sqrt{L^2 - h^2\cos^2\phi}}{L}. \tag{9.5}$$

9.1.2 The dynamics

The reader is referred to Bleistein et al. (1997) for the derivation of the following formulas:

1. *Reflection coefficient.* The oblique acoustic reflection coefficient R is given by

$$R = \frac{z_1 - z_2}{z_1 + z_2}, \tag{9.6}$$

where

$$z_1 = \frac{\cos\theta}{v_1}; \tag{9.7}$$

$$z_2 = \sqrt{1/v_2^2 + \left[\cos^2\theta - 1\right]/v_1^2} \tag{9.8}$$

2. *Spreading effect due to curvature:*

$$\sqrt{\frac{\rho\cos^2\theta}{r_0 + \rho\cos^2\theta}}. \tag{9.9}$$

3. *Geometrical point-source spreading factor:*

$$\frac{1}{4\pi(r_s + r_g)} = \frac{1}{8\pi L}, \tag{9.10}$$

4. *Phase function:*

$$\frac{2\omega L}{v_1}. \tag{9.11}$$

We combine all these elements to build the finite offset section according to

$$U(y, w, h) = \frac{F(\omega)R}{8\pi L}\sqrt{\frac{\rho\cos^2\theta}{r_0 + \rho\cos^2\theta}}\exp\left\{2i\,\omega/v_1\right\}, \tag{9.12}$$

as described in Bleistein et al. (1997). After applying inverse Fourier transform I obtain the finite offset data $u(y, t, h)$. The spreading effect due to curvature in a zero–offset section is given by

$$\sqrt{\frac{\rho}{r_0 + \rho}}; \tag{9.13}$$

and the zero–offset geometrical spreading is given by

$$\frac{1}{8\pi\, r_0}. \tag{9.14}$$

Note that modeling equations (9.1) through (9.11) are given as functions of zero-offset location x_0. Equation 9.12 however is evaluated in midpoint y. Formula 9.2 defines the midpoint y as a function of zero–offset point x_0. The inversion of this

equation for x_0 in terms of y requires the solution of a high–order polynomial without a closed–form analytical solution. Also note that due to the symmetry of the model, we need only to compute one side of the cylinder. Fortunately on either side, the function $y = y(x_0)$ is a monotonic function and hence can be uniquely inverted . I sampled the recording surface finely in x_0 and then did numerical interpolation to find a function $x_0 = x_0(y)$ uniformly sampled in midpoint. Figure 9.2 shows the common–offset data corresponding to midpoints between -2 km and 2 km.

9.2 Transformation to zero–offset

A TZO formula consistent with our definition of "true amplitude" (chapter 1) is numerically implemented. The TZO output data is studied and the main principles of SDM are demonstrated.

Bleistein et al. (1997) derived a TZO formula for a constant velocity medium which satisfies the "true amplitude" requirements of data mapping. The TZO formula in the frequency (ω) domain, for input data in the wave–number (k) domain, is given by

$$u(x_0, w, h) = \frac{1}{2\,\pi} \int \frac{dk\,dt_n}{A} \left[1 \div \frac{2\,k^2\,h^2}{\omega_0^2\,t_n^2}\right] U(k, t, h) \exp i(k\,x_0 \div \omega_0\,t_n\,A) \tag{9.15}$$

Here the NMO corrected time t_n is given by

$$t_n = \sqrt{t^2 - \frac{2\,h}{v_i}}, \tag{9.16}$$

and the factor A is given by

$$A = \sqrt{1 \div \frac{k\,h}{\omega_0\,t_n}^{\,2}}. \tag{9.17}$$

TZO equation (9.15) differs from Hale (1984) by the factor in square braces under the integral sign.

I now show that SDM as applied to this model in the form of TZO produces zero–offset data with the point–source and curvature geometrical spreading factors appropriate for the zero–offset configuration and with the reflection coefficient corresponding to the input (finite–offset) configuration.

Figure 9.3 shows the output of the TZO equation (9.15) applied to the data in Figure 9.2. The wavelets are centered at the zero–arrival time. The peak amplitudes are the product of the geometrical effects (point–source and curvature) of the zero–offset configuration and the reflection coefficient corresponding the input (common–offset)

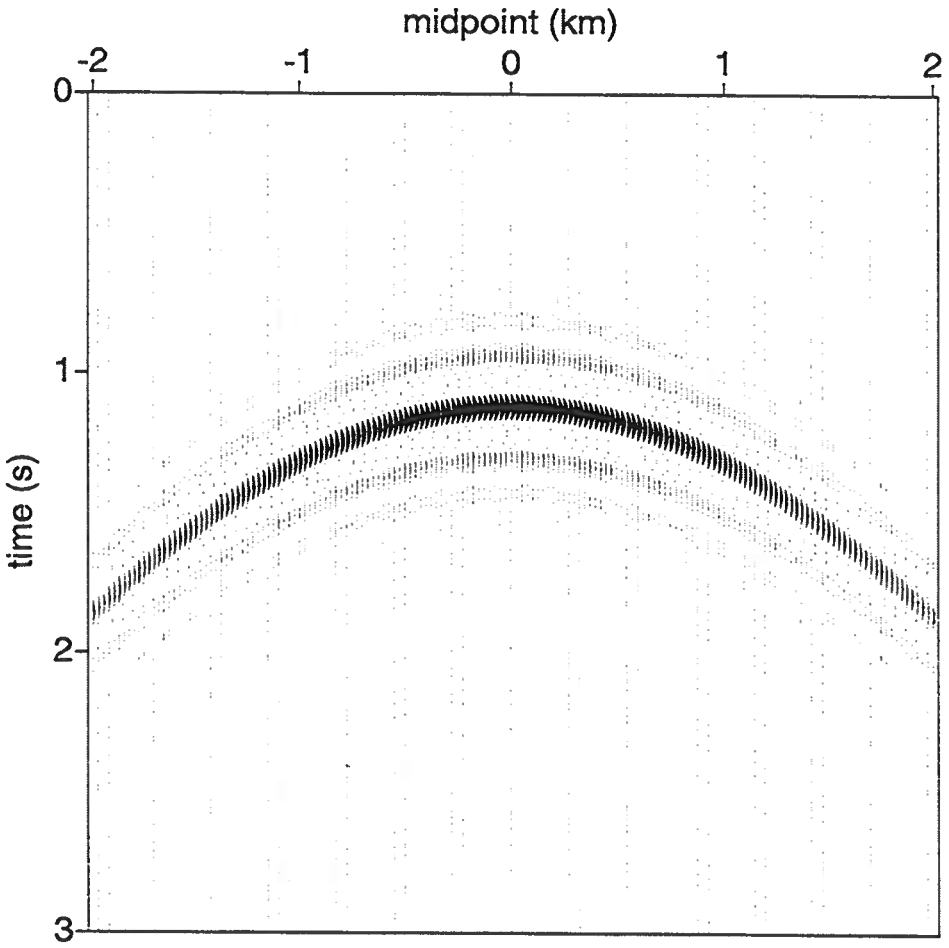

FIG. 9.2. Modeled common-offset for data for the cylindrical reflector experiment sketched in Figure 9.1.

configuration. Also we have to take into account the area of the filter function $F(\omega)$. To demonstrate this we use the analytical expressions for the geometrical effects listed above to scale the peak amplitudes and produce reflection coefficients that should be compared with the theoretical oblique acoustic reflection coefficients given by equation (9.6). I also compute a TZO section using Hale's (1984) algorithm. Figure 9.4 shows the differences between the TZO section computed using Bleistein et al. (1997) and Hale's (1984) formulas. Here we observe that the differences between the two sections are relatively small for small and large dips and larger for intermediate dips. A quantitative analysis of the error is done by using the point source and curvature geometrical factors listed above. I extracted the reflection coefficient of the TZO data using both Bleistein et al. (1997) and Hale (1984). Figure 9.5 displays these reflection coefficients. We see that the relative error between the analytical reflection coefficients and the computed reflection coefficients using Bleistein et al. (1997) formula are under the one percent. The relative error between the analytical reflection coefficients and the computed reflection coefficients using Hale (1984) is small for small and large dips, and larger (still under 10 per cent) for intermediate dips. The accuracy that I achieve in the computation of the zero–offset times and reflection coefficients from the peak amplitudes in the TZO data, proofs the validity of the kinematic and dynamic statements related to SDM. While Hale's (1984) DMO formula, also produces a good approximation of the reflection coefficients, the cost of the evaluation of both formulas is exactly the same. I want to emphasize, however, that the purpose of this section is not to compare Bleisteinet al. (1997) method with Hale's (1984) method, but to illustrate the kinematic and dynamic properties of SDM through this specific example. The comparison with Hale's (1984) work is done as an additional exercise to provide ties with this general theory with well known algorithms in DMO.

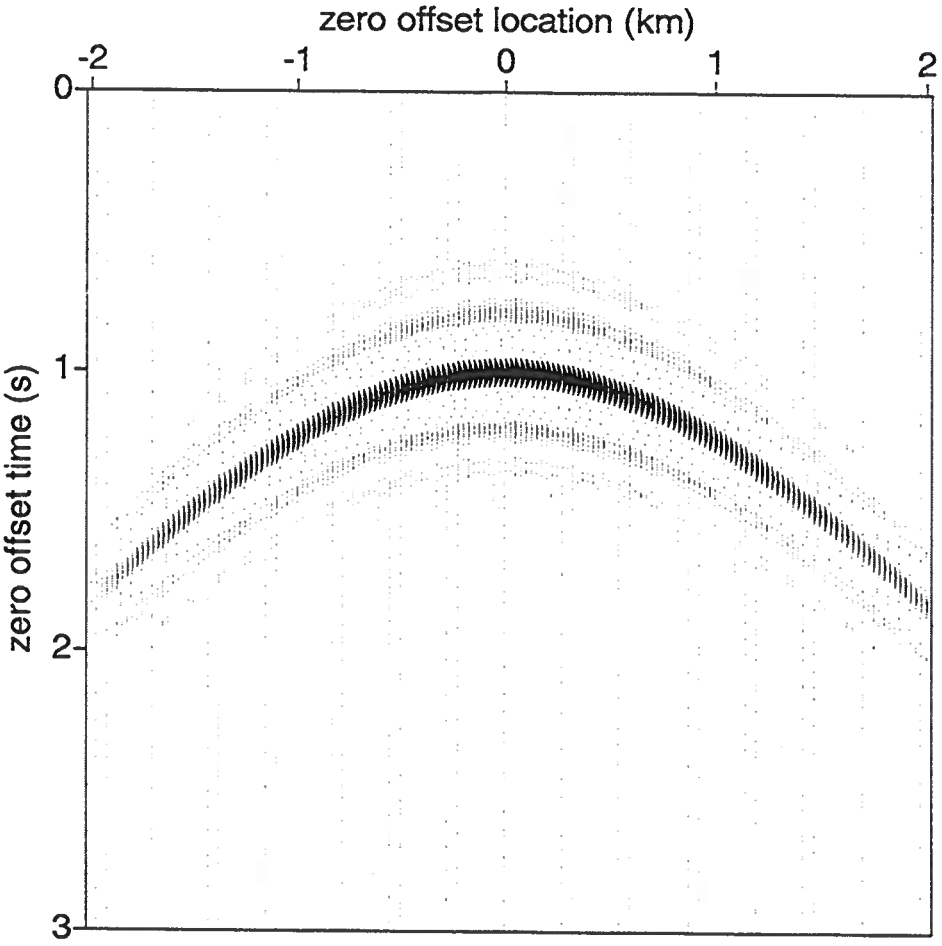

FIG. 9.3. Zero–offset data computed from the data in Figure 9.2 using equation (9.15).

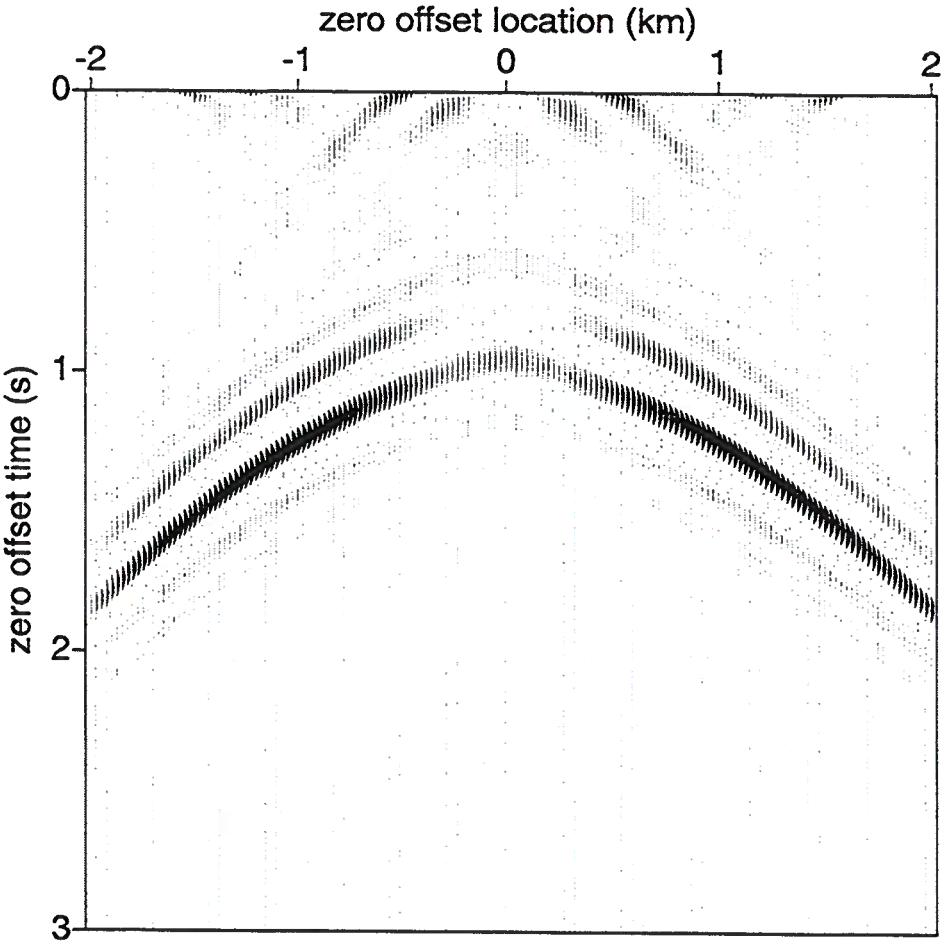

FIG. 9.4. TZO Differences between the TZO sections produced by Bleistein et al. and Hale's formulas.

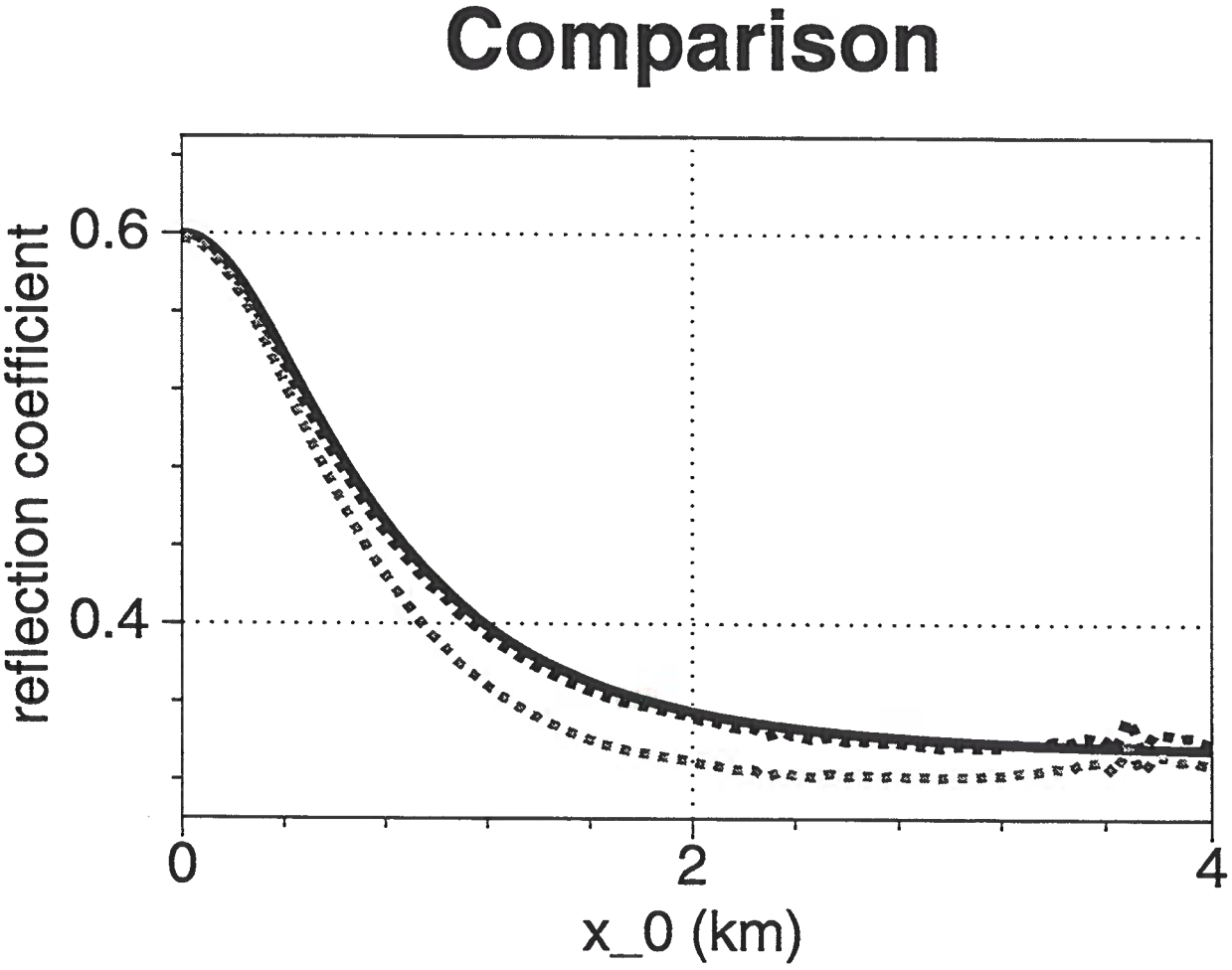

FIG. 9.5. Reflection coefficients as a function of zero–offset location for the model in Figure 9.1. Solid black represents the analytical solution, dashed black the numerical solution using Bleistein et al. formula and dashed gray the reflection coefficient using Hale's DMO formula. The erratic behavior fo the numerical computed curves close to the zero–offset location $x_0 = 4$ km, is due to edge effects at the right end of the model.

Chapter 10

CONCLUSIONS

Here I derived a number of operators that can be implemented numerically to solve a variety of geophysical problems. These operators are: demigration, migration and Seismic Data Mapping (SDM) operators for 2.5D and 3D media. Some of these operators were derived previously by using different techniques and are used here to check the validity of the newly derived results. Most of the operators are new and provide a basis for many new alternative approaches in seismic data processing. The newly derived results for SDM in 2.5D and 3D data are based on a formulation of the Configuration Transformation (CT) problem by Hubral et. al (1996) and Tygel et. al (1996).

The operators presented here are "true–amplitude" in the following sense:

- The amplitude on the *demigrated* data should account for the proper geometrical spreading due to a point–source and reflector curvature, and it should preserve the reflection coefficient corresponding to the configuration for the input data.
- The *migration* operator locates the events in the correct place with amplitudes that are proportional to the oblique incidence reflection coefficient.
- In SDM, the correct point–source and curvature geometrical spreading effects of the input is mapped into the correct point–source and curvature geometrical spreading effects of output. The oblique–incidence reflection coefficient from the input data is preserved in the output data.

The SDM results derived in this thesis are very general. They can be used to solve a variety of interesting seismic data processing problems. Among the specific problems that can be solved with the derived SDM equations are:

- Offset continuation and Transformation to Zero Offset (TZO). Some of the uses of offset continuation are binning, reconstruction of missing offsets for multiple suppression or any other process that requires these missing data.
- Amplitude preserving azimuthal continuation. Given that marine data have azimuths that are near zero, software developed for marine data could be used for land "acoustic" data after the azimuths are rotated to near zero azimuth.

- Transformation of P–S scalar to "P–P" seismic data. The 'P-P' data is not true P–P data in the sense that the main elastic properties (like the polarization and P–S reflection coefficient) are preserved. However the kinematics is that of a P–P wavefield under the same modeling conditions.
- Datuming. This technique is convenient for downward or upward continuing sources and receivers to map an irregular acquisition topography into a planar topography.
- Combinations of the above.

Actually all the operations mentioned above can be seen individually as SDM operators. We can make use of SDM also to perform velocity analysis. This could be done in combination with TZO. After all offsets are mapped to zero–offset, events should line up.

The derivations of the diffraction and isochron stacks were done in the time domain, and for the case of data from inhomogeneous isotropic media. These derivations were based on scattering theory. They continue the work of Bleistein (1987) and builds a bridge through the more general derivation in de Hoop and Bleistein (1996) for anisotropic media. One particular difference between the derivations presented here, and those done previously using scattering theory, is that both the forward and the inverse operators in this thesis, are derived from the Kirchhoff approximate modeling formula, while the other derivations published are based on the Born approximate modeling formula. A simplified derivation of the Kirchhoff approximate modeling formula is presented in Appendix B. I also carried out a derivation of a criterion for convergence of the Neumann series for monotype (P-P or S-S) seismic waves. This derivation is presented in Appendix A.

From the previous demigration and migration operators, I derived two alternative operators based on the superposition principle, to perform migration and demigration. These are the isochron superposition (to do migration) and the diffraction superposition (to do demigration). While those concepts are not new (Hubral *et al.*, 1996; Schneider, 1971), I give here a precise mathematical formulation of the problem that was lacking in previous publications. The amount of input or output data to process determines which operator (stacking or superposition) should be more computationally efficient. An extreme (and non–realistic) example is that of migrating a single scatter. While this could be done by superposition of all isochrons that touch it, the most efficient way to migrate it is by summing all the energy on the data along the corresponding diffraction response. On the other hand, if the input data consists of a single spike (also non–realistic) then it is more efficient to smear all the energy along its corresponding isochron than summing all the energy on the data along all the diffractions responses for scatter points on the isochron.

An analytical solution for the common–shot TZO in a 3D medium with linear velocity

gradient in the vertical velocity problem is provided in Chapter 6.

To demonstrate and verify the kinematic and dynamic properties of the SDM operator, an specific model in a constant velocity medium was chosen. Based on the analytical knowledge of the kinematic and dynamic properties for this specific model, I was able to show the agreement between the expected SDM features and the numerical results obtained.

Finally, as mathematical by–product of this research, I found a justification for the half–derivative operator through the Fourier transform. This new insights build more solid foundations for the mathematical analysis of 2.5D operators.

10.1 Future work

I describe some extensions and/or future applications of the research developed here

- Extension of the SDM operators to include anisotropy.
- Use of the 2.5D and 3D SDM operators to develop "true–amplitude" software for offset continuation, TZO, datuming, velocity analysis, transformation of converted data etc.
- I believe that more testing should be performed using the TZO technique explained in Chapter 8.

REFERENCES

Abramowitz, M., & Stegun, I. A. 1965. *Handbook of Mathematical Functions.* Dover.

Artley, C. 1994. *Dip-moveout processing for depth-variable velocity.* M.Sc. thesis, Colorado School of Mines.

Artley, C., & Hale, I. D. 1994. Dip-moveout processing for depth-variable velocity. *Geophysics*, **59**(4), 610–622.

Beylkin, G. 1985. Imaging of discontinuities in the inverse scattering problem by inversion of a causal generalized Radon transform. *J. Math. Phys.*, **26**, 99–108.

Biondi, B., & Chemingui, N. 1994. Transformation of 3–D prestack data by Azimuthal Moveout. *64th Annual Internat. Mtg., Soc. Expl. Geophys., Expanded Abstracts*, 1541–1144.

Bleistein, N. 1984. *Mathematical Methods for Wave Phenomena.* Academic Press, Inc, New York.

Bleistein, N. 1986. Two–and–one–half dimensional in–plane wave propagation. *Geophyscial Prospecting*, **34**, 686–703.

Bleistein, N. 1987. On the imaging of reflectors in the Earth. *Geophysics*, **52**(7), 931–942.

Bleistein, N., Cohen, J.K., & Stockwell, J. 1996. *Mathematics of Multidimensional Seismic Inversion.* In preparation.

Bleistein, N., Cohen, J.K., & H., Jaramillo. 1997. True Amplitude Transformation of Data from Curved Reflectors to Zero Offset. *Geophysics*, **submitted.**

Bracewell, R. N. 1986. *The Fourier Transform and Its Applications.* McGraw–Hill, Inc., New York.

Burridge, R., de Hoop M.V., & E., Miller D. 1995. Multi-parameter inversion in anisotropic media using the generalized Radon transform. *Geoph. J. Int.*, **in review**.

Chan, W., & Stewart, R. 1996. Transformation of P–S to P–P seismic data. *Crews Research Report*, **8**, 18–1,18–25.

Chemingui, N., & Biondi, B. 1995. Amplitude preserving AMO from true amplitude DMO and inverse DMO. *SEG–84*, 153–168.

Claerbout, J. F. 1985. *Imaging the Earth's Interior.* Blackwell Scientific Publications. Pages 209–213.

de Hoop, A. 1991. Convergence criterion for the time–domain iterative Born approximation to scattering by an inhomogeneous, dispersive object. *Journal of the Optical Society of America*, 8, 1256,1260.

de Hoop, M.V., & Bleistein, N. 1996. Generalized Radon Transform inversions for reflectivity in anisotropic elastic media. *Inverse Problems*, **13**, 669–690.

Deregowski, S. M., & Brown, S. M. 1983. A theory of acoustic diffractors applied to 2–D models. *Geophysical Prospecting*, **31**, 293–333.

Dietrich, Michel, & Cohen, Jack K. 1993. Migration to zero offset (DMO) for a constant velocity gradient: An analytical formulation. *Geophysical Prospecting*, **41**, 621–644.

Evans, E. J. 1997. *Geophysical Monograph Series.* Soc. Expl. Geophys. Page 1.

G., Beylkin, & R., Burridge. 1990. Linearized inverse scattering problems in acoustics and elasticity. *Wave Motion*, 15–52.

Gauss, K. F. 1965. *General Investigations of curved surfaces.* Springer-Verlag, Berlin.

Gel'fand, I. M., & Shilov, G. E. 1964. *Generalized functions.* Academic Press, New York.

Gray, S. H. 1992. Frequency-selective design of the Kirchhoff migration operator. *Geophysical Prospecting*, **40**, 565–571.

Grünwald, A. K. 1987. Über 'begrenzte' Derivationen und deren Anwendung. *Math. Phys.*, 1121.

Hagedoorn, J. G. 1954. A process of seismic reflection interpretation. *Geophysical Prospecting*, **2**(2), 85–127.

Hale, I. D. 1984. Dip moveout by Fourier transform. *Geophysics*, **55**, 595–607.

Hale, I. D. 1991. A nonaliased integral method for dip moveout. *Geophysics*, **56**, 795–805.

Hale, I. D. 1992. *Dip Moveout Processing.* Society of Exploration Geophysicists, Tulsa.

Hubral, P., Schleicher, J., & Tygel, M. 1996. A unified approach to 3-D seismic reflection imaging, Part I: Basic concepts. *Geophysics*, **61**(3), 742–758.

Jaramillo, H., & Bleistein, N. 1997. A simplified derivation to migration and demigration in isotropic inhomogeneous media. *Center for Wave Phenomena Annual Report, CWP-248.*

Jaramillo, H., & Fowler, P. 1997. P-S converted–wave DMO in depth–variable velocity. *67th Annual Internat. Mtg., Soc. Expl. Geophys., Expanded Abstracts*, 1591–1994.

Jaramillo, H., Schleicher, J., & Tygel, M. 1997. Discussion and Errata to: A unified approach to 3–D seismic reflection imaging, Part II: Theory, by M. Tygel, J. Schleicher, and P. Hubral. *Geophysics*, **63**, 670–673.

Ji, Jun. 1995. *Sequential Seismic Inversion using Plane wave Synthesis.* Ph. D. thesis, Stanford University.

Jorden, T. E. 1987. *Transformation to zero offset.* M.Sc. thesis, Colorado School of Mines.

Kaufman, A. 1992. *Geophysical field theory and method, part A.* Academic Press, New York. Pages 155–156.

Kreyszig, E. 1978. *Intruductory functional analysis with applications.* Wiley, New York.

Kreyszig, E. 1991. *Differential Geometry.* Dover, New York.

Laugwitz, D. 1965. *Differential and Riemannian Geometry.* Academic Press, New York. Page 54.

Lindsey, J. P., & Herman, A. 1985. Digital migration. *Pages 70–74 of:* Gardner, G. H. F. (ed), *Migration of seismic data.* Soc. Expl. Geophys.

Lumley, D. E., Claerbout, J. F., & Bevc, D. 1994. Anti-aliased Kirchhoff 3-D migration. *64th Annual Internat. Mtg., Soc. Expl. Geophys., Expanded Abstracts*, 1282–1285.

Miller, D., Oristaglio, M., & Beylkin, G. 1984. A new formalism and an old heuristic for seismic migration. *Page Session:S19.6 of: 54th Annual Internat. Mtg., Soc. Expl. Geophys., Expanded Abstracts.* Soc. Expl. Geophys.

Norton, S. G., & M., Linzer. 1981. Ultrasonic scattering potential imaging in three dimensions: Exact inverse scattering solutions for plane, cylindrical, and spherical apertures. *Intst. Elctr. Electron. Eng. Trans. on Biomedical Engineering*, **BME-28**, 202–220.

Oldham, K. B., & Spanier, J. 1974. *The Fractional Calculus.* Academic Press.

Osler, T. J. 1972. The integral analog of the Leibniz's rule. *Math. Comp.*, 903.

Post, E. L. 1930. Generalized differentiation. *Trans. Amer. Math. Soc.*, 273.

Press, W. T., Flannery, B. P., Teukilsky, S. A., & Vetterling, W. T. 1986. *Numerical recipes.* Cambridge Univ. Press., Cambridge.

Rockwell, D. W. 1971. Migration stack aids interpretation. *Pages 75–81 of:* Gardner, G. H. F. (ed), *Migration stack aids interpretation.* Soc. Expl. Geophys.

Salinas, T. 1996. *The influence of Near–surface Time Anomalies in the Imaging Process.* M.Sc. thesis, Colorado School of Mines.

Scales, J. A. 1995. *Theory of seismic imaging.* Springer-Verlag, Berlin. Pages 113–118.

Schleicher, J., Tygel, M., & Hubral, P. 1993. 3-D true-amplitude finite-offset migration. *Geophysics*, **58**(8), 1112–1126.

Schneider, William A. 1971. Developments in seismic data-processing and analysis (1968-1970). *Geophysics*, **36**(6), 1043–1073.

Schneider, William A. 1978. Integral formulation for migration in two-dimensions and three-dimensions. *Geophysics*, **43**(1), 49–76.

Sheaffer, S. D., & Bleistein, N. 1998. 2.5D Downward Continuation Using Data Mapping Theory. *Center for Wave Phenomena Annual Report.*

Slotnick, Morris M. 1959. *Lessons in seismic computing *.* Soc. Expl. Geophys., Tulsa.

Tygel, M., Schleicher, J., & Hubral, P. 1994. Pulse distortion in depth migration. *Geophysics*, **59**(10), 1561–1569.

Tygel, M., Schleicher, J., & Hubral, P. 1995. Dualities involving reflectors and reflection-time surfaces. *Journal of Seismic Exploration*, 123–150.

Tygel, M., Schleicher, J., & Hubral, P. 1995a. True-amplitude migration to zero offset (MZO) by diffraction stack. *preprint Insitituto de Matemática Estatística e Ciência da Computação Universidade Estadadual de Campinas, Brazil.*

Tygel, M., Schleicher, J., & Hubral, P. 1996. A unified approach to 3-D seismic reflection imaging, Part II: Theory. *Geophysics*, **61**(3), 759–775.

Červený, V. 1995. *Lecture notes: Seismic Wave Fields in Three–Dimensional Isotropic and Anisotropic Structures.* University of Trondheim.

Verschuur, D. J. 1991. *Surface–related multiple elimination: an inversion approach.* Ph. D. thesis, Delf University of Technology, The Netherlands.

Verschuur, D. J., & Berkhout, A. J. 1992. Surface-Related Multiple Elimination: Practival Aspects. *Pages 1100–1103 of: 62th Annual Internat. Mtg., Soc. Expl. Geophys., Expanded Abstracts.* Soc. Expl. Geophys.

Yilmaz, Ö. 1987. *Seismic Data Processing.* Soc. Expl. Geophys. Pages 370–383.

Appendix A

A.1 Criterion for convergence of the Neumann series

This appendix is inspired in the work by de Hoop (1991). He shows the conditions for convergence of the Neumann series for electromagnetic waves. Here, I show the equivalent result for monotype scattered (*P-P* or *S-S*) seismic waves in a homogeneous isotropic background.

In Chapter 2, we defined

$$Tu_s = \int_D d^3x\, G(\boldsymbol{x},\boldsymbol{r},\omega)\,\frac{\omega^2}{c^2}\alpha_0\, u_s(\boldsymbol{x},\boldsymbol{x}_s,\omega),$$

and said that the convergence of the Neumann series is guaranteed by making

$$\epsilon\|T\| < 1, \tag{A.1}$$

where ϵ is a parameter related to the perturbation α by the formula $\alpha = \epsilon\alpha_0$. Here α_0 is bounded by one. By definition

$$\|T\| = \sup_{\|u_s\|=1} \|Tu_s\|,$$

where $\|Tu_s\|$ is the norm of Tu_s defined by the equation

$$\sup_{\boldsymbol{r}\in\mathbb{R}^3} |Tu_s(\boldsymbol{r})|. \tag{A.2}$$

We have then,

$$\begin{aligned}\|Tu_s\| &= \sup_{\boldsymbol{r}\in\mathbb{R}^3} \left| \int d^3x\, G(\boldsymbol{x},\boldsymbol{r},\omega)\,\frac{\omega^2}{c^2}\,\alpha_0\, u_s(\boldsymbol{x},\boldsymbol{x}_s,\omega) \right| \\ &\leq \frac{\omega^2}{4\pi\, c^2} \sup_{\boldsymbol{r}\in\mathbb{R}^3} \int_D d^3x \frac{1}{|\boldsymbol{r}-\boldsymbol{x}|}\end{aligned} \tag{A.3}$$

Here, we have used the causal Green function

$$G(\boldsymbol{x},\boldsymbol{r},\omega) = \frac{e^{i\omega|\boldsymbol{r}-\boldsymbol{x}|/c}}{4\pi\,|\boldsymbol{r}-\boldsymbol{x}|},$$

and the fact that $\|u_s\| = 1$ and $|\exp\{i\omega|\boldsymbol{r}-\boldsymbol{x}|/c\}| \leq 1$. Let us define B as the

smallest sphere such that $D \in B$ and let R be its radius. We have then that

$$\int_D d^3x \frac{1}{|\boldsymbol{r} - \boldsymbol{x}|} \leq \int_B d^3x \frac{1}{|\boldsymbol{r} - \boldsymbol{x}|}.$$

The right hand side of this equation, up to a scale factor, has the physical interpretation of the gravity (or electrical) potential at $\boldsymbol{r}$ due to a sphere B with unit mass (charge) density. Kaufman, (1992) shows a derivation of the gravity field due to a constant density sphere. This gravity field depends only on the radial component r. By integrating along r we find the gravity (electric) potential, and after ignoring the gravitational (dielectric) constant we find

$$\frac{1}{4\pi} \int_B d^3x \frac{1}{|\boldsymbol{r} - \boldsymbol{x}|} = \begin{cases} R^2/2 - r^2/6 & \text{if } r \leq R \\ R^3/3r & \text{if } r \geq R \end{cases}$$

Then,

$$\sup_{\boldsymbol{r} \in \mathbb{R}^3} \frac{1}{4\pi} \int_D d^3x \frac{1}{|\boldsymbol{r} - \boldsymbol{x}|} \leq \frac{R^2}{2}.$$

To satisfy the inequality (A.1) we then must have

$$\alpha(\boldsymbol{x}) < \frac{2\,c}{\omega^2 R^2}.$$

Appendix B

B.1 From Born to Kirchhoff

This appendix was "Born" as an effort to find justification for the name reflection coefficient for the factor R_B defined in equation (3.19). The approach presented here is a Bleistein's variation of the approach presented by Jaramillo and Bleistein (1997).

Here, I will show a derivation of the Kirchhoff approximate modeling formula (2.16) from the Born–approximate modeling formula (2.11). I start with equation (3.10) which can be rewritten as

$$D_B(\boldsymbol{\xi},t) = \int d^3x\, \frac{\alpha(\boldsymbol{x})}{c^2(\boldsymbol{x})} a(\boldsymbol{x},\boldsymbol{\xi}) \nabla_x H(\Sigma_R(\boldsymbol{x})) \cdot \boldsymbol{u} \frac{\delta'(t-\phi)}{\boldsymbol{u}\cdot\nabla_x\phi}.$$

Let us know pick $\boldsymbol{u} = \boldsymbol{u}_\Sigma$ where $\boldsymbol{u}_\Sigma$ is a normal vector to the reflecting surface Σ_R pointing upwards. We have then that

$$\boldsymbol{u}\cdot\nabla_x H(\Sigma_R(\boldsymbol{x})) = -\gamma(\boldsymbol{x}),$$

where $\gamma(\boldsymbol{x})$ is the singular function of the reflecting surface. The minus sign comes from the fact that $\nabla_x H(\Sigma_R(\boldsymbol{x}))$ is a unit vector normal to the surface pointing in the positive z direction. While $\boldsymbol{u}$ was chosen to be oppositely directed.

From the definition of the singular function we have, then, that

$$D_B(\boldsymbol{\xi},t) = -\int d\Sigma_R\, \frac{\alpha(\boldsymbol{x})}{c^2(\boldsymbol{x})} a(\boldsymbol{x},\boldsymbol{\xi}) \gamma(\boldsymbol{x}) \frac{\delta'(t-\phi)}{\boldsymbol{u}_\Sigma\cdot\nabla_x\phi}.$$

If we use the fact that

$$\frac{\alpha(\boldsymbol{x})}{c^2(\boldsymbol{x})(\boldsymbol{u}_\Sigma\cdot\nabla_x\phi)^2} \sim \frac{\alpha(\boldsymbol{x})}{4\cos^2\theta} = R_B,$$

where, as before, θ is half the angle between the source/receiver rays at the reflector, then we find

$$D_B(\boldsymbol{\xi},t) = -\int d\Sigma_R\, R_B\, \boldsymbol{u}_\Sigma\cdot\nabla_x\phi\, \delta'(t-\phi).$$

By taking the direct Fourier transform of the previous equation we obtain

$$D_B(\boldsymbol{\xi}, \omega) = i\omega \int R_B \; a(\boldsymbol{x}, \boldsymbol{\xi}) \; \boldsymbol{u}_\Sigma \cdot \nabla_x \phi \; e^{i\omega\phi(\boldsymbol{x},\boldsymbol{\xi})} \, d\Sigma.$$

If we replace R_B by R_K, then we will have that the previous equation is the Kirchhoff modeling (approximation) formula (2.16), where $\boldsymbol{u}_\Sigma = \hat{\boldsymbol{n}}$. This, then, explicitly shows, that the Kirchhoff modeling formula is an extension to the Born approximation formula, with a less restrictive reflection coefficient, also justifying the name "Linearized Born reflection coefficient".

Appendix C

C.1 The Fractional Calculus

The need for this appendix stems from the fact that there is no formal theory of fractional calculus in terms of Fourier transforms. In this dissertation, fractional derivatives arise from the stationary phase analysis in 2.5D. Those derivatives are written in terms of Fourier filters of the type $(-i\omega)^q$. In our particular case $q = 1/2$. Then this appendix is about how to find and how to justify half–derivatives under the Causal Fourier Transform theory.

We want to do this in a general context. Here the concept of n-th derivative or n-th iterated integral is extended from the natural number n to generic complex number q. This extension unifies both integration and differentiation in a single *differintegral* operator. The term *differintegral* as well as all definitions and some of the properties that we illustrate below are taken from the book "The Fractional Calculus" (Oldham & Spanier, 1974). We do not pretend to make an extensive self consistent discussion of the topic. So we will not define the space of differintegral operators and assume that the functions that we deal with here are in that space (and they are). For mathematical details of this, the reader can consult Oldham and Spanier (1974), where he can find many other references about the topic.

C.2 Definitions

The basic definition of the *differintegral* operator was first given by Grünwald (1987) and later extended by Post (1930). Here I present the Oldham and Spanier's version:

$$\frac{d^q f}{[d(x-a)]^q} = \lim_{N\to\infty} \left\{ \frac{\left[\frac{x-a}{N}\right]^{-q}}{\Gamma(-q)} \sum_{j=0}^{N-1} \frac{\Gamma(j-q)}{\Gamma(j+1)} f\left(x - j\left[\frac{x-a}{N}\right]\right) \right\}, \tag{C.1}$$

where the Γ function is used, and q can be an arbitrary complex number. The number a represents the lower limit of integration (for $q = -n$) and it is irrelevant for the usual differentiation $q = n$. So for $q = n$ we could just drop a from this formula and obtain the usual finite–difference forward representation of the n-th derivative. This formula can be obtained by starting with the forward finite difference representation of the n-th derivative operator. You can see that the change of n by q will preserve the

algebraic structure of the formula. Another way to derive this formula is by starting with the Riemman sum of the n-th iterated integral. The formula will come up when n is replaced by $-n$ and then this by $-q$. The derivation of this formula for a natural number n would require some manipulation of the binomial coefficient

$$\binom{n}{j} = \frac{\Gamma(n+1)}{\Gamma(j+1)\,\Gamma(n-j+1)}. \tag{C.2}$$

While Oldham and Spanier's definition is valid for any complex number q, its algebraic complexity make it difficult to use. There are some simpler definitions that can be shown to agree with this definition in a smaller domain (subset of the complex numbers), then by analytic continuation they all should be equivalent (in their domain of analitycity) to the Oldham and Spanier's definition. For convenience we will use here the so called Riemman–Liouville definition

$$\frac{d^q f}{[d(x-a)]^q} = \frac{1}{\Gamma(-q)} \int_a^x \frac{f(y)dy}{[x-y]^{q+1}}, \qquad q < 0. \tag{C.3}$$

The way to extend this formula to positive q's ($q \geq 0$), is by using the *composition law*

$$\frac{d^n}{dx^n} \frac{d^q f}{[d(x-a)]^q} = \frac{d^{n+q} f}{[d(x-a)]^{n+1}}. \tag{C.4}$$

valid for all q and any natural number n. In this way we find any positive fractional by picking the negative fraction and doing iterated differentiation n times. Here n is the next integer grater or equal to $-q$. Then we can cover the whole real line. The Riemman–Liouville definition is shown (Oldham & Spanier, 1974) to be equivalent to the Oldham and Spanier's definition, so again that definition is the analytic continuation to the entire plane of this more restricted, but at the same time, simpler definition. One way to derive the Riemman–Liouville definition is by naturally extending the Cauchy's formula for repeated (iterated) integration after substituting n by $-q$.

C.3 Properties

I list (besides the composition law) the main properties of the differintegral operators

1. Linearity

$$\frac{d^q[f_1 + f_2]}{[d(x-a)]^q} = \frac{d^q f_1}{[d(x-a)]^q} + \frac{d^q f_2}{[d(x-a)]^q}. \tag{C.5}$$

2. Term by term differintegration

$$\frac{d^q}{[d(x-a)]^q}\sum_{j=0}^{n} f_j = \sum_{j=0}^{n}\frac{d^q f_j}{[d(x-a)]^q}. \tag{C.6}$$

3. Homogeneity

$$\frac{d^q[Cf]}{[d(x-a)]^q} = C\frac{d^q[f]}{[d(x-a)]^q}, \qquad C \quad \text{anyconstant.} \tag{C.7}$$

4. Leibinz's Rule. This is an important property for asymptotic analysis and we will make use of it below.

$$\frac{d^q[\phi\,\psi]}{[d(x-a)]^q} = \sum_{j=0}^{\infty}\binom{n}{j}\psi^{(j)}\frac{d^{q-j}\phi}{[d(x-a)]^{q-j}}. \tag{C.8}$$

A further generalization of Leibniz's rule due to Osler (1972) is the integral form

$$\frac{d^q[\phi\,\psi]}{[d(x-a)]^q} = \int_{-\infty}^{\infty}\frac{\Gamma(q+1)}{\Gamma(q-\gamma-\lambda+1)\,\Gamma(\gamma+\lambda+1)}\frac{d^{q-\gamma-\lambda}\phi}{dx^{q-\gamma-\lambda}}\frac{d^{\gamma+\lambda}\psi}{dx^{\gamma+\lambda}}\,d\lambda \tag{C.9}$$

5. The Chain rule. The chain rule is perhaps the most difficult property to extend beyond $n = 1$. If for example the chain rule could be extended to $n = -1$ then the process of integration would pose no greater difficulty than does differentiation. Since any general formula for $d^q\,g(f(x))/[d(x-a)]^q$ must encompass integration as a special case, little hope can be held out for a useful chain rule for arbitrary q. A known formula for the chain rule for a natural number n is shown in Abramowitz and Stegun (1965) and named as Faa de Bruno's formula. This formula is so complicated that I chose not to include it here.

C.4 Fractional derivatives as seen from the Causal Fourier Transform point of view

We are interested on the differintegral operators of causal functions, and want to find an expression for them in terms of the Fourier Transform. We want prove that

$$\mathcal{F}\left\{\frac{d^q f}{dt^q}\right\} = (-i\omega)^q\,\mathcal{F}(f) \tag{C.10}$$

Where q is any real number, $\mathcal{F}$ is the forward Fourier transform operator as defined in equation (2.1) and f is a causal real function ($f(t) = 0, t < 0$). That is we can compute the q-th derivative of $f(t)$ by taking the forward Fourier transform, filtering this with $(-i\omega)^q$ and finally taking the inverse Fourier transform of the result. In

other words

$$\frac{d^q f}{dt^q} = \mathcal{F}^{-1}\left\{(-i\omega)^q F(\omega)\right\}. \tag{C.11}$$

This is a well known result for a natural number n (Bracewell, 1986) [1]. We want to extend it to all real numbers, even though, in our particular case, we are only interested only in $q = 1/2$. We use the Riemman-Liouville definition

$$\frac{d^q f}{dt^q} = \frac{1}{\Gamma(-q)} \int_0^t \frac{f(\tau)}{(t-\tau)^{q+1}} d\tau, \qquad q < 0 \tag{C.12}$$

The convolution theorem for causal functions can be written as (Bracewell, 1986)

$$\mathcal{F}\left\{\int_0^t d\tau f_1(t-\tau)\, f_2(\tau)\right\} = \mathcal{F}\left\{f_1\right\} \mathcal{F}\left\{f_2\right\}. \tag{C.13}$$

So

$$\mathcal{F}\left\{\frac{d^q f}{dt^q}\right\} = \frac{1}{\Gamma(-q)} \mathcal{F}\left\{t^{-1-q}\right\} \mathcal{F}\left\{f\right\} = (-i\omega)^q \mathcal{F}(f), \qquad q < 0. \tag{C.14}$$

For noninteger positive q, we use the composition rule (C.4) where $n-1 < q < n$, so

$$\begin{aligned} \mathcal{F}\left\{\frac{d^q f}{dt^q}\right\} = \mathcal{F}\left\{\frac{d^n}{dt^n}\left[\frac{d^{q-n} f}{dt^{q-n}}\right]\right\} &= (-i\omega)^n \mathcal{F}\left\{\frac{d^{q-n}}{dt^{q-n}}\right\} \\ &= (-i\omega)^n (-i\omega)^{q-n} \mathcal{F}\left\{f\right\} \\ &= (-i\omega)^q \mathcal{F}\left\{f\right\}. \end{aligned} \tag{C.15}$$

This proves the statement.

C.5 Asymptotic analysis of the fractional derivative operator

Here we find the leading order term of the fractional derivative of the product of a "smooth" function $s(t)$ by a "sharp" function $\delta(t-\tau)$. The Leibniz's rule (C.8) for the signal $s(t)\,\delta(t-\tau_R(\sigma))$ is given by

$$\frac{d^q}{dt^q}\left[s(t)\,\delta(t-\tau_R(\xi))\right] = \sum_{j=0}^{\infty} \binom{n}{j} s(t)^{(j)} \frac{d^{q-j}\delta(t-\tau_R(\xi))}{dt^{q-j}}. \tag{C.16}$$

We can asymptotically approximate this equation by using its leading order term ($j = 0$, which represents the highest power of $(-i\omega)$ in the frequency domain) as

[1] Actually, Bracewell does it only for n=1, but higher–order derivatives follow the rule due to the composition law

follows:

$$\frac{d^q}{dt^q}\left[s(t)\,\delta(t-\tau_R(\xi))\right] \sim s(t)\frac{d^q\delta(t-\tau_R(\xi))}{dt^q}. \tag{C.17}$$

So, asymptotically, the smooth function $s(t)$ behaves like a constant with respect to the sharp delta function, under the q-th differentiation ($q > 0$).

Appendix D

In this Appendix I find a relation between the curvature of the difference between the input and output configuration isochrons and the Hessian matrix Φ, corresponding to the 3D DM chain operator.

For exposition purposes, I will omit the arguments of the phase function ϕ. In any case ϕ is the total travel time of the source–scatterer–receiver ray, but in some cases this travel time is taken with respect to the input configuration isochron and in other cases with respect to the output configuration isochron. To distinguish between these two choices, I use the tilde for the coordinates of the output configuration isochron. Also for simplification purposes, I use Einstein summation convention. That is, a sum is assumed over repeated indexes.

Let us begin by rewriting the stationary phase condition (6.12)

$$\frac{\partial \phi}{\partial \sigma_i} = \frac{\partial \phi}{\partial x_l} \frac{\partial \tilde{x}_l}{\partial \sigma_i} = 0. \tag{D.1}$$

By using the chain rule for partial differentiation we have that

$$\frac{\partial^2 \phi}{\partial \sigma_i \sigma_j} = \frac{\partial^2 \phi}{\partial x_l \partial x_k} \frac{\partial \tilde{x}_l}{\partial \sigma_i} \frac{\partial \tilde{x}_k}{\partial \sigma_j} + \frac{\partial \phi}{\partial x_l} \frac{\partial^2 \tilde{x}_l}{\partial \sigma_i \partial \sigma_j}. \tag{D.2}$$

where $i, j = 1, 2$ and $l, k = 1..3$. Now, let us take the input isochron, defined by $t = \phi(\boldsymbol{x}(\boldsymbol{\sigma}), \boldsymbol{\xi})$. Given that t is constant along the isochron,

$$\frac{\partial t}{\partial \sigma_i} = \frac{\partial \phi}{\partial x_l} \frac{\partial x_l}{\partial \sigma_i} = 0, \tag{D.3}$$

and

$$\frac{\partial^2 t}{\partial \sigma_i \partial \sigma_j} = \frac{\partial^2 \phi}{\partial x_l \partial x_k} \frac{\partial x_l}{\partial \sigma_i} \frac{\partial x_k}{\partial \sigma_j} + \frac{\partial \phi}{\partial x_l} \frac{\partial^2 x_l}{\partial \sigma_i \partial \sigma_j} = 0. \tag{D.4}$$

From equations (D.1) and (D.3) and the fact that the point $\boldsymbol{x}_0$ belongs both to the input and to the output isochron, we find that both isochrons share the same tangent plane at the point $\boldsymbol{x}_0$. Let us then parameterize the input configuration isochron as

$$\begin{pmatrix} x_1(\sigma_1, \sigma_2) \\ x_2(\sigma_1, \sigma_2) \\ x_3(\sigma_1, \sigma_2) \end{pmatrix} = \begin{pmatrix} \sigma_1 \\ \sigma_2 \\ x_3(\sigma_1, \sigma_2) \end{pmatrix} \tag{D.5}$$

and the output configuration isochron as

$$\begin{pmatrix} \tilde{x}_1(\sigma_1,\sigma_2) \\ \tilde{x}_2(\sigma_1,\sigma_2) \\ \tilde{x}_3(\sigma_1,\sigma_2) \end{pmatrix} = \begin{pmatrix} \sigma_1 \\ \sigma_2 \\ \tilde{x}_3(\sigma_1,\sigma_2) \end{pmatrix} \tag{D.6}$$

where the parameters σ_1 and σ_2 define an orthogonal coordinate system along the common (σ_1,σ_2) tangent plane and the components x_3 and $\tilde{x}_3$ are seen as plotted along the normal direction to this plane.

Now, since $\partial x_3/\partial\sigma_k = \partial\tilde{x}_3/\partial\sigma_k = 0$, under the specific chosen parameterization, then $\partial x_l/\partial\sigma_k = \delta_{lk}$, $l = 1..3$, $k = 1,2$ Then, at $\boldsymbol{x} = \boldsymbol{x}_0$ equations (D.2) and (D.4) reduce to

$$\frac{\partial^2\phi}{\partial\sigma_i\partial\sigma_j} = \frac{\partial^2\phi}{\partial x_l\partial x_k}\,\delta_{li}\,\delta_{kj} + \frac{\partial\phi}{\partial x_l}\,\frac{\partial^2\tilde{x}_l}{\partial\sigma_i\partial\sigma_j} = \frac{\partial^2\phi}{\partial x_i\partial x_j} + \frac{\partial\phi}{\partial x_l}\,\frac{\partial^2\tilde{x}_l}{\partial\sigma_i\partial\sigma_j} \tag{D.7}$$

and

$$\frac{\partial^2 t}{\partial\sigma_i\partial\sigma_j} = \frac{\partial^2\phi}{\partial x_l\partial x_k}\,\delta_{li}\,\delta_{kj} + \frac{\partial\phi}{\partial x_l}\,\frac{\partial^2 x_l}{\partial\sigma_i\partial\sigma_j} = \frac{\partial^2\phi}{\partial x_i\partial x_j} + \frac{\partial\phi}{\partial x_l}\,\frac{\partial^2 x_l}{\partial\sigma_i\partial\sigma_j} = 0. \tag{D.8}$$

We subtract equation (D.8) from equation (D.7) and find that

$$\frac{\partial^2\phi}{\partial\sigma_i\partial\sigma_j} = \frac{\partial\phi}{\partial x_l}\,\frac{\partial^2(\tilde{x}_l - x_l)}{\partial\sigma_i\partial\sigma_j} = |\nabla_x\phi|\;\boldsymbol{n}\cdot\boldsymbol{b}_{ij}, \tag{D.9}$$

where $\boldsymbol{n}$ is a unit vector normal to both isochrons at $\boldsymbol{x}_0$ and

$$\boldsymbol{b}_{ij} = \left[\partial^2(\tilde{x}_l - x_l)/\partial\sigma_i\partial\sigma_j\right].$$

The inner product is taken for each i,j fixed. The tensor L_{ij} defined as

$$L_{ij} = \boldsymbol{n}\cdot\boldsymbol{b}_{ij} \tag{D.10}$$

is known as the *second fundamental tensor for the surface* $(\sigma_1,\sigma_2,(\tilde{x}_3 - x_3)(\sigma_1,\sigma_2))$, (Laugwitz, 1965). This surface is the difference of between the output and input isochrons, as seen in the (σ_1,σ_2) tangent plane. Laugwitz shows that

$$L = \det(L_{ij}) = K\,g_d = \kappa_1\,\kappa_2\,g_d, \tag{D.11}$$

where K is the Gaussian curvature and κ_1, κ_2, are the main curvatures, or curvatures along the principal directions [1]. Here g_d is the determinant of the first fundamental

[1] maximum and minimum normal curvatures through the surface at the point $\boldsymbol{x}_0$.

tensor for the surface

$$\begin{pmatrix} \sigma_1 \\ \sigma_2 \\ (\tilde{x}_3 - x_3)(\sigma_1, \sigma_2) \end{pmatrix}. \tag{D.12}$$

Now the metric tensor g_{ij}, for this surface, is found as follows

$$g_{ij} = \frac{\partial x_k}{\partial \sigma_i} \frac{\partial x_k}{\partial \sigma_j} = \delta_{ik}\, \delta_{jk} = \delta_{ij}, \tag{D.13}$$

so that $g_d = 1$. Note that here, we renamed $\tilde{x}_3 - x_3$ as the third Cartesian coordinate (x_3).

We have that the determinant of the Hessian matrix Φ at the stationary point $\boldsymbol{x}_0$ becomes

$$\det \Phi = |\nabla_x \phi|^2 \, K g_d. \tag{D.14}$$

and since for this parameterization $g_d = 1$ then

$$\det \Phi = |\nabla_x \phi|^2 \, K. \tag{D.15}$$

Also, $\mathrm{sgn}(\Phi) = \mathrm{sgn}(L_{ij})$. Let us now rewrite the DM weight w_{DM}

We now show that this determinant is independent of any parameterization of the isochron surfaces.

Since the parameterization was done along a tangent plane at the stationary point, the determinant of the first fundamental form at this point, for the output configuration isochron is $g = 1$. To better understand this, think that g is a stretching factor that can be thought of as the deviation of a local infinitesimal tangent plane from the (σ_1, σ_2)–plane. At the stationary point, the two normal vectors to those planes are colinear. The factor $g = \sec^2 \alpha = 1$, where α is the angle between those two normal vectors.

Given that K is independent of the coordinate system (Laugwitz, 1965), this weight is independent of the particular parameterization chosen and so this derivation is still valid for any *allowable* [2] parameterization of the output isochron.

If the parameters (σ_1, σ_2) were running in a plane whose normal makes an angle α with $\nabla_x \phi$, then it can be shown (Jaramillo *et al.*, 1997) that the relation between the Hessian matrix in this new plane and in the old one is given by

$$\Phi = U \, \Phi_n \, U^T. \tag{D.16}$$

[2]Here we deal with smooth parameterizations with a large enough number of derivatives to find the surface curvatures. The term *allowable* is explain in Kreyszig (1991)

Here $\Phi_n = (\partial^2\phi/\partial\gamma_1\,\partial\gamma_2)$ is the Hessian matrix along the new coordinates γ_1, γ_2. Also [3]

$$U = \begin{pmatrix} \cos\alpha & 0 \\ 0 & 1 \end{pmatrix}. \tag{D.17}$$

so

$$\sqrt{|\det\Phi_n|} = \sqrt{\frac{|\det\Phi|}{\cos^2\alpha}} = \sqrt{g\,|\det\Phi|} \tag{D.18}$$

We find that in any case, the the factor $\sqrt{g}$ is canceled. This is consistent with the fact that the result is independent of the chosen coordinate system.

[3] In fact, U is the product of three matrices. Two of those matrices are rotations with unit determinant, and the other one is the projection that I call U here.

Appendix E

E.1 Curvature analysis for input and output isochron configurations for the Common–shot TZO in a medium with vertically velocity gradient in the vertical direction

We show below that the output isochron is a sphere. This fact implies that, for the output isochron, any direction along the tangent plane is a principal direction of curvature, since the principal curvature is constant and equal to the reciprocal of the radius. Let us define this principal curvature of the output isochron as $\tilde{\kappa}$ and the two principal curvatures of the input isochron as κ_1 and κ_2. In the direction of the minimum value of curvature, for the input isochron, we have that the curvature of the difference between the output and the input isochron is given by $\tilde{\kappa} - \kappa_1$, while in the direction of maximum curvature this difference curvature is given by $\tilde{\kappa} - \kappa_2$. Note that in the general case of offset continuation we could not say that the curvature of the difference between the input and output isochron is equal to the difference of curvatures of the input and output isochrons. For this we would have to prove that the principal directions of both surfaces are collinear(which is not true, in general), and then apply the linearity of the partial derivatives operators as we just did here. We have then that:

$$K = (\tilde{\kappa} - \kappa_1)(\tilde{\kappa} - \kappa_2) = \tilde{K} - 2H\tilde{\kappa} + K_I, \tag{E.1}$$

where $\tilde{K} = \tilde{\kappa}^2$ is the Gaussian curvature of the output isochron (sphere), $H = (\kappa_1 + \kappa_2)/2$ is known as the mean curvature and K_I is the Gaussian curvature of the input isochron.

To find these curvatures, I will compute an explicit solution of both (input and output) isochrons $z = z_I(\boldsymbol{\xi}, t, \boldsymbol{\rho})$ and $z = \tilde{z}_I(\tilde{\boldsymbol{\xi}}, \tilde{t}, \boldsymbol{\rho})$. Here we follow closely Dietrich and Cohen (1993) derivations. They derived the isochrons in the common–offset configuration; we derive them in the common–shot configuration.

E.1.1 The finite-offset (input) isochron

Let us introduce the dimensionless variables:

$$\gamma_s(\boldsymbol{x}_s, \boldsymbol{x}) = \cosh^{-1}\left[\frac{x^2 + y^2 + \hat{z}^2 + {\hat{z}_0}^2}{2\hat{z}\hat{z}_0}\right], \tag{E.2}$$

and

$$\gamma_g(\boldsymbol{x}_s, \boldsymbol{x}) = \cosh^{-1}\left[\frac{(x-\xi_1)^2 + (y-\xi_2)^2 + \hat{z}^2 + \hat{z}_0{}^2}{2\hat{z}\hat{z}_0}\right], \tag{E.3}$$

where

$$\hat{z} = v/k = z + v_0/k = z + \hat{z}_0. \tag{E.4}$$

We then have $\gamma_s + \gamma_g = k\,t$, or

$$\cosh(\gamma_s + \gamma_g) = \cosh k\,t. \tag{E.5}$$

From the previous equation we derive the identity

$$2\cosh\gamma_s \cosh\gamma_g \cosh k\,t - \cosh^2\gamma_s - \cosh^2\gamma_g = \sinh^2 k\,t. \tag{E.6}$$

To check this result, write equation(E.5) as

$$\sinh\gamma_s\ \sinh\gamma_g = \cosh k\,t - \cosh\gamma_s \cosh\gamma_g$$

and square both sides to find that

$$2\cosh\gamma_g\ \cosh\gamma_g\ \cosh k\,t \cos^2 kt + \sinh^2\gamma_s\ \sinh^2\gamma_g - \cosh^2\gamma_s\ \cosh^2\gamma_g = \cosh^2 k\,t.$$

Then use the identity $\cosh^2\alpha - \sinh^2\alpha = 1$, first for $\alpha = k\,t$ on the right hand side, then for $\alpha = \gamma_s$ and for $\alpha = \gamma_g$ on the left hand side, so as to eliminate the sinh factors. After collecting terms identity (E.6) is obtained.

We use the identities:

$$\cosh\gamma_s \cosh\gamma_g = \left(\frac{x^2 + y^2 + \hat{z}^2 + \hat{z}_0{}^2}{2\hat{z}\hat{z}_0}\right)\left(\frac{(x-\xi_1)^2 + (y-\xi_2)^2 + \hat{z}^2 + \hat{z}_0{}^2}{2\hat{z}\hat{z}_0}\right), \tag{E.7}$$

and

$$\begin{aligned}\cosh^2\gamma_s + \cosh^2\gamma_g &= \left(\frac{x^2 + y^2 + \hat{z}^2 + \hat{z}_0{}^2}{2\hat{z}\hat{z}_0}\right)^2 \\ &+ \left(\frac{(x-\xi_1)^2 + (y-\xi_2)^2 + \hat{z}^2 + \hat{z}_0{}^2}{2\hat{z}\hat{z}_0}\right)^2\end{aligned} \tag{E.8}$$

to find that

$$a\,\hat{z}^4 + b\,\hat{z}^2 + c = 0. \tag{E.9}$$

Here

$$a = 2\cosh k\,t - 2, \tag{E.10}$$

$$b = b(x,y) = 2\cosh k\,t\,(\rho^2 + \rho_\xi^2 + 2\hat{z}_0^2) - 2\,(\rho^2 + \rho_\xi^2) - 4\,\hat{z}_0^2\cosh^2 k\,t, \tag{E.11}$$

$$c = c(x,y) = 2\cosh k\,t\,(\rho^2 + \hat{z}_0^2)(\rho_\xi^2 + \hat{z}_0^2) - (\rho^2 + \hat{z}_0^2)^2 - (\rho_\xi^2 + \hat{z}_0^2)^2, \tag{E.12}$$

and

$$\rho = \sqrt{x^2 + y^2} \qquad \rho_\xi = \sqrt{(x-\xi_1)^2 + (y-\xi_2)^2}. \tag{E.13}$$

Equation (E.9) is a quartic equation in the variable $\hat{z}$. From the four roots of this equation we pick the physical (positive) solution

$$\hat{z} = \sqrt{\frac{-b + \sqrt{b^2 - 4ac}}{2a}}, \tag{E.14}$$

and from E.4, the input (finite offset) isochron is given by

$$z = z_I(\boldsymbol{\xi}, t, \boldsymbol{\rho}) = \sqrt{\frac{-b + \sqrt{b^2 - 4ac}}{2a}} - \hat{z}_0. \tag{E.15}$$

The domain of validity for this isochron is limited to those (x,y) such that $c(x,y) < 0$ and $z \geq 0$, for each fixed (ξ_1, ξ_2) and t.

E.1.2 The zero-offset (output) isochron

Here we define the dimensionless variable $\tilde{t}_s$ as

$$\tilde{t}_s = \cosh^{-1}\left[\frac{(x-\tilde{\xi}_1)^2 + (y-\tilde{\xi}_2)^2 + \hat{z}^2 + \hat{z}_0^2}{2\hat{z}\hat{z}_0}\right], \tag{E.16}$$

and $2\,\tilde{\gamma}_s = k\,t_0$. As in the previous section, we find the identity

$$2\cosh^2\tilde{\gamma}_s\,(\cosh k\,t_0 - 1) = \sinh^2 k\,t_0, \tag{E.17}$$

that is

$$2\left[\frac{(x-\tilde{\xi}_1)^2 + (y-\tilde{\xi}_2)^2 + \hat{z}^2 + \hat{z}_0^2}{2\hat{z}\hat{z}_0}\right]^2 (\cosh k\,t_0 - 1) = \sinh^2 k t_0. \tag{E.18}$$

This equation can be transformed into

$$\frac{(x-\tilde{\xi}_1)^2 + (y-\tilde{\xi}_2)^2 + \hat{z}^2 + \hat{z}_0^2}{2\hat{z}\hat{z}_0} = \cos\frac{kt_0}{2} \tag{E.19}$$

and then into

$$(x-\tilde{\xi}_1)^2 \div (y-\tilde{\xi}_2)^2 \div (\tilde{z}-\hat{z}_0\,(\cosh\frac{k\,t_0}{2}-1))^2 = \hat{z}_0^2\sinh^2\frac{k\,t_0}{2}. \tag{E.20}$$

Equation (E.20) represents a sphere with center at the point $(\tilde{\xi}_1, \tilde{\xi}_2, \hat{z}_0\,(\cosh(k\,t_0/2)-1))$ and radius $\hat{z}_0\sinh(kt_0/2)$. So

$$\tilde{\kappa} = -\frac{1}{\hat{z}_0\sinh(k\,t_0/2)}. \tag{E.21}$$

The minus sign comes from the fact that the isochron is convex up and the coordinate z is positive in the lower half space. Slotnick (1959) showed that the wavefronts for a medium with linear velocity with depth, in the vertical plane (x,z), are circular. Equation (E.20), shows this fact, given that the wavefronts are kinematically equivalent to zero–offset isochrons after the medium velocity has been halved. From equation (E.20) we find that:

$$\tilde{z} = \hat{z}_0\,(\cosh\frac{k\,t_0}{2}-1) \div \sqrt{\hat{z}_0^2\sinh^2\frac{k\,t_0}{2}-\rho_\xi^2}, \tag{E.22}$$

with ρ_ξ defined in equation E.13. This is the zero offset (output) isochron. Here we are choosing the lower hemi–sphere. To process dips larger than $\pi/2$ the upper hemi–sphere should be picked.

Our next task is to find the curvatures on the finite–offset isochron.

E.1.3 Curvatures on the finite (input) offset isochron

In this section I find the Gaussian and the mean curvatures of the finite (input) offset isochron. Let me refrase the fact that the Gaussian curvature for the difference between the output and the input configuration isochrons can be written in terms of the mean and the Gaussian curvatures of both (input and output) isochrons, as shown in equation E.1.

The Gaussian curvature of the finite (input) offset isochron Let us first, for convenience in notation, use the short hand notation:

$$\cdot_{,i} = \frac{\partial\,\cdot}{\partial x_i} \qquad \text{and} \qquad \cdot_{,ij} = \frac{\partial^2\,\cdot}{\partial x_i\,\partial x_j} \tag{E.23}$$

where $i,j = 1,2$, $x_1 = x$ and $x_2 = y$. All equations derived in this section are valid and so applied, at the stationary point $\boldsymbol{x}_0 = (x,y,z)$. This point is common to both the input and the output configuration isochrons. The first goal is to find expressions for $z_{,ij}$. Since by equation E.4 $\hat{z} = z \div \hat{z}_0$, all partial derivatives of $\hat{z}$ are the same

as those of z. Moreover, it was shown above that, when both the input and output configuration isochrons are parameterized in depth, their first partial derivatives are equal to each other respectively.

Let us now take partial differentiation twice in equation (E.9):

$$z_{,ij} = -\frac{(12\,a\,\hat{z}^2 + 2b)\,z_{,i}\;z_{,j} + b_{,ij}\,\hat{z}^2 + 2\,\hat{z}\,b_{,i}\;z_{,j} + c_{,ij}}{4\,a\,\hat{z}^3 + 2\,b\,\hat{z}}. \tag{E.24}$$

We can use the fact that the stationary phase condition provides the equality of the first partial derivatives for the input and output isochron configurations. In this way we use the first (simpler) derivatives of the output configuration isochron. That is we take partial differentiation in equation (E.20) and find that

$$z_{,i} = -\frac{(x_i - \tilde{\xi}_i)}{\hat{z} - \hat{z}_0 \cosh k\,t_0/2}. \tag{E.25}$$

We still need to know the expressions for $b_{,i}$, $c_{,i}$, $b_{,ij}$ and $c_{,ij}$, for $i, j = 1, 2$. A direct differentiation of the coefficients b and c results in

$$\begin{aligned}
b_{,i} &= (\cosh kt - 1)(8x_i - 4\xi_i), \\
c_{,i} &= 4\cosh kt\left[x_i\,(\rho_\xi^2 + \hat{z}_0^2) + (\rho^2 + \hat{z}_0^2)\,(x_i - \xi_i)\right] \\
&\quad -4\left[(\rho_\xi^2 + \hat{z}_0^2)\,(x_i - \xi_i) + x_i\,(\rho^2 + \hat{z}_0^2)\right], \\
b_{,ij} &= 8\,\delta_{ij}\,(\cosh kt - 1); \\
c_{,ij} &= 4\cosh kt\left[\delta_{ij}\,(\rho_\xi^2 + \hat{z}_0^2) + 2\,x_i(x_j - \xi_j) + 2x_j(x_i - \xi_i) + \delta_{ij}(\rho^2 + z_0^2)\right] \\
&\quad - 4\left[2\,(x_j - \xi_j)(x_i - \xi_i) + \delta_{ij}(\rho_\xi^2 + \hat{z}_0^2) + \delta_{ij}(\rho^2 + \hat{z}_0^2) + 2x_i x_j\right].
\end{aligned} \tag{E.26}$$

The Gaussian curvature can be found then by using Gauss formula (Gauss, 1965).

$$K_I = \frac{\det|Z|}{g^2} = \frac{z_{,11}\;z_{,22} - {z_{,12}}^2}{(1 + {z_{,1}}^2 + {z_{,2}}^2)^2}. \tag{E.27}$$

Where $g = 1 + {z_{,1}}^2 + {z_{,2}}^2$.

The mean curvature of the finite (input) offset isochron The mean curvature H of a surface is given by the formula

$$H = \frac{\kappa_1 + \kappa_2}{2} = \frac{g_{11}\,L_{11} - 2\,g_{12}\,L_{12} + g_{22}\,L_{11}}{2g}, \tag{E.28}$$

(Laugwitz, 1965). The components of the first fundamental tensor for the surface $z = z_I(\boldsymbol{\xi}, t, \boldsymbol{\rho})$ are

$$g_{ij} = \boldsymbol{x}_{,i} \cdot \boldsymbol{x}_{,j} = (\delta_{1i}, \delta_{2i}, z_{,i}) \cdot (\delta_{1j}, \delta_{2j}, z_{,j}) = \delta_{ij} + z_{,i}\;z_{,j}. \tag{E.29}$$

Here $\boldsymbol{x} = (x, y, z(x,y) = z_I(\boldsymbol{\xi}, t, \boldsymbol{\rho}))$. To find the components of the second fundamental tensor L_{ij} we use equation (D.10). For the specific parameterization that we are using here the normal vector to the surface is given by

$$\boldsymbol{n} = \frac{\boldsymbol{x}_{,1} \times \boldsymbol{x}_{,2}}{|\boldsymbol{x}_{,1} \times \boldsymbol{x}_{,2}|} = \frac{(-z_{,1}\,, -z_{,2}\,, 1)}{\sqrt{1 + {z_{,1}}^2 + {z_{,2}}^2}} = \frac{(-z_{,1}\,, -z_{,2}\,, 1)}{\sqrt{g}}. \tag{E.30}$$

Note that $g = \det(g_{ij})$. We then find that

$$L_{ij} = z_{,ij} \,/\sqrt{g}, \tag{E.31}$$

and so

$$2\,H = \frac{(1 + {z_{,1}}^2)\, z_{,22} - 2\, z_{,1}\; z_{,12}\; z_{,2} + (1 + {z_{,2}}^2)\, z_{,11}}{(1 + {z_{,1}}^2 + {z_{,2}}^2)^{\frac{3}{2}}}. \tag{E.32}$$

It is my guess that there should be a simpler way to express these curvature factors (K_I and H), but, unfortunately, I have not been able to solve this problem. What I showed was basically an algorithmic sequence of equations that tells us how to compute them, but the back substitution in terms of the primitive variables (x, y, z), (ξ_1, ξ_2) and v_0, k results in a long expression for which a simplification represents a real challenge.

E.1.4 Signature of the Hessian Matrix

As I explained at the beginning of Chapter 5, the signature of a matrix is the given by the number of positive eigenvalues minus the number of negative eigenvalues. We already know that at the stationary point, $\boldsymbol{x}_0$, $\tilde{z}_{,i} = z_{,i}$. This fact implies that, there, the components of the first fundamental tensor for the surface $[x, y, (\tilde{z} - z)(x, y)]$ are $g_{ij} = \delta_{ij}$. The principal curvatures of this surface satisfy the equation for λ

$$\det(\hat{L}_{ij} - \lambda g_{ij}) = 0, \tag{E.33}$$

(Laugwitz, 1965). Here $\hat{L}_{ij}$ is the second fundamental tensor for the difference between the output and the input configuration isochron surfaces. This means [1] $\tilde{\kappa} - \kappa_1$, and $\tilde{\kappa} - \kappa_2$ are the eigenvalues of (L_{ij}), and so $\operatorname{sgn} L_{ij} = \operatorname{sgn}(\tilde{\kappa} - \kappa_1) + \operatorname{sgn}(\tilde{\kappa} - \kappa_2)$. We already found $\tilde{\kappa}$ (see equation (E.21)). To find κ_1 and κ_2 we use the fact that $K_I = \kappa_1\,\kappa_2$ and $H = (\kappa_1 + \kappa_2)/2$, so that κ_1 and κ_2 are the solutions of the quadratic equation

$$\lambda^2 - 2\,H\,\lambda + K_I = 0 \tag{E.34}$$

[1] we mentioned at the beginning of this section that the output isochron is a sphere, so the principal directions of the finite offset and zero–offset isochron should coincide, given that a sphere is invariant under any rotation

in λ. We then have that

$$\kappa_1 = H - \sqrt{H^2 - K_1} \qquad \text{and} \qquad \kappa_2 = H + \sqrt{H^2 - K_1}. \tag{E.35}$$

With this, sgn (Φ) is completely defined.

We use continuity arguments to find the signature number. Let us assume a horizontal reflector. In this case, at the stationary point, $z_{,i} = 0$. The reflector point is directly below the source–receiver line, so $\xi_2 = x_2 = 0$. By direct evaluation we find, then, that $c_{,12} = 0$ and that the determinant of the first fundamental tensor for input isochron is $g = 1$. From equation (E.31) we find that the tensor for the second fundamental form for the input isochron is given by

$$L_{ij} = z_{,ij}\,. \tag{E.36}$$

Now from equation (E.24) we find that $z_{,12} = z_{,21} = 0$, so that the principal directions for the input isochron at the stationary phase point $\boldsymbol{x}_0$ are the in–line and cross–line directions. Furthermore $\kappa_1 = z_{,11}$ and $\kappa_2 = z_{,22}$.

To find the Hessian signature for a horizontal layer reflection we use the following continuity argument. Along the in–line direction and in the limit as $k \to 0$, the stationary phase point (specular reflection point) is the global minimum of an ellipse (finite offset configuration isochron) and a circle (zero–offset configuration isochron) with curvatures given by

$$z_{,11} = \kappa_1 = -\frac{v^2 t^2 - \xi_1^2}{v^2 t^2 z} \qquad \text{and} \qquad \tilde{z}_{,11} = \tilde{\kappa} = -\frac{1}{z}, \tag{E.37}$$

respectively. Here z is the reflector depth. We then have that

$$\tilde{\kappa} - \kappa_1 = -\frac{1}{z}\left[1 - \frac{v^2 t^2 - \xi_1^2}{v^2 t^2}\right] \tag{E.38}$$

and given that $0 \leq v^2 t^2 - \xi_1^2 < v^2 t^2$ then $\tilde{\kappa} - \kappa_1 \leq 0$. This means that

$$\text{sgn}\,(\tilde{\kappa} - \kappa_1) = -1. \tag{E.39}$$

While it can be argued that the 3–D TZO is degenerate –this means that the operator collapses in one of its directions– when $k \to 0$, we still can claim that this degeneration is found along the cross–line direction and not along the in–line direction. Then, by a continuity argument we can say that for a small velocity gradient k, $\text{sgn}(\tilde{\kappa} - \kappa_1) = -1$.

Let us now do the analysis along the cross–line direction where $x = \xi_1/2$ and $\xi_2 = 0$. By using these two expressions in equations (E.6) through equation (E.8) we find that the cross-line curve is a circle with center at the point $(\xi_1/2, 0, \hat{z}_0^2 \cosh k\,t/2 - 1)$ and

radius $\sqrt{z_0^2 \sinh^2 k\,t/2 - \xi_1^2/4}$. So that

$$\kappa_2 = -\frac{1}{\sqrt{\hat{z}_0^2 \sinh^2 \frac{k\,t}{2} - \frac{\xi_1^2}{4}}}. \tag{E.40}$$

At this point we have to decide whether $\tilde{\kappa} \geq \kappa_2$ or $\tilde{\kappa} < \kappa_2$. This fact can not be seen directly from the expressions for $\tilde{\kappa}$ and κ_2. Let us work with the radii of both circles representing the input and output isochrons. We define

$$r_0^2 = \hat{z}_0^2 \sinh^2 \frac{k\,t_0}{2}, \tag{E.41}$$

and

$$r_c^2 = z_0^2 \sinh^2 \frac{k\,t}{2} - \frac{\xi_1^2}{4}. \tag{E.42}$$

Here r_0 is the radius of the output configuration isochron, while r_c is the radius of the cross-line circle, representing the input configuration isochron. To evaluate the difference between these two radii we need to know the travel times t_0 and t. From equation (6.62) and recognizing that for the zero–offset case $x = \tilde{\xi}_1$ and $y = \xi_2 = 0$ we find

$$t_0 = \frac{2}{k} \cosh^{-1} \left[\frac{(v_0 + kz)^2 + v_0^2}{2\,v_0\,(v_0 + kz)} \right]. \tag{E.43}$$

This is the time of a vertical ray going from the surface directly to the reflector point below it. Along the same lines we find that the finite offset time, from the source $\boldsymbol{x}_s = (0, 0, 0)$ to the reflector point $\boldsymbol{x}_0 = (\xi_1/2, 0, z)$ and then to the receiver position $\boldsymbol{x}_g = (\xi_1, 0, 0)$ is given by

$$t = \frac{2}{k} \cosh^{-1} \left[\frac{k^2\xi_1^2/4 + (v_0 + kz)^2 + v_0^2}{2\,v_0\,(v_0 + kz)} \right]. \tag{E.44}$$

It follows then that

$$\cosh(\frac{k\,t_0}{2}) = \frac{(v_0 + kz)^2 + v_0^2}{2\,v_0\,(v_0 + kz)}, \tag{E.45}$$

and

$$\cosh(\frac{k\,t}{2}) = \frac{k^2\xi_1^2/4 + (v_0 + kz)^2 + v_0^2}{2\,v_0\,(v_0 + kz)}. \tag{E.46}$$

We have

$$\sinh^2 \frac{k\,t}{2} = \cosh^2 \frac{k\,t}{2} - 1$$

$$= \left[\frac{k^2\xi_1^2/4 + (v_0 + kz)^2 + v_0^2}{2\,v_0\,(v_0 + kz)}\right]^2 - 1$$

$$= \sinh^2\frac{k\,t_0}{2} + \frac{(k^2\xi_1^2/4)((v_0 + k\,z)^2 + v_0^2)}{2\,v_0^2(v_0 + k\,z)^2} + \frac{k^4\,\xi_1^2}{64\,v_0^2\,(v_0 + k\,z)^2}. \tag{E.47}$$

Now multiplying the previous equation by $\hat{z}_0^2 = v_0^2/k^2$ we find

$$\hat{z}_0^2\,\sinh^2\frac{k\,t}{2} = \hat{z}_0^2\,\sinh^2\frac{k\,t_0}{2} + \frac{\xi_1^2}{8}\,\frac{(v_0 + k\,z)^2 + v_0^2}{(v_0 + k\,z)^2} + \frac{k^2\,\xi_1^4}{64\,(v_0 + k\,z)^2}, \tag{E.48}$$

and after subtracting the term $\xi_1^2/4$ from this result,

$$\hat{z}_0^2\,\sinh^2\frac{k\,t}{2} - \frac{\xi_1^2}{4} = \hat{z}_0^2\,\sinh^2\frac{k\,t_0}{2} + \frac{\xi_1^2}{8}\left[\frac{(v_0 + k\,z)^2 + v_0^2}{(v_0 + k\,z)^2} + \frac{k^2\,\xi_1^2}{8\,(v_0 + k\,z)^2} - 2\right].$$

Now, using the definitions for r_0 and r we find that

$$r^2 - r_0^2 = \frac{\xi_1^2}{8}\left[\frac{(v_0 + k\,z)^2 + v_0^2}{(v_0 + k\,z)^2} + \frac{k^2\,\xi_1^2}{8\,(v_0 + k\,z)^2} - 2\right]. \tag{E.49}$$

To investigate the sign of this expression it is useful to do it in terms of its zeros. One zero is found by making $k = 0$. This is a singular point of the Hessian matrix Φ. This is in agreement with what we showed above, about the constant velocity 3D TZO problem. Another zero is given when the equation

$$k\,\xi_1^2 = 16\,v_0 kz + 8k^2z^2 \tag{E.50}$$

is satisfied. The depth for this to happen is given by

$$z^{\pm} = \frac{-16\,v_0 \pm \sqrt{(16\,v_0)^2 + 32\,k^2\xi_1^2}}{8\,k}. \tag{E.51}$$

At this depth there is a sign change on equation (E.49). That is the sign of (E.49) should be negative for $z > z^{\pm}$ and positive for $z < z^{\pm}$. That is, for $z < z^{\pm}$

$$\tilde{\kappa} - \kappa_2 = -\frac{1}{r_0} + \frac{1}{r} < 0, \tag{E.52}$$

and for $z > z^{\pm}$

$$\tilde{\kappa} - \kappa_2 = -\frac{1}{r_0} + \frac{1}{r} > 0 \tag{E.53}$$

We found then that $\mathrm{sgn}(\tilde{\kappa} - \kappa_2) = -1$ for $z < z^{\pm}$ and $\mathrm{sgn}(\tilde{\kappa} - \kappa_2) = 1$ for $z > z^{\pm}$. In words, if $k = 0$ then the Hessian matrix Φ has a singularity and the stationary

phase technique fails. If $k \neq 0$, then for depths between 0 and $z^{\mp}$ the stationary phase point corresponding to horizontal reflections is a elliptic point of the isochron surface ($\text{sgn}(\Phi) = -2$), for points below the depth $z^{\mp}$ the stationary phase point corresponding to horizontal reflections is hyperbolic ($\text{sgn}(\Phi) = 0$), and at the point $z^{\mp}$ there is a singularity that cannot be handled by simple–order stationary phase analysis. Let us recall –see discussion below equation E.39–that we are constrained to small values for k along the in–line direction. If it happens that a combination of parameters k and reflector dip changes the signature of Φ, then again, by a continuity argument, this curvature would have to go through zero at some point, and that point would be a cylindrical (parabolic) point. The simple stationary phase result is invalid close to this point and we need an alternative method. The study of these possible singularities is left for future research.